

**Plasma-Assisted Fabrication of Microporous and Nanoporous
Composite Coatings on Titanium Implants for Orthopedic Applications**

Monica Thukkaram

Doctoral dissertation submitted to obtain the academic degree of
Doctor of Engineering Physics

Supervisors

Prof. Nathalie De Geyter, PhD* - Prof. Lieven De Wilde, PhD** - Prof. Kim Verbeken, PhD***

* Department of Applied Physics
Faculty of Engineering and Architecture, Ghent University

** Department of Human Structure and Repair
Faculty of Medicine and Health Sciences, Ghent University

***Department of Materials, Textiles and Chemical Engineering
Faculty of Engineering and Architecture, Ghent University

September 2021



**Plasma-Assisted Fabrication of Microporous and Nanoporous
Composite Coatings on Titanium Implants for Orthopedic Applications**

Monica Thukkaram

Doctoral dissertation submitted to obtain the academic degree of
Doctor of Engineering Physics

Supervisors

Prof. Nathalie De Geyter, PhD* - Prof. Lieven De Wilde, PhD** - Prof. Kim Verbeken, PhD***

* Department of Applied Physics
Faculty of Engineering and Architecture, Ghent University

** Department of Human Structure and Repair
Faculty of Medicine and Health Sciences, Ghent University

***Department of Materials, Textiles and Chemical Engineering
Faculty of Engineering and Architecture, Ghent University

September 2021

ISBN 978-94-6355-521-0

NUR 971

Wettelijk depot: D/2021/10.500/69

Members of the Examination Board

Chair

Prof. Filip De Turck, PhD, Ghent University

Other members entitled to vote

Prof. Ondrej Kylian, PhD, Charles University, Czech Republic

Prof. Christophe Leys, PhD, Ghent University

Prof. Ann Martens, PhD, Ghent University

Prof. Andre Skirtach, PhD, Ghent University

Prof. Alexander Van Tongel, PhD, Ghent University

Supervisors

Prof. Nathalie De Geyter, PhD, Ghent University

Prof. Lieven De Wilde, PhD, Ghent University

Prof. Kim Verbeken, PhD, Ghent University

This research has received funding from the Research Foundation Flanders (FWO) under the strategic basic research (1S13017N). The authors would also like to acknowledge the financial support from the Ministry of Education, Youth and Sports of the Czech Republic under the framework of the grant LTC17062.

Summary

Every year more than 1000 tons of titanium-based devices of every description and function are implanted in patients. Titanium (Ti) and its alloys are widely used in biomedical implants for musculoskeletal disorders such as joint prostheses, fracture fixation devices and dental implants for many years due to their outstanding mechanical properties and excellent corrosion resistance. Even though Ti implants are expected to last for at least a decade or more, they often fail prematurely, resulting in revision surgery that is usually characterized by a higher level of complexity thereby forming a heavy burden on the current healthcare systems. The causes of implant failure are varying in nature, with bacterial infections on the implant surface being one of the prime reasons. It has been reported that the annual rate of implant-associated infections in orthopedic implants is between 2% and 5% in recent years. Risk of bacterial infection is high, especially for fracture fixation devices where open fractured bones are involved. Implant-associated infections are the result of bacterial adhesion to an implant surface and subsequent biofilm formation at the implantation site. Once the bacteria adhere on the implant surface, they undergo cellular proliferation under favorable conditions to form a protective envelope consisting of an exopolysaccharide layer that leads to the formation of a biofilm (bacterial colonies). Subsequently, the bacteria will detach from this biofilm to form planktonic cells which can then continue the formation process of a new biofilm. The most common organisms causing biofilm formation are gram-positive bacteria such as *S. aureus* and *S. epidermidis* but gram-negative bacteria such as *E. coli* have also been linked to this phenomenon. Nowadays, minor bacterial infections are in most cases successfully treated with oral antibiotics. Nevertheless, these antibiotic treatments can sometimes be very challenging due to the continuous bacterial adherence on the implant surface resulting in biofilm formation, which is highly resistant to antibiotics and the host's defense mechanism. Also, many bacterial species, especially those involved in nosocomial infections are multidrug resistant which poses a crucial problem to the healthcare industry. Consequently, there currently is an increasing demand to develop alternative antibacterial Ti implants. Therefore, several surface modification strategies focused on loading organic (chitosan, collagen) and inorganic (silver, copper, gold) antibacterial

agents onto the surface of implants were implemented. However, all current approaches are still failing in controlling the release of antibacterial agents and in maintaining their therapeutic level.

Next to implant-associated infections, another problem associated with Ti-based implants is their insufficient osseointegration and osteoconductive properties. An appropriate adhesion between the bone and the metal surface has still not been observed because of insufficient bone-implant contact and fibrous encapsulation. This may lead to improper biomechanical fixation and loosening of the implants causing implant failure. Therefore, the need to improve the osseointegration of Ti with the host tissue is still a crucial topic. Osteoconductivity can however be enhanced if successful tissue integration occurs before bacterial adhesion takes place during the race for colonization of the implant surface. In addition to these aspects, an implant material should also possess appropriate mechanical properties to achieve higher efficiency and durability under more sliding conditions. Thus, an ideal implant material should be bi-functional as it should possess both antibacterial and osteoconductive properties together with improved hardness and durability. Therefore, the aim of this dissertation is to design and test novel microporous and nanoporous composite coatings loaded with antibacterial agents such as silver and copper on medical grade Ti substrates possessing the ideal topographical and chemical cues triggering a bi-functional character, i.e. providing both a high efficiency against biofilm formation and at the same time promoting osseointegration.

From this point of view, there are several criteria that need to be achieved. Firstly, the process of the coating fabrication has to be fast, simple and convenient. Secondly, the coating should be hard and possess adequate bonding strength to Ti substrates. Thirdly, the choice of matrix which can serve as a reservoir of the antibacterial agents should allow a continuous release of antibacterial agents (silver ions, copper ions) and should prevent any unwanted high release. Finally, and most importantly, the designed coating should possess the desired bi-functional property. To fulfil these general requirements, two different non-thermal plasma-based surface modification strategies, plasma electrolytic oxidation (PEO) and a cluster source process combining a gas aggregation source (GAS) with plasma enhanced

chemical vapour deposition (PECVD) were used and compared in this study.

Plasma, also known as the fourth state of matter, is produced by electrical discharges in which energetic electrons collide with the available molecules. The first technique employs PEO which provides a plasma-assisted electrochemical conversion of metal surfaces into oxide ceramic layers in the presence of an electrolyte. During PEO, Ti and a stainless-steel tank act as an anode and cathode respectively and the Ti substrate is exposed to an electrolyte placed within the tank at an applied high voltage. When the applied voltage is less than the breakdown voltage, an amorphous oxide layer is deposited, whereas when the voltage is higher than the breakdown voltage, the process tends to produce plasma spark discharges leading to the formation of a ceramic oxide layer, which thickens into a native passivating titanium dioxide (TiO₂) layer. The ceramic oxide coatings produced on metal surfaces are microporous and rough which enables better performance of bone implants as they can improve the growth of bone tissue. In addition, the deposited oxide layers can offer a wide variety of mechanical, tribological, and antibacterial properties via the incorporation of several ions and particles present in the electrolyte. The porous oxide layer can in fact act as a reservoir and can stimulate the release of antibacterial agents from the Ti implants into its surroundings. As such, the bioactivity and antibacterial properties of the coating can be tuned by controlling the applied voltage, electrolyte composition, treatment time, and current density.

The second technique used in this dissertation employs a cluster source based on plasma enhanced chemical vapour deposition (PECVD) to deposit thin plasma polymer films and a magnetron-based gas aggregation source for the production of nanoparticles (NPs). PECVD deposits thin films from the gaseous state (vaporious or gaseous precursors) to the solid state on a substrate. Creation of plasma of the reactive gas takes places with the subsequent formation of chemically active species. Thin plasma polymer films are then deposited on the cathode (typically the radiofrequency (RF) electrode) or any object exposed to the plasma region. In PECVD, thin films with different properties can be obtained by changing the nature of the precursor, the working gas mixture and the intensity of ion bombardment of the growing film. The use of plasma polymers such as amorphous hydrocarbon (a-C:H) is very advantageous due to their

superior bonding strength to various substrates and their possibility to regulate the release of antibacterial agents from the plasma polymerized matrix and thus to control the antibacterial performance of the produced coatings. By combining the PECVD technology and the GAS system, it is possible to independently control the properties of the matrix material that can be adjusted by the parameters employed for PECVD (e.g. applied power, type of precursor, working gas mixture, bias on the substrate) and the size distribution and flux of NPs that solely depend on the parameters in the GAS. As such, coatings with appropriate surface properties and biocompatibility can be attained simply by varying the operational parameters in the PECVD and/or GAS system.

Thus, the above discussion serves as the rationale for choosing the proposed method to accomplish the goal of this dissertation. i.e. to fabricate microporous and nanoporous composite coatings on Ti implant surfaces for orthopaedic applications. The dissertation's first experimental part focused on the fabrication of bi-functional coatings by PEO while the second experimental part focused on the fabrication of bi-functional coatings using the cluster technology (PECVD + GAS). A profound and well-thought step-by-step approach is adopted in this dissertation gradually paving the way towards the fabrication of an ideal implant surface.

In the first experimental phase of this dissertation, Ag-free and Ag-doped porous TiO₂ coatings were fabricated. To attain this, commercially pure Ti samples were subjected to PEO in a sodium dihydrogen phosphate and sodium hydroxide containing base electrolyte with and without the addition of silver nanoparticles (AgNPs). AgNPs were chosen as antibacterial agent due to their larger surface to volume ratio and their broad antibacterial spectrum. After PEO treatment, porous Ag-free and Ag-doped TiO₂ coatings were formed on the surface of the Ti substrates. In the latter case, AgNPs were successfully incorporated into the coating and distributed as clusters and stand-alone NPs on the coating surface and inside the pores of the coating. The obtained results revealed that by increasing the concentration of AgNPs in the electrolyte the amount of Ag in the oxidized coatings increased. In contrast, the microstructure, phase composition, surface roughness and surface wettability of the TiO₂ coatings were not affected by the incorporation of AgNPs. Additionally, the coatings synthesized in the alkaline base electrolyte with added

AgNPs exhibited excellent antibacterial activity against *E. coli* and *S. aureus* in comparison to the coating formed in the Ag-free base electrolyte. Moreover, the antibacterial activity of the coating was found to increase with an increase in AgNPs amount in the electrolyte. Although the exact mechanism of the antibacterial activity of AgNPs is still not clear and under debate, it is believed that it is caused by the synergistic effects of both AgNPs and released Ag⁺ ions. Despite exhibiting superior antibacterial efficacy, the incorporated AgNPs were observed to aggregate as clusters on the coating surface and the clustering effect was more pronounced at increased Ag content. This finding is unfavorable as a uniform deposition of Ag in the oxide layer is essential to have a constant release of Ag⁺ which can in turn provide a better antibacterial performance as aggregates of silver are known to lead to bacterial resistance and may cause potential cytotoxic effect on cell lines. Therefore, in the next step of this dissertation, the focus was shifted to harness the antibacterial properties of Ag⁺ without actually using AgNPs by delivering Ag⁺ from silver acetate or silver nitrate present within a suitable matrix. The bi-functional character (antibacterial ability and osseointegration) of the PEO coatings was investigated for the first time by incorporating antibacterial Ag⁺ ions together with osteoconductive Ca and P ions on Ti implant surfaces. Porous bi-functional oxide coatings on Ti discs were synthesized by means of PEO in a base electrolyte containing calcium acetate monohydrate, sodium dihydrogen phosphate dehydrate with and without the addition of different amounts of silver acetate as supplier of Ag⁺ ions. The electrolyte concentration used in this study was optimized to attain the ratio characteristic for stoichiometric hydroxyapatite (HA) (Ca/P = 1.6) which mimics the bone apatite properties. The attained results revealed that the formation of crystalline phases such as rutile TiO₂ and Ca- and P-containing phases (hydroxyapatite, CaTiO₃) on the coating can be increased by increasing the silver acetate concentration in the electrolyte. This increased crystallinity was found to be a crucial factor in promoting successful protein adsorption and tissue integration. Increasing the concentration of silver acetate in the electrolyte increased the amount of silver in the coatings from 0.8 at% to 2.2 at%. On the other hand, the porous microstructure of the coatings, their moderate surface roughness (0.8-1 μm) and high wettability (approximately 20°) were not altered by the incorporation of Ag. The produced coatings exhibited

good antibacterial performance and osseointegration and promoted osteoblast cell adhesion and proliferation in comparison to the untreated Ti surface.

In the second experimental phase of this doctoral dissertation, the cluster technology was employed (a combination of magnetron sputtering and PECVD) to deposit an a-C:H matrix loaded with antibacterial agents such as AgNPs and CuNPs. This cluster technique, in contrast to PEO, enables to control the properties of the a-C:H matrix, and the amount of antibacterial agents loaded into the matrix as well as its release rate independently. a-C:H films were chosen as matrix because of their superior mechanical properties, biocompatibility and haemocompatibility. In this work, Ag-containing a-C:H nanocomposites with varying AgNPs concentration were deposited on Ti substrates using the cluster technique. This deposition strategy made it possible to tune the silver content in the nanocomposites independently of the properties of the matrix material. This in turn also allowed to precisely control the antibacterial efficiency of the produced coatings which was connected with their ability to release Ag⁺ into an aqueous environment. The incorporated AgNPs were strongly fixed into the a-C:H matrix as the NPs did not migrate from the coatings into surrounding water even after prolonged immersion times. As such, the undesirable release of AgNPs into an aqueous environment was prevented in case of the nanocomposite coatings developed in this dissertation. The obtained results revealed that all Ag/a-C:H coatings exhibited good antibacterial efficacy against *S. aureus* and *E. coli* and that the antibacterial effect was more pronounced for the coating with the highest Ag amount. Besides the very good antibacterial performance of the produced Ag/a-C:H films, all coatings were also able to promote osteoblast adhesion and proliferation independent of the Ag content in the coating as osteoblast adhesion and proliferation was higher than on the uncoated Ti surfaces. These excellent antibacterial efficacies and enhanced cellular response were attributed to the superior physico-chemical properties (favorable surface wettability, roughness and chemical composition) of the a-C:H matrix together with the controlled release of Ag⁺. As the Ag-rich amorphous hydrocarbon thin films (Ag/a-C:H) developed in this work showed promising results, the bi-functional character of a novel thin a-C:H matrix loaded with CuNPs on Ti substrates has also been examined in this dissertation,

an approach which has not yet been explored in the past. CuNPs are used because, apart from their use as an antibacterial agent, Cu ions released from CuNPs are also beneficial to the cardiovascular system by stimulating the proliferation and differentiation of endothelial cells and a sustained release of trace amounts of Cu ions could also promote osteogenesis. As such, in the last experimental chapter of this thesis, cluster beam deposition of CuNPs was combined with PECVD of a-C:H thin films for the fabrication of three different types of Cu/a-C:H coatings with approximately the same amount of embedded CuNPs but with a different arrangement of the NPs inside the a-C:H matrix. The obtained results revealed that different structures of the produced coatings have significantly different release rates of Cu ions from the coatings into aqueous media. This in fact is connected with the antibacterial efficiency and osteoblast cell viability of the fabricated coatings. Even the coatings with the highest amount of CuNPs resulted in excellent antibacterial efficiency and osteoblast cell adhesion and proliferation. Consequently, the coating, formed with a properly tailored number of CuNPs and a-C:H structure offer a strong antibacterial effect without any harm to osteoblast cells.

Overall, it can be concluded that both investigated surface modification technologies (PEO and PECVD+GAS) have a great potential in fabricating bi-functional coatings as they can both deposit coatings exhibiting sufficient osseointegration and antibacterial properties, thus making them highly interesting materials for orthopaedic applications. As a general conclusion, the results obtained in this dissertation thus prove that favourable surface properties such as surface wettability, surface roughness and surface chemical composition together with a controlled release of Ag ions or Cu ions are the determining factors for the success of an implant material.

Samenvatting

Titanium en zijn legeringen worden al jaren uitgebreid gebruikt bij musculoskeletale aandoeningen zoals gewrichtsprothesen en osteosynthese van fracturen vanwege hun buitengewone mechanische eigenschappen en hun excellente corrosieweerstand. Ondanks een verwachte levensduur van minstens 10 jaar falen Ti implantaten echter vaak prematuur, met soms noodzakelijke chirurgische revisies als gevolg en deze gaan vaak gepaard met een hogere complexiteit.

Er zijn verschillende oorzaken waarom Ti implantaten falen, maar de meest voorkomende oorzaak is een bacteriële infectie op het oppervlak van het implantaat. Onderzoek heeft aangetoond dat de voorbije jaren het jaarlijks percentage van infecties geassocieerd met orthopedische implantaten tussen de 2 en 5% ligt. Implantaat-geassocieerde infecties zijn het resultaat van bacteriële adhesie op het oppervlak van het implantaat. Eens de bacteriën zich hechten aan het oppervlak van het implantaat, ondergaan deze in gunstige omstandigheden cel proliferatie om zo een beschermende biofilm te creëren bestaande uit een exopolysaccharide laag. De meest voorkomende organismen die biofilm vorming veroorzaken zijn grampositieve bacteriën zoals *S. aureus* en *S. epidermidis* maar ook gramnegatieve bacteriën zoals *E. coli*. Dergelijke biofilms zijn zeer resistent tegen antibiotica en het verdedigingsmechanisme van de patiënt. Bijgevolg is er momenteel een sterk toenemende vraag om 'antibacteriële' Ti implantaten te ontwikkelen die de bacteries doden vooraleer een biofilm kan worden gevormd. Dit kan door het oppervlakte van het implantaat te modificeren. In dit kader zijn reeds verschillende oppervlakte modificatie strategieën geïmplementeerd die gefocust zijn op het laden van organische (chitosan, collageen) en anorganische (zilver, koper, goud) antibacteriële agenten op het implantaat. Jammer genoeg falen alle huidige strategieën nog steeds in het controleren van de vrijgave van de antibacteriële agenten en in het onderhouden van hun therapeutisch niveau.

Infecties zijn echter niet het enige probleem geassocieerd met Ti-gebaseerde implantaten. Een ander gekend nadeel is hun ontoereikende osseo-integratie en osteoconductieve eigenschappen. Dit kan leiden tot het loskomen en het falen van het implantaat.

Daarom is onderzoek naar het verbeteren van de osseo-integratie van Ti belangrijk..

Een ideaal materiaal voor een implantaat moet dus bi-functioneel zijn aangezien het zowel antibacteriële als osteoconductive eigenschappen moet bezitten

Het doel van dit onderzoek is het ontwerpen en testen van nieuwe micro poreuze en nano poreuze composiet deklagen geladen met antibacteriële agenten zoals zilver en koper. Deze deklagen worden afgezet op medische gekeurd Ti materialen zodat deze de ideale topografische en chemische signalen bezorgen aan Ti om zowel een hoge efficiëntie tegen de vorming van biofilmvorming te bieden als osseo-integratie promoten. Vanuit dit oogpunt zijn er verschillende criteria nodig. Eerst en vooral, het vervaardigen van de deklagen moet snel, simpel en gemakkelijk gebeuren. Daarnaast moeten de deklagen hard zijn en moeten ze een adequate bindingskracht bezitten aan het onderliggende Ti substraat. Ten derde moet er een geschikte matrix gekozen worden die kan fungeren als een reservoir voor de antibacteriële agenten. Deze matrix moet een voortdurende vrijgave van antibacteriële agenten toelaten (zilver ionen, koper ionen) en moet een te hoge vrijgave voorkomen. Tot slot, en uitermate belangrijk, moet de ontworpen deklaag de gewenste bi-functionele eigenschap bezitten. Om deze algemene vereisten te vervullen werden twee verschillende niet-thermische, plasma-gebaseerde, oppervlakte modificatie strategieën gebruikt en vergeleken tijdens dit onderzoek: plasma elektrolytische oxidatie (PEO) en een cluster bron proces dat een gasaggregatiebron (GAS) combineert met plasma-versterkte chemische damp depositie (PECVD).

Plasma, ook gekend als de vierde aggregatietoestand, wordt geproduceerd door elektrische ontladingen waarin energetische elektronen botsen met beschikbare atomen/moleculen. De eerste onderzochte techniek in dit werk (PEO) is gebaseerd op een door plasma geassisteerde elektrochemische conversie van metaal oppervlakken naar oxide keramische lagen in het bijzijn van een elektrolyt. Tijdens het PEO proces fungeren het Ti substraat en een roestvrij stalen tank respectievelijk als anode en kathode. Het Ti substraat wordt blootgesteld aan een elektrolyt geplaatst in de stalen tank terwijl er hoogspanning wordt toegepast. Wanneer de

aangebrachte hoogspanning lager is dan de doorslagspanning dan wordt er een amorfe oxide laag gedeponerd. Daarentegen, wanneer de aangelegde spanning hoger is dan de doorslagspanning, dan zal in veel gevallen het proces vonkontladingen produceren, welke op hun beurt leiden tot het vormen van een keramische oxide laag. Deze laag zal vervolgens verdikken tot een passieve titanium dioxide (TiO_2) laag. De keramische oxide deklagen geproduceerd op de oppervlakte van de Ti substraten zijn micro poreus en ruw waardoor deze een betere werking als bot implantaten mogelijk maken aangezien de ruwheid de groei van het beenweefsel kan bevorderen. Bovendien kunnen deze gedeponerde oxide lagen een grote variatie aan mechanische, tribologische en antibacteriële eigenschappen bieden via de incorporatie van verschillende ionen en partikels aanwezig in het elektrolyt. De poreuze oxide laag kan fungeren als een reservoir en kan het vrijgeven van antibacteriële agenten van de Ti implantaten naar zijn omgeving stimuleren. Zodoende kunnen de bioactiviteit en antibacteriële eigenschappen van de deklaag worden afgestemd door de aangelegde hoogspanning, de elektrolyt samenstelling, de behandelingstijd en de stroomdichtheid te controleren.

De tweede techniek die wordt toegepast in dit onderzoek maakt gebruik van (1) een cluster bron gebaseerd op PECVD om dunne plasma polymeer films te deponeren en (2) een magnetron gebaseerde gasaggregatiebron voor de productie van nanopartikels (NPs). PECVD deponert dunne films startende van een gasvormige toestand (verdampte of gasvormige precursoren) op een vast substraat. Plasma wordt gecreëerd van het reactieve gas wat op zijn beurt leidt tot de vorming van chemisch actieve deeltjes. Dunne plasma polymeer films worden dan vervolgens gedeponerd door reacties tussen deze chemisch actieve deeltjes op de kathode (in de meeste gevallen een radiofrequente (RF) elektrode) of op elk ander object dat is blootgesteld aan de plasma regio. In PECVD kunnen dunne films met verschillende eigenschappen worden verkregen door de aard van de precursor, de gebruikte gasmengsels en de intensiteit van het ionenbombardement van de groeiende film aan te passen. Het gebruik van plasma polymeren zoals amorf koolwaterstof (a-C:H) is zeer bevorderend omdat deze uitstekend bindt aan diverse substraten en omdat deze in staat zijn om het vrijgeven van antibacteriële agenten van de plasma gepolymeriseerde matrix te reguleren en dus de antibacteriële

werking van de geproduceerde deklagen te kunnen controleren. Door het combineren van de PECVD technologie met het GAS systeem is het mogelijk om onafhankelijk de eigenschappen van de matrix en de NPs te controleren. De eigenschappen van de matrix kunnen worden aangepast door de parameters, gebruikt voor PECVD (e.g. het vermogen, het type precursor, het gasmengsel, de substraatbias), te veranderen, terwijl de grootteverdeling en de flux van NPs kan gevarieerd worden door de parameters van de GAS te wijzigen. Op deze manier kunnen deklagen met de juiste oppervlakte eigenschappen en biocompatibiliteit verkregen worden door het variëren van de operationele parameters in het PECVD en/of GAS systeem.

Deze bovenstaande discussie heeft een beter inzicht van de gekozen methodes om het doel van dit onderzoek te behalen. i.e. het fabriceren van micro poreuze en nano poreuze composiet deklagen op het oppervlak van Ti implantaten voor orthopedische applicaties. Het eerste deel van dit onderzoek is gefocust op het deponeren van bi-functionele deklagen door PEO terwijl het tweede deel van het onderzoek focust op de productie van bi-functionele deklagen door het gebruik van de cluster technologie (PECVD + GAS). Dit onderzoek werd benaderd via een grondige, stap voor stap methode om zo geleidelijk aan te werken in de richting van de productie van een ideaal Ti implantaat oppervlak.

Tijdens de eerste experimentele fase van dit onderzoek werden zilver (Ag)-vrije en Ag-bevattende poreuze TiO₂ deklagen ontwikkeld. Om dit te verkrijgen werden commercieel verkrijgbare, puur Ti stalen blootgesteld aan PEO in een natrium diwaterstof fosfaat en natrium hydroxide bevattende basis elektrolyt met en zonder de toevoeging van zilver nanopartikels (AgNPs). AgNPs werden gekozen als antibacteriële agent omdat deze een grotere oppervlakte tot volume verhouding hebben en een breed antibacterieel spectrum bezitten. Na de PEO behandeling vormden poreuze Ag-vrije en Ag-bevattende TiO₂ deklagen op het oppervlak van de Ti substraten. In het laatste geval werden AgNPs succesvol geïncorporeerd in de deklagen en verspreid als clusters en alleenstaande NPs op het bedekte oppervlak en binnenin de poriën van de deklaag. De verkregen resultaten toonden aan dat door het verhogen van de concentratie van AgNPs in het

elektrolyt de hoeveelheid zilver in de geoxideerde deklaag verhoogde. In contrast, de microstructuur, de fase samenstelling, de ruwheid van het oppervlak en de bevochtiging van het oppervlak van de TiO₂ deklagen werden niet beïnvloed door de incorporatie van AgNPs. Daarbovenop vertoonden de deklagen verkregen in het alkalische basis elektrolyt met toegevoegde AgNPs uitstekende antibacteriële eigenschappen tegen *E. coli* en *S. aureus* in vergelijking tot de deklaag gevormd in het Ag-vrije basis elektrolyt. Daarbij werd de antibacteriële activiteit van de deklaag verhoogd wanneer de concentratie aan AgNPs werd verhoogd in het elektrolyt. Ondanks het feit dat het exacte mechanisme van de antibacteriële activiteit van AgNPs nog niet volledig duidelijk is en nog veel discussie teweeg brengt, kan er verondersteld worden dat de antibacteriële eigenschappen van AgNPs veroorzaakt worden door de synergetische effecten van zowel AgNPs zelf als van de vrijgegeven Ag⁺ ionen. Ondanks de sterk verbeterde antibacteriële werking, werd toch geobserveerd dat de geïncorporeerde AgNPs zich vooral aggregeerden als clusters op het deklaagoppervlak en dat dit cluster effect meer uitgesproken was bij een verhoging van het zilveragehalte. Deze bevinding is ongunstig aangezien een uniforme depositie van Ag in de oxide laag essentieel is om een constante vrijgave van Ag⁺ te hebben, wat op zijn beurt kan zorgen voor een betere antibacteriële werking aangezien aggregaten van zilver gekend zijn voor hun bacteriële resistentie en potentieel cytotoxisch effect op cellijnen kunnen veroorzaken. Om die reden werd in de volgende stap van dit onderzoek de focus verlegd ten einde de antibacteriële eigenschappen van Ag⁺ te benutten zonder AgNPs te gebruiken door Ag⁺ te bezorgen van zilver acetaat of zilver nitraat binnenin een gepaste matrix. Het bi-functioneel karakter (antibacteriële eigenschappen en osseo-integratie) van de PEO lagen werd voor het eerst onderzocht door antibacteriële Ag⁺ ionen samen met osteoconductieve Ca en P ionen op de Ti implantaat oppervlakken te incorporeren. Poreuze bi-functionele oxide lagen op de Ti substraten werden ontwikkeld door een PEO proces uit te voeren in een basis elektrolyt dat calcium acetaat monohydraat en natrium diwaterstof fosfaat dehydraat bevat met en zonder de toevoeging van verschillende hoeveelheden zilver acetaat als leverancier van Ag⁺ ionen. De elektrolyt concentratie die in deze studie werd gebruikt was geoptimaliseerd om de Ca/P verhouding te verkrijgen die karakteristiek is voor stoichiometrisch hydroxyapatiet

(HA) (Ca/P = 1.6) welke in staat is boteigenschappen na te bootsen. De verkregen resultaten onthulden dat de samenstelling van de kristallijne fasen zoals rutiel TiO_2 en Ca- en P-bevattende fasen (hydroxyapatiet, CaTiO_3) op de deklaag kan worden verhoogd door het verhogen van de concentratie van zilver acetaat in het elektrolyt. Deze verhoogde kristalliniteit werd bevonden als een cruciale factor in het promoten van succesvolle proteïne adsorptie en weefselintegratie. Het verhogen van de concentratie zilver acetaat in het elektrolyt verhoogde de hoeveelheid zilver in de deklagen; hun gemiddelde oppervlakte ruwheid ($0.8\text{-}1\ \mu\text{m}$) en hoge hydrofliciteit (contacthoek van ongeveer 20°) wijzigden echter niet door de incorporatie van Ag. De geproduceerde deklagen vertoonden een goede antibacteriële werking en osseo-integratie en bevorderden osteoblast hechting en proliferatie in vergelijking met het onbehandelde Ti oppervlak.

In de tweede experimentele fase van deze doctoraatsthesis werd de cluster technologie toegepast (een combinatie van magnetron sputtering en PECVD) om een a-C:H matrix geladen met antibacteriële agenten te deponeren zoals AgNPs en CuNPs. Deze cluster techniek, in contrast tot PEO, zorgt ervoor dat de eigenschappen van de a-C:H matrix en de hoeveelheid van antibacteriële agenten geladen in de matrix net als hun afgiftesnelheid onafhankelijk kunnen worden gecontroleerd. a-C:H films werden gekozen als matrix omdat deze uitstekende mechanische eigenschappen, biocompatibiliteit en hemocompatibiliteit bezitten. In dit werk werden Ag-bevattende a-C:H nano composieten met verschillende AgNPs concentraties gedeponerd op Ti substraten met behulp van de cluster techniek. Deze manier van deponeren maakt het mogelijk om het zilveragehalte af te stemmen in de nano composieten onafhankelijk van de eigenschappen van de matrix. Dit gaf ook de mogelijkheid om de antibacteriële efficiëntie van de geproduceerde deklagen precies te controleren, wat op zijn beurt verbonden was aan hun mogelijkheid om Ag^+ vrij te geven in een waterig milieu. De geïncorporeerde AgNPs waren sterk gefixeerd in de a-C:H matrix aangezien de NPs niet migreerden vanuit de gedeponerde lagen in omliggend water, zelfs niet na een lange immersie periode. De ongewenste vrijlating van AgNPs in een waterig milieu werd dus voorkomen in geval van de nano composiet lagen ontwikkeld in deze thesis. De vastgestelde resultaten toonden ook aan dat alle Ag/a-C:H

deklagen een goede antibacteriële werking tegen *S. aureus* en *E. coli* vertoonden en dit antibacterieel effect was meer uitgesproken voor de deklaag met het hoogste Ag gehalte. Naast de zeer goede antibacteriële werking van de geproduceerde Ag/a-C:H films waren alle lagen ook in staat om osteoblast adhesie en proliferatie te promoten, onafhankelijk van de Ag content in de laag aangezien osteoblast adhesie en proliferatie steeds hoger was dan op de onbedekte Ti oppervlakken. Deze uitstekende antibacteriële effecten en verhoogde cellulaire reacties waren het gevolg van de superieure physico-chemische eigenschappen (gunstige oppervlakte bevochtiging, ruwheid en chemische samenstelling) van de a-C:H matrix samen met de gecontroleerde vrijgave van Ag⁺. Aangezien de Ag-rijke amorfe koolwaterstof dunne films (Ag/a-C:H) ontwikkeld in dit werk veelbelovend waren, werd het bi-functioneel karakter van een a-C:H matrix geladen met koper nanopartikels (CuNPs) op Ti substraten ook bestudeerd in deze thesis, iets wat nog niet werd onderzocht in het verleden. CuNPs werden gebruikt omdat deze, los van hun kwaliteit als antibacteriële agent, Cu ionen vrijlaten en deze ionen bevorderend zijn voor het cardiovasculair systeem omdat deze zorgen voor stimulatie van de proliferatie en differentiatie van endotheel cellen en een langdurige vrijgave van minimale hoeveelheden van Cu ionen ook osteogenesis kan promoten. In het laatste deel van deze thesis werd opnieuw de cluster technologie toegepast: CuNPs werden gecombineerd met PECVD van a-C:H dunne films voor het vervaardigen van drie verschillende types Cu/a-C:H lagen met ongeveer dezelfde hoeveelheid geïntegreerde CuNPs maar met een verschillende schikking van de NPs in de a-C:H matrix. De verkregen resultaten toonden aan dat verschillende structuren van de geproduceerde lagen aanzienlijk verschillende afgiftesnelheden van Cu ionen uit de deklagen hebben in waterig milieu. Deze afgiftesnelheid is op zijn beurt verbonden met de antibacteriële effectiviteit en osteoblast cel adhesie en proliferatie van de ontwikkelde deklagen. Zelfs de deklagen met de hoogste hoeveelheid CuNPs vertoonden een uitstekende antibacteriële efficiëntie en excellente osteoblast adhesie en proliferatie. Bijgevolg zorgt een deklaag met een geschikte a-C:H structuur en de juiste hoeveelheid CuNPs voor een sterk antibacterieel effect zonder dat de vrijgelaten Cu ionen schade veroorzaken aan osteoblasten.

Algemeen kunnen we concluderen dat beide onderzochte oppervlakte modificatie technologieën (PEO en PECVD+GAS) veel potentieel hebben in het vervaardigen van bi-functionele deklagen aangezien beide technieken deklagen deponeren die voldoende osseo-integratie en antibacteriële eigenschappen vertonen. Bijgevolg zijn deze gecoate Ti materialen dus heel interessant voor orthopedische toepassingen. De verkregen resultaten in deze thesis bewijzen dat gunstige oppervlakte eigenschappen zoals bevochtiging, ruwheid en chemische samenstelling samen met een gecontroleerde vrijgave van Ag of Cu ionen doorslaggevende factoren zijn voor het succes van orthopedische implantaten.

Acknowledgements

I would like to express my sincere gratitude towards Prof. Nathalie De Geyter and Prof. Rino Morent for giving me an opportunity to pursue a PhD at the Research Unit Plasma technology. Without their guidance, I would not have been able to successfully finish my master thesis, achieved my FWO strategic basic research grant, and successfully completed my PhD dissertation. They both gave me an opportunity to expand my scientific background and perform high-quality research. I would always be thankful to both of you for believing in me and accepting me as your PhD student. I am indebted to you both forever.

I am also very grateful to my co promoters Prof. Kim Verbeken, Prof. Dr. Lieven De Wilde for their excellent support. Special thanks to both of you for your encouraging words and impeccable support for the last 4 years.

I would like to thank Dr. Anton Nikiforov for his constant support, stimulating ideas, expertise and discussions that made my research interesting. Our discussions improved my knowledge and helped me in analyzing the scientific outcomes. I am always grateful to you for showing interest in my research and for all your valuable suggestions. You have been an very important role in my PhD carrier. Thank you very much Anton.

A profound thankfulness goes to Prof. Christophe Leys, head of the Department of Applied Physics where my Ph.D. took place. I was honored by his acceptance together with Prof. Ann Martens, Prof. Andre Skirtach, Prof. Alexander Van Tongel and Prof. Ondrej Kylian to be members of my PhD examination board. I am grateful for the time they spent in reading my thesis.

Special thanks to RUPT technical team Tim Poelman and Joris Peelman. These people were of critical importance in the design of the reactors and always helped me whenever a technical problem arose.

XVII

Special thanks to my colleague and friend Parinaz and Rouba for XPS support, Mahtab and Sheida for their cell test support. I would also like to thank all the members of RUPT for their direct and indirect support during my Phd.

During my research, I had the chance to coloborate with many people and I would like extend my gratitude to them and recognize their efforts: Prof Tom Coenye, Petra Rigole, Prof. Gijs Du Liang, Joachim, and Prof. Pascal Van der Voort.

One of the most memorable period during my PhD was my short research stay in Department of Macromolecular Physics, Charles University in Prague, Czech Republic. From the very first day everyone made me feel very welcomed and helped me with anything I needed. Thanks to Prof. Hynek Biederman and Prof. Ondrej Kylian in hosting me in their group. Special thanks to Dr. Mykhajlo Vaydulych (Misha), Anna, Daniël. I really enjoyed my time in Prague and its definitely because of you all. My sincere thanks to Prof. Ondrej Kylian for all your valuable comments and encouragement that incented me to widen my research from various perspectives.

Finally, I would like to thank my family for all their support, love and encouragement and motivation. My father Thukkaram, My mom Renuka, my two sisters Divya and Prashanthi, my brothers in law Parthi and Sudan and my loving niece Mithra and cute little nephews Ahbi & Dhruv. Lastly I would like to thank my Husband Vignesh. Has anyone can tolerate me for this long is a miracle. I doubt if I could finish this work without you. You were always ready to help with any tasks. You gave me the motivation and encouragement and full support to go through any obstacle. I may not have thank you enough. Thanks a lot Vignesh.

Table of Contents

Summary.....	I
Samenvatting.....	VIII
Acknowledgements	XVI
List of Figures	XXV
List of Tables.....	XXXIV
List of Abbreviations and Acronyms.....	XXXVI
List of Publications	XL
Chapter 1. Introduction	1
1.1 Musculoskeletal disorders and their treatment	3
1.1.1 History of artificial implantation.....	4
1.1.2 Infection.....	8
1.1.3 Implant loosening.....	9
1.1.4 Strategies to prevent implant failure	9
1.2 Objective of this thesis:	12
1.3 Structural organization of this PhD dissertation.....	14
Chapter 2. Role of biomaterials in implant therapy: Challenges, perspectives and opportunities.....	19
2.1 Nature of bone overview	21
2.1.1 Bone properties.....	21
2.1.1.1 Physicochemical properties.....	21
2.1.1.2 Mechanical properties.....	24
2.2 Bone implants: an overview	26
2.2.1 Properties of an ideal bone implant material:	27
2.2.1.1 Biocompatibility:	27
2.2.1.2 Osteoconductivity.....	28
2.2.1.3 Biomechanical capability	28

2.3 Biomaterials used in implant therapy	28
2.3.1 Metallic biomaterials overview	30
2.3.1.1 Titanium and titanium alloys	31
2.3.1.2 Magnesium	33
2.3.1.3 Tantalum	34
2.3.1.4 Stainless steel	35
2.3.1.5 Cobalt - Chromium	36
2.4 Problems associated with implant therapy	36
2.4.1 Implant - associated infection	36
2.4.2 Poor osseointegration	39
2.4.3 Mechanical failure: wear of metallic implants	39
2.5 Surface modification techniques	41
2.5.1 Thermal spraying	41
2.5.2 Sol-Gel	43
2.5.3 Physical vapor deposition (PVD)	44
2.5.3.1 Thermal Evaporation PVD	45
2.5.3.2 Sputtering PVD	45
2.5.4 Ion implantation	48
2.5.5 Chemical vapor deposition (CVD)	49
2.5.6 Anodization	52
2.5.7 Plasma immersion ion implantation and deposition (PIIID)	52
2.5.9 Plasma electrolytic oxidation	53
Chapter 3. Deposition of functional coatings on Ti surfaces: Improved biocompatible, antibacterial, and tribological properties	57
3.1 Introduction	59
3.2 Coatings with biocompatible and bioactive properties:	60

3.2.1 HA coating	61
3.2.2 Bioactive oxide coating.....	70
3.2.3 Bioactive glass (BG).....	75
3.3 Coatings with antibacterial properties.....	80
3.3.1 Coating loaded with antibiotics	80
3.3.2 Coatings containing non-antibiotic organic antibacterial agents.....	83
3.3.3 Coatings containing inorganic antibacterial agents.....	87
3.3.3.1 Silver- release coatings.....	87
3.3.3.2 Copper-release coatings.....	94
3.3.3.3 Nitric oxide releasing coatings.....	97
3.4 Coatings with improved tribological performance	98
3.4.1 Titanium dioxide(TiO_2) coating.....	98
3.4.2 Titanium nitride coatings.....	103
3.4.3 Diamond-like carbon (DLC) coatings.....	106
4 Conclusion	111
Chapter 4. Materials and Methods	113
4.1 Introduction	115
4.2 Preparation of Ti test specimens	115
4.3 Coating deposition methods.....	116
4.3.1 PEO deposition	116
4.3.1.1 Deposition of Ag-doped oxide coatings	116
4.3.1.2 Deposition of Ca/P/Ag-doped oxide coatings	116
4.3.1.3 PEO deposition process	116
4.3.2 Cluster source deposition	117
4.3.2.1 Deposition of amorphous hydrocarbon (a-C:H) plasma polymer thin films	118
4.3.2.2 Deposition of NPs by GAS.....	120

4.3.2.3 Plasma activation	120
4.3.2.4 Fabrication of functional antibacterial coatings ..	121
4.4 Coating characterization techniques	123
4.4.1 Surface chemical analysis: X-ray photoelectron spectroscopy (XPS).....	123
4.4.2 Coating crystallinity: X-ray powder diffraction crystallography (XRD).....	125
4.4.3 Surface wettability analysis : water contact angle (WCA).....	126
4.4.4 Surface morphology analysis : Scanning electron microscopy – Energy dispersive X-ray spectroscopy (SEM-EDS)	127
4.4.5 Surface topographical analysis	129
4.4.5.1 Stylus profilometer: 2D roughness measurements	130
4.4.5.2 AFM	131
4.4.6 Silver/copper ion release characteristics of the coating : Inductively coupled plasma mass spectrometry (ICP-MS)	132
4.5 Evaluation of the coating’s mechanical properties	133
4.5.1 Microhardness test	133
4.5.2 Scratch test.....	133
4.5.3 Adhesion tests.....	134
4.6 <i>In-vitro</i> antibacterial studies	134
4.6.1 CFU assay.....	135
4.6.2 Fluorescent staining (Resazurin assay)	135
4.6.3 Visualization of bacterial cell morphology using SEM	135
4.7 <i>In-vitro</i> cell studies	136
4.7.1 Cell culture	136

4.7.2 Live/dead staining and fluorescent microscopy.....	137
4.7.3 Visualization of cell morphology using SEM	137
4.7.4 Cell proliferation - MTT assay	137
4.8 Protein testing.....	138
4.8.1 Protein adsorption assay by sodium dodecyl sulfate- polyacrylamide gel electrophoresis (SDS-PAGE).....	138
4.8.2 Protein adsorption by fluorescence microscopy.....	139
Chapter 5. Antibacterial activity of a porous silver doped TiO ₂ coating on Ti substrates synthesized by PEO.....	141
5.1 Introduction	143
5.2 Experimental methods	143
5.3 Results and discussions	144
5.3.1 Coating morphology and distribution of AgNPs	144
5.3.2 Surface crystallinity	150
5.3.3 Surface wettability.....	152
5.3.4 Surface roughness.....	152
5.3.5 Surface microhardness.....	153
5.3.6 Silver ion release characteristics of the coatings	154
5.3.7 Evaluation of the <i>in-vitro</i> antibacterial activity of the coatings.....	155
5.4 Conclusion.....	158
Chapter 6. Fabrication of microporous coatings on Ti implants with improved mechanical, antibacterial and cell-interactive properties	159
6.1 Introduction	161
6.2 Experimental methods	162
6.3 Results and discussions	163
6.3.1 Influence of the silver acetate concentration on the current density of the PEO process.....	163

6.3.2 Morphologies, chemical states and crystalline phases of the coatings.....	164
6.3.3 Surface roughness, wettability and microhardness	171
6.3.4 Frictional coefficient of the coatings	172
6.3.5 Silver ion release kinetics.....	173
6.3.6 <i>In-vitro</i> antibacterial activity of the coatings	176
6.3.7 Protein adsorption to the coatings	178
6.3.8 Osteoblast cell response.....	181
6.4 Conclusion.....	186
Chapter 7. Fabrication of Ag/a-C:H nanocomposite coatings on Ti implants with improved mechanical, antibacterial and cell-interactive properties	189
7.1 Introduction	191
7.2 Experimental methods	192
7.3 Results and discussions	193
7.3.1 Characterization of AgNPs	193
7.3.2 Physico-chemical properties of Ag/a-C:H nanocomposites.....	195
7.3.3 Silver ion release of the nanocomposite coatings.....	200
7.3.4 Antibacterial efficiency of the Ag/a-C:H coatings	203
7.3.5 Cytocompatibility of the Ag/a-C:H coatings	204
7.4 Conclusions	209
Chapter 8. Biological activity and antimicrobial properties of Cu/a-C:H nanocomposites and nanolayered coatings on titanium substrates	211
8.1 Introduction	213
8.2 Experimental methods	213
8.3 Results and discussions	216
8.3.1 Physico-chemical characterization of the coatings	216

8.3.2 Cu ion release study	221
8.3.3 Antimicrobial efficiency of the produced coatings	223
8.3.4 Cytotoxicity study	228
8.4 Conclusion.....	234
Chapter 9. Conclusions and outlook	235
9.1 Conclusions	237
9.2 Outlook and future work.....	241
References	243

List of Figures

Figure 1. 1. Titanium hip joint (A), knee joint (B) and elbow joint (C).	6
Figure 1. 2. Titanium plates and screws	7
Figure 1. 3. Total knee arthroplasty revision causes during first early, first late and re-revision [17].....	7
Figure 1. 4. The chart represents the rate of failure mechanism following hip arthroplasty revision [18].....	8
Figure 2.1. Bone cells [64]	22
Figure 2.2. Structure of cortical and trabecular bone [65]	23
Figure 2.3. Confocal microscopy of human cortical bone from the femoral shaft. (a) Image showing the entire cortex (b) network of lacuna-canalicular porosity and (c) Detail of the lacuna-canalicular porosity depicting the nutrient arteries[68]	25
Figure 2.4. Porous tantalum implant: total shoulder arthroplasty (A), Zimmer dental trabecular implant (B) [88]	35
Figure 2.5. SEM image of S.aureus (left) and E.coli (right) biofilm ...	37
Figure 2.6. Biofilm formation on an implant surface [92]	38
Figure 2.7. An infected external fixation device forming skin necrosis	39
Figure 2.8. Radiographs of failed implants: (A) Spinal rod failure (B) Intramedullar nail fracture(C) plate fracture failure (D) Femur fracture failure [109]	41
Figure 2.9. Schematic diagram of Plasma spraying [118]	42
Figure 2.10. Schematic representation of sol-gel processing [123]	44
Figure 2.11. Magnetron sputtering mechanism [146]	47

Figure 2.12. Schematic diagram of mechanism of magnetron sputter coating machine [135]	47
Figure 2.13. Schematic description of gas transport and reaction process contributing to CVD film [156]	51
Figure 2.14. Schematic illustration of the direct current plasma immersion ion implantation (D-PIII) into planar substrates [167]	53
Figure 2.15. Schematic diagram of plasma electrolytic oxidation (PEO) experimental device	55
Figure 2.16. Schematic of the formation process of PEO coating [170]	55
Figure 3.1. The outline of this chapter	60
Figure 3.2. SEM images of the HA coatings prepared via electrochemical deposition after immersion in SBF solution for (a) 1 day; (b) 4 days and (c) 7 days [190]	66
Figure 3.3. SEM micrographs of MG63 osteoblasts cells grown for 10 days on (a) uncoated titanium, (b) plasma sprayed coating, (c) sputtered coating, (d) sol-gel coating	67
Figure 3.5. Morphology of human osteosarcoma (MG63) cells attached on untreated Ti disc(a), TiO ₂ films (b) and ZrO ₂ films (c) after 24h at 200x magnification (bar – 50 μm) [223]	75
Figure 3.6. Field emission SEM micrographs of the surface morphology after 5 days immersion in SBF : Pure HA (a,b), 90% HA with 10% Zr (c,d), 70% HA with 30% Zr (e,f) [225]	76
Figure 3.7. S. aureus bacteria colonies on agar plates (a) untreated Cp Ti, (b) 0.5h-Ag-PIII and E. coli colonies (c) untreated Cp Ti, (d) 0.5h-Ag-PIII [168]	89
Figure 3.8. Laser scanning confocal microscope images of MG63 osteoblast cells cultures for 1h (i-1), 3 h (i-2), 5 h (i-3), and 24 h (i-4) on the various surfaces with F-actin stained with rhodamine phalloidin	

(red) and the nucleus stained with DAPI (blue) (i = a, b, c and d represent Cp Ti, 0.5h-Ag-PIII, 1.0h-Ag-PIII, and 1.5h-Ag-PIII, respectively) [168] 90

Figure 3.9. Fluorescence microscopy images of adhered bacterial cells, *S. aureus* (A,B,C), *S. epidermidis* (D,E,F), *E. coli* (G,H,I), and *P. aeruginosa* – (J,K,L), after 3 h of incubation with bacterial cell suspension. The tested surfaces were: Ti (A,D,G,J), TiO₂-NT (B,E,H,K), and Ag/TiO₂-NT (C,F,I,L). In brackets: the average number of cells per mm² and the standard deviation of this value. .. 92

Figure 3.10. viabilities of the cells cultured on untreated Ti and Cu doped TiO₂ for 1 h, and 1 and 3 days [336]..... 96

Figure 3.11. Hardness (A) and elastic modulus (B) as a functional of the applied voltage before and after HT, Frictional coefficient as a function on sliding distance for the PEO samples before(A) and after HT(B) [362] 101

Figure 4.1. Schematic diagram of the titanium disc along with its measurements 115

Figure 4.2. Schematic diagram of the PEO experimental device used for the fabrication of microporous oxide coating. 117

Figure 4.3. Schematic representation of the cluster source utilized for the fabrication of metallic nanoparticles and thin plasma polymeric films..... 118

Figure 4.4. Schematic arrangement utilized for the deposition of amorphous hydrocarbon thin films (a-C:H) thin films, plasma activation and plasma etching of as prepared nanocomposite and nanolayered coating. 119

Figure 4.5. Schematic arrangement of the GAS utilized for the fabrication of metallic nanoparticles. 121

Figure 4.6. Schematic representation of the experimental setup (A) used for the fabrication of a-C:H films (B), nanocomposite (C) and nanolayered (D) coatings. 123

Figure 4.7. Schematic representation of XPS physical principle of photoelectron extraction from atom or molecules electronic orbitals (A) and simplified apparatus (B).....	124
Figure 4.8. Schematic representation of XRD principle.	126
Figure 4.9. Principle of WCA measurements.	127
Figure 4.10. Schematic representation of electron beam-surface interactions (A) and simplified SEM setup(B) [3].	129
Figure 4.11. Schematic of surface profilometer and its principle [5].	130
Figure 4.12. Schematic representation of the AFM.	131
Figure 4.13. Schematic of ICP-MS [6].	132
Figure 4.14. Schematic representation of the scratch tester.	134
Figure 5.1. Surface SEM micrographs of Ag-free (Ag0) and Ag-doped (Ag1, Ag2, Ag3) TiO ₂ coatings at 1000x magnification (A) and 10,000x magnification (B) and their corresponding EDS spectra (C).	145
Figure 5.2. SEM-BSE images of the surface of antibacterial coatings (Ag1, Ag2, Ag3) clearly showing the presence of AgNPs (scale bar: 10 μm (A) and 100 nm (B)). The arrows indicate the incorporation of AgNPs inside the coating pores.	146
Figure 5.3. Cross-sectional SEM-BSE images and EDS mapping corresponding to the framed area in the upper SEM-BSE images of the Ag0, Ag1, Ag2 and Ag3 coatings (Scale bar: 5 μm).	147
Figure 5.4. XPS survey spectra of the coatings.	148
Figure 5.5. XPS deconvoluted high resolution O1s peaks of the coatings.	150
Figure 5.6. XRD spectra of untreated Ti, Ag-free and Ag-doped TiO ₂ coatings.	151

Figure 5.7. WCA (A), roughness (B), microhardness (C) of untreated Ti, Ag0, Ag1, Ag2 and Ag3 samples and evolution of the microhardness as a function of loading force for the untreated Ti, Ag0 and Ag3 samples (D).	153
Figure 5.8. Cumulative Ag ⁺ release (ppb) (A) and Ag ⁺ release rate (ppb/day)(B) when immersed in water up to 7 days for Ag1, Ag2 and Ag3 samples.....	155
Figure 5.9. Number of CFU (A) and metabolic activity (B) after 24 hours of incubation with different samples. The data are expressed as mean ± SD of 4 independent experiments (n=4). Asterisk (*) denotes significant difference at p<0.05 compared to the control sample (untreated Ti).	157
Figure 6.1. Current density characteristics of PEO-treated Ti discs at varying silver concentrations (Ag0, Ag1, Ag2, Ag3).	164
Figure 6.2. Surface SEM micrographs of Ag-free (Ag0) and Ag-doped (Ag1, Ag2, Ag3) TiO ₂ coatings at (Scale bar: 10 μm) (A) and (Scale bar: 5 μm) (B).....	165
Figure 6.3. Cross-sectional SEM-BSE images of Ag-free (Ag0) and Ag-doped (Ag1, Ag2, Ag3) TiO ₂ coatings (Scale bar: 5 μm).	166
Figure 6.4. Cross-sectional SEM-BSE images and EDS mapping corresponding to the framed area in the upper SEM-BSE images of Ag-free (Ag0) and Ag-doped (Ag1, Ag2, Ag3) TiO ₂ coatings (Scale bar: 5 μm).	166
Figure 6.5. XPS survey spectra of the coatings (A), deconvoluted high-resolution Ti2p (B), Ag3d (C), O1s (D), P2p (E) and Ca2p (F) peaks of the Ag3 coating.....	169
Figure 6.6. XRD spectra of the Ag-doped TiO ₂ coatings.	170
Figure 6.7. Roughness (A), WCA (B) and microhardness (C) of untreated Ti, Ag0, Ag1, Ag2 and Ag3 samples.	172

Figure 6.8. Coefficient of friction of untreated and PEO-treated Ti discs evaluated by a pin-on-disc scratch tester at varying loads.	173
Figure 6.9 Cumulative Ag ⁺ release (ppb) (a) and Ag ⁺ release rate (ppb/day) when immersed in water up to 7 days for Ag1, Ag2 and Ag3 samples.	175
Figure 6.10. Number of CFU after 24 hours of incubation for different samples. Asterisk (*) denotes a significance difference at $P < 0.05$ compared to the control sample (untreated Ti).	177
Figure 6.11. SEM images of MRSA strain cultured on uncoated and coated Ti samples (scale bar: 5 μm , insert : 1 μm).	178
Figure 6.12. SDS-PAGE analysis of FBS and BSA proteins for different Ti samples under study: (A) gel image of one of the triplicate measurements showing the protein bands (A) and percentage of the intensity of the FBS/BSA bands calculated from the gel images using ImageJ (B).	180
Figure 6.13. Fluorescent images of Ti samples after incubation in FITC-labelled albumin for 1 hour.	181
Figure 6.14. Fluorescence and SEM images of MC3T3 cells cultured on uncoated and coated Ti samples 1 day after cell seeding (scale bar: 100 μm (1 st column), 10 μm (2 nd column) and 500 μm (3 rd column)).	182
Figure 6.15. Fluorescent and SEM images of MC3T3 cells cultured on uncoated and coated Ti samples 7 days after cell seeding (scale bar: 100 μm (1 st column), 10 μm (2 nd column) and 500 μm (3 rd column)).	185
Figure 6.16. Cell viability results 1 day and 7 days after cell seeding on different titanium samples. Asterisk (*) denotes a significant difference at $P < 0.05$	186
Figure 7.1. Histogram of the diameter of the AgNPs (A) and evolution of the number of deposited AgNPs and their size as a function of DC magnetron current(B). The deposition time was fixed at 2.5 mins...	194

Figure 7.2. UV-vis spectra of Ag monolayer films for different applied DC magnetron currents (A) and UV-Vis spectra recorded at different positions on the sample (magnetron current: 500 mA) (B). 195

Figure 7.3. Deconvoluted high resolution C1s spectra measured on an a-C:H coating (A) and on Ag/a-C:H nanocomposites prepared at a DC magnetron current of 200 mA (B) and 500 mA (C). 197

Figure 7.4. AFM images of the a-C:H coating and different Ag/a-C:H nanocomposite coatings. 198

Figure 7.5. R_a and WCA values of the a-C:H coating and Ag/a-C:H films (a) and photography of the Ag/a-C:H coating (500 mA) after the scratch test (b). 199

Figure 7.6. Cumulative silver ion release of the Ag/a-C:H nanocomposite coatings as a function of water immersion time. 201

Figure 7.7. SEM images of Ag/a-C:H nanocomposite coatings deposited at 500 mA before and after 7 days of immersion in water and PBS: comparison of SEM images acquired in secondary electron (SE) and backscattered electron (BE) imaging modes (scale bar = 100 nm) (A) and SE images of Ag/a-C:H coatings acquired at 30° tilt (scale bar = 1 μ m) (B). 202

Figure 7.8. CFU assay of gram negative E. coli (a) and gram positive S. aureus (b) after 6 and 24 hours of incubation. The data are reported as mean \pm SD of 3 independent experiments (n=3). Asterisk (*) represents a significant difference at $P < 0.05$ compared to the control (untreated Ti). 204

Figure 7.9. Fluorescence images of live/dead stained MC3T3 cells 1 and 7 days after cell seeding on a bare Ti substrate and different coated Ti samples (scale bar = 200 μ m). 206

Figure 7.10. Cell viability 1 day and 7 days after cell seeding on different titanium samples. The data are reported as mean \pm SD of 3 independent experiments (n=3). Asterisk (*) represents significant difference at $P < 0.05$ compared to the control sample (untreated Ti). 207

Figure 7.11. SEM images of MC3T3 cells 1 and 7 days after cell seeding on different Ti samples(scale bar = 100 μm).....	208
Figure 8.1. Schematic representation of the produced samples: Cu/a-C:H nanocomposites (A), O ₂ plasma etched Cu/a-C:H nanocomposites(B) and nano-layered a-C:H/Cu/a-C:H film (C).....	215
Figure 8.2. <i>SEM-BSE images of the coated Ti samples (Scale bar: 100 nm)</i>	217
Figure 8.3. High-resolution XPS spectra of the Cu2p peak of uncoated and coated Ti disks.....	219
Figure 8.4. Evolution of the copper surface concentration as a function of water incubation time for the coated Ti samples under study (XPS surface analysis)	221
Figure 8.5. Cumulative Cu ²⁺ release (ppb) (A) and Cu ²⁺ release rate (ppb/day) (B) when immersed in water up to 7 days for Cu/a-C:H, Cu/a-C:H etched, 10 nm and 20 nm barrier samples.....	223
Figure 8.6. CFU assay of gram-negative E. coli (A) and gram-positive S. aureus (B) after 24 hours of incubation. Asterisk (*) denotes significant difference at P<0.05 compared to control (untreated Ti).226	
Figure 8.7. CFU assay of gram-negative E. coli (A) and gram-positive S. aureus (B) after pre-incubation (up to 7 days) of coated Ti samples.	227
Figure 8.8. Fluorescence (scale bar : 500 μm & 200 μm) and SEM images (scale bar: 100 μm) of MC3T3 cells 1 day after cell seeding on uncoated and coated Ti samples.....	229
Figure 8.9. Quantification of the cell shape factor 1 day after cell seeding on uncoated and coated Ti disks. Asterisk (*) denotes a significantly different sample (P<0.05).....	230
Figure 8.10. Fluorescence scale bar : (500 μm & 200 μm) and SEM images (scale bar: 100 μm) of MC3T3 cells 7 days after cell seeding on uncoated and coated Ti.	232

Figure 8.11. Cell viability results 1 day and 7 days after cell seeding on different titanium samples. Asterisk (*) denotes a significant difference at $P < 0.05$ compared to the control sample (uncoated Ti). 233

List of Tables

Table 2.1. Mechanical properties of a human bone	26
Table 2.2. Overview of different implants, their functions in body systems.....	29
Table 2.3. Materials used in biomedical application and their	30
Table 2.4. Classification of titanium and titanium based alloys	32
Table 2.5. Comparison of the mechanical properties of natural bone with magnesium implants [84].....	34
Table 2.6. Different types of CVD	50
Table 3.1. Summary of different techniques used to deposit HA coating.....	61
Table 3.2. Overview of literature on HA coating on Ti and its alloys not discussed in the text	68
Table 3.3. Overview of literature on BG coating on Ti and its alloys not discussed in the text	78
Table 3.4. Overview of literature on antibiotics loaded coating on Ti and its alloys not discussed in the text.....	82
Table 3.5. Overview of literature on non-antibiotics organic antibacterial agents loaded on Ti and its alloys not discussed in the text	86
Table 3.6. Overview of literature on Ag doped coatings on Ti and its alloys not discussed in the text.	93
Table 3.7. Overview of literature on titanium dioxide (TiO ₂) coating on Ti and its alloys with improved tribological properties not discussed in the text.....	101

Table 3.8. Overview of literature on titanium nitride (Ti-N) coating on Ti and its alloys not discussed in the text	104
Table 3.9. Overview of literature on diamond like carbon (DLC) coating on Ti and its alloys not discussed in the text	110
Table 4.1. Results of EDX analysis of the titanium disc (wt%).....	Error!
Bookmark not defined.	
Table 5.1. Experimental methods	143
Table 5.2. Elemental composition of Ag-free and Ag-doped TiO ₂ coatings obtained from XPS analysis.....	149
Table 6.1. Experimental methods	162
Table 6.2. Elemental composition of Ag-free and Ag-doped TiO ₂ coatings obtained from XPS analysis.....	168
Table 7.1. Experimental methods	192
Table 7.2. Operational parameters used for the deposition of Ag/a-C:H nanocomposites.	193
Table 7.3. Surface elemental composition of Ag free and Ag incorporated a-C:H films.	197
Table 8.1. Experimental methods	214
Table 8.2. Operational parameters used for the deposition of Cu/a-C:H nanocomposites and nano-layered a-C:H/Cu/a-C:H coatings.....	215
Table 8.3. R _a roughness, water contact angles and elemental surface composition of coated Ti disks.	218

List of Abbreviations and Acronyms

A

AA: Acetic acid
AACVD: Aerosol assisted chemical vapor deposition
Aam: Allylamine
a-C:H: Amorphous hydrocarbon
AC: Acetone
AFM: Atomic force microscopy
AgNPs: Silver nanoparticles
ALP: Alkaline phosphatase
APCVD: Atmospheric pressure chemical vapor deposition
Ar: Argon

B

BE: Backscattered electrons
BG: Bioactive glass
BSA: Bovine serum albumin

C

CaCO₃: Calcium carbonate
CAE: Cathodic arc evaporation
CCP: Capacitively coupled plasma
CF₄: Tetrafluoromethane
C₂H₂: Ethylene
COOH: Carboxylic group
CO₂: Carbon dioxide
Cps: Counts per second
CW: Continuous wave

D

DC: Direct current
DLC: Diamond like coating
DLICVD: Direct liquid injection chemical vapor deposition
DTA: Diethylnetriamine

E

ECM: Extracellular matrix
EC: Endothelial

EDS: Energy dispersive X-ray spectroscopy

eV: Electron volt

E_b: Binding energy

F

FA: Formic acid

FBS: Fetal bovine serum

FC: Fluorocarbon

FWHM: Full width at half maximum

H

HAc: Hyaluronic acid

HA: Hydroxyapatite

He: Helium

HFFs: Human foreskin fibroblasts

hMSCs: Human mesenchymal stem cells

H&E: Hematoxylin-Eosin

H₂SO₄: Sulphuric acid

HMDSO: Hexamethyldisiloxane

I

ICP-MS: Inductively coupled plasma mass spectroscopy

L

LC-MS: Liquid chromatography coupled with mass spectroscopy

LPPECVD: Low pressure plasma enhanced chemical vapor deposition

M

MC3T3: Mouse calvaria cells

MEFs: Mouse embryonic fibroblasts

MEO: Micro-arc electrolytic oxidation

mESCs: Mouse embryonic stem cells

MSCs: Human mesenchymal stromal cells

MS: Mass spectrometry

MS: Magnetron sputtering

MTT: ((3-[4,5-dimethylthiazol-2-yl]-2,5-diphenyltetrazolium bromide)

Mn: Molecular weight

MW: Microwave

N

NaOH: Sodium hydroxide

N₂: Nitrogen

NMP: 1-methyl-2-pyrrolidone

NO; Nitric oxide

NTP: Non-thermal plasma

O

O₂: Oxygen

OES: Optical emission spectroscopy

P

PA: Plasma activation

PA: Peptide-amphiphile

PA: Polyacrylamide gel

PBS: Phosphate buffered saline

PCL; Poly- ϵ -caprolactone

PDLA: Poly-DL-lactic acid

PEO: Polyethylene oxide

PES: Polyethersulphone

PET; Polyethylene terephthalate

PGA; Polyglycolic acid

PHBV: Poly(hydroxybutyrate-co-hydroxyvalerate)

PLLA: Poly-L-lactic acid

PLA: Polylactic acid

PLGA: Poly(lactic-co-glycolic acid)

pMSCs: Porcine mesenchymal stem cells

PTFE: Polytetrafluoroethylene

PP: Plasma polymerization

PPT: 1-propanethiol

PPF: Plasma polymer film

PS: Polystyrene

PECVD: Plasma enhanced chemical vapor deposition

PEPVD: Plasma enhanced physical vapor deposition

PIID: Plasma immersion ion implantation

PPAA: Plasma polymer of acrylic acid

R

RF: Radio frequency

RGD: Tripeptide arginine-glycine-aspartate

RMS: Root mean square

ROS: Reaction oxygen species

RPECVD: Remote plasma enhanced chemical vapor deposition

S

Saos-2: Human primary osteosarcoma cells
Scm: Standard cubic centimetre per minute
SDS-PAGE: Sodium dodecyl sulphate polyacrylamide gel electrophoresis
SEM: Scanning electron microscopy
SE: Secondary electrons
SF6: Sulphur hexafluoride
SF: Silk fibroin
SS: Stainless steel

T

TCPS: Tissue culture polystyrene
TE: Tissue engineering
TEM: Transmission electron microscopy
TiO₂: Titanium dioxide
TNF: Tumor necrosis factor

U

UHV: Ultra high vacuum
UHVCVD: Ultra high vacuum chemical vapor deposition
UPLC: Ultra performance liquid chromatography
USSCs; Unrestricted somatic stem cells
UV: Ultraviolet

V

VECs: Vascular endothelial cells

W

WCA: Water contact angle

X

XPS: X-ray photoelectron spectroscopy
XRD: X-ray diffraction

List of Publications

A.1 International journal publications

1. **Thukkaram M.**, Vaidulych M., Kylian O., Rigole P., Aliakbarshirazi S., Asadian M., Nikiforov A., Biederman H., Coenye T., Du Laing G., Morent R., Van Tongel A., De Wilde L., Verbeken K., De Geyter N.
“Biological activity and antimicrobial property of Cu/aC:H nanocomposites and nanolayered coatings on titanium substrates”
Material Science and Engineering C, 2020,
IF 2019: 5.88, Q1
2. **Thukkaram M.**, Coryn R., Asadian M., Tabaei PSE., Rigole P., Rajendhran N., Nikiforov A., Sukumaran J., Coenye T., Van der Voort P., Du Laing G., Morent R., Van Tongel A., De Wilde L., De Baets P., Verbeken K., De Geyter N.
“Fabrication of microporous coatings on titanium implants with improved mechanical, antibacterial, and cell-interactive properties”
ACS Applied Materials & Interfaces, 2020, 10 (27), pp 30155-30169.
IF 2019: 8.75, Q1
3. **Thukkaram M.**, Vaidulych M., Kylian O., Hanus J., Rigole P., Aliakbarshirazi S., Asadian M., Nikiforov A., Biederman H., Coenye T., Du Laing G., Morent R., Van Tongel A., De Wilde L., Verbeken K., De Geyter N.
“Investigation of Ag/a-C:H nanocomposite coatings on titanium for orthopedic applications”
ACS Applied Materials & Interfaces, 2020, 12 (21), pp 23655-23666.
IF 2019: 8.75, Q1
4. **Thukkaram M.**, Cools P., Nikiforov A., Rigole P., Coenye T., Van der Voort P., Du Laing G., Vercruyssen C., Declercq H., Morent R., De Wilde L., De Baets P., Verbeken K., De Geyter N.
“Antibacterial activity of a porous silver doped TiO₂ coating on titanium substrates synthesized by plasma electrolytic oxidation”
Applied Surface Science, 2020, 500, pp 144235.
IF 2019: 6.1, Q1

5. Tabaei PSE., Asadian M., Ghobeira R., Cools P., **Thukkaram M.**, Derakhshadeh PG., Abednatanzi S., Van der Voort P., Verbeken K., Vercruyssen C., Declercq H., Morent R., De Geyter N.
“*Combinatorial effects of coral addition and plasma treatment on the properties of chitosan/polyethylene oxide nanofibers intended for bone tissue engineering*”
Carbohydrates Polymers, 2020, 117211.
IF 2019: 7.182, Q1

6. Sivan M., Madheswaran D., Asadian M., Cools P., **Thukkaram M.**, Van der Voort P., Morent R., De Geyter N., Lukas D.
“*Plasma treatment effects on bulk properties of polycaprolactone nanofibrous mats fabricated by uncommon AC electrospinning: A comparative study*”
Surface & coatings technology 2020, 399, pp 126203.
IF 2019: 3.78, Q1

7. Asadian M., Onyschenko I., **Thukkaram M.**, Tabaei PSE., Van Guyse J., Cools P., Declercq H., Hoogenboom R., Morent R., De Geyter N.
“*Effects of dielectric barrier discharge (DBD) treatment on chitosan/polyethylene oxide nanofibers and their cellular interactions*”
Carbohydrate Polymers, 2018, 201, pp 402-415.
IF 2019: 7.18, Q1

8. Aziz G., **Thukkaram M.**, Morent R., De Geyter N.
“*Plasma parameters effects on the properties, ageing and stability behaviors of allylamine plasma coated ultra-high weight polyethylene(UHMWPE) films*”
Applied Surface Science, 2017, 409, pp 381-395.
IF 2019: 6.1, Q1

B.2 Book chapter

1. Cools P., Astoreca L., Tabaei PSE., **Thukkaram M.**, De Smet H., Morent R., De Geyter N.
Book title: Surface treatment of polymers by plasma
Editor: Pinson. J., Thiry. D.
Publ: Wiley, New Jersey, USA (2019)

C.1 Publication in conference

1. **Thukkaram M.**, Cools P., Nikiforov A., Rigole P., Coenye T., Morent R., De Wilde L., Verbeken K., De Geyter N.

“Antibacterial activity TiO₂ coating on titanium substrates by plasma electrolytic oxidation”

Oral presentation

Conference on Cold Plasma Sources and Applications (COPSA), Ypres, Belgium (2018)

C.4 Active Conference participations

1. **Thukkaram M.**, Vaidulych M., Kylian O., Biederman H., Morent R., De Wilde L., Verbeken K., De Geyter N.

“Deposition of antibacterial Ag/a-C:H nanocomposites on titanium substrates using a gas aggregation cluster source”

Oral presentation

Workshop on Plasma-Based synthesis of Nanomaterials, Prague, Czech Republic (2020)

2. **Thukkaram M.**, Rigole P., Coenye T., Morent R., Verbeken K., De Geyter N.

“Study of antibacterial efficiency of Cu-doped TiO₂ coatings produced by plasma electrolytic oxidation”

Oral presentation

33rd International Conference of Surface Modification Techniques, Naples, Italy (2019)

3. **Thukkaram M.**, Cools P., Kylian O., Morent R., De Geyter N.

“Antimicrobial Ag/a-C:H nanocomposite coated titanium substrates for implant application”

Oral presentation

44th International Conference on Plasma Science, Denver, USA (2018)

Chapter 1. Introduction

1.1 Musculoskeletal disorders and their treatment

The world health organization (WHO) recognizes that musculoskeletal disorders significantly occur across all regions of the world, and these disorders become a widespread human health problem [1]. Musculoskeletal conditions comprise more than 100 diagnoses that affect the locomotor system, such as muscles, bone, joints, tendons, and ligaments [2]. According to the musculoskeletal disease data released by the United States, nearly half of the American population is affected by musculoskeletal diseases such as osteoporosis, arthritis, bone fracture, hip, knee, foot, and ankle fractures as well as trauma due to sports or injuries. Due to the aging population and increase in life expectancy, the number of patients is expected to double by 2030.. In 2015, more than 9 million knee-replacement surgeries were performed in the United States, and this trend is progressing until now and is even expected to further increase in the future [3]. Using bone fractures and osteoporosis as typical examples as they account for 16% (6.3 million bone fractures) and 18% (8.9 million osteoporotic fracture) of all musculoskeletal injuries worldwide annually [4], it is reported that worldwide 1 in 2 women and 1 in 5 men over the age of 50 are experiencing osteoporotic or bone fractures. According to the osteoporosis data released by the European Union, the number of new fractures in 2015 is 3.5 million comprising approximately 620,000 hip fractures, 520,000 knee fractures, 560,000 forearm fractures, and 180,000 other fractures. The number of deaths related to fractures in the EU was found to be 43000 in the year 2015 [5]. Therefore, the orthopedic and biomedical implants industry (hip, knee, shoulder, bone, and cartilage) is one of the fastest-growing industries, worldwide [6]. In a market analysis report provided by the research group Lucintel, it is stated that the global orthopedic device industry is expected to reach an estimated 62.6 billion dollars by 2022 and is forecasted to grow at a rate of 5.5 % from 2017 to 2022 [7]. In the US alone, more than 100 billion dollars is spent each year on health care for musculoskeletal disorders, resulting in more than 100 million patient visits [8].

As bone is a highly dynamic tissue, it can undergo the processes of remodeling and self-repairing to accommodate changing mechanical stress and fatigue fractures [9]. However, the bone cannot reset properly when the bone tissue is affected by a disease, trauma or if the

defect is too large. Different strategies using natural and synthetic materials are followed to regain the bone function. Autografts, allografts, and xenografts use natural materials, while artificial substitution and autologous implantation are based on synthetic materials. Out of these methods, autografts are preferred as the grafts originate from other body parts of the same patient. As these materials already contain patient's bone growing cells and proteins, they do not have any risk of disease transmission. However, autografts are restricted due to the limited amount of bone that can be taken from the patient's body and the intensive surgical interventions. The use of allografts and xenografts is a potential alternative to autografts as bone is taken from another person or an animal. However, these autografts have a high risk of immunogenic response and possible transfer of diseases.

1.1.1 History of artificial implantation

The history of artificial implants dates back to the ancient Egyptian times during which the concept of bioactivity was not known [10]. Therefore, surgeons used synthetic materials such as wood, bamboo and animal bone as implant materials, which undoubtedly resulted in the failure of the implant and more often even led to the death of the patient. It was also during this period that prostheses such as wooden legs, iron hands, and artificial feet were used. It was only in the 18th century that a plaster cast made of plaster of Paris was used in orthopedics due to the accidental discovery of soda lime. Implants made of soda lime were the first biocompatible implants, and after that, they were replaced by metal alloys as the latter exhibited better mechanical properties as an implant material [11]. The first textbook to deal with osteosynthesis was published in 1870 by J.B Berenger- Feraud, chief naval physician who summarized literature of more than 400 cases of fractures that were operated on. He used lead wires to surgically fix fractures, a technique known as "la synthesisation", the precursor of osteosynthesis. Later in the 1886, Carl Hansmann proposed an high performance fracture fixation plate. Following that, in 1890, orthopedic surgeon Thomas Gluck described ivory ball joints that could be used as joint replacement implants. At the beginning of the twentieth century, plate osteosynthesis started spreading in Europe, mainly due to William Arbuthnot Lane and Albin Lambotte. Albin Lambotte

(father of external fixation) used plates for the fixation of fractures of the distal humerus, distal femur, proximal tibia and the mandible. He developed plates in aluminum, steel, silver, copper and self – absorbable magnesium fixation plates[12]. The design of the Lambotte fixator was highly sophisticated and was very similar to the current tubular fixator. The screws were self-threading and self-tapping and the clamps provided the fixator with different degrees of freedom. Later, after the 2nd world war when an orthopedic surgeon named Martin Kirschner tried to improve the methods of fracture fixation using wires and pins. After comprehensive research, a new generation of implant materials and orthosis was developed for the treatment of arthritis and complicated bone fractures. In the post-war era, significant progress was also made in the development of external fixation when an amateur carpenter designed his own external fixator. After modification by different surgeons, the external fixator became the most popular device in traumatology due to its straightforward application. In 1960, a more modern total hip replacement was initiated by John Charnley, which laid the foundation of most designs that we have today [13,14]. Since then, significant progress has been made concerning material choice and design optimization.

In the field of metallic implants, titanium is referred to as “wonder metal” since Kroll’s innovative process development in 1936, which made this material a commercial possibility [15]. Titanium was first applied in medical devices after world war II and since then titanium and its alloys have been widely used as hard tissue replacements in load-bearing applications such as in artificial joints, bones and dental implants due to its superior mechanical properties and excellent biocompatibility. Artificial hip joints consisting of an articulating bearing (femoral head & cup) and stem, artificial knee joints consisting of a femoral, patella and tibial component and artificial elbow joints consisting of a humeral, ulnar and radial component are the most common applications of titanium and its alloys (**Figure 1.1**). These artificial joints must be able to reproduce the joint’s natural movement and should provide secure positioning with the other joint component. Implant materials made of titanium are also used for osteosynthesis applications such as bone fracture fixation devices, bone plates, bone screws and internal/external fixators (**Figure 1.2**). Though an increasing number of progress has been made in the field of

biomaterials, long term studies have reported that the rate of premature failure of implants and the associated revision surgery are critically high. Using total hip replacement surgery as an example, it was reported that up to 30 % of the patients require revision surgery within a period of 10 years [15,16]. Among the different causes for implant failure, the two factors that are considered prominent are infections and implant wear/loosening, which account for 70% of the failures. For instance, Postler et al. [17] assessed the underlying causes leading to revision surgery in total knee arthroplasty (TKA) in tertiary care hospitals between 2010 and 2015. The study reported that infection and implant loosening are the two most common reasons for revision (early and late revision) and re-revision of TKA (**Figure 1.3**). Similarly, Mehdi Jafari et al. [18] revealed that infection is the most common cause of revision of hip arthroplasty, which accounts for 30 % of the cases among the considered 256 failed hip replacements (**Figure 1.4**).

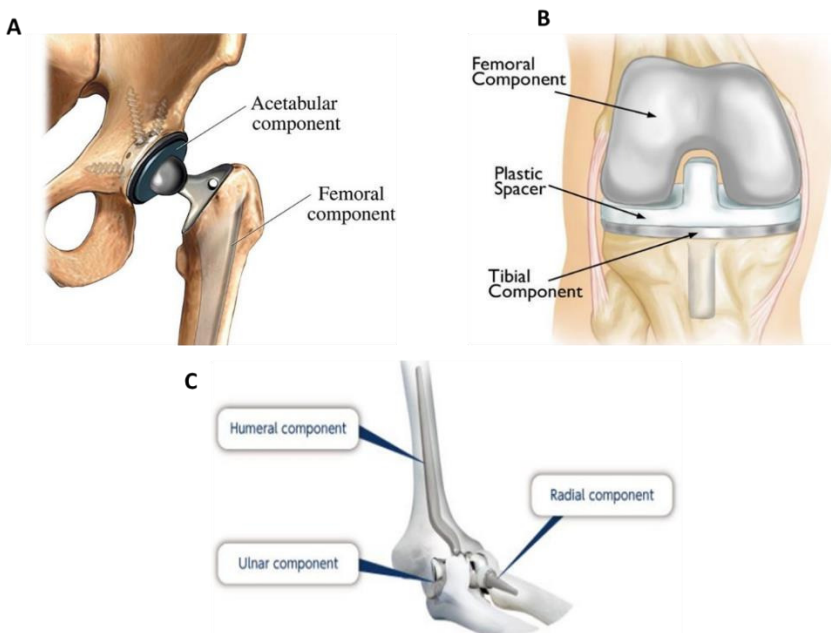


Figure 1.1. Titanium hip joint (A), knee joint (B) and elbow joint (C)



Figure 1.2. Titanium plates and screws

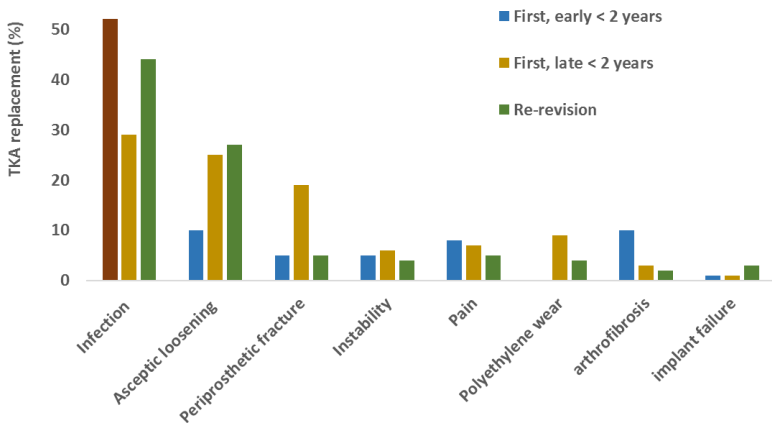


Figure 1.3. TKA revision causes during first early revision, first late revision and re-revision [17]

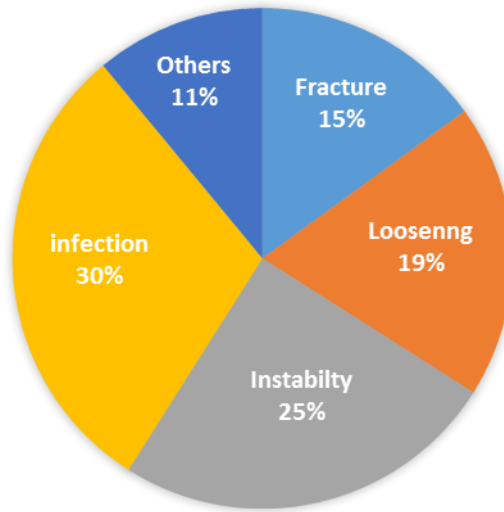


Figure 1.4. Pie chart representing the rate of different failure mechanisms following hip arthroplasty revision [18]

1.1.2 Infection

The occurrence of bacterial infection is a widely occurring problem often leading to implant failure. In case of early revision surgeries which occur within the first five years after the primary surgery, bacterial infection is even the main reason for implant revision [18]. The risk of bacterial infection is high, especially for fracture fixation devices (bone plates, wires, pins and rods) where open fractured bones are involved [19,20]. Once an infection settles, it is a challenging task to treat it, and, more often than not, the infection leads to premature implant removal. In more severe cases, the infection can expand to the surrounding tissues or bloodstream, which in turn results in multiple surgeries, and could in the worst case lead to amputation or mortality. Implant associated infections are the result of bacterial adhesion to an implant surface and subsequent biofilm formation at the implantation site. The biofilm formation takes place in several stages, starting with rapid surface attachment, followed by multi-layered bacterial proliferation and intracellular adhesion in an extracellular polysaccharide matrix. Due to the presence of biofilms, a chronic inflammatory response may develop at the infection site, as treatment

with antibiotics is often unsuccessful in removing the biofilm-associated bacteria [21–23]. Therefore, understanding the bacterial routes of infection and the physico-chemical factors that influence the bacterial adhesion on to an implant surface is essential to develop an antibacterial coating that can provide a long term antibacterial effect.

1.1.3 Implant loosening

There are many reasons for the occurrence of implant loosening such as inadequate implant fixation, mechanical/biological loss of fixation, and generation of wear debris. However, one prominent factor that triggers implant loosening is considered to be particle accumulation or failure in osseointegration [24]. As the surface properties of an implant material are different from those of natural bone, excessive wear takes place due to the mismatch between the bone and implant material properties. These particles invoke a subtle inflammatory response, which becomes more prominent as the particles accumulate over time, thus resulting in tissue toxification. This consequently increases the wear rate of the implant and the adjacent bone, which ultimately results in implant failure [24,25]. Evidently, studies have reported that particulate debris and particle composition are crucial factors in the osteolytic process. Therefore, researchers are investigating and evaluating alternative weight-bearing surfaces to determine optimal implant materials that can minimize particle generation over time. The use of ceramics, highly cross-linked polymers, and metal-on-metal articulations has been found to lead to a reduction in the production of wear particles. Consequently, osseointegrated implants have more resistance to implant loosening than non-osseointegrated implants [19].

1.1.4 Strategies to prevent implant failure

The underlying cause of implant failure and the lowered success rate for the treatment of patients suffering from musculoskeletal disorders is due to the improper surface characteristics of the implant material. To address this issue, extensive research has been performed to improve the mechanical and biological properties of an implant material beyond its natural capability. Unfortunately, fabricating a new material with appropriate bulk and surface properties is up to this date impossible. Therefore, research on this subject is focused on modifying the surface of existing materials. From a historical point of

view, mechanical or chemical treatment of Ti surfaces are the standards used in industry today. However, these processes are considered to be time-consuming and often result in low treatment efficiencies. Moreover, these strategies have failed to prevent implant-associated infections, a dominant cause of implant failure. Therefore, researchers are now more focusing on loading therapeutic agents onto the implant material to improve the biological performance of the material. For example, organic therapeutic agents such as chlorhexidine, collagen, chloroxylenol and poly (hexamethylenebiguanide) [26–29], inorganic antibacterial metallic nanoparticles (NPs) like Ag [30–32], Cu [33–35] and Zn [36–38] and other bioactive enzymes and proteins have been incorporated onto the implant surface to improve its biological performance. Among these therapeutic agents, anti-bacterial metallic NPs such as Ag and Cu NPs have attracted large attention due to their larger surface area to volume ratio, their wide therapeutic window, their good stability, their low risk of producing bacterial resistant strains and their comparatively low toxicity to human cells [39,40]. Because of these excellent properties, these NPs have been incorporated into the surfaces of various medical devices such as fracture fixation devices, heart valve orthesis, devices, catheters, orthopedic implants, and dental implants [41–43]. *In-vitro* studies have demonstrated excellent biocompatibility of silver deposited stainless-steel coatings without any cytotoxic effect [44], while *in-vivo* studies have indicated that Ag ion containing cobalt-chromium coatings have no local or systemic side effects [45]. Also, both *in-vitro* and *in-vivo* studies have demonstrated that a sustained release of trace amounts of Cu ions could promote osteogenesis [46–49]. In contrast, other studies have also reported that a high release of silver, copper and zinc causes cytotoxicity in various cell lines in a dose-dependent manner [37,50]. For instance, a high amount of silver was observed in the blood samples of patients treated with silver-coated implants since most of the incorporated silver was not immobilized in the coating, enabling silver to freely circulate through the blood stream [51]. Consequently, the issue of regulating the antibacterial agent release has been a substantial concern as the burst release of antibacterial agents from the coatings can have cytotoxic effects [44]. In addition, the majority of the coatings investigated so far are soft and have a low resistance to wear or abrasion and are thus not suitable as coatings of bone implants [52–

54]. Hence, these coatings can be easily damaged or delaminated from the implant surface which may in turn also lead to implant loosening. To address these issues, a coating strategy is needed which can lead to the deposition of a hard and stable coating and which can regulate the release of therapeutic agents while maintaining normal biological functions as the success of an implant therapy lies in achieving both functionalities: an improved antibacterial effect and favorable cellular interactions. In this PhD dissertation, we will, therefore, focus on fabricating such a bifunctional coating using plasma-based surface modification techniques.

The term “plasma” was first coined by Langmuir in 1929, and is used to describe the fourth state of matter. Plasma is defined as a ionized gas consisting of a mixture of electrons, ions, photons, and neutrals and is commonly produced upon gas excitement. In nature, the occurrence of plasma is quite common, and some examples include the stars, the space between the star systems, the solar wind, lightning, and the Earth’s magnetosphere. In the lab, plasmas are generally produced by supplying an electric field to a gas, which can be done using direct current (DC), radio frequency (RF), or microwave (MW) excitation. An important distinction has to be made between thermal and non-thermal plasmas based on the relative temperature of the electrons, ions, and neutrals. In thermal plasmas, both the electrons and the heavy particles are at the same temperature (up to 10,000 K) and are considered to be in thermal equilibrium. In non-thermal plasmas, only the electrons are excited to higher temperatures while the ions and neutrals stay close to the room temperature creating a temperature difference between light and heavy particles. Thanks to this non-equilibrium in temperature, non-thermal plasmas can be used for the surface modification of biomedical materials. Non-thermal plasma-assisted surface modification has emerged as a unique and versatile method to effectively modify the surface properties of a material without changing the bulk properties. Moreover, this strategy is environmentally friendly and it can lead to the deposition of coatings with a thickness ranging from nano- to micrometre. In addition, it is a highly versatile technique as a wide variety of surface functional groups, bioactive agents and/or antibacterial agents can be incorporated into the coatings. Consequently, non-thermal plasma-assisted surface modification has already been extensively used to

improve the surface properties and the biological performance of implant materials.

1.2 Objective of this thesis:

Acknowledging the literature, it is evident that current designs of coated titanium implant surfaces still lack the optimal combination of properties namely: 1) an antibacterial coating with a controlled release of the antibacterial agent; 2) a surface promoting tissue integration and biocompatibility; 3) a hard coating possessing superior mechanical properties. Therefore, this dissertation is driven by the need to fabricate titanium implant surfaces that can mimic the properties of natural bone to provide implant durability and longevity, while preventing bacterial infections. To achieve this, two different plasma-based surface modification techniques have been used in this dissertation to fabricate hard ceramic and diamond-like composite coatings incorporating antibacterial agents such as silver and copper on medical-grade titanium discs.

The rationale behind choosing the proposed surface modification techniques and the coating strategies is as follows:

- 1) **Controlled release of the antibacterial agent:** Release of antibacterial agents from a coating should not be considered as a universal treatment in preventing implant-associated infections. Instead, they should be considered as only a fundamental need to control the risk of infections as there are still several questions and challenges that must be overcome for any antibacterial coating to become a genuinely useful tool in the fight against implant-associated infections. One critical challenge to overcome is a controlled release of the antibacterial agents from the coating and a long-term stable release. Over the years, a broad range of antibacterial compounds has been developed for release-based coatings, yet, due to the absence of a particular bonding mechanism to the coating, these compounds are often released at a too high rate. Matrix materials acting as a reservoir for the antibacterial agents consisting of polymeric compounds, ceramics, and hydrogels prepared by chemical or heat treatment have been widely studied. However, these matrix materials still lack in controlling the release rate and release stability as the overall

timeframe and release kinetics of the antibacterial agents are greatly application dependent. Therefore, in this dissertation, a carefully chosen matrix material as a reservoir for antibacterial agents is essential to achieve a controlled release of antibacterial agents.

- 2) **Surface promoting tissue integration and biocompatibility:** Even if the fabrication of a coating with a controlled release of antibacterial agents capable of preventing bacterial infection was achieved, it would not be successful unless the developed surface promotes tissue integration. Indeed, as previously mentioned, the success of implant therapy lies in preventing infection and promoting favorable tissue integration. That is, when a foreign material is placed in the body, the first mechanism that takes place is the deposition of a protein layer from the blood and the body fluids onto the surface of the implant. The presence of this film influences the interactions between the material, cells, and the bacteria, and this in turn, will determine who will win the race for colonization of the implant surface. Therefore, it is imperative that successful tissue integration should occur before bacterial adhesion takes place. To achieve this, the chosen coating technique should possess favorable surface properties to promote sufficient tissue integration.
- 3) **Coating with superior mechanical properties:** Implant applications require a sliding contact thereby subjecting the implant material to aggressive environments. Therefore, a coating with adequate antibacterial properties and excellent biocompatibility is still not sufficient to achieve a near-perfect implant material when the material does not have appropriate mechanical and tribological properties. To achieve a higher efficiency and durability under more severe sliding conditions a hard coating is required which can exhibit a low frictional coefficient and low wear rates and hence a longer durability.

Bearing this knowledge in mind, within this dissertation, two different coating strategies have been chosen to address the aforementioned concerns. The first surface modification technique employs plasma electrolytic oxidation (PEO) to deposit hard ceramic-like titanium dioxide (TiO₂) coatings loaded with bioactive agents and antibacterial

agents. This technique is chosen as it can produce porous, adhesive, bioactive coatings, and most importantly, the content of antibacterial and bioactive elements on the PEO treated surfaces can be tuned by controlling the PEO operational parameters. This, in turn, helps to tune the degree of bioactivity and antibacterial efficacy of the produced coatings. Furthermore, using TiO_2 as a reservoir of antibacterial agents facilitates improved biocompatibility and mechanical properties. The second technique employs a cluster source (a combination of magnetron sputtering and plasma-enhanced chemical vapor deposition) to deposit an amorphous hydrocarbon matrix (a diamond-like carbon coating) loaded with antibacterial agents. This technique enables to independently control the properties of the hydrocarbon matrix, the amount of antibacterial agents loaded into the matrix as well as their release rate. Moreover, amorphous hydrocarbon (a-C:H) films are known for their biocompatibility, haemocompatibility, and superior mechanical properties [55–58]. In particular, a-C:H films are currently used in cardiovascular applications for blood-contacting devices such as heart valves, coronary stents, and guide wires [59–61].

1.3 Structural organization of this PhD dissertation

A profound and well-defined step-by-step approach is followed in this dissertation to reach the ultimate goal of fabricating titanium implant surfaces suitable for orthopedic applications. In all phases of this dissertation, a detailed investigation of the physical, biochemical, bio-responsive, and mechanical properties of the fabricated materials is performed to optimize and pave the way towards the development of an optimized implant surface. This PhD dissertation is divided into 4 main sections which are expressed in the following way:

Section 1: Literature review

Chapter 2 provides the description of the nature of bone and its properties followed by a review of bone implant materials, and biomaterials used in implant therapy. The chapter will also give an extensive review of metallic biomaterials used in implant therapy, their properties, their classifications and the problems associated with these materials to understand the basis on which researchers have been focusing to fabricate coatings to improve implant material properties. After that, a short review will be given dealing with surface

modification techniques used to improve the surface properties of implant materials and the theory behind each technique.

Chapter 3 gives an extensive review of the functional coatings or films fabricated on titanium surfaces for orthopedic applications. This chapter is divided into 3 sections based on the properties of the functional coatings: 1) their biocompatible and bioactive properties; 2) their antibacterial properties and 3) their tribological properties. This chapter primarily focuses on the functions of the coatings as well as their influencing factors and a description of their advantages and disadvantages. For the basic knowledge of the techniques mentioned in this chapter, readers can refer to **chapter 2**.

Section 2: Materials and Methods

Chapter 4 is devoted to the materials, methodology and experimental set-ups used in this dissertation. The coating's fabrication methods, plasma-assisted deposition strategies, surface characterization techniques, mechanical tests, *in-vitro* antibacterial tests and cell tests will be described.

Section 3: Experimental results

Chapter 5 studies the effect of PEO treatment in sodium dihydrogen phosphate and sodium hydroxide containing base electrolyte with and without the addition of AgNPs on the surface of commercially pure titanium substrates. AgNPs are chosen as antibacterial agent due to their larger surface to volume ratio, their broad antibacterial spectrum, and the non-toxicity of the active Ag ions to human cells. The influence of the AgNPs concentration in the electrolyte on the properties of the coating such as surface morphology, phase composition, roughness, wettability, microhardness, and silver ion release is examined in detail. Additionally, the *in-vitro* antibacterial activity of the coatings against *E. coli* (Gram-negative bacterium) and *S. aureus* (Gram-positive bacterium) has also been performed to evaluate the antibacterial efficacy of the coatings. In the next experimental chapter (**Chapter 6**), the focus has been shifted to harness the antibacterial properties of Ag⁺ without actually using AgNPs but delivering Ag⁺ from silver acetate present within a suitable matrix. PEO coatings with a bifunctional character (antibacterial ability and osseointegration) have been fabricated for the first time by incorporating antibacterial Ag⁺ ions together with osteoconductive Ca

and P ions on Ti implant surfaces. To do so, a base electrolyte containing calcium acetate monohydrate, sodium dihydrogen phosphate dihydrate with and without the addition of different amounts of silver acetate as supplier of Ag^+ ions is used. A detailed examination has been carried out to elucidate the effect of varying silver content in the electrolyte on the surface physical, chemical, and mechanical properties of the deposited coatings. In addition to this, the dose-dependent effect of silver on the *in-vitro* antibacterial performance, protein interactions, and osteoconductivity of the prepared coatings is also investigated. To conclude, the first two experimental chapters of this dissertation are thus focused on the fabrication of microporous oxide coatings with improved mechanical, antibacterial, and cell-interactive properties.

In the second part of this dissertation (**Chapters 7 and 8**), a cluster technology (a combination of magnetron sputtering and plasma-enhanced chemical vapor deposition) has been employed to deposit an amorphous hydrocarbon (a-C:H) matrix loaded with antibacterial agents such as AgNPs and CuNPs. An a-C:H film is chosen as matrix due to its superior mechanical properties, biocompatibility, and haemocompatibility. In **Chapter 7**, Ag containing a-C:H nanocomposites with varying AgNPs concentration have been simultaneously deposited on Ti substrates. Subsequently, a profound characterization of the surface properties and the biological performance of the coated Ti discs was performed. The obtained results will show that this deposition strategy made it possible to tune the silver content in the nanocomposites independently of the properties of the matrix material. This, in turn, also allows to precisely control the antibacterial efficiency of the produced coatings, which was connected with their ability to release Ag^+ into an aqueous environment. In the final experimental chapter of this dissertation (**Chapter 8**), the potential of using the cluster technique for the fabrication of novel thin a-C:H matrices loaded with CuNPs on titanium discs has been explored as this particular approach was not yet explored before. Thus, **Chapter 8** focuses on the fabrication of different types of Cu/a-C:H coatings with approximately the same amount of embedded CuNPs but with a different arrangement of the NPs inside the a-C:H matrix. The chapter will reveal that different structures of the produced coatings lead to significantly different

release rates of Cu ions from the coatings into aqueous media. The obtained results will also reveal that the release rate of Cu ions is closely connected to the antibacterial efficiency and osteoblast cell viability of the fabricated coatings. To conclude, the last two experimental chapters of this dissertation thus focus on the fabrication of nanoporous composite coatings with improved mechanical, antibacterial, and cell-interactive properties.

Section 4: Conclusion

Chapter 9 gives a general conclusion on the performed work as well as the advantages and disadvantages of the used techniques, and ends with an outlook on future perspectives.

Chapter 2. Role of biomaterials in implant therapy: Challenges, perspectives and opportunities

2.1 Nature of bone overview

Bone is a complex living tissue composed of cells and a mineralized extracellular matrix. It harnesses the energies from various tissues such as osseous tissue, cartilage, connective tissues, epithelium, adipose tissue, and nervous tissue. It contains about 25% organic matrix, 10% water, and the rest are crystallized mineral salts. Bone as a functional organ in the human body protects various organs of the body, provides blood cell production sites, stores minerals, and provides structure and support for the body enabling mobility in human activity.

2.1.1 Bone properties

2.1.1.1 Physicochemical properties

Four types of cells (**Figure 2.1**) are present in bone tissue, such as osteogenic cells, osteoblasts, osteocytes, and osteoclasts, which are responsible for bone formation, resorption, and maintenance. Osteogenic cells undergo cell division and develop into osteoblasts. These osteoblasts are bone-forming cells: they secrete type 1 collagen fibers, which are mineralized and saved in the extracellular matrix as hydroxyapatite (HA). This calcified collagen essentially makes the bone matrix. It consists out of minerals of calcium phosphate and calcium carbonate, which can be thought of as an advanced composite material. The calcium phosphate is responsible for maintaining the bone matrix hardness and resistance to external stress, while collagen holds the bone matrix together, preventing brittleness. In general, the calcium and phosphorous ratio of natural bone ranges between 1.50 and 1.67 depending on the location of the bone. Osteocytes are inactive osteoblasts that are trapped in the bone matrix during the formation. They seem to play a vital role in preventing the brittleness of the bone matrix and also have a significant role in detecting and coordinating bone responses when subjected to shocks. Finally, osteoclasts are huge cells with multiple nuclei that are responsible for bone resorption [62,63]. Thus, bone is actively constructed and remodeled throughout life by the previously mentioned bone cells.

Within any bone, the bone tissue (osseous tissue) is composed of two main structures: cortical bone (compact bone tissue) and cancellous bone (spongy bone tissue), each with different appearance and characteristics.

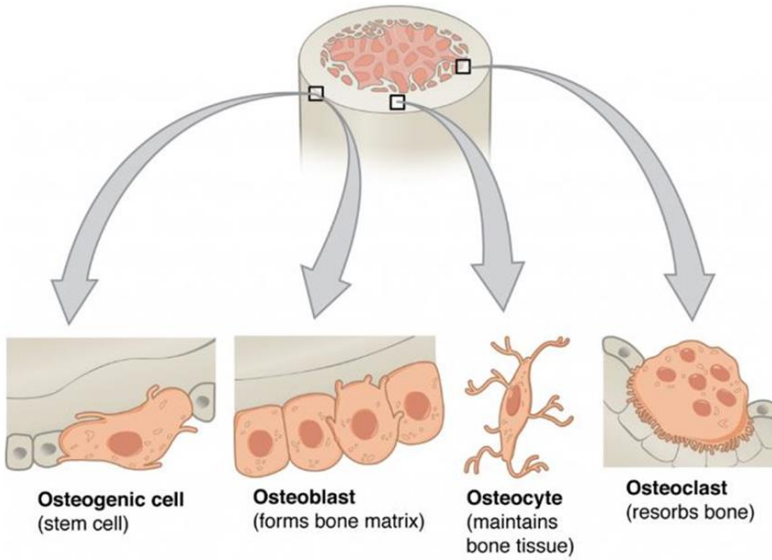


Figure 2.1. Bone cells [64].

Figure 2.2 shows the structure of cortical and trabecular bone. Cortical bone is denser and more durable than cancellous bone, and about 80% of the human skeleton is made of cortical bone. This bone structure support the body's primary function, such as protecting the organs, facilitating movement, and processing chemical elements, mainly calcium and phosphorous.

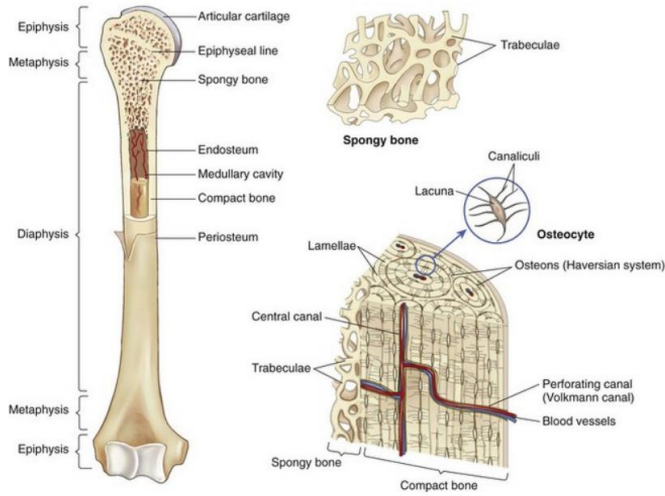


Figure 2.2. Structure of cortical and trabecular bone [65].

Cancellous bone, also known as spongy or trabecular bone, makes up the remaining 20% of the total bone mass. This bone structure is less dense and has a higher surface area than cortical bone, which makes it more flexible.

Bone can be classified into five types based on its shape, such as long, short, flat, irregular, and sesamoid bones. Long bones include the femur, which is the longest bone in the body. These long bones support the weight of the body and assist in mobility. Short bones are present in the wrist and ankle joints, and they provide stability and movement. On the other hand, the function of the flat bones is to protect the internal organs such as the brain, heart, and pelvic organs, and they are mostly present in the skull, thoracic cage, and the pelvis. Irregular bones are irregular in shape as the name implies, and they come in sophisticated shapes that help to protect internal organs. Some bones of the spine, pelvis, and skull are irregular bones. Finally, sesamoid bones are embedded in tendons, and they are mostly found in the tendons of hands, knees, and feet. Their function is to protect tendons from stress and wear and to optimize biomechanical muscular properties [66,67].

2.1.1.2 Mechanical properties

The most important mechanical properties of the human bone are listed in **Table 2.1**. It is however important to mention that the mechanical properties of bone are also characterized by its porosity. The bone structure consists of structures with macro, micro, and nanoscale porosity that have different functions and characteristics. For example, the porosity of the cortical bone is due to a complex network of intracortical canals and spaces, while the porosity of the cancellous bone is due to intertrabecular spaces. The cortical porosity plays a crucial role due to its mechanical properties, its impact on bone materials, and its role in the bone remodeling process [68]. Cortical bone contains multiple levels of porosity to perform different functions such as marrow cavities to provide channels for nutrients to transfer the cortex, vascular porosity to facilitate vascularization and cell migration within the cortex, lacuna-canalicular porosity to contribute to the process of bone modeling and remodeling, and nanoporosity at the level of collagen which acts as a framework for cell and mineral bonding [69]. **Figure 2.3** presents a confocal microscopy image of human cortical bone showing different levels of porosity.

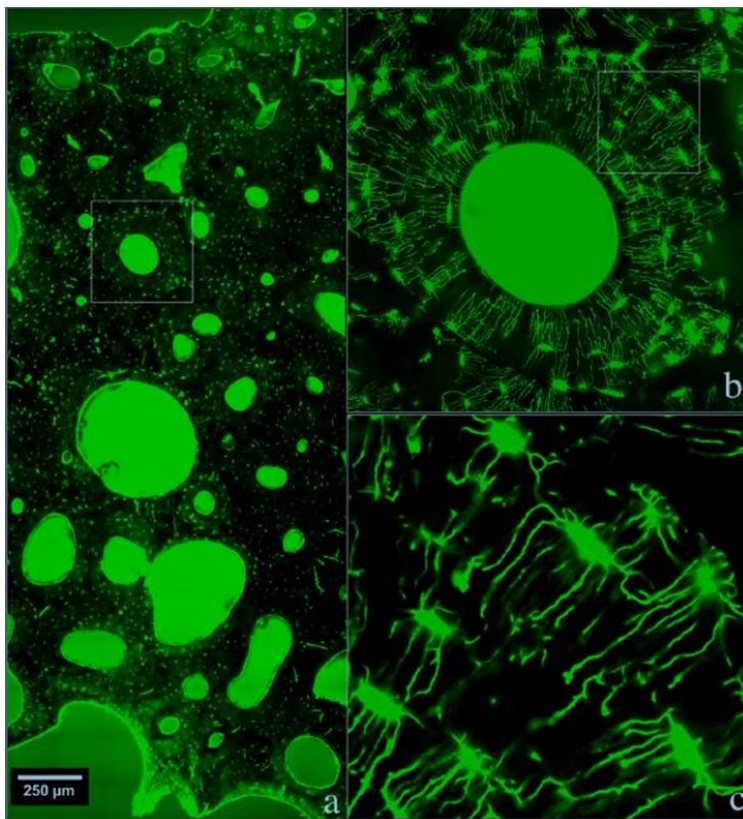


Figure 2.3. Confocal microscopy image of human cortical bone from the femoral shaft: (a) Image showing the entire cortex, (b) network of lacuna-canalicular porosity and (c) detail of the lacuna-canalicular porosity depicting the nutrient arteries[68].

Table 2.1. Mechanical properties of a human haversian canal [70]

Mechanical properties	Human Haversion MPa
Tensile strength	158
Tensile yield stress	128
Compressive strength	213
Compressive yield stress	180
Shear strength	71

2.2 Bone implants: an overview

The history of implants started with the application of bone grafts, which is a surgical procedure to treat bone or joints. Bone grafting is advantageous in fixing problems that are caused by trauma or joints problems. It is also useful for growing bone around an implanted device such as total knee replacement[71]. The bone used in a bone graft can come either from the patient who needs a bone graft or from a donor, or can be constructed from any artificial material. The bone graft accepted by the body can contribute to a new framework where a living bone can grow. The two most common types of bone grafts are autografts and allografts. Autografts use tissues from other parts of the same patient's body, while allografts use tissues from a donor or cadavers that are cleaned and stored in a bone bank. Unfortunately, both methods suffer from severe drawbacks, such as their limited availability, possible rejection of the bone grafts, inflammation, infections at the implant site, reabsorption of the graft, and nerve injuries. To overcome these limitations, artificial grafts are currently widely used, as these lower the risk of disease transmission, reduce the risk of infection, and facilitate the implant availability as several biomaterials can be used. Therefore, the following section will give (1) an overview of the properties of an ideal implant material, (2) a review on the different biomaterials used in bone implant therapy, and (3) a description of some of the current challenges faced in bone implant therapy.

2.2.1 Properties of an ideal bone implant material:

An ideal implant material should mimic the bone properties as much as possible in order to be successful as a bone implant. Hence, the implant material should at least have the following properties:

- Biocompatibility
- Osteoconductivity
- Biomechanical capability

Each of the above mentioned properties will be discussed briefly in the following sections:

2.2.1.1 Biocompatibility:

An essential property of an implant material is to perform its desired function without causing any inflammatory or adverse reaction to the recipient of the therapy and thus to be biocompatible. The biocompatibility of a material is not only dependent on the host response induced by the materials but also by the degradation of the material in the body environment. Heimke et al. [72] classified the biocompatibility of orthopedic implant materials into three categories:

1. Bioactive implants
2. Bio-inert implants
3. Bio-tolerant implants

Bioactive materials are materials which allow bone formation onto their surface with the help of chemical or biological bonding to the surface. Bio-inert materials allow bone formation by direct contact with the material, while bio-tolerant materials are materials that are not rejected when implanted but that are surrounded by fibrous tissue in the form of a capsule. The biocompatibility of the material also depends on the toxicity of the products that are leached from the material and the corrosion resistance of the material. Firstly, cytotoxicity may be caused by substances that are released from the material into the biologic system affecting the cells, organs, or the whole organism. Secondly, biomaterials with weak corrosion resistance may release substances from the surface to the surrounding environment. This may result in bone reabsorption, which in turn affects the adhesion of the implant, and may ultimately result in implant failure.

2.2.1.2 Osteoconductivity

Next to biocompatibility, osteoconductivity is another essential property of a bone implant material. Osteoconductivity is the ability of the implant surface to grow bone on its surface. A successful implant surface should have the ability to induce osteogenesis, an inductive agent that will stimulate undifferentiated pluripotent stem cells to form pre-osteoblasts (bone-forming cells). Another aspect required for the long-term success of an implant is osseointegration. It is the ability to cater to enduring structural and functional coexistence between living bone and the load-bearing implant surface without triggering any rejection mechanisms [73]. Proper integration of implant materials within the bone is essential to ensure the safety and efficacy of the implant throughout its lifetime.

2.2.1.3 Biomechanical capability

When implant materials are intended to be used as bone substitutes, the mechanical properties of these implant materials must match with that of the bone that it replaces to prevent fractures and to provide functional stability. Hardness, compressive strength, tensile strength, and shear strength are most often used to characterize the mechanical behavior of bone substitutes. Other fundamental requirements for an ideal orthopedic biomedical implant include high wear resistance and good fatigue properties if used under cyclic loading

2.3 Biomaterials used in implant therapy

A biomaterial is any synthetic material that interacts with a biological environment. Biomaterials have already been used centuries ago when Mayan culture used natural materials in their primordial dentistry [74]. Later on, metals such as gold, silver, and titanium were used in different parts of the body, including teeth. Recent developments in biomaterials include bioactive and porous materials with improved efficiency to promote new bony tissue ingrowth after implantation. These novel biomaterials can be fabricated from polymers, metals, ceramics, and composites to target specific functionalities. Regardless of their origin, they have to be biocompatible as they will be used in replacing/restoring living tissues such as heart valves, hip replacements, and knee orthosis. Consequently, they are expected to prevent any immune response. Biomaterials can also be biodegradable and bioresorbable in some

cases to be able to disappear from the organism after fulfilling their function. In this context, biomaterials are widely used in drug delivery systems as capsules for carrying drugs towards the target and in regenerative therapy as scaffolds to facilitate the growth of specific tissues [75]. A wide range of biomaterials is used in different implant therapies making it difficult to discuss all available biomaterials in detail. Therefore, a tabular overview of different implants and their functions in body systems is presented in **Table 2.2**. In addition, an overview of biomaterials used in implant therapy and their corresponding properties is also given in **Table 2.3**.

Table 2.2. Overview of different implants, their functions in body systems.

Organs	Examples of implants	Function of implants
Heart	Stents, artificial valves, cardiac pacemakers	Correct functional abnormalities
Bone	Artificial hip joints, knee joints	Replacement of damaged or diseased parts
	Bone fixation (plates, screws, pins)	Assist in healing
Kidney and bladder	Probes, catheters, stents	Aid to diagnosis
Eye	Contact lenses, intraocular lenses	Correct cosmetic problems
Teeth, jaw	Orthodontic wire fillings	Replacement of diseased parts
Ear	Cochlea implants	Replacement of damaged parts

Table 2.3. Materials used in biomedical applications and their main properties and corresponding implant examples.

Material	Properties	Example of implants
Metals: Titanium and alloys (Ti) Magnesium (Mg) Tantalum (Ta) Stainless steel (SS) Cobalt chromium (CC)	<ul style="list-style-type: none"> • Excellent mechanical strength • High corrosion resistance (Ti and Ta) • Ductile • Light weight • Biocompatible (Ti, SS) • Poor osteointegration • Low corrosion resistance (Mg) 	Bone fixation (plates, screws, pins) artificial joints, artificial valves, stents
Polymers: Polyester (PET) Polyethylene (PE) Polymethylmetacrylate (PMMA) Polypropylene (PP), Polytetrafluoroethylene (PTFE)	<ul style="list-style-type: none"> • Biodegradable • Ductile • Light weight • Easy to fabricate • Low mechanical strength • Bio-inert 	Catheters, vascular grafts, heart valves, orthopedic implants, implantable sutures,
Ceramics: Bioglass Hydroxyapatite Oxide coatings	<ul style="list-style-type: none"> • Biodegradable • Bioactive • Strong in compression • Low impact resistance 	Orthopedic implants, ear implants (Bioglass)

2.3.1 Metallic biomaterials overview

As mentioned in chapter 1, metallic implants are commonly used in the orthopedic field, such as bone implants for the treatment of musculoskeletal disorders. In the following section, a brief review of the application of the most important metals as implant materials, their properties, and their limitations will be discussed.

2.3.1.1 Titanium and titanium alloys

The earliest work of titanium as a material for medical, surgical, and dental applications dates back to post-world war II, as during this war titanium manufacturing processes were widely applied for aerospace and military requirements. The four commercially pure titanium (cpTi) grades were the first titanium biomaterials introduced in implantable components and devices. They are classified based on their oxygen content, and due to the minute amount of contaminants present, they possess different mechanical properties. Ti and its alloys have specific properties such as a high corrosion resistance, a high tensile strength, and a high strength to density ratio that enables them to be used as bone substitutes under load-bearing conditions. Another valuable property that makes Ti and its alloys one of the most promising biomaterials for implant therapy is their inherent formation of a secure, adherent thin passivation oxide layer on the top surface which forms naturally in the presence of oxygen. Indeed, these oxide films are responsible for the excellent biocompatibility of Ti and its alloys [76]. Consequently, Ti and its alloys are being successfully used as implant materials as screws, plates, hip and knee prostheses for bone fractures, and bone replacements. Due to the increased application of Ti, new materials, and improved versions of older materials have also been developed to fulfil the needs of specific biomedical applications.

As Ti is an allotropic element, it can exist in more than one crystallographic form. The hexagonal closed packed crystal structure (hcp), also called the alpha (α) phase, exists at room temperature. It transforms into a beta (β) phase or a body-centered cubic (bcc) structure when solid titanium is heated to temperatures above 883°C. These two crystal structures are the basis for naming the three generally accepted classes of titanium alloys: α , ($\alpha + \beta$) and β [74,77]. The properties of these 3 types of titanium alloys are summarized in **Table 2.4**. α stabilizers, β stabilizers, and neutrals are three types of alloying elements. The material characteristics are affected based on the alloying conditions and the choice of the stabilizer. The alloying elements used to stabilize the α phase include aluminum, tin, oxygen, carbon, nitrogen, gallium, and zirconium, while those used to stabilize the β phase include vanadium, molybdenum, tantalum, niobium, chromium, and iron. Many alloys combine a carefully chosen

combination of two types of elements, and these are classified as ($\alpha + \beta$) alloys. Certain alloying elements attract biomedical applications such as tantalum, tin, niobium, and zirconium due to their superior properties such as a high corrosion resistance, non-cytotoxicity, and biocompatibility. Some β and ($\alpha + \beta$) alloys have been extensively studied due to their lower elastic modulus and improved mechanical strength. Ti-6Al-4V, Ti-13Nb-13Zr, and Ti-24Nb are some of the β alloys widely used in bone implant applications. ($\alpha + \beta$) alloys have some advantages over β alloys such as a high tensile strength and fracture toughness [74]. Ti-6Al-4V is a commonly used material in implant applications containing both α and β stabilizers. However, studies have revealed that the release of aluminum and vanadium metal ions can cause harmful effects in the human body. Thus, alloying elements must be carefully chosen to reduce any biologically adverse reactions.

Table 2.4. Classification of titanium and titanium based alloys [78–82].

Alloys	Properties	Example of typical materials
α - type Hexagonal closed packed structure (hcp)	<ul style="list-style-type: none"> • Excellent resistance to plastic deformation • Lower ductility • Excellent creep resistance • Poor osteointegration • Superior weldability • Low to medium tensile strength • Favorable for low and high temperature applications 	cpTi Ti-6Al-2Sn-4Zr-2Mo Ti-8Al-1Mo Ti5Al-2.5Sn
($\alpha + \beta$) type	<ul style="list-style-type: none"> • Contains a mixture of α and β phases • Good mechanical strength • A lower tensile strength • Good creep resistance 	Ti-6Al-4V Ti-6Al-7Nb Ti-5Al-2.5Fe Ti-5Al-3Mo-4Zr

β - type Body centered cubic structure(bcc)	<ul style="list-style-type: none"> • A lower elastic modulus • Good strength and fatigue resistance • Higher ductility 	Ti-8Mo-8V-2Fe-3Al Ti-13V-11Cr-3Al Ti-42Nb Ti-30Ta Ti-50Ta-20Zr Ti-6Al-4V
------------------------------------------------------------	---------------------------------------------------------------------------------------------------------------------------------------------------------	-----------------------------------------------------------------------------------------

2.3.1.2 Magnesium

Magnesium is a well-known mineral in our daily lives as it plays a vital role in the human metabolism. Magnesium is known for its biocompatibility, biodegradability, and its non-toxicity to the human body. Its mechanical properties, such as fracture toughness and elastic modulus, and its density are quite similar to the human bone, making magnesium an attractive candidate for hard tissue applications [83,84]. Studies have reported that porous magnesium has a Young's modulus in the range 4 – 18 GPa, which is close to the Young's modulus of natural bone [85]. Moreover, studies have also reported that the deformation strength of magnesium is within the range of natural bone [86]. **Table 2.5** gives an overview of the mechanical properties of magnesium and natural bone. Despite its favorable properties, magnesium and its alloys are not commonly used as an implant material. This is due to the high corrosion rate of magnesium, which promotes a fast degradation of its mechanical properties, leading to premature failure of magnesium implants. Therefore, various alloying strategies and surface modification techniques have been investigated to improve the corrosion resistance of magnesium.

Table 2.5. Comparison of the mechanical properties of natural bone with magnesium implants [86].

Mechanical properties	Magnesium	Natural bone
Density (g/cm ³)	1.74 - 2.0	1.7 - 2.0
Elastic modulus (MPa)	41 - 45	3 - 20
Tensile strength (MPa)	170 - 270	80 - 150
Compressive yield strength (MPa)	65 - 100	130 - 180
Elongation failure (%)	6 - 20	1 - 7
Fracture toughness (MPa m ^{1/2})	15 - 40	3 - 6

2.3.1.3 Tantalum

Tantalum is another successful metallic material due to its bio performance. Tantalum has an excellent corrosion resistance and biocompatibility, and due to this, it has been widely used in various medical devices such as pacemaker electrodes, spinal implants, shoulder implants, and femoral orthosis [87]. The corrosion resistance and biocompatibility of tantalum is due to the native, stable Ta₂O₅ protective film formed on the implant surface. This native oxide layer facilitates bone ingrowth under *in-vivo* conditions via the development of bone-like apatite, which promotes hard and soft tissue adhesion. Furthermore, tantalum is very hard, ductile, and has an excellent chemical resistance with good apposition to human bone. However, the widespread use of this metal is limited due to its high elastic modulus and low frictional properties compared to the natural bone. To overcome this limitation, porous tantalum was developed and examples of porous tantalum implants are presented in **Figure 2.4**. The introduction of porous tantalum has attracted researchers to further explore its potential in bone tissue applications and porous tantalum was found to exhibit improved osseointegration and to

possess reasonable mechanical properties [88]. Studies have also reported that the geometry of porous tantalum represents a polyhedron with twelve flat faces (dodecahedron), which is similar to the structure of cancellous bone [89]. Due to this, porous tantalum exhibits distinct properties such as an excellent corrosion resistance, bioactivity, a lower elastic modulus, and high frictional properties. These superior mechanical properties of porous tantalum make it an excellent candidate as an orthopedic implant material.

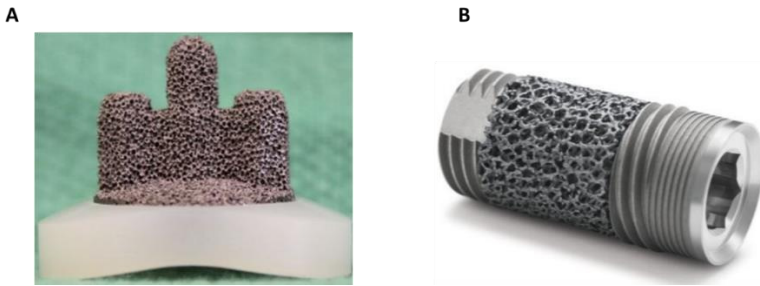


Figure 2.4. Porous tantalum implants: total shoulder arthroplasty (A), a Zimmer dental trabecular implant (B) [90].

2.3.1.4 Stainless steel

Stainless steel that is used as an implant material is classified as conventional stainless steel or nickel(Ni)-free stainless steel. Ni-free stainless steel should not possess any Ni content as it reduces the biocompatibility of the material while increasing the corrosion resistance. Moreover, Ni-containing stainless steel may cause allergies after implantation; therefore, nitrogen is commonly alloyed with stainless steel to reduce the content of Ni in the implant material[91]. Though stainless steel is inferior to titanium in terms of biocompatibility, osseointegration, corrosion resistance, and fatigue resistance, the cost of a titanium implant is relatively high compared to steel. Therefore, in most cases, stainless steel is used for temporary implants such as fixation devices due to its liability to resist to plastic deformation.

2.3.1.5 Cobalt - Chromium

Cobalt (Co)-chromium (Cr) alloys are the second generation implant materials, widely used in artificial knee and hip joints. The wear resistance properties of Co-Cr alloys are higher than for stainless steel and titanium alloys. Moreover, Co-Cr alloys also have a high corrosion resistance in body fluids and possess a high heat resistance. Therefore, high strength cobalt-chromium-molybdenum (Co-Cr-Mo) alloys are predominantly used in hip joints due to the high occurrence of wear in these joints [92]. However, the biocompatibility of Co-Cr is not as optimal as in case of titanium alloys. This is due to the fact that the release of Co, Cr and Ni ions from Co-Cr alloys are reported to cause inflammatory reactions and cytotoxicity. *In-vitro* studies have reported that released Co inhibits the synthesis of type 1 collagen, osteocalcin, and alkaline phosphatase in culture medium and is toxic to osteoblast cell lines. Therefore, various surface modification techniques have been investigated to improve the biocompatibility of Co-Cr alloys [93].

2.4 Problems associated with implant therapy

With the increased need for artificial joints, limbs, and other body part replacements, it is crucial to be aware of the problems associated with implant therapy and to investigate new strategies to overcome these limitations. Hence, the following section gives an extensive review of some of the common problems faced in implant therapy and strategies to overcome them.

2.4.1 Implant - associated infection

Implant surfaces are designed to encourage adhesion of soft and hard tissue, eventually leading to osseointegration. Unfortunately, this phenomenon may also encourage bacterial adhesion. About half a million cases of implant-associated infections are reported in the US associated with indwelling medical devices [94]. The risk of bacterial infection is high, especially for fracture fixation devices where open fractured bones are involved [95,96]. Once an infection settles, it is a challenging task to treat it, and, more often than not, it leads to premature implant removal. In more severe cases, the infection expands to the surrounding tissues or bloodstream, which results in multiple surgeries, and finally, this could lead to amputation or mortality. The common causes of implant-associated infections are the

following microorganisms: *Staphylococci aureus* (*S. aureus*), *Staphylococci epidermidis* (*S. epidermidis*), *Pseudomonas aeruginosa* (*P. aeruginosa*) and *Escherichia coli* (*E. coli*). Staphylococci are gram-positive bacteria, non-motile, non-spore forming anaerobes that grow by aerobic respiration or fermentation, and their size varies from 0.5 to 1.5 μm in diameter. They are characterized by individual cocci, which can divide in more than one plane to form cluster-like structures. *E.coli* are gram-negative bacteria, rod-shaped, non-spore forming anaerobes that grow by aerobic respiration or fermentation and are approximately 0.25 – 1.0 μm in diameter. Many strains of *Staphylococci* and *Escherichia* can produce a biofilm (**Figure 2.5**) and this biofilm formation takes place in several stages, as shown in **Figure 2.6**. It starts with the adhesion of free-floating bacteria on the surface, which undergo cellular proliferation under the right conditions to form clusters in an extracellular polysaccharide matrix and secrete a protective exopolysaccharide layer leading to the formation of a biofilm. Subsequently, the bacteria will detach from this mature biofilm leading to planktonic cells, which can then restart the cycle. Due to the presence of biofilms, a chronic inflammatory response may develop at the infection site, as treatment with antibiotics is often unsuccessful in removing biofilm-associated bacteria [21–23].

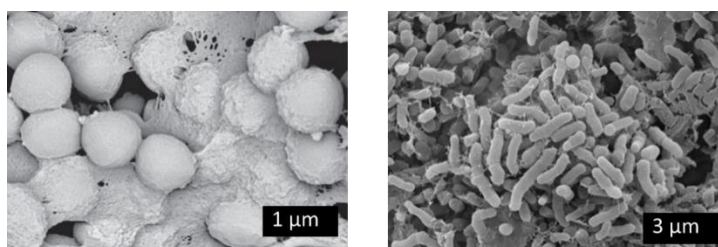


Figure 2.5. SEM image of S.aureus (left) and E.coli (right) biofilm[97].

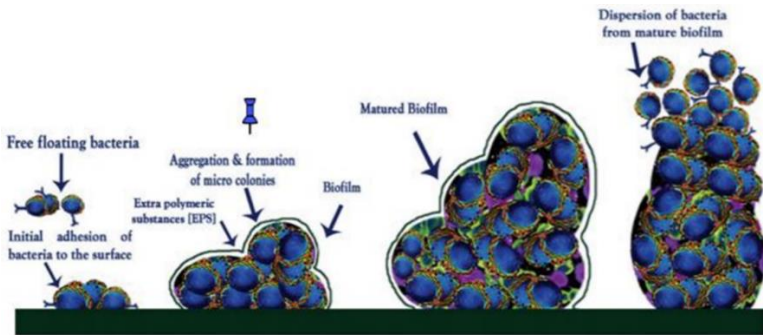


Figure 2.6. Biofilm formation on an implant surface [95].

As stainless steel and Ti are the most commonly used metal implants in load-bearing applications, the rate of bacterial infection is also higher with these implant surfaces. A photograph of an infected external fixation device is presented in **Figure 2.7**. However, studies have reported that stainless steel implants are associated with significantly higher infection rates than Ti-based implants [96,98]. This may be because the Ti surface facilitates improved soft tissue adhesion while a stainless steel implant forms a fibrous capsule enclosing a liquid-filled void. In this non vascularized space, bacteria can quickly spread and proliferate freely [99,100]. Although Ti is known for its biocompatibility, an *in-vitro* study has reported that the adhesion and proliferation of fibroblast cells are inhibited on commercially available Ti alloys [101]. This could cause a potential problem *in-vivo* due to the presence of bacteria. However, no significant differences are observed between the adhesion of *S. aureus* to Ti and stainless steel surfaces [102]. Besides, from various studies [103–107] it is known that once a biofilm is formed on the surface, it could be challenging to treat clinically as these biofilms are strongly protected from phagocytosis and antibiotics. This calls attention to researchers to develop new strategies to prevent initial bacterial adhesion by modifying the implant surface.



Figure 2.7. An infected external fixation device forming skin necrosis[20].

2.4.2 Poor osseointegration

Once an implant material is placed in the body, numerous biological and physico-chemical interactions take place, determining the osseointegrity of the material. Although Ti and its alloys are widely used for orthopedic applications due to their good biocompatibility, they lack in bone-bonding ability. An appropriate adhesion between the bone and the metal surface has still not been observed because of insufficient bone-implant contact and fibrous encapsulation. This may lead to improper biomechanical fixation and loosening of the implants leading to implant failure. Therefore, the need to improve the osseointegration of an implant material with the host tissue is still a crucial topic.

2.4.3 Mechanical failure: wear of metallic implants

Wear is another major factor that limits the long-term clinical performance of an implant. Approximately 1 million joint implants are expected to fail in the US after 10 years of use due to wear. In the case of joint implants, wear debris generated at the bearing surfaces can induce osteolysis resulting in implant loosening [108]. It is useful to divide the wear mechanisms into a number of different categories, such as adhesive, abrasive, corrosion, fretting and fatigue wear [109]. Adhesive wear occurs when the pressure between the sliding surfaces is high enough to cause plastic deformation due to which a segment of an opposing material is ripped away. This may result in pin indentations and scratches along the impacted surface. Abrasive wear

occurs when a hard material passes over a soft surface and creates a groove in the softer material. However, the abrasive grooves can be found on the wear tracks of the sliding friction between similar metal surfaces [110]. This can reduce the surface roughness and hence the rate of wear. Abrasion also removes oxide layers and other protective layers present on the implant surface. Corrosion wear generally occurs when a corrosion product is formed on the metal surface and is eventually removed by mechanical action. Fretting is a combination of adhesive and abrasive wear, where a normal load would cause damage to the surface in the contact region due to small sliding motions between the surfaces [111]. Fatigue wear occurs when a repetitive, cyclic loading on the implant weakens the surface to produce cracks, consequently leading to fragmentation and pitting [112]. A study of metal implants showed that 90% of surface fractures were caused by one of the wear mechanisms mentioned above [113]. A study on a cobalt alloy hip orthosis reported that a fracture of the femur component is due to the corrosion attack and cyclic fatigue loading of the stem [114]. Surgically removed stainless steel hip screw plates were also found to result in significant wear, corrosion, and damage to the surrounding tissue [115]. These observations were also seen in Ti-based bone implants [116]. **Figure 2.8** presents radiographs of mechanically failed implants.

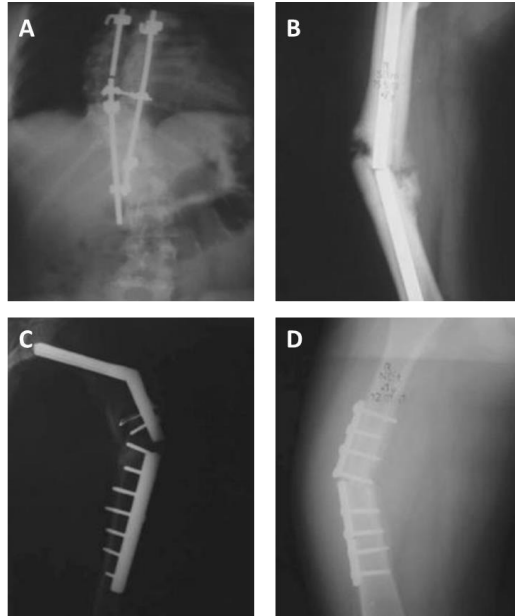


Figure 2.8. Radiographs of failed implants: (A) a spinal rod failure, (B) an intramedullary nail fracture and osteosynthesis failure, (C) subtrochanteric plate (jewet) fracture failure, (D) femur diaphyseal fracture failure of a compression plate [113].

2.5 Surface modification techniques

The underlying cause for the failure of implants is often their improper surface characteristics. To address this issue, extensive research has been performed to modify the surface of an implant material as surface engineering can play an important role in improving the performance of a material such as its biocompatibility, its osseointegration, and its mechanical properties beyond its natural capability. Surface modification is a process to change the composition, microstructure, and/or morphology of the surface while retaining the bulk properties of the material. This section provides an overview of various surface modification techniques relevant for biomedical implant materials.

2.5.1 Thermal spraying

Thermal spraying is a versatile technique that can be applied for a wide variety of materials such as metals, polymers, and ceramics [117,118]. Thermal spraying can be used to coat materials with different melting points and 3D shapes and it is a cost-effective method

offering a high deposition rate. Thermal spray-coated orthopedic and dental implants have been commercially used in the healthcare industry [119]. However, thermal spray coatings in long term implantation have failed due to coating delamination, coating resorption, coating biodegradation and mechanical instability of the coatings [120,121]. Thus, improving the adhesion strength of thermal spray coatings remains a major concern for bone or dental applications. There are several methods of thermal spraying, such as plasma spraying, flame spraying, and cold spraying [121]. The plasma spraying technique has attracted much attention due to the advantages of low cost, high efficiency, and its ability to control coating thickness. Moreover, plasma spraying can produce thick coatings for metallic corrosion protection. The schematic diagram of a plasma spraying equipment is shown in **Figure 2.9**. It can be seen that the system comprises an electrical power source, a gas flow, a cooling water system and a powder feeder.

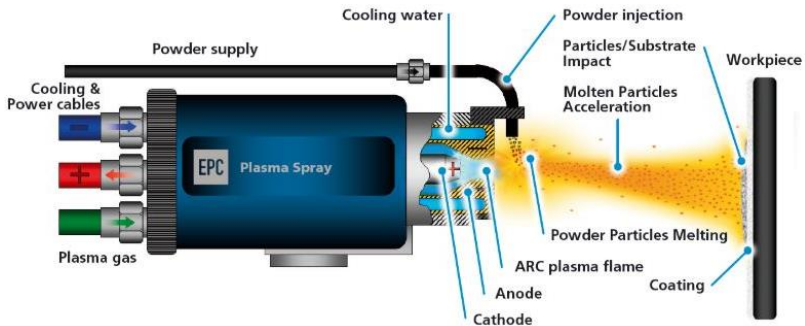


Figure 2.9. Schematic diagram of a plasma spraying device [122].

During plasma spraying, plasma is generated from a high-density arc current in the space between the cathode and anode, which is filled with inert gases. Consequently, ionized gases heat up to a temperature of approximately 15,000°C and expand the nozzle reaching supersonic velocities. Many parameters can be controlled and optimized to produce a high-quality coating such as cathode-nozzle arrangement, gas type, gas mixture, and electric arc settings [122]. Plasma sprayed ceramic coatings provide favorable mechanical properties, and facilitate the growth of bone cells and tissues. Moreover, they improve

bonding strength, hardness, wear, and corrosion resistance [123,124]. In the case of flame spraying, a combustion flame is used to melt a solid precursor. The solid precursor held in a high-pressure chamber propels the material through a small orifice to form a supersonic jet. High-velocity oxygen fuel (HVOF) is another flame spraying technique that employs high spray velocities to form durable bond coatings [125]. Cold spraying is a new member of the thermal spraying technique which uses small particles of size ranging between 1 and 50 μm and employs a supersonic jet of compressed gas to accelerate these particles. Cold spraying provides dense coatings maintaining the material chemistry and phase composition of the original particles [126].

2.5.2 Sol-Gel

Sol-gel technology is a versatile wet-chemical synthesis technology that has been developed to fabricate metal oxides, glassy, and ceramic materials. The sol-gel technique transforms a liquid (sol) into a gel-like network containing both the liquid phase and a solid phase. The details of the sol-gel process are shown in **Figure 2.10** [127] and the steps involved in sol-gel processing are as follows [127,128]:

1. Preparation of a homogenous solution of a liquid precursor in an organic solvent miscible with water/other common reagents.
2. Conversion of the homogeneous solution into a sol, via hydrolysis or polycondensation with a suitable reagent. In this step, molecular-level manipulations are possible like adjustment of the hydrolysis conditions to obtain precisely controlled particle sizes and the addition of dopants to add unique properties to the desired product.
3. Conversion of the sol into a gel, film, powder or a fiber, which takes place via heating, evaporation, precipitation or spinning. This sol-gel conversion can lead to a wide number of applications in catalysis and in the biomedical field.
4. Sintering the gel into ceramic materials with the desired shape.

The advantages of using the sol-gel technique include the ease in controlling the initial and final chemical composition of the raw materials, ease in controlling the thickness of the final material, the ability to coat complex shapes, its cost-effectiveness, and its low

process temperature. Coatings such as TiO₂ and hydroxyapatite prepared by sol-gel are reported to have improved corrosion resistance, as well as an improved cellular response in terms of cell attachment, growth and proliferation [129–131]. However, the coatings suffer at the same time from weak adhesive strength to titanium substrates. Therefore, to improve the adhesion and to optimize the mechanical properties of sol-gel coatings, other coating technologies are currently combined with sol-gel to produce an improved biological coating [132].

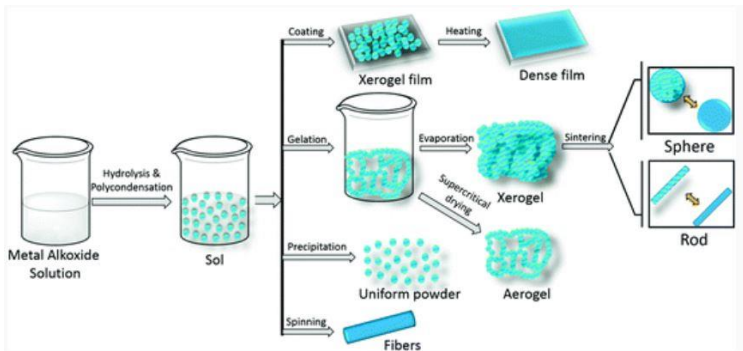


Figure 2.10. Schematic representation of sol-gel processing [127].

2.5.3 Physical vapor deposition (PVD)

Physical vapor deposition is a vacuum-based deposition process used to produce thin films and coatings. The process is similar to chemical vapor deposition (CVD), except that in PVD, the precursors, i.e., the material to be deposited, start out in solid form, whereas in CVD, the precursors are introduced in the reaction chamber in the gaseous phase. The PVD process involves the following steps [133] :

1. The material to be deposited is evaporated by a high energy source such as an electron beam or ions evaporating atoms from the surface.
2. The produced vapor is transported to the substrate to be coated.
3. The reaction takes place between the metal atoms and the appropriate reactive gas (such as oxygen, nitrogen or methane).
4. Deposition of the coating at the substrate surface.

The most common PVD process is thermal evaporation and sputtering and both methods will be described in detail hereafter.

2.5.3.1 Thermal Evaporation PVD

In thermal evaporation PVD, the coating material is heated up to the evaporation point through a resistance heat source, high-energy arc, or an electron beam. The phase change from solid to vapor phase is performed under vacuum conditions during which the evaporation atoms of a solid precursor placed in a crucible can travel directly and condense onto the surface of a substrate [134]. In the case of using PVD to coat metallic samples, the resistance source can be used to heat the crucible containing the powder form of the coating [135]. However, this method can only be applied for metals with a low melting point as it does not allow the evaporation of metals with high melting temperatures. Silver incorporated calcium phosphate films deposited by evaporation PVD have been reported to be effective against gram positive and gram negative bacterial strains [136]. In fact, the HA-coated films had a bond strength of 64.8 MPa, which was significantly higher than the bond strength of HA coatings deposited by plasma spraying (5.3 MPa).

In the case of cathodic arc evaporation (CAE) PVD, a high energy arc is used to heat the target generating an ionized metal vapor. This vapor accelerates towards the substrate kept at negative bias. This results in a highly dense coating with better adhesion [137]. The quality and the performance of the deposited coating depends on various parameters such as substrate temperature, target composition, bias voltage, gas flow, and ion bombardment rates. Magnesium-doped titanium nitride coatings deposited on Ti substrates by CAE resulted in the formation of magnesium substituted HA nodules when immersed in simulated body fluid [138]. These coatings present the potential to fabricate implants that facilitate nanostructured HA production promoting osseointegration.

2.5.3.2 Sputtering PVD

Sputter PVD is a process in which atoms, molecules or molecular ions, both neutral or ionize, are ejected from a target surface by energetic particle bombardment and propelled towards the substrate. It is mainly used for the deposition of thin films with a thickness of up to 5 μm on metals, alloys, and compound textiles [139]. The underlying

mechanism of magnetron sputtering and the schematic of a sputter coating machine are depicted in **Figures 2.11 and 2.12** respectively. The target or metal precursor that is desired to be deposited is bombarded with energetic ions of inert gases (argon or helium), which can quickly be accelerated towards the cathode employing an applied electric potential. The forceful collision of these energetic ions with the target ejects target atoms into the surrounding space. These ejected atoms are then transferred and condensed onto the substrate to form a coating. The target is typically cooled by water to reduce heat generation. There are several sputtering methods such as direct current (DC), glow discharge, ion beam sputtering (IBS), and reactive sputtering using a wide range of metals as target, including silver, copper, brass, titanium, silicon, silicon nitride and carbon nitride [140,141].

The simplest model for sputtering is the diode plasma consisting of a pair of planar electrodes: an anode, and a cathode. The sputtering target mounted on the cathode under appropriate potential difference between the electrodes will ionize the gas, creating a plasma discharge. The ionized ions (pleonasm) will then be attracted and accelerated towards the sputtering target. Such ion bombardment on the target will result in the displacement of some of the target atoms. This results in the emission of electrons which subsequently collide with gas atoms to form more ions that sustain the discharge [142]. Another type of sputtering employs a radiofrequency (RF) diode that operates at high frequency. RF magnetron sputtering is an improved ion sputtering method as thin films deposited by RF sputtering possess a higher adhesion to the substrate compared to the evaporation method.

Concerning the coating deposition, studies have reported that the magnetron sputtering technique offers several advantages such as the ability to coat complex 3D shapes, its cost-effectiveness, the deposition of smooth, homogenous dense coating surfaces, and the deposition of thin films with a thickness of 0.1 – 3 μm [143,144]. Magnetron sputtering has been used to deposit an HA coating onto a Ti substrate with varying thickness [145,146]. The deposited HA coating was observed to be dense comprising NPs, and the crystallinity of the coatings increased after thermal treatment. To improve the adhesion strength of the HA-coated Ti substrate, a Ti interlayer was also used

to improve the bonding strength. In addition, a layered coating and a functionally graded coating (FGC) have also been demonstrated to improve the adhesion strength between dissimilar materials [147–149].

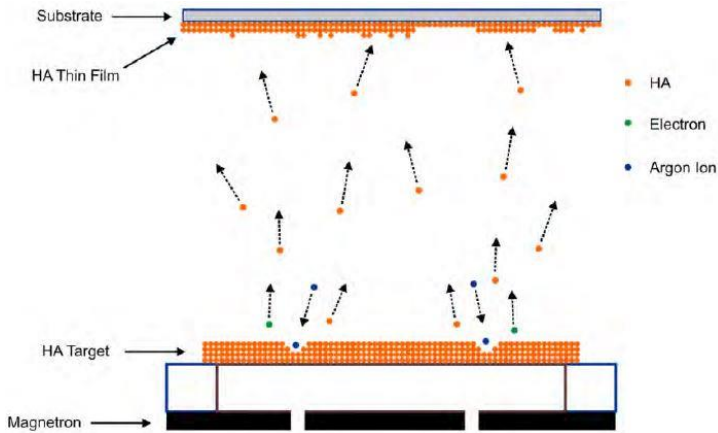


Figure 2.11. Magnetron sputtering mechanism [150].

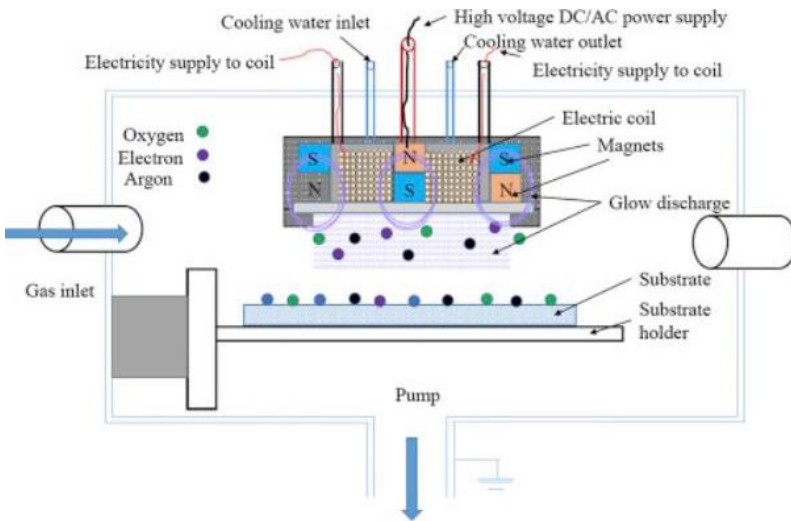


Figure 2.12. Schematic diagram of a mechanism of magnetron sputter coating machine [139].

2.5.4 Ion implantation

Ion implantation is a kinetic doping process in which accelerating ions are focused on the surface of a target material by an applied electric field, causing a change in the surface physical and chemical properties [151]. Ion implantation involves an ion source (the generated ions penetrate the surface layer as they have a high initial energy in the range of 20-200 keV), an accelerator (where the ions are electrostatically accelerated to high energy), and a target (where the ions impinge on). The energy of the ions, as well as the ion species and target material's composition determine the functions acquired and the penetration depth of the ions in the solid substrate [152]. Among other surface modification techniques, ion implantation offers distinctive advantages, making this technique suitable for biomedical applications. The process is performed at low substrate temperatures, thus preventing changes to the bulk properties of the material. Moreover, any kind of dopants can be introduced into any solid material to enhance the surface functional properties. In addition, high purity layers can be synthesized as the process takes place under vacuum conditions. Finally, the technique also offers good adhesion on a wide variety of substrates due to the absence of an interface between the implanted layer and the substrates [153,154]. Recent studies are focused on investigating ion implantation strategies towards the improvement of Ti implants for bone integration. For example, sodium (Na) ion implantation on a Ti surface resulted in an enhancement of HA precipitation, which in turn led to improved cell densities compared to untreated surfaces. Specific ions have also been implanted onto the surface of Ti and Ti alloys to improve their bioactivity, wear properties and tribological performances. Implantation of carbon (C⁺) and carbon monoxide (CO⁺) onto a Ti surface significantly improved bone integration, with stronger contacts between the bone and the implant material [155]. An increased wear resistance of Ti was observed after oxygen and nitrogen implantation due to the formation of surface oxide layers [94–96]. However, oxygen implanted samples showed better wear resistance than nitrogen implanted samples. Ion implantation techniques are also suited for the enhancement of other biomedical interactions. Fluorine ion-implanted polystyrene surfaces were observed to have an improved adhesion and viability of vascular smooth muscle cells. In addition, ion implantation has also been found

to improve the bioactivity of polyurethane, polystyrene, and polyethersulfones for the construction of vascular grafts [154].

2.5.5 Chemical vapor deposition (CVD)

Chemical vapor deposition is a vacuum-based deposition method used to produce high-performance thin films. In this process, a thin film of materials is deposited from the vapor phase by the decomposition of chemicals on the surface of a substrate [156]. CVD is widely used in industry to fabricate organic and inorganic films on metals, semiconductors, and other materials [157]. CVD exists in a multitude of processes, as listed in **Table 2.6**. The sequential steps that occur in every CVD process are schematically presented in **Figure 2.13**. It includes the convective and diffusive transport of reactants from the gas inlet to the reaction zone, the production of new reactive species and byproducts due to chemical reactions that occur in the gas phase, the transport of initial reactants to the substrate surface and the physical and chemical adsorption and diffusion of these species onto the substrate surface. Various researchers have demonstrated the excellent biocompatibility, corrosion resistance of diamond-like carbon (DLC) and TiO₂ films produced by CVD [158,159]. While this process does offer significant merits, the near volatility of the precursors at room temperature and the temperature at which the process takes place, up to 1600°C, are notable disadvantages [135].

Table 2.6. Different types of CVD.

Type	Description
Low-pressure CVD (LPCVD)	Process at sub-atmospheric pressures. At low pressures, unwanted gas-phase reactions are reduced which improves film homogeneity across the substrate.
Ultrahigh vacuum CVD (UHVCVD)	Process at very low pressure, typically below 10^{-6} Pa.
Aerosol assisted CVD (AACVD)	Precursors are transported to the substrate by means of a liquid/gas aerosol that is ultrasonically generated.
Direct liquid injection CVD (DLICVD)	Liquid precursors (liquid/solid dissolved in a solvent) are injected in a vaporization chamber towards injectors. In a next step, the precursor vapors are transported to the substrate as in classical CVD.
Plasma enhanced CVD (PECVD)	Process at low temperatures which utilizes plasma to enhance the chemical reaction rates of the precursors. The use of low temperatures allows deposition of organic coatings such as plasma polymers.
Remote plasma enhanced CVD (RPECVD)	Similar to PECVD. Process is conducted at room temperature as the substrate is not directly in the plasma discharge region.
Low energy PECVD	Process at high density, a low energy plasma is used to obtain semiconductor materials at high rates and low temperatures.

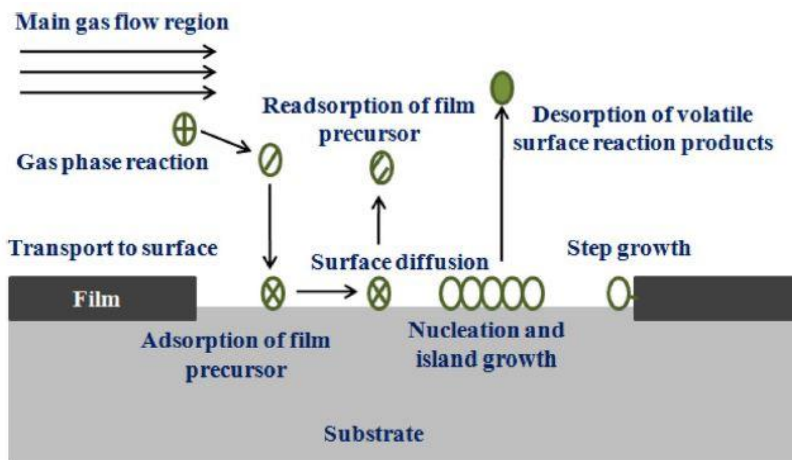


Figure 2.13. Schematic description of gas transport and reaction processes contributing to CVD film formation [160].

PECVD belongs to the group of coating deposition techniques where plasma is used to initiate the deposition process. It deposits solid thin films starting from the gaseous state (vaporous or gaseous precursors) on a substrate [156]. The addition of a small amount of gaseous precursors such as hexamethyldisiloxane, n-hexane, and acetylene to an RF discharge leads to the fragmentation of the precursor molecules with the subsequent formation of chemically active species. Thin plasma polymer films are then deposited on the cathode (typically the RF electrode) or any object exposed to the plasma region. The use of plasma polymers is very advantageous due to their superior bonding strength to various substrates. PECVD has been used to create TiO₂ coatings, hydroxyapatite coatings, DLC coatings, and many other plasma polymers on metals and polymer surfaces [161–163]. The osseointegration of TiO₂ coated implants significantly improved in both cortical and cancellous bone. PECVD deposited diamond films were also found to be as biocompatible as Ti, since they adsorb and denature a small amount of fibrinogen [159]. In PECVD, thin films with different functional properties can be obtained by changing the nature of the precursor, the working gas mixture and the intensity of ion bombardment of the growing film [164]. This is particularly

interesting from a biomedical point of view as differences in properties of the thin films can play a crucial role in cellular interactions.

2.5.6 Anodization

The anodization technique was discovered in the early 1930s, and since then, it has been widely studied. It is a well-established technique used for the production of protective layers on valve metals [165]. During anodization, a constant voltage or current is applied between the anode and cathode, leading to electrode reactions in combination with ion diffusion. This results in the formation of an oxide layer on the anode surface. The anodization process is complex and depends on several parameters, such as current density, electrolyte medium, treatment time, pH, and temperature [166,167]. A higher clinical success rate was observed for anodized Ti implant surfaces in comparison with polished Ti surfaces of similar shapes [168] as the anodized film can enhance the anchor points of the implants to the bone. Anodization is also used to fabricate biologically inspired nanosurfaces using specific anodization parameters. Nanoporous structures can be created by anodizing Ti in an electrolyte containing chromic acid at a voltage of 10 – 40 V. Another unique surface morphology which can be obtained through Ti anodization is an ordered nanotubular structure [169,170]. This nanotubular morphology can be produced by anodizing Ti in a fluorine containing electrolyte, at a voltage lower than the dielectric breakdown voltage. Moreover, microporous titanium surfaces can also be produced by potentiostatic or galvanostatic anodization at high current density or potential in an electrolyte solution containing H_2SO_4 , H_3PO_4 , HNO_3 , or HF [158]. In addition to the morphological modification of the surfaces, the crystallinity of the Ti surfaces can also be changed. Thus, another benefit of anodization is the possibility of adjusting both the chemical composition and the crystalline structure of the produced oxide layers.

2.5.7 Plasma immersion ion implantation and deposition (PIIID)

PIIID is a recently developed technique that has been showing progressive potential due to its adaptable process of plasma modification, ion implantation, and the fact that it is a non-line of sight process, which makes it suitable for biomedical applications. The schematic representation of direct current PIIID is illustrated

in **Figure 2.14**. In PIII, the material is immersed in plasma, and the ions are introduced to the entire surface at the same time, accordingly providing a faster and more cost-effective treatment. It is a low-temperature process; therefore, the material does not undergo any thermal deformation. Another main advantage of this technique is that it can conduct multiple processes such as simultaneous and consecutive implantation, deposition, and etching [171]. Over the past decade, a wide range of gases have been examined and different therapeutic and antibacterial elements have been introduced to improve the biocompatibility, antibacterial ability, and mechanical properties of a material by PIIID [172,173]. For example, calcium, nitrogen, and tantalum PIII were observed to increase the bioactivity and biocompatibility of a substrate, while Ag and Cu PIII improved the antibacterial properties of a substrate. Furthermore, DLC films and Ti oxide films were also produced by PIII to increase the haemocompatibility and wear resistance of a material.

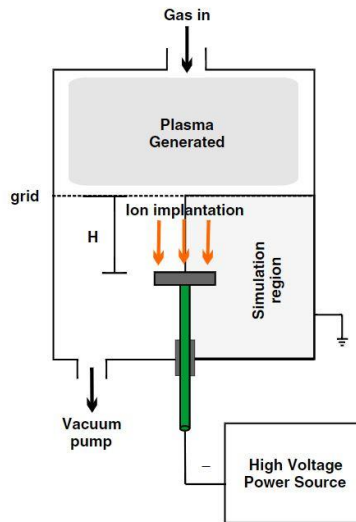


Figure 2.14. Schematic illustration of the direct current plasma immersion ion implantation (D-PIII) on planar substrates [171].

2.5.9 Plasma electrolytic oxidation

Plasma electrolytic oxidation (PEO) is a member of the anodization family, but it employs a voltage higher than the breakdown voltage to

generate a plasma-assisted anodic oxidation process. The schematic of a PEO experimental device is presented in **Figure 2.15**. During PEO, the material to be treated acts as an anode, while a stainless-steel electrolyte bath is regarded as the cathode. A circulating water treatment system is typically used to sustain the temperature of the electrolyte below 30°C. The growth mechanism of a coating deposited using PEO is explained in **Figure 2.16** [174]. As soon as the specimen to be treated is exposed to the electrolyte, the voltage increases rapidly and exponentially with time, which in turn results in the formation of an anodic barrier film (passivating film) on the surface of the substrate (**Figure 2.16a**). With a further increase in voltage (up to the breakdown voltage), oxygen bubbles and a porous oxide layer are formed on the surface of the substrate. At this stage, the voltage and current flow follow Faraday's law, which corresponds to the anodization stage (**Figure 2.16b**). With an even further increase in voltage (higher than the breakdown voltage), dielectric breakdown occurs leading to the formation of a micro-arc spark discharge (**Figure 2.16c**). The current flow concentrates on regions of breakdown, and the elements from the electrolyte and the substrate enter into the breakdown regions by diffusion and electrophoresis at local high temperatures resulting in localized thickening of the porous structure oxide layer. The micro-arc discharges gradually grow more prominent and are transformed into powerful arc discharges (**Figure 2.16d**). When the newly generated oxide layer is capable of resisting the current flow, the other regions are vulnerable to breakdown due to their smaller resistance, and the electrochemical reaction interface moves towards the entire surface of the substrate (**Figure 2.16e**). With prolonging the treatment time, large discharge channels develop with intense sparking and gas bubbles leading to the formation of larger distending pores (**Figure 2.16f**). The continuous formation and breakdown of the oxide coating (**Figure 2.16g**) cause the potential to vary. Both the dissolution of the base material and gasification of the electrolyte enables the formation of a porous ceramic oxide coating (**Figure 2.16h**).

The microstructure and mechanical properties of the PEO-based oxide films are mainly controlled by the electrolyte type and matrix composition [175]. Hence, an appropriate selection of the electrolyte is essential to obtain a satisfactory coating performance. Generally, different antibacterial agents and bioactive elements are doped into

the oxide layer to fabricate antibacterial and bioactive coatings [176–178]. Thus, these doped coatings can determine the interactions between implants and surrounding tissues, and can thus affect cell adhesion, proliferation, and differentiation on implants.

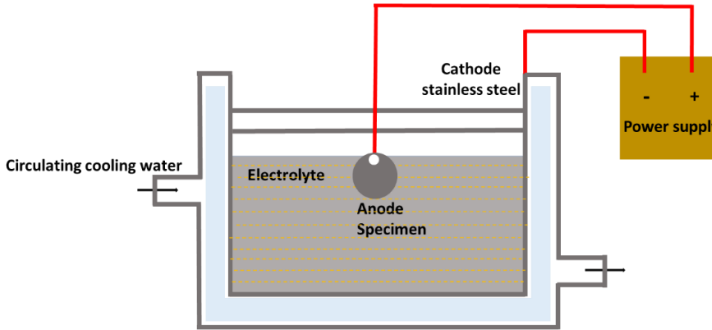


Figure 2.15. Schematic diagram of a (PEO) experimental device.

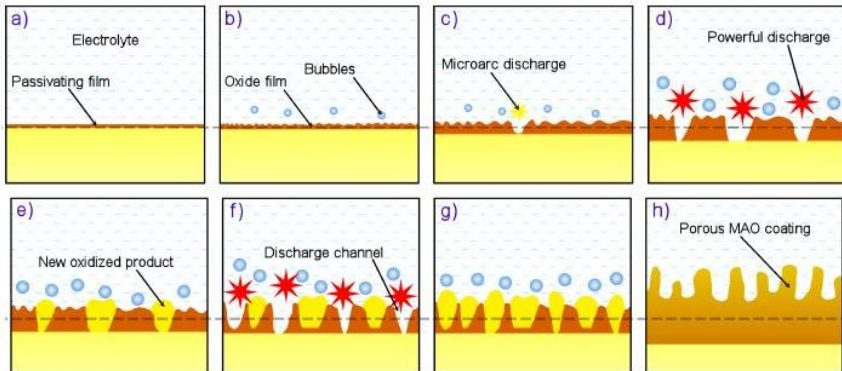


Figure 2.16. Schematic representation of the formation process of a PEO coating [174].

Chapter 3. Deposition of functional coatings on Ti surfaces: Improved biocompatible, antibacterial, and tribological properties

3.1 Introduction

Ti and its alloys have been widely used as artificial hip joints, bone plates, knee joints and dental implants due to their excellent corrosion resistance, biocompatibility and mechanical strength. These criteria, generally accepted as valid, are mainly attributed to the Ti properties resulting from a spontaneous building up of a stable Ti oxide layer. However, the clinical success of temporary and permanent implants and prostheses does not rely only on the implant surface properties but also on the functional design of the implant. The first priority when designing a medical device is indeed to perform its intended function, whether it is to provide support, to provide stability or to replace a diseased/damaged part of the body. However, many case studies of premature implant failures have reported that the cause of failure of the implants under study is mainly due to inadequate surface properties of the material such as low bio inertness, low surface hardness, poor wear resistance, poor osseointegration and inadequate osteoconductive properties. Moreover, implant associated infections also remain a major impediment to the utility of medical implants despite the use of sterilization techniques. Due to this, researchers are striving to develop functional coatings to improve the biocompatibility, antibacterial, and tribological properties of implant materials.

This chapter aims to give an extensive review of functional coatings deposited on Ti substrates and the outline of this chapter is presented in **Figure 3.1**. The chapter primarily focuses on the functions of the coatings as well as on their influencing factors, and describes their advantages and disadvantages. For the basic knowledge of the deposition techniques mentioned in this chapter, readers can refer to the previous chapter (Chapter 2).

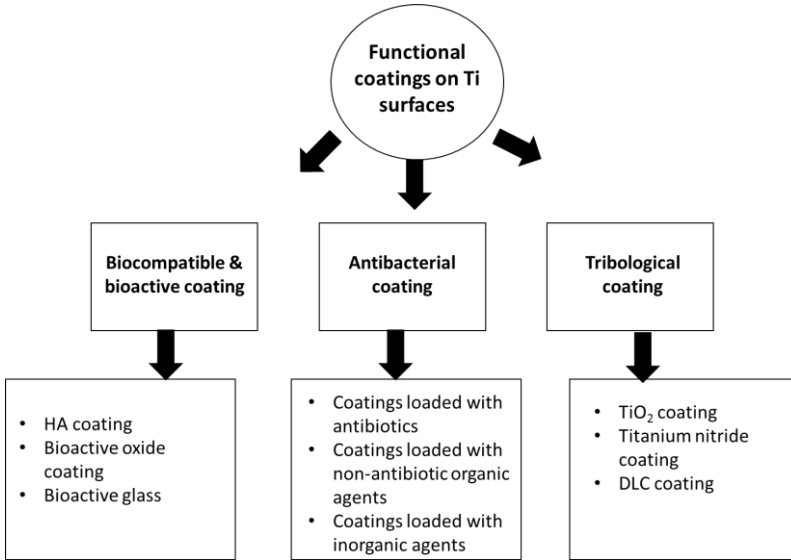


Figure 3.1. The outline of chapter 3.

3.2 Coatings with biocompatible and bioactive properties:

As implant materials are employed in direct contact with living tissues, it is essential that the implant surface exhibits biocompatibility. Biocompatibility is defined as the capability of the implant material to exist in harmony with surrounding tissues and with the body as a whole without causing any deleterious changes [179]. Recently, Williams reevaluated the current knowledge status regarding the factors that determine the clinical success of an implant material and proposed that a material should also possess bioactive properties [179]. A bioactive material is defined as a material which can induce a specific biological activity. Upon implantation, bioactive materials thus for example have the ability to induce the formation of bony tissue around the implant material (which is called osseointegration) thereby resulting in an excellent integration of the implant surface. For bone implant materials, bioactive materials are those that can induce bone-like apatite formation both *in-vitro* and *in-vivo* [180,181]. In fact, insufficient osseointegration can lead to the formation of fibrous tissues around the implant surface resulting in implant loosening.

Hence, a biomaterial should include all features of bio functionalities during its interactions with tissues and cells. However, Ti-based implants or metallic implants in general have a weak bone-bonding ability caused by the large difference in chemical and physical properties of the implant and the bone. Therefore, the bioactivity and biocompatibility of Ti implants needs to be improved by matching the surface properties (topography, porosity, roughness, microstructure) of the Ti implant with that of natural bone. Recent progress on coatings developed to improve the biocompatibility and bioactivity of Ti implants is reviewed below.

3.2.1 HA coating

Calcium phosphates are the most essential inorganic constituents of biological hard tissues. Consequently, many researchers have incorporated HA ($\text{Ca}_{10}(\text{PO}_4)_6 \text{OH}_2$) and alpha and beta tri calcium phosphates ($\alpha/\beta - \text{Ca}_3 (\text{PO}_4)_2$) as a bioactive material on metallic implants to enhance their bone-bonding ability. HA is biocompatible and bioactive in the human body due to its similarity to the mineral component of natural bone. It can directly adhere to bony tissue and helps in promoting osseointegration. Besides calcium phosphate, calcium carbonate (CaCO_3) is also an important biomaterial which has been widely used in bone implants. There are three crystalline and one amorphous phase of calcium carbonate. Studies have demonstrated that calcium carbonate is biocompatible and osteoconductive material. Therefore, calcium carbonate are application candidate to prepare resorbable coating with improved biodegradation rates due to its higher solubility. Also, CaCO_3 has been used as a inorganic precursor to induce the formation of HA containing bone minerals [182,183]. Various surface modification techniques have been applied to incorporate Ca-P and CaCO_3 on Ti substrates such as plasma spraying, sol-gel [184], anodization, electrophoretic deposition [185], sputtering, ion beam assisted deposition, pulsed laser deposition, high-velocity suspension plasma deposition (HVSPS) [132].

Table 3.1 gives a summary of different surface modification techniques used for the deposition of HA coatings on Ti surfaces and their corresponding advantages/disadvantages.

Table 3.1. Summary of different techniques used to deposit HA coatings.

Surface modification methods	Characteristics
Sol-gel and dip coating	<ul style="list-style-type: none"> - Inexpensive method using low processing temperatures - A high surface uniformity and the possibility to coat complex shapes - Requires a high sintering temperature which can degrade the metal strength and cause HA coating decomposition
Plasma spraying	<ul style="list-style-type: none"> - Rapid deposition, less risk of coating degradation and a lower cost - Non-uniformity of the coating, poor adhesion and possible alteration of the HA structure - High temperature procedure causing phase transformation
Electrophoretic deposition	<ul style="list-style-type: none"> - Rapid deposition, uniform coatings and the possibility to coat complex shapes - A low bond strength to substrates and possible formation of cracks - Requires a high sintering temperature which can degrade the metal strength and cause HA coating decomposition
Sputtering	<ul style="list-style-type: none"> - Uniform coatings with a high adhesion strength - Low deposition rate and expensive method
Electrochemical deposition	<ul style="list-style-type: none"> - Rapid deposition, uniform coatings, low cost and the possibility to coat complex shapes - Limited bond strength to substrates

Thermal spaying	<ul style="list-style-type: none"> - Rapid deposition and low cost - A high temperature procedure which can cause HA decomposition
Biomimetic deposition	<ul style="list-style-type: none"> - Low processing time, ability to coat complex shapes, possible to incorporate bioactive agents and bone growth stimulating factors in the coatings - Time consuming process
Plasma electrolytic oxidation	<ul style="list-style-type: none"> - Rapid deposition, low cost and the ability to coat complex shapes - A high adhesion and bond strength to substrates - Possibility to incorporate bioactive and antibacterial agents

Plasma spraying is one of the commonly used methods to deposit HA coatings onto Ti implant surfaces [186]. Groot et al. [187] fabricated the first plasma sprayed HA coating in 1987 to improve the bonding strength between the bone and the implant. Later on, in the following year, Furlong et al. performed clinical trials of plasma sprayed HA coatings in the femoral stem [188]. The observed findings suggested that the use of an HA coating allowed early and secondary fixation of implants. Since then, HA coatings have been extensively studied and their application has been extended to various implant materials such as joint prostheses, fracture fixation devices and dental implants. The bioactivity and biocompatibility of HA coatings depend on their fabrication method and can be categorized based on thickness, phase composition, roughness and porosity. For instance, Lynn et al. investigated the effect of coating thickness on the fatigue behavior of HA-coated Ti alloys deposited by plasma spraying. An HA coating thickness of 150 μm significantly diminished the fatigue strength while a thickness in the range of 25 – 100 μm did not have this negative effect [189]. The reduction in fatigue strength at high coating thickness could be attributed to the residual stresses and heat inputs generated during the deposition and the propagation of cracks towards the substrate from within the coating [189]. In some cases, a heat

treatment is used to improve the structure and bonding properties of HA coatings after the deposition process as an annealing process can transform the amorphous HA coating into a crystalline layer. Annealing at high temperatures such as at 700°C was observed to enhance the HA coating purity, the amount of hydroxyl groups and the coating crystallinity [190], while annealing between 400 and 600°C was found to result in HA coatings with less crystallinity [191]. An optimum crystallinity of deposited HA coatings is not known till now, however, Overgaard et al. showed that HA coatings with low crystallinity (50% crystallinity) had a higher tendency to dissolve in body fluids, thus accelerating early mechanical fixation and bone ingrowth as compared to highly crystalline HA coatings (75%) [192]. The surface roughness of HA coatings was also observed to have a significant effect on the implant's mechanical stability and osseointegration. The surface roughness of plasma sprayed HA coatings is in the order of several micrometers and is known to be strongly influenced by the operational deposition parameters. Studies have reported that a rougher surface exhibited superior biocompatibility and bioactivity, enhancing osteoblast cell adhesion and proliferation and improving mechanical fixation with the natural bone [193,194].

Although HA coatings fabricated by plasma spraying have shown promising results, a major limitation of this type of coating is its low bonding strength and the non-uniformity of the structure of the deposited coatings. To overcome these limitations, researchers began to investigate HA coating deposition by means of an electrochemical deposition. In 2002, Yen et al. first deposited HA coatings on Ti substrates via electrochemical deposition using dicalcium phosphate dihydrate and b-tricalcium phosphate. The deposited coating was transferred into an HA coating by immersing the coating in an aqueous solution containing calcium and phosphorus salts. The deposited coatings exhibited an improved adhesion strength [195]. Similarly, Isa et al. fabricated HA coatings via electrochemical deposition and reported an increased formation of bone-like apatite crystals on the coating surface after 7 days of immersion of the treated samples in a simulated body fluid (SBF) solution (**Figure 3.2**) [196]. Although HA coating fabrication by conventional electrochemical methods increased the adhesion strength and decreased coating

degradation, it did result into the formation of defects onto the coating surfaces [197]. Therefore, anodization has been used to post-treat Ti substrates coated by electrochemical deposition [198]. This anodization process improved the mechanical interlocks between the Ti substrate and the HA coating. In fact, anodization could also be used to deposit uniform and homogenous HA coatings without any post-treatment and calcium phosphate formation was observed on the grooves of the anodized metal after immersing in SBF [199]. In addition to its improvement in biocompatibility, previous research has reported that HA coatings deposited via electrochemical deposition and anodization on Ti surfaces exhibited an improved corrosion resistance [200].

Sol-gel combined with dip-coating has also been widely investigated to deposit HA coatings on metal substrates to improve the bioactivity and adhesion strength of the coatings [132,201]. Moreover, Massaro et al. conducted a comparative study on the surface properties and biological performance of HA-based coatings on Ti employing plasma spraying, sol-gel and sputtering techniques [202]. All three techniques deposited a homogeneous coating exhibiting a rough morphology while a porous morphology was also observed in case of the sol-gel coatings. Although all deposition techniques showed HA diffraction peaks on the coatings, the sputtered and sol-gel coatings were found to have a composition most similar to HA while sol-gel coatings also exhibited a high concentration of hydroxyl ions. The activity of alkaline phosphatase (ALP) is considered as an indicator of the osteoblast cells and the formation of new bone. It hydrolysis inorganic pyrophosphate which is a naturally occurring inhibitor of mineralization. Bone ALP also provides inorganic phosphate for the synthesis of HA. Therefore, measure of ALP activity has proven to be a reliable and adequate marker for osteogenic activity. *In-vitro* cell culture studies demonstrated that the sol-gel coating promoted cell proliferation, showed a higher alkaline phosphatase (ALP) activity and led to a greater osteocalcin production compared to the other two coatings under study (**Figure 3.3**). This suggests that a favorable surface morphology and chemical composition such as a porous and rough structure and the presence of hydroxyl groups can improve osteoblasts interactions stimulating cell differentiation. An overview of other

studies focusing on HA coating deposition not described in the paragraphs above is given in **Table 3.2**.

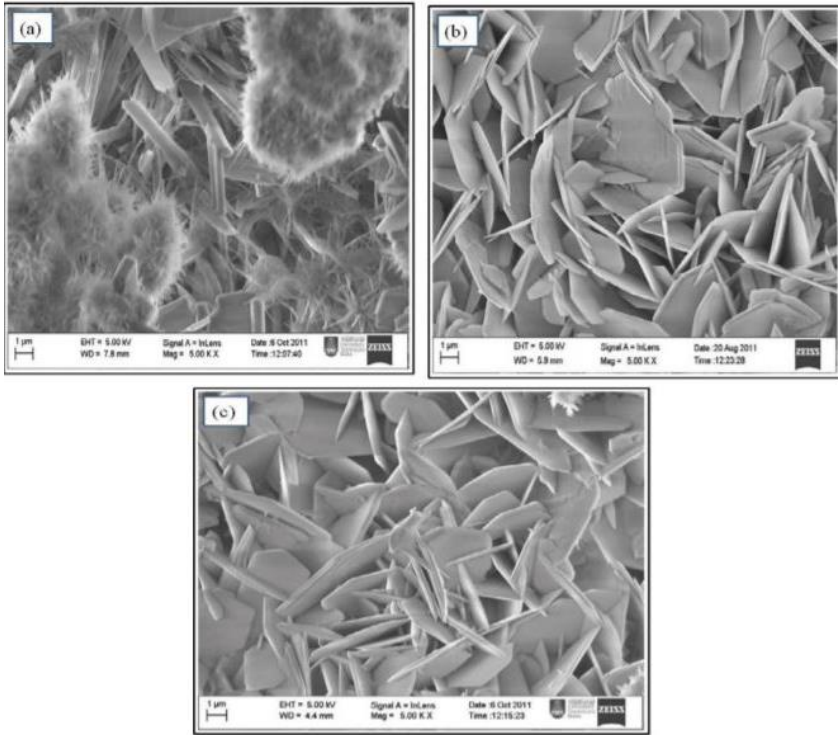


Figure 3.2. SEM images of the HA coatings prepared via electrochemical deposition after immersion in an SBF solution for (a) 1 day; (b) 4 days and (c) 7 days [196].

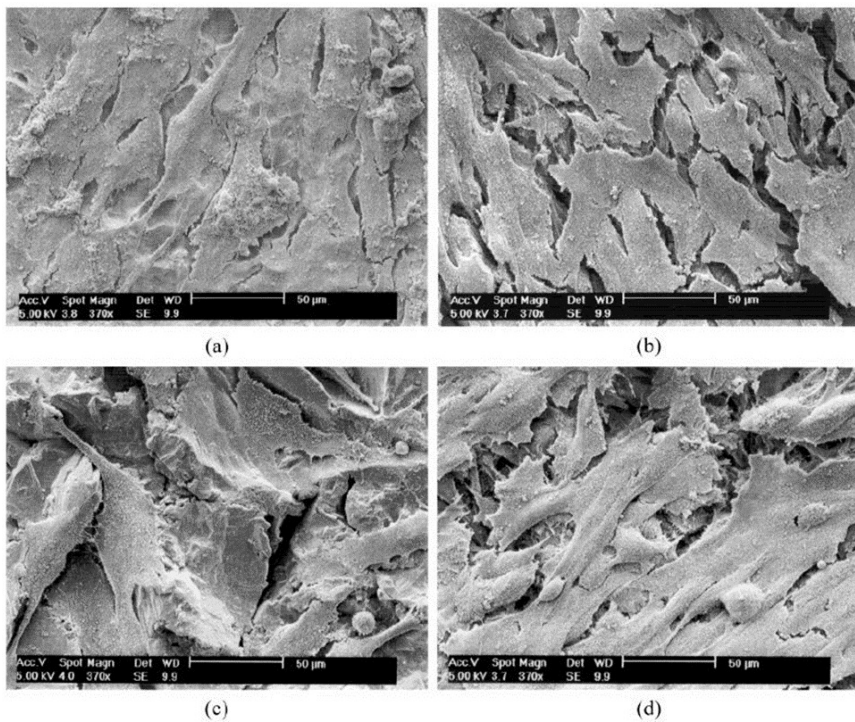


Figure 3.3. SEM micrographs of MG63 osteoblasts cells grown for 10 days on (a) uncoated Ti, (b) Ti covered by a plasma sprayed HA coating, (c) Ti covered by a sputtered HA coating, (d) Ti covered by a sol-gel HA coating.

Table 3.2. Overview of literature on HA coatings on Ti and its alloys not discussed in the text.

Coating method	Physico-chemical property	<i>In-vitro/in-vivo</i> experimental model	Biocompatible/bioactive property	Ref
Sol-gel	-Phase: rutile, anatase, HA -Increased bonding strength	<i>In-vitro</i> - osteosarcoma cells (HOS)	-Better cell proliferation -Enhanced ALP activity	[203]
Plasma electrolytic oxidation + Sol – gel	-Phase: anatase, HA -Increased surface roughness.	<i>In-vitro</i> - human osteosarcoma cells (HOS)	-Better cell proliferation -Enhanced ALP activity	[204]
Plasma electrolytic oxidation	-Phase: anatase, rutile, CaTiO_3 , $\beta\text{-Ca}_2\text{P}_2\text{O}_7$, $\alpha\text{-Ca}_3(\text{PO}_4)_2$ -Pore size increases with increasing thickness	-	-Increased apatite formation in SBF	[205]
Plasma spraying	-	<i>In-vitro</i> - osteoblasts cells (OSTEO) <i>In-vivo</i> – mandibular dog model	-Formation of mineralized extracellular matrix -Increased presence of Ca and P rich globular deposits <i>in-vitro</i> & <i>in-vivo</i>	[206]

Plasma electrolytic oxidation	<ul style="list-style-type: none"> -Phase: anatase, rutile, CaTiO₃, HA -Increased HA phase with increase voltage and increase concentration of Ca & P in electrolyte -Exhibited more porous 	<ul style="list-style-type: none"> <i>In-vitro</i> - Osteoblasts cells (MC3TC) <i>In-vivo</i> – distal femur rabbit model 	<ul style="list-style-type: none"> -Increased cell adhesion and differentiation with -Increased HA phase -Higher bonding strength -Improved osseointegration 	[207]
Sol-gel	<ul style="list-style-type: none"> -Increased crystalline peaks and HA peak intensity increases with sintering temperature -Exhibited more porous morphology 	<ul style="list-style-type: none"> <i>In-vitro</i> - human mesenchymal cells (hMSCs) 	<ul style="list-style-type: none"> -Improved cell adhesion, differentiation and osseointegration 	[208]
Biomimetic approach	<ul style="list-style-type: none"> -Presence of sodium and titanate phase -Appearance of HA phase after soaking in SBF for 24 	-	<ul style="list-style-type: none"> -Increased apatite formation in SBF 	[209]
Aerosol deposition + Hydrothermal annealing	<ul style="list-style-type: none"> -Increased crystalline peaks and HA peak -Increased roughness and more porous morphology 	<ul style="list-style-type: none"> <i>In-vitro</i> - Osteoblasts cells (MC3T3) 	<ul style="list-style-type: none"> -Increased apatite formation in SBF -Enhanced cell viability and cell differentiation 	[210]

Biomimetic deposition	<ul style="list-style-type: none"> - Improved nanoporosity - Increased formation of oxide groups and crystalline phases - Increased hardness and superior corrosion resistance 	<i>In-vitro</i> - Osteoblasts cells (MG-63)	<ul style="list-style-type: none"> - Enhanced cell attachment, cell proliferation and differentiation 	[211]
Sol-gel	<ul style="list-style-type: none"> - Formation of crystalline phase of HA - Deposited HA particles are polycrystalline - Increased surface roughness and wettability 	-	-	[212]

3.2.2 Bioactive oxide coating

Thin oxide films or coatings such as TiO₂, ZrO₂, and Al₂O₃ over a metallic bone-interfacing implant play an important role in improving the implant properties such as implant fixation, bioactivity, wear and corrosion resistance. It is commonly known that when Ti and Ti alloys are exposed to air or water they immediately form a thin oxide layer known as the passive condition of Ti. The formed Ti oxide layer is responsible for the bioactivity of Ti implants as it is in direct contact with the bone tissue. The oxide film minimizes the metallic ion release from the surface to the surrounding tissues as well as adverse toxic reactions [213,214]. Therefore, researchers are currently investigating the deposition of oxide coatings on bone implants to improve the osseointegration process between the implant and the surrounding bone tissue. Within this context, various surface modification methods such as electrochemical treatment, chemical vapor deposition, anodization [215,216], thermal oxidation [217], plasma spraying, sol-gel [218], ion implantation and PEO have been employed to develop a functional implant surface by improving the surface properties of the

oxide layer to improve the implant bioactivity [219]. The quality of the fabricated oxide coatings strongly depends on the used surface modification method and can be examined using the following properties: crystallinity, surface morphology, roughness, thickness, microstructure and wettability.

Santiago-Medina et al. investigated the bioactive factor responsible for osteoblast differentiation on differently oxidized Ti alloys [220]. To study this, Ti alloys were subjected to thermal oxidation at varying temperatures (500°C and 800°C) and PEO at varying times (3 min and 4 min) to deposit a TiO₂ layer. Osteoblast cell differentiation was found to increase on both oxidized surfaces compared to untreated Ti due to the presence of Ti oxide. However, a much higher cell differentiation was observed on the PEO-treated samples as can be observed in **Figure 3.4**. This is due to the increased presence of crystalline phases such as anatase and rutile which are not present on thermally oxidized Ti as these phases are responsible for nucleation and precipitation of apatite. This finding thus confirmed that the phase composition of the deposited Ti oxide layer is responsible for its bioactivity. In addition, researchers have postulated that the surface topography is another factor affecting the degree of bioactivity of TiO₂ coatings. For instance, Vandrovcova et al. [221] evaluated the influence of materials of different chemical composition (with and without TiO₂) and different surface roughness (R_a varying from 0 to 170 nm) prepared by magnetron sputtering on the behavior of osteoblast cell adhesion, proliferation and differentiation. Enhanced cell adhesion and proliferation were observed on TiO₂ coated samples in comparison to uncoated samples. Moreover, on all investigated materials, the cell population density achieved on day 7 increased with increasing surface roughness with a more pronounced effect on rougher TiO₂ films ($R_a = 100$ and 170 nm). Thus, it was stated that the cell-material interactions were controlled by the interplay between material chemistry and surface topography, and that these interactions were usually better on rough surfaces. Popescu et al. reported a similar effect on fibroblast cell adhesion and growth on TiO₂ films prepared by low pressure CVD [222,223]. In addition, Majeed et al. investigated osteoblast behavior on TiO₂ films prepared by magnetron sputtering with different surface roughness ($R_a = 10$ nm and 120 nm) and different surface hydrophilicity. The authors reported that the water contact angle decreases with increased roughness and depending on

the surface roughness, the cells intend to attach via direct (rough surfaces) or indirect (smooth surfaces) adhesion processes [224]. In addition, Tsukimura et al. [225] and Taeg Sul et al. [226] investigated TiO₂ coatings prepared by different techniques (PEO, sputtering, sandblasting and machined turned) to evaluate if the rate of osseointegration was influenced by surface chemistry or topography. Their findings revealed that surface chemistry plays an important role in osseointegration as it can facilitate rapid and robust integration of implants in bone. Moreover, the sol-gel method has also demonstrated good bioactivity due to the high amount of hydroxyl (OH) groups present on the surface which promotes mineralization of calcium phosphate and improves osseointegration [218,227]. Furthermore, the functionality of the deposited TiO₂ coatings can also be further improved by adding several dopants into TiO₂ films to improve its physico-chemical, antibacterial and tribological properties. These doped TiO₂ coatings will be discussed later in this chapter.

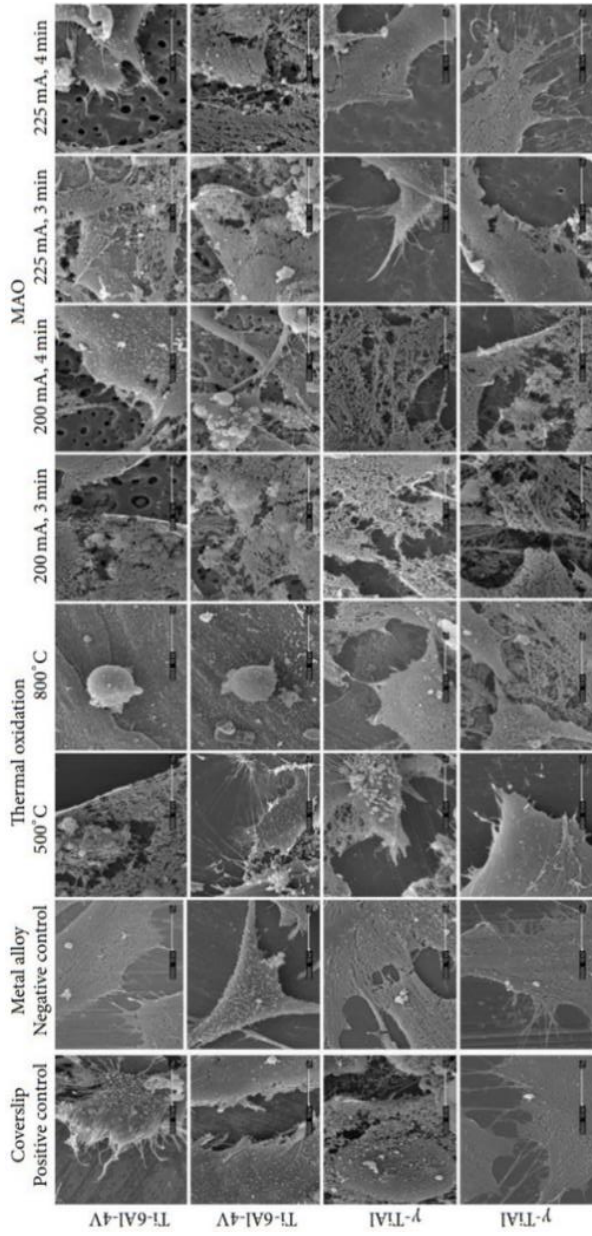


Figure 3.4. SEM micrographs of osteoblast cells 10 days after cell seeding on a glass coverslip (positive control), untreated Ti disks(negative control) and treated Ti disks (negative control), thermally oxidized Ti disks and Ti disks treated by Micro arc oxidation(MAO), which is a synonym of PEO [214].

Besides TiO₂, also zirconium oxide (ZrO₂) has attracted considerable attention for implant applications due to its antimicrobial activity, good chemical stability, corrosion resistance and wear resistance [228]. Zhang et al. [229] have investigated human osteosarcoma cell behavior on ZrO₂ and TiO₂ thin films deposited on Ti discs by cathodic arc deposition. It was observed that the cell adhesion and proliferation were significantly enhanced on both oxide coatings compared to untreated Ti as shown in **Figure 3.5**. Due to the observed positive influences of TiO₂, ZrO₂ and HA coatings on cell behavior, researchers also began to fabricate composite coatings containing more than one bioactive element. For instance, Tsai et al. [230] used a PEO process to fabricate composite coatings containing Ti and Zr oxide films on Ti substrates to investigate the biological performance of human osteosarcoma and fibroblast cells on the fabricated coatings. The study demonstrated that the oxide coatings deposited by PEO exhibited a higher cell viability due to the presence of crystalline phases such as anatase/rutile TiO₂ and tetragonal/monoclinic ZrO₂. Similarly, Rafieerad et al. prepared pure HA and HA/ZrO₂ composite coatings via electrophoretic deposition to evaluate the influence of zirconia content on the phase composition, wettability and *in-vitro* biocompatibility of the coatings. The study revealed that increasing the zirconia content dramatically changed the morphology of the apatite layer formed after 5 days of incubation in an SBF solution, as shown in **Figure 3.6**. A rough apatite layer with spherical particles (**Figure 3.6(a, b)**) was formed on the pure HA coated sample immersed in SBF, while plate-shaped HA crystals were formed in the case of HA/ZrO₂ composite films (**Figure 3.6(c-f)**). These latter morphological features are favorable for osseointegration, due to their effectiveness in anchoring bone cells, while encouraging vascular and bone tissue in-growth. Furthermore, the HA/ZrO₂ composite coating exhibited an increased hydrophilicity (water contact angle of 14°) and an enhanced osteoblast cell adhesion and these positive effects were more pronounced in the case of composite coatings with a high content of zirconia [231]. Furthermore, calcium stabilized zirconia coatings fabricated by means of plasma spraying were also found to improve the biocompatibility and apatite formation of implant materials [232]. Recently, Alagarsamy et al. investigated the osteoconductivity and bioactive properties of HA/ZrO₂ composite coatings prepared by PVD. The results indicated that the coated Ti substrates possessed an

accelerated bone formation compared to untreated Ti [233]. The Zr-OH groups formed on the coating surface during the phase transformation from the cubic or tetragonal phase to the monoclinic phase was thought to be a key factor in the implant bioactive performance due to its apatite forming ability.

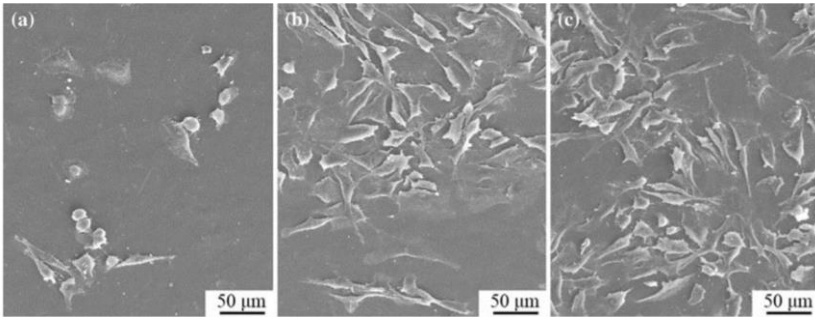


Figure 3.4. Morphology of human osteosarcoma (MG63) cells attached on an untreated Ti disc (a), TiO₂ films (b) and ZrO₂ films (c) 24h after cell seeding at 200x magnification (bar – 50 μ m) [229].

3.2.3 Bioactive glass (BG)

Another important material in the bioactive coating family is bioactive glass (BG), also known as bioglass, bioceramic or glass-ceramic. Bioactive glasses are composed of SiO₂, CaO, P₂O₅ and Na₂O, but their properties are different from the properties of soda-lime-silica glasses used in non-biologic applications. Hench et al. first developed BG in 1969 and since then, bioglass-based materials have been studied extensively. The bioactivity of BG is due to its ability to evoke complex interactions with living body fluids and tissues, releasing Ca²⁺ and P⁵⁺ ions and forming a bioactive S-OH group. This subsequently favors the growth of bone tissue due to the formation of hydroxycarbonate apatite (HCA). The biologic response to BG includes attachment of bone, yet interactions between the bioglass and bone are restricted to the surface, preventing both bone ingrowth and resorption [234–236].

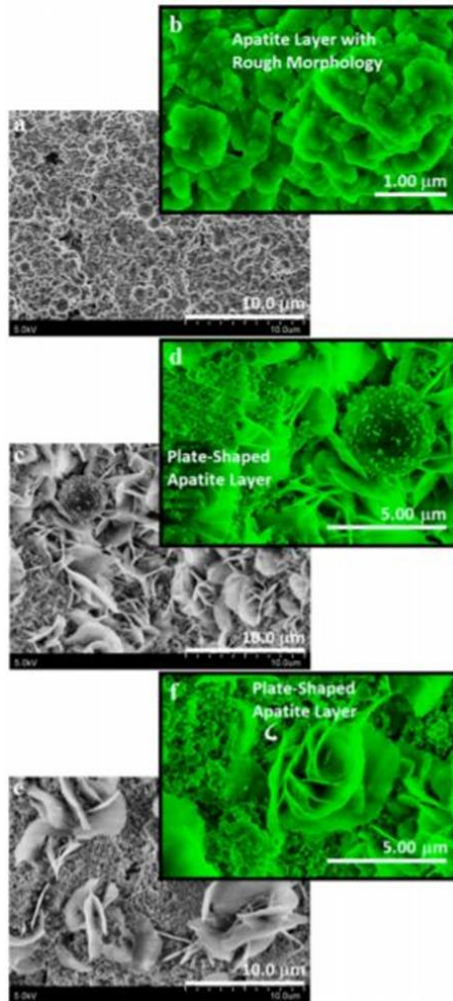


Figure 3.5. Field emission SEM micrographs of the surface morphology of different coatings after 5 days of immersion in SBF : Pure HA (a, b), 90% HA with 10% Zr (c, d), 70% HA with 30% Zr (e, f) [231].

The final bioactivity of BG for bone and soft tissue applications is determined by its composition. Silicate-based BG promotes the growth and the osteogenic differentiation of primary osteoblasts due to the release of Si^{4+} . In this case, interfacial bonding is the main factor responsible for the bioactivity, which is greatly connected to the

formation of an HCA layer. Consequently, the rate of bone-bonding depends on the amount of SiO₂: in particular, glasses with a silica content above 60 wt% induce the formation of a fibrous tissue whereas low bioactivity is observed for glasses with a silica content between 55 and 60 wt%. On the other hand, a higher bioactivity is again observed on glasses with a silica content below 55 wt% [234,237].

BG is brittle and does not withstand bending and tension; therefore, it cannot be used as base material for implants. However, it is possible to combine the superior properties of BG and Ti by depositing a BG coating on the surface of Ti implants. For this purpose, several coating techniques have been explored including plasma spraying, sol-gel, enameling, magnetron sputtering, electrophoretic deposition, pulsed laser ablation, and air abrasion [238–244]. CaO-SiO₂ based bioceramic coatings such as wollastonite (CaSiO₃) have been widely studied by many researchers [245–247]. Bone-like apatite is formed on the surface of CaO-SiO₂ based bioceramic coatings after immersion in SBF indicating the high bioactivity of the deposited coatings. Although the bioactivity is increased by the deposition of CaO-SiO₂ coatings, these coatings are harmful in the long-term as they are mechanically unstable due to the high dissolution rates of the coatings. To deal with this issue, composites of CaO and SiO₂ with a certain amount of TiO₂ and ZrO₂ have been used to improve the mechanical properties without impairing the bioactivity. For instance, Liu et al. [246] deposited wollastonite/TiO₂ composite coatings on Ti substrates using plasma spraying to improve the coating properties. In this study, four different types of coatings were prepared consisting of pure wollastonite, a composite coating containing 30% TiO₂, a composite coating containing 70% TiO₂ and pure TiO₂. Increased osteoblast cell adhesion and proliferation was observed on all coatings under investigation. However, HCA and silica-rich layers were formed on the surface of the wollastonite coating and the composite coating with 30% TiO₂ after immersion in SBF, while these layers were not found on the other two surfaces. This observation proved that coatings with wollastonite possessed a higher bioactivity.

The first *in-vivo* tests on BG-coated Ti implants were performed on rabbit hips [248]. Subsequent *in-vivo* studies indicated that the BG-coated implant group integrated well into the host bone without the

presence of a connective tissue capsule and that this implant group was surrounded with significantly more bone than the control group [249,250]. Mistry et al. evaluated and compared the *in-vivo* behavior of BG-coated and HA-coated Ti dental implants in the human jaw bone of 31 patients. The HA coatings were applied on Ti by air microplasma spraying, while the BG coatings were applied by a conventional enameling technique at 800 – 810°C in an ambient atmosphere. It was reported that among the implant types, the implant failure rate of BG-coated implants was less than in the case of HA-coated implants. However, both the HA- and BG-coated Ti implants were non-toxic and biocompatible, and overall results showed that both coatings were equally successful in achieving osseointegration [251,252]. Other *in-vitro* and *in-vivo* studies on BG-coated Ti and Ti alloys are summarized in **Table 3.3**.

Table 3.3. Overview of literature on BG-coated Ti and its alloys not discussed in the text

Coating	Coating method	Physico-chemical property	<i>In-vitro</i> / <i>in-vivo</i> experimental model	Biocompatible/ bioactive property	Ref
BG	CO ₂ laser beam	- Formation of a calcium phosphate layer and an HA phase - Formation of porous structure	-	- BG coated Ti shown to precipitates calcium phosphate in SBF	[253]
BG	Plasma spraying + thermal treatment	- Formation of a porous layer - The calcium to phosphorous ratio (1:7) corresponds to mineralization of bone	<i>In-vivo</i> - rabbit tibia model	- Improved bone ingrowth in to the coated porous Ti implant - Complete resorption of BG	[254]

Porous silica/ BG nanocomposite coating	Sol gel + dip coating	<ul style="list-style-type: none"> - Formation of a nanoporous structure 	<p>In-vitro - bioactivity assay with bone marrow stem cells (BMSCs)</p> <p><i>In-vivo</i> - rat tibia model</p>	<ul style="list-style-type: none"> - Formation of apatite in SBF - Enhanced osteogenic differentiation of stem cells - Formation of bone tissue in the periphery of the implant <i>in-vivo</i> 	[255]
BG	RF magnetron sputtering + heat treatment	<ul style="list-style-type: none"> - Formation of calcium, phosphorous and silicate containing crystalline phases - Improved adhesion strength 	-	<ul style="list-style-type: none"> - Incorporation of enstatite, forsterite and calcium magnesium phosphate phases in SBF 	[256]
ZnO + HA + BG nanocomposite coating	Enameling	<ul style="list-style-type: none"> - Formation of a microporous structure - Formation of crystalline phases 	<p>In-vitro - bioactivity assay with fibroblast cells</p>	<ul style="list-style-type: none"> - Incorporation of calcium and phosphate ions resulting in an HCA layer in SBF - Improved cell viability 	[257]
BG	Plasma spraying	<ul style="list-style-type: none"> - Formation of nano granules and pancake-like splats - Formation of calcium and silicate containing crystalline phases 	-	<ul style="list-style-type: none"> - Increased formation of an HCA layer in SBF 	[258]

HA/BG composite coating	Plasma spraying	<ul style="list-style-type: none"> - Formation of HA phases - Formation of spherical and ellipsoidal HA particles with microstructure 	In-vitro - bioactivity assay with osteoblast cells	<ul style="list-style-type: none"> - Formation of bone-like apatite in SBF - Enhanced cell proliferation and differentiation 	[259]
BG	Magnetron sputtering	<ul style="list-style-type: none"> - Formation of HA phases 	-	<ul style="list-style-type: none"> - Formation of bone like apatite in SBF 	[240]

3.3 Coatings with antibacterial properties

Implant surfaces are typically designed to facilitate adhesion of soft and hard tissue, eventually leading to osseointegration. Unfortunately, this phenomenon may also facilitate bacterial adhesion. About half a million cases of implant-associated infections are reported in the US associated with indwelling medical devices [94]. The risk of bacterial infection is high, especially for fracture fixation devices where open fractured bones are involved [95,96]. Bacterial infections not only cause severe pain and suffering to patients but also increase health care costs and burden the healthcare system. In more severe cases, the infection can expand to the surrounding tissues or bloodstream, often resulting in multiple surgeries, and in some cases even to amputation or mortality. Consequently, there is a pressing urge in the research community to develop implant coatings with improved antibacterial performance. The recent progress on antibacterial coatings on Ti implants is reviewed in the following paragraphs.

3.3.1 Coating loaded with antibiotics

Implant-associated infections are currently clinically treated by systemically administering a high concentration of antibiotic prophylaxis such as vancomycin, gentamycin, tobramycin, cephalothin, carbenicillin, amoxicillin and cefamandol. Although

systemic administration of antibiotics can prevent biofilm formation, potential cytotoxicity and poor distribution of drugs at the implant site are considerable limitations. Therefore, a controlled and local antibacterial release system is needed to replace the conventionally used systemic therapy. According to previously published studies, the limitations of systemic antibiotic therapy can be overcome by a controlled release system which has less susceptibility in promoting antibiotic resistance strain, which can administer a low dosage if required, and which has a greater control over toxicity and long-term release.

Gentamicin is more commonly used as antibiotic due to its thermostable properties and its broad spectrum of antibacterial activity. Therefore, it is one of the widely used antibiotics in antibiotics-loaded coatings on Ti implants [260,261]. Different coatings consisting of polymers such as polyurethane (PU), polylactic acid (PLA), polyglycolide (PGA), polymethyl methacrylate (PMMA) or calcium phosphates have been used as reservoirs containing the antibacterial agents due to their biocompatibility [262]. For instance, antibiotics-loaded calcium phosphate coatings on Ti implants exhibited a significant improvement against bacterial infections [263–265]. However, due to the high processing temperature that is required during the coating deposition, the antibiotics cannot be incorporated into the calcium phosphate coatings during their formation. Furthermore, the release characteristics and the amount of loaded drugs were limited due to the physical absorption of the antibiotics onto the surface of calcium phosphates [266,267]. Moreover, Radin et al. and Yamamura et al. reported that antibiotics loaded by the dipping method also resulted into burst releases of drugs, and observed that more than 90% of the antibiotics were released from the calcium phosphate coatings within the first 60 minutes [266,267]. Moreover, lipophilicity between the drug and the calcium phosphate coatings can lead to a homogenous distribution within the coating, which in turn influences the release profile of the drug. However, researchers have observed that the application of an additional lipid layer did not improve the release kinetics on the long-term [267]. A controlled antibiotic release system can be achieved by using a polymer matrix, however, the polymers are required to have a controllable hydrophilicity and should have an appropriate balance of

biostability and biodegradability [268,269]. Lucke et al. developed biodegradable gentamicin-loaded poly (dl-lactic acid) (PDLLA) coatings to prevent implant-associated infections in rats [270]. The release rate of gentamicin from PDLLA was slower than in case of calcium phosphate coatings, however, 90% of the drug was still released within the first 48h. Additionally, multilayered vancomycin sol-gel films [271], gentamicin-loaded Ti nanotubes [272,273], vancomycin-loaded Ti samples prepared by anodization and covalent bonding [274,275] were also fabricated. Although all fabrication strategies mentioned above were able to reduce bacterial adhesion and colonization in the short term, they still had inherent problems. First of all, antibiotic resistance strains were reported from the bacteria isolated from the treated surfaces [276]. Secondly, it was extremely challenging to design an antibiotics coating with a long-term antibacterial action at efficient concentrations. Finally, although antibiotics are considered to be biocompatible, studies have reported toxic effects of certain antibiotics on human cells [277–280]. Therefore, choosing the right antibiotic into an implant surface is crucial, and further studies have to be performed to explore the effect of antibiotics on tissue integration around the implant *in-vitro* and *in-vivo*. **Table 3.4** gives an overview of studies reporting on antibiotics-loaded coatings on Ti surface

Table 3.4. Overview of literature on antibiotics-loaded coating on Ti and its alloys not discussed in the main text

Type of coating	Surface modification method	Experimental model	Results	Ref
Tobramycin-loaded calcium phosphate coating	Biomimetic co-precipitation	<i>In-vitro S. aureus</i>	- Inhibition of bacterial growth - Release rate depends on the Ti	[261]
Vancomycin loaded calcium phosphate	Immersion	<i>In-vitro S. aureus</i>	- Effective bacterial inhibition up to 72h	[266]

Cephalothin-, carbenicillin-, amoxicillin-, cefamandol-, tobramycin, gentamycin, vancomycin-	Biomimetic precipitation	<i>In-vitro</i> <i>S.aureus</i>	- Inhibition of bacterial growth - Release rate is related to the antibiotics structure	[260]
Gentamicin-loaded titania nanotubes	Anodization technique	<i>In-vitro</i> <i>S. epidermidis</i> and MG63 osteoblast cells	- Reduced bacterial adhesion - Increased osteoblast differentiation	[272]
Gentamicin loaded PDLA coatings	Dipping	<i>In-vivo</i> Rat acute osteomyelitis model inoculated by <i>S. aureus</i>	- Reduced implant-associated infections	[270]
Vancomycin loaded sol-gel films	Dipping	<i>In-vitro</i> <i>S. aureus</i> <i>In-vivo</i> Rat femur model	- Inhibition of bacterial adhesion both <i>in-vitro</i> and <i>in-vivo</i>	[271,281]
Vancomycin-bonded coatings	Covalent bonding	<i>In-vitro</i> <i>S. aureus</i> , <i>S.epidermidis</i>	- Reduced bacterial colonization	[274,275,282–284]
Daptomycin bisphosphonates-loaded coatings	Covalent bonding	<i>In-vitro</i> <i>S. aureus</i>	- Reduced bacterial growth to 50%	[285]

3.3.2 Coatings containing non-antibiotic organic antibacterial agents

As antibiotics-containing coatings are associated with the risk of developing antibiotic-resistant bacteria, non-antibiotics organic antibacterial agents such as chlorhexidine and chloroxylenol have also been integrated into implant coatings. Organic antibacterial agents, especially chlorhexidine (CHX), are widely used in dental applications due to their broad antibacterial spectrum and their lower risk of developing drug-resistant strains. CHX is thus often used to combat bacterial infections by immobilizing it on the surface of Ti implants [286–288]. Studies have investigated the interaction of CHX on TiO₂-coated Ti surfaces and reported that the release kinetics of CHX depend on the surface roughness, the crystal structure of the oxide

layer and the buffer used [27,29]. CHX in N-morpholino ethane sulfonic acid (MES) buffer was adsorbed rapidly to both anatase and rutile surfaces while CHX in phosphate buffered solution (PBS) adsorbed more on rutile than anatase. However, studies did not give any evidence if the difference in CHX adsorption was due to the surface chemistry or due to the surface topography. Besides TiO₂ coatings, many other complex coatings have also been utilized to achieve a controllable and continuous release of organic antibacterial agents. For example, studies have investigated different kinds of polymer coatings such as poly(trimethylene furandicarboxylate) (PTF), poly(vinylpyrrolidone) (PVP), PDLLA, PLA as a matrix for CHX adsorption. An improved cytocompatibility, slower CHX release kinetics, and favorable mechanical properties were observed for PDLLA coatings [26,289]. In these studies, the Ti substrate was first anodized and subsequently coated in a mixed solution of polymer and CHX by spraying or impregnation. Cortizo et al. prepared an effective antibacterial coating architecture with different concentrations of CHX within a poly butyl acrylate (PBA) polymer matrix on Ti dental implants. A high concentration of CHX was found to demonstrate harmful effects indicating cytotoxicity on osteoblasts, while a low concentration of CHX was successful in reducing bacterial growth and maintaining sufficient osteogenic activity [290]. It is therefore crucial to optimize the CHX content to achieve a balance between cytocompatibility and antibacterial properties.

More recent utilization of organic antibacterial agents to treat implant-associated infections is focused on organic polymers such as proteins, peptides, liposomes, dendrimers, and cyclodextrins [288,291–293]. Within this field, antimicrobial peptides (AMPs) attract much attention due to their broad antibacterial spectrum and their low cytotoxicity [294,295]. Furthermore, AMPs act as the first line of defense mechanism against invading pathogens in multicellular organisms, as they rarely induce bacterial resistance on account of a complex mechanism [288,296,297]. Renxun et al. used an AMP called melamine on *S. aureus* and *P. aeruginosa*. In this particular case, AMP was loaded on amine-functionalized Ti surfaces. According to the authors, the melamine-loaded surfaces significantly reduced the *in-vitro* bacterial adhesion and biofilm formation of both bacteria. The coating was also able to reduce the bacterial load by 2 logs in both

mouse and rat subcutaneous infection models [291]. Another cationic peptide called Tet213 loaded on calcium phosphate coated Ti surfaces also demonstrated antibacterial effects against *P. aeruginosa* and *S. aureus* within 30 min *in-vitro* [298]. Several studies followed to confirm the antibacterial and biocompatible properties of AMPs such as Tet213, GL13K, hLf-11, and cecropin B [298–301]. Unfortunately, the reduced biocidal activity of AMPs upon tethering to solid supports can compromise their effectiveness as antibacterial coating materials [302–304]. The antibacterial action of AMPs is influenced by the AMPs concentration, the AMPs lateral mobility, the AMPs orientation, and the properties of the intermediate polymeric matrix such as its length and its flexibility [302,305]. For example, the length of the spacer was found to influence the lateral diffusion of the peptides in the lipid bilayer of bacterial membranes [304]. In such a situation, the bactericidal function of the peptide is diminished, and only the peptide properly bonded to the polymer matrix is capable of killing the bacteria upon contact. In addition, a costly design of synthetic peptides is necessary to fabricate coatings with potent antibacterial activity and bioactivity. Moreover, studies also indicate that it is challenging to control the activity of AMPs due to their various interlinked factors and their complex interplay mechanisms. A good understanding of the AMP structure-function relationship is therefore essential for the formulation of a more general approach in obtaining antibacterial surfaces loaded with AMPs. More studies on coatings containing non-antibiotic organic antibacterial agents deposited on Ti and its alloys are summarized in **Table 3.5**.

Table 3.5. Overview of literature on non-antibiotics organic antibacterial agents loaded on Ti and its alloys not discussed in the main text.

Type of coating	Surface modification method	Experimental model	Results	References
Chlorhexidine-incorporated polymer coatings	Grafting + dip coating + polymerisation	<i>In-vivo</i> - Rat intramedullary fixation model	- Reduced bacterial colonization in contaminated Rats - Reduced osteolysis	[306]
Chlorhexidine incorporated polybenzyl acrylate coatings	Solvent casting	<i>In-vitro</i> - <i>S. mitis</i> , <i>S. salivarius</i> Osteosarcoma cells	- Effective bacterial reduction - Toxicity at higher concentration of chlorhexidine	[290]
Chlorhexidine incorporated hydroxyapatite coatings	Surface induced mineralization	<i>In-vitro</i> - <i>S. aureus</i>	- Large inhibition zone	[307]
Chlorhexidine containing PLA coatings	Anodization + spraying deposition	<i>In-vitro</i> - <i>S. aureus</i>	- Large inhibition zone	[308]
Chlorhexidine containing PDLLA, PTF, PU, PVP and calcium phosphate	Impregnation	<i>In-vitro</i> - <i>S. aureus</i> , <i>S. epidermidis</i> and human fibroblast	- Effective bacterial reduction - Reduced fibroblast viability	[289]
Coatings with antiseptic combination of chlorhexidine and chloroxylenol	Not mentioned	<i>In-vitro</i> - <i>S. aureus</i> , <i>S. epidermidis</i> , <i>P.aeruginosa</i> , <i>E. coli</i> , <i>C. albicans</i>	- Good antibacterial activity against all the tested species	[309]
Chlorhexidine containing epoxy based resins	Spin coating + dip coating	<i>In-vitro</i> - <i>S. aureus</i> ,	- Effective bacterial inhibition	[310]

Antimicrobial peptides (Melimine)	Covalent grafting	<i>In-vitro</i> - <i>P. aeruginosa</i> Osteoblasts <i>In-vivo</i> rat model	- Excellent antibacterial activity <i>in-vitro</i> and <i>in-vivo</i> . - No toxicity to osteoblast cells	[311]
Antimicrobial peptides (HHC- 36) containing calcium phosphate and	Anodization + physical deposition	<i>In-vitro</i> <i>S. aureus</i> , <i>P. aeruginosa</i> , Osteoblasts	- Highly effective against both the bacteria. - No toxicity to osteoblast cells	[292]
Antimicrobial peptides (cecropin B) containing polydopamine films	Physical deposition	<i>In-vitro</i> <i>B. subtilis</i> , <i>S. aureus</i> , <i>E. coli</i> , <i>P. aeuroginosa</i> , Osteoblasts	- Inhibited adhesion and growth of bacteria. - Improved cytocompatibility	[312]
Antimicrobial peptides (Tet - 20) containing polymer	Covalent grafting	<i>In-vitro</i> <i>P.aeuroginosa</i> , Osteoblasts <i>In-vivo</i> rat infection model	-Inhibited biofilm formation -No toxicity to osteoblast cells <i>in-vitro</i> and	[311]

3.3.3 Coatings containing inorganic antibacterial agents

Inorganic antibacterial agents are excellent alternatives in implant applications because they offer many advantages such as a good antibacterial activity, less toxicity to cells, and sufficient stability. Among various dopants, active metals such as silver, copper, zinc, and nitric oxide (NO) have been examined and embedded in different matrices. In the following sections, different inorganic antibacterial release-based coatings on Ti surfaces are reviewed.

3.3.3.1 Silver- release coatings

Silver (and silver ions) have extensively been applied in antibacterial doping applications due to the following advantages :

- A broad antibacterial spectrum against gram-negative, gram-positive, and drug-resistant bacterial strains such as methicillin-resistant staphylococcus aureus (MRSA)
- The antibacterial effect of silver is long-lasting

- Easy to dope silver into different matrices, including polymers, ceramics, and metals

Due to these advantages, silver has been introduced into Ti implants to prevent implant-associated infections. Various surface modification techniques have been explored to incorporate silver and its compounds onto Ti surfaces including ion implantation, electrochemical methods, PEO, magnetron sputtering, plasma-assisted chemical/physical deposition, anodization and so on [176,313]. For example, Ewald et al. incorporated silver at different concentrations onto Ti alloys using physical vapor deposition. The silver-loaded samples were able to inhibit bacterial growth (*S. epidermidis*, *K. pneumonia*) and to facilitate osteoblast and epithelial cell activity [314]. Similarly, Cao et al. investigated the influence of silver PIII on the antibacterial performance and the osteoblast cell growth on Ti implants [172]. In this study, commercially pure Ti samples were subjected to Ag-PIII at different times (0.5h, 1.0h and 1.5h). The results indicated that the Ag-PIII Ti samples inhibited the growth of both *S. aureus* and *E. Coli* (**Figure 3.7**) while enhancing the osteoblast cell proliferation. The authors also reported that the *in-vitro* cell culture assay revealed no significant cytotoxicity, and even good cytocompatibility was observed on the Ag-PIII Ti samples. However, a significant difference was observed in the initial cell adhesion process between the untreated Ti and the different Ag-implanted samples under investigation. Although the cells exhibited a round morphology in the first hour on all surfaces, the expression of filamentous F-actin on the Ag-implanted samples was slightly lower than in case of untreated Ti (**Figure 3.8**). While mitosis phase cells were observed on untreated Ti within 3h (**white arrow in Figure 3.8**), hardly any mitosis phase was observed on Ag-implanted samples within 5h (white arrows in **Figure 3.8** b-3, c-3, d-3). This finding thus indicates that the untreated Ti surface was more preferable than that of the Ag-implanted samples in the initial cell adhesion stage. The observed difference in cell proliferation and cell attachment in the initial stage was attributed to the difference in surface wettability as the surface wetting characteristics play a crucial role in cell adhesion. This study thus proved that the physico-chemical properties of the Ag-loaded coatings are a crucial factor in controlling the cytotoxicity [36,172].

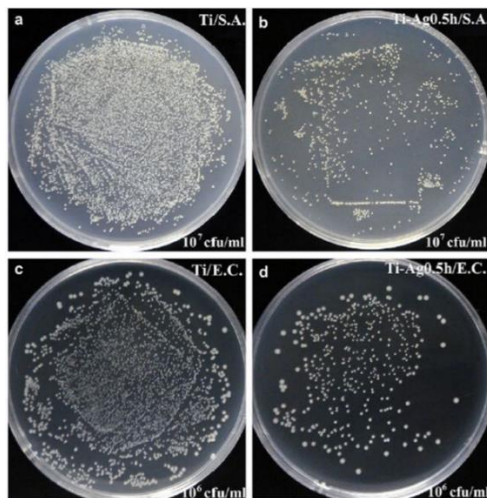


Figure 3.6. *S. aureus* bacteria colonies on agar plates (a) untreated Ti, (b) 0.5h-Ag-P/III and *E. coli* colonies on (c) untreated Ti, (d) 0.5h-Ag-P/III [172].

It has been reported that combination therapy of systemic antibiotics treatment and local delivery of silver NPs is also an effective way of enhancing both the antibacterial effect and decreasing the usage of antibiotics [315]. Within this context, an AgNPs loaded TiO₂ nanotube array was fabricated on Ti by anodization for a customized release of Ag⁺ ions. Enhanced antibacterial activity of combination therapy was observed on gram-positive, gram-negative, and MRSA bacterial strains *in-vitro* and in an *in-vivo* rat model. Although various strategies have been explored to dope silver into Ti implants, anodization is believed to be effective in bacterial inhibition, yet the reason remains unclear. It has been reported that the silver ions generated at the anode electrode with direct current are more effective against bacterial growth [313,316]. Secinti et al. reported that silver-coated Ti screws could prevent implant-associated deep bone infections when they have polarized anodically [317]. Improved antibacterial efficacy and biocompatibility have also been reported for silver-polymer composites on Ti surfaces [318,319] and TiO₂ nanotubes loaded with AgNPs [320–323]. **Figure 3.9** presents fluorescence microscopy images of adhered bacterial cells, *S. aureus*

and *S. epidermidis*, after 3h of incubation on an untreated Ti surface, TiO₂ nanotubes, and TiO₂ nanotubes loaded with AgNPs [320].

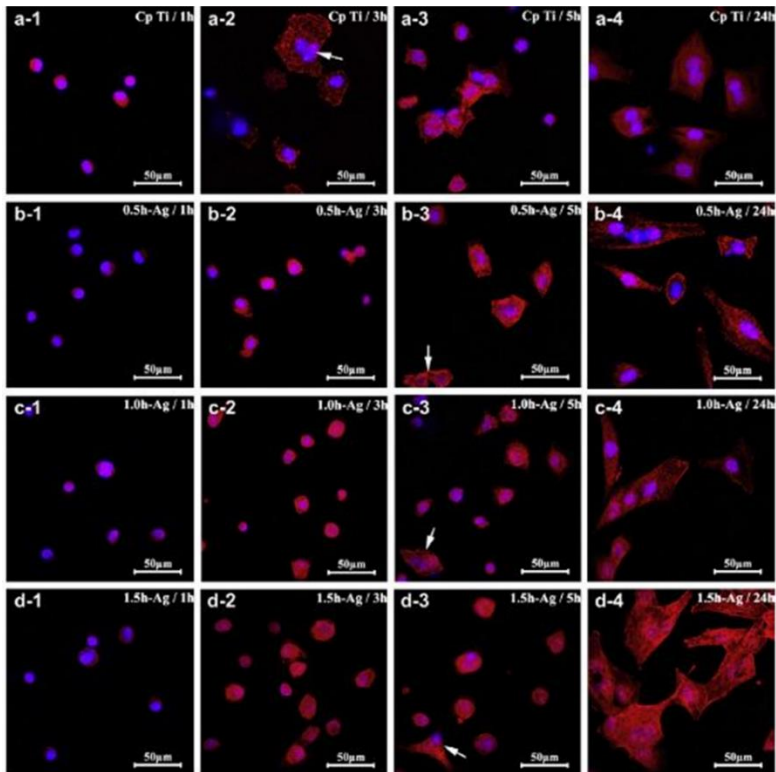


Figure 3.7. Laser scanning confocal microscope images of MG63 osteoblast cells cultured for 1h (i-1), 3 h (i-2), 5 h (i-3), and 24 h (i-4) on the various surfaces with F-actin stained with rhodamine phalloidin (red) and the nucleus stained with DAPI (4,6-diamidino-2-phenylindole) (blue) (i = a, b, c and d represents Ti, 0.5h-Ag-P/III, 1.0h-Ag-P/III, and 1.5h-Ag-P/III, respectively)[172].

Although the exact mechanism of silver resistance against bacteria is still under debate, various findings suggest that the antibacterial activity of Ag-doped coatings is due to the close contact between bacteria and AgNPs and/or the release of Ag⁺ ions from the coating to the aqueous medium [324]. Direct contact of bacteria with AgNPs can cause physical damage to the bacterial membrane leading to cell death. In addition, it has been proven that the bacterial cell membrane has a negative charge, which confers electrostatic attraction to the

positively charged AgNPs. This helps the AgNPs to attach onto bacterial cell membranes followed by membrane damage [325,326]. There is also evidence suggesting that released Ag⁺ ions from AgNPs are crucial contributors to the antibacterial activity and that long term release of Ag⁺ from an implant surface is essential to provide long term efficiency. The release rate of silver ions is influenced by many factors including the pH of the medium, the wettability of the coating, and the initial silver loading. In a recent study, Shivaram et al. [327] investigated the long term silver ion release for a period of minimum 6 months at two different pHs (pH 7.4 and 5.0), and two different silver loading rates from silver-coated surface modified porous Ti implants. The implants were fabricated using a powder-based additive manufacturing technique with and without TiO₂ nanotubes. The results indicated that the cumulative rate of silver ions in both mediums, and for both loading rates, were well within the potential toxic limit of 10 ppm specified for human cells. Also, the *in-vivo* rat distal femur model indicated good interfacial bonding between the implant and the surrounding bone tissue up to 12 weeks. From these findings, it can be concluded that porous Ti implants with enhanced wettability and strongly adherent silver coatings have a long term efficiency. Other, not yet discussed studies on Ag-doped coatings deposited on Ti and its alloys are summarized in **Table 3.6**.

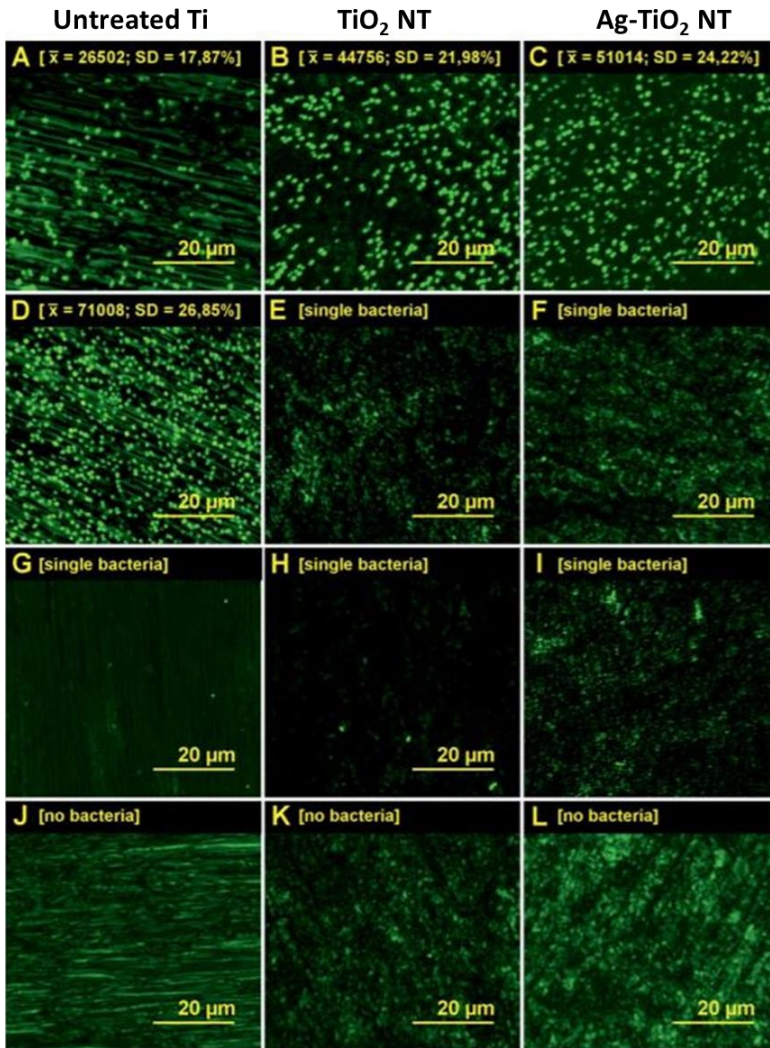


Figure 3.8. Fluorescence microscopy images of adhered bacterial cells (*S. aureus* (A, B, C), *S. epidermidis* (D, E, F), *E. coli* (G, H, I), and *P. aeruginosa* – (J, K, L), after 3 h of incubation with bacterial cell suspensions. The tested surfaces were Ti (A, D, G, J), TiO₂-nanotubes (TiO₂NT) (B, E, H, K), and Ag-TiO₂NT (C, F, I, L). In brackets: the average number of cells per mm² and the standard deviation of this value [320].

Table 3.6. Overview of literature on Ag doped coatings on Ti and its alloys not discussed in the text.

Type of coating	Surface modification method	Experimental model	Results	Ref
Ag/HA composite coatings	Hydrothermal treatment	<i>In-vitro</i> <i>S. aureus</i> , <i>E.coli</i> & MG63 osteoblast cells	- Improved antibacterial effect - Reduced cell proliferation and differentiation on Ag-containing samples while improved cell proliferation & differentiation on	[328]
Ag/TiO ₂ /HA composite coatings	Electroplating + anodization + sintering	<i>In-vitro</i> <i>S. sanguinis</i>	- 100% mortality of bacterial growth in the surrounding media - Biofilm formation reduced by 97.5%	[329]
Ag/carbon composite coatings	Pulsed dual cathodic arc	<i>In-vitro</i> <i>S. aureus</i>	- Reduced bacterial adhesion on Ag-containing samples	[330]
Ag/Pt/HA composite coatings	PEO	<i>In-vitro</i> <i>S.aureus</i> , <i>E. coli</i> & MG63 human osteosarcoma (HOS) cells	- Improved antibacterial effect on Ag-containing samples - Coatings with low Ag content were biocompatible while coatings with high Ag	[331]
Ag/TiO ₂ composite coatings	High current anodization	<i>In-vitro</i> <i>S.aureus</i> & MC3T3-E1 osteoblast cells	- Improved antibacterial effect and cytocompatibility on Ag-containing samples	[332]
Ag/hydrocarbon plasma polymer films	Unbalanced magnetron sputtering	<i>In-vitro</i> <i>E. coli</i> & pulmonary artery endothelial cells	- All Ag containing coatings reduced the growth of bacteria - Films with high Ag content showed cytotoxic effects	[56]

TiN/Ag coatings	Magnetron sputtering	<i>In-vitro</i> <i>E. coli</i> (with and without whole blood proteins)	- Improved antibacterial effect on all treated surfaces - Reduced antibacterial effect in the presence of both bacteria and whole blood proteins on all	[333]
Ag/CaP coatings Ag/Sr/CaP coatings	Hydrothermal treatment	<i>In-vitro</i> <i>S.aureus</i> , <i>E. coli</i> & MG63 osteoblast cells	- Improved antibacterial effect and reduced cell proliferation and differentiation on Ag containing coatings - Incorporation of Strontium improved the biocompatibility of Ag-containing	[334]

3.3.3.2 Copper-release coatings

Copper is an essential trace element for survival. It is present in all body tissues and plays a significant role in making red blood cells, maintaining nerve cells, and in the immune system. Deficiency of copper is associated with impairment of blood, liver and the immune system. Copper is responsible for cellular actions in the human body, such as destabilization of membranes, is responsible for energy production and is responsible for the induction of apoptosis. Furthermore, copper also has a broad spectrum of antibacterial activity against numerous bacteria. Due to these properties, copper-based release coatings may be a good alternative to silver-release coatings.

Although the exact mechanism of antimicrobial activity of CuNPs is not clear and still under debate, it is believed that the antibacterial activity of CuNPs is connected with (1) their ability to perforate the bacterial membrane that results in the release of intracellular material [335,336], (2) the capability of CuNPs to generate reactive oxygen species (ROS) and (3) last, but not least, with the release of Cu ions from the surface of CuNPs in the aqueous environment that may interact with phosphorous- and sulfur-containing biomolecules such as DNA and proteins which inhibits the bacterial cells [337]. Apart

from their use as an antibacterial agent, previous studies have shown that Cu ions are also beneficial to the cardiovascular system by stimulating the proliferation and differentiation of endothelial cells [177,338–341]. Recent literature reports have explored antibacterial coatings loaded with CuNPs that were prepared by various means such as ion-beam deposition, electrolytic oxidation [39,176,342], magnetron sputtering [343], plasma source ion implantation and deposition [344,345].

Shirai et al. evaluated the antibacterial activity of a Ti-copper alloy on implant infections to determine the potential use of copper in a biomaterial. Both Ti alloys under study (with 1% and 5% of copper) inhibited the colonization of *E. coli* and *S. aureus*. *In-vivo* implantation of Ti-Cu external fixation pins on a rabbit model was observed to significantly inhibit infections and inflammation and also resulted into excellent osteoid formation. Copper levels measured before and 14 days after the operation did not show significant differences [346]. Additionally, hard copper coatings with improved corrosion resistance have been deposited on pure Ti and Ti-Al-Nb alloys by means of ion implantation [344,347,348], while copper-containing HA coatings have also been produced on Ti by PEO [177,342,349–351]. The aforementioned studies all reported that the copper-doped surfaces exhibit antibacterial properties and sufficient biocompatibility. Thus, copper doping can effectively inhibit bacterial adhesion and growth without compromising the activity of osteoblasts, fibroblasts and endothelial cells [177,342,351]. Even more, cells cultured on copper-coated Ti substrates were found to exhibit better spreading and proliferation and even the cell density was higher compared to untreated Ti. For instance, Zhang et al. fabricated a microporous TiO₂ coating doped with different doses of copper (0-1.93 wt%) on Ti surfaces using PEO, after which the antibacterial ability of and the fibroblast interactions on the produced coatings were investigated. The obtained results showed that all Cu-doped coatings exhibited good antibacterial properties. Compared to untreated Ti, cell adhesion and proliferation were significantly enhanced on the coating with low Cu content while greatly inhibited on the coating with high Cu content (**Figure 3.10**) [342]. This study thus demonstrated that an appropriate Cu dose could accelerate the proliferation and up-regulation of a specific protein of cells, however, an increased Cu dose is thought to

interact non-specifically with various macromolecules causing site-specific damage and increasing clinical oxidative stress [341]. To examine the balance of antibacterial activity versus adverse tissue effects, Hoene et al. evaluated Cu-coated Ti implants in an *in-vivo* rat model. The Cu-coated Ti implants reduced the growth of *S. aureus* within 24h, accompanied by an increased inflammatory response in the early post-implantation phase [350]. Although the prepared coatings demonstrated the anti-infective potential of Cu, accumulation of Cu from the implants was found in the liver depending on its concentration and its chemical state. Therefore, further studies are required to investigate the long-term effect of Cu-based coatings and to optimize the release by varying the operational parameters during the coating fabrication.

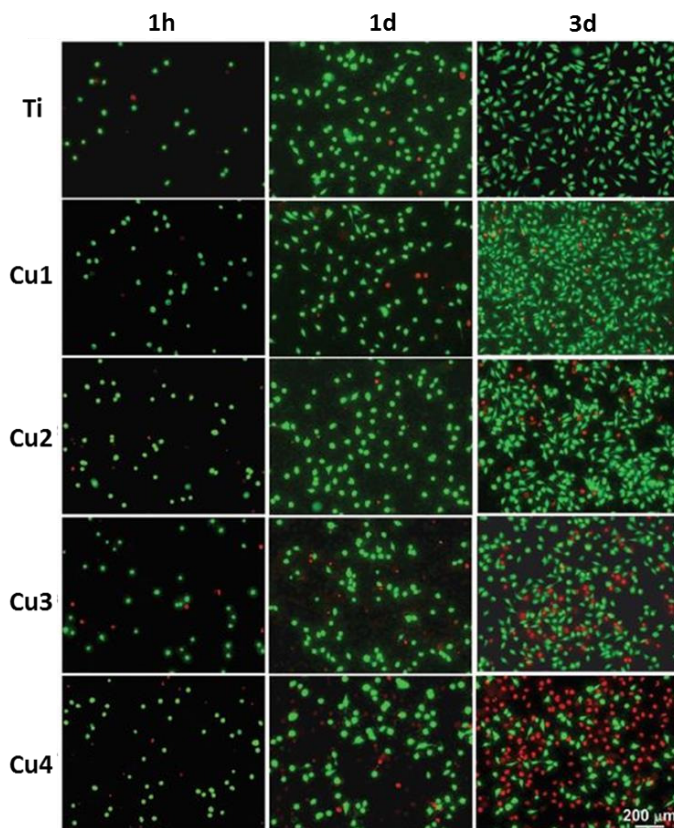


Figure 3.9. Viabilities of fibroblast cells cultured on untreated Ti and Cu-doped TiO_2 coatings on Ti for 1 h, 1 day and 3 days [342].

3.3.3.3 Nitric oxide releasing coatings

Nitric oxide is a diatomic free radical that plays a role in many biological processes such as in the immune system, the cardiovascular system, vasodilation, angiogenesis, wound healing, and phagocytosis [352]. NO can be naturally synthesized in the body by different nitric oxide synthase (NOS), and it is continually released by the endothelium. It has been demonstrated that NO is a potent antibacterial agent against both gram-positive and gram-negative bacteria and it possesses a broad antibacterial spectrum due to the superoxide generated by its byproducts [353,354]. The primary mechanism of antibacterial action of NO is via lipid peroxidase generated membrane destruction, irreversible DNA damage and inhibition of critical proteins found in bacterial respiration [354]. Therefore, several research groups have suggested the use of NO coatings on polymeric substrates polyethylene glycol (PEG), polycaprolactone (PCL), polyethylenimine (PEI), polyvinyl chloride (PVC), (PEG, PET) via a sol-gel method to improve the antibacterial and biocompatible properties of implants [354–357]. The results of these studies showed that an NO flux generated from the sol-gel coatings significantly reduced the bacterial adhesion of *S. aureus*, *P. aeruginosa* and *S. epidermidis* [352,355–357]. In particular, Naghavi et al. have reviewed NO coatings deposited on different polymeric substrates for cardiovascular implant applications [358]. In addition, to assess their antibacterial efficacy for orthopedic implants, NO-releasing coatings were also incorporated on stainless steel [359] and Ti substrates by the sol-gel method [360]. Results showed that the deposited coatings had better stability on both metal substrates and that the coatings significantly reduced the bacterial adhesion. Besides, an *in-vivo* rat model was performed to further evaluate the results of obtained *in-vitro* tests. After 28 days of implantation, no pin tract infection was seen in the NO-releasing group [360]. This study thus confirms that NO-release coatings on Ti are an alternative method, however, there are still many characteristics that have to be studied, such as the coating bonding strength, the interaction of the coating with bone tissue and the long-term release characteristics. Therefore, further studies are required to investigate the long-term effect of NO-based coatings.

3.4 Coatings with improved tribological performance

Corrosion is an unwanted electro chemical reaction that can result in the degradation of metal to oxides, hydroxides and other toxic compounds. This degradation leads to an inflammatory reaction, which may lead to implant loosening. Most Ti implanted materials tend to lose electrons in a solution and therefore, they show a high potential to corrode. Another critical factor which determines implant success is its wear and abrasion properties. Poor wear resistance can lead to the formation of wear debris, which may cause varied unwanted reactions in the body and thus increase the chance of implant failure. There is therefore a pressing urge to design implant materials with enhanced corrosion and wear resistance. The recent progress on coatings with improved tribological properties on Ti implants is reviewed below.

3.4.1 Titanium dioxide(TiO₂) coating

As mentioned in section 3.2.2 TiO₂ coatings are known for their bioactive and biocompatible properties. In addition, they are also known for their good corrosion resistance and high hardness. The corrosion resistance of TiO₂ has been studied on different metal substrates, including Ti and its alloys, aluminum, magnesium and stainless steel. As previously mentioned, TiO₂ can be generated on Ti surfaces via different surface modification techniques such as thermal oxidation, anodization, PEO, oxygen ion implantation and the sol-gel technique.

Thermal oxidation is the most commonly used technique to deposit thin oxide films on Ti surfaces [361,362]. It is performed by exposing Ti samples to air/oxygen and nitrogen atmospheres at temperatures ranging from 400 to 700°C. Ti substrates treated by thermal oxidation were found to exhibit improved wear resistance compared to untreated Ti during a block on ring test under dry sliding conditions [362]. This is due to the formation of a hard oxide layer and an oxygen diffusion zone below it. Similar findings were observed by other researchers, who stated that the hard oxide layer and oxygen diffusion zone formation on Ti contributed to the improvement of wear resistance and corrosion resistance [363–366]. Aniolek et al. determined the influence of temperature and treatment time on the growth process, mechanical properties and roughness of oxide layers obtained on Ti via thermal

oxidation [367]. The researchers found that the temperature had a more important influence on the formation of the oxide layers on Ti than the treatment time. The hardness of the obtained oxide layers grew with increasing temperature and extended time of oxidation. In addition, the surface roughness also increased when increasing the temperature from 600 to 700° C [367].

PEO is the second most commonly used surface modification technique applied to produce hard, thick oxide coatings on the surface of light alloys such as Ti, aluminum and magnesium. PEO is based on conventional anodization with a similar configuration, but higher voltages (200 to 500 V) are used. Therefore, the samples are anodically polarized to high voltages exceeding the dielectric breakdown voltage generating short-lived plasma micro discharges on the metal surface. In PEO, the substrates are not subjected to thermal damage as the developed micro discharges undergo extinction within microseconds. Ti substrates treated via PEO exhibited improved hardness, wear and corrosion resistance. The improved tribological properties are due to the formation of a crystalline oxide structure composed of anatase and rutile TiO₂. Although the anatase phase was found to exhibit poor corrosion resistance against certain acids, rutile typically has shown superior protection properties exhibiting higher stability, and higher corrosion resistance [368]. The microstructure of PEO coatings is influenced by several parameters such as the type and concentration of the electrolyte used, the substrate composition and the process parameters used during the PEO treatment. Moreover, the formed oxide layers are also greatly influenced by the applied polarization conditions such as DC, AC, pulsed DC (unipolar or bipolar) with control of current density, as well as the voltage and time applied during the treatment [369]. Laurindo et al. demonstrated the influence of applied voltage on the mechanical properties of oxide layers produced by PEO on Ti substrates with and without heat treatment. The hardness, elastic modulus and wear resistance of the newly formed TiO₂ films increased with increasing the PEO applied voltage in the range of 250 – 400 V (**Figure 3.11**) [368]. This observation is due to the formation of the rutile TiO₂ phase at increased temperatures. An increase in wear resistance due to the rutile phase formation was also described by Yetim et al. [370], Krishna et al. [371] and Aniolek et al. [372]. These authors proposed

that the improved wear resistance of the PEO-treated Ti substrates is related to the harder rutile oxide layer formed on the oxidized surface. Also, Fei et al. [373] and Usta et al. [374] reported similar results, as these authors found that the PEO treatment increases the wear resistance of Ti and its alloys by increasing the thickness, crystallinity and hardness of the oxide layers. In fact, superior wear resistance and high frictional coefficients were observed at applied loads up to 50 N. This is due to the presence of hard and thick oxide layers that supported the applied load protecting the substrate [375]. Furthermore, the use of alkaline electrolytes makes the PEO process sustainable and environmentally friendly.

Chemical methods such as sol-gel are also used to improve the tribological properties of Ti implant materials. TiO₂ coatings deposited on Ti alloys using the sol-gel method were found to exhibit improved corrosion resistance [376,377]. Zhang et al. investigated the tribological properties of SiO₂, TiO₂ and HA ceramic films deposited on Ti surfaces by the sol-gel method and the wear resistance of all sol-gel ceramic films was superior compared to the untreated Ti substrate. However, among them, the TiO₂ coating showed good wear resistance under a load below 1 N, while the HA coating exhibited the best resistance and the SiO₂ coating had the worst resistance under loads below 1 N and above 3 N [378]. The superior tribological properties of the HA coatings is due to the limited plastic deformation and the specific microstructure of these deposits [378,379].

Several authors have also used physical methods such as ion implantation to improve the mechanical properties and biocompatibility of Ti surfaces [155,380]. For instance, Leng et al. have shown that the PIII of oxygen ions on Ti is very effective in improving the wear resistance of Ti alloys under low load. The microhardness of the oxidized TiO_x films increased with increasing the oxygen partial pressure in the range 0-3x10⁻² Pa and reached a maximum value of 17 GPa at an oxygen pressure of 3x10⁻² Pa. Despite these positive results, the thickness of the prepared coatings was too thin and therefore suboptimal for bone applications [381]. Moreover, Mohan et al. demonstrated that PIII of oxygen facilitated the growth of the apatite phase on Ti alloys, which greatly improved the wear resistance and lowered the frictional coefficient. In addition, oxygen implanted Ti

exhibited a better passivation behavior in Hank's solution [382]. Tian et al. also showed that increasing the oxygen implantation time and RF power can further improve the wear and corrosion resistance of Ti surfaces. This may be due to the formation of a thick oxide layer formed after oxygen ion implantation, which significantly hinders the charge transformation as the treated samples returned a reduced corrosion current [383]. An overview of TiO_2 coatings with improved tribological properties is presented in **Table 3.7**.

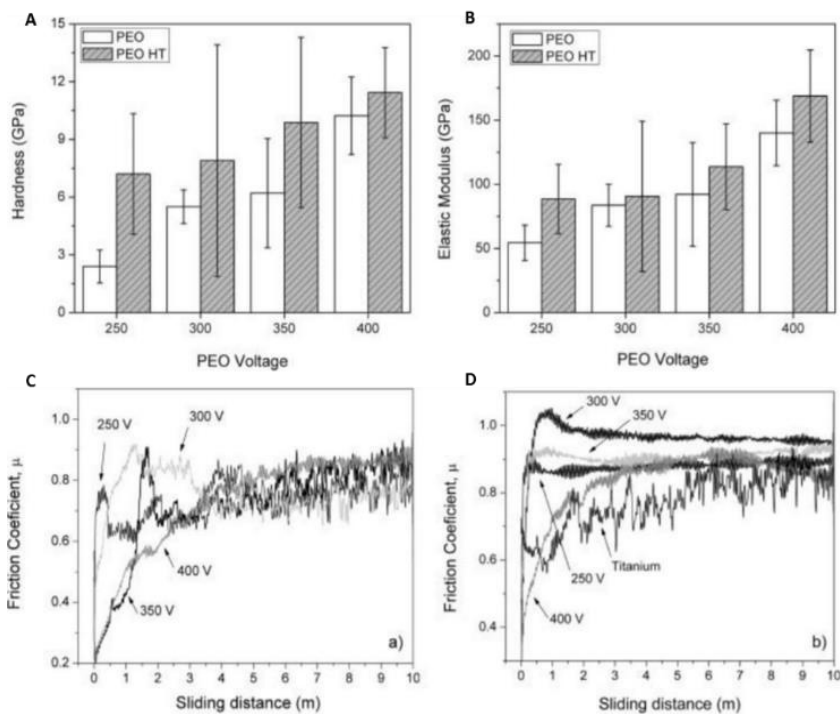


Figure 3.10. Hardness (A) and elastic modulus (B) as a function of the applied voltage before and after heat treatment (HT), frictional coefficient as a function of sliding distance for PEO samples before (C) and after HT (D) [368].

Table 3.7. Overview of literature on TiO_2 coatings deposited on Ti and its alloys with improved tribological properties not discussed in the main text.

Coating	Technique	Experimental model	Results	Ref
TiO ₂ (electrolyte solution: H ₂ SO ₄ + H ₃ PO ₄)	PEO	Tribo-electrochemical test	<ul style="list-style-type: none"> - Higher corrosion resistance due to low capacitance of the oxide layer - Fretting fatigue cracks present in PEO-treated Ti - Abrasive wear cracks present in PEO-treated Ti-6Al-4V 	[384]
TiO ₂ (electrolyte solution: Na ₂ SiO ₃ + Na ₂ CO ₃ + ethylenediaminetetraacetic acid (EDTA))	PEO	Wear test: ball-on-disk (dry friction)	<ul style="list-style-type: none"> - Formation of rutile phases - Increased surface roughness - Reduced frictional coefficient from 0.5 to 0.4 	[373]
TiO ₂ (electrolyte solution: Na ₂ SiO ₃)	PEO	Fretting fatigue test (dry and oil lubrication)	<ul style="list-style-type: none"> - Reduced frictional coefficient under oil lubrication 	[385]
Al ₂ O ₃ /TiO ₂ & ZrO ₂ /Al ₂ O ₃ /TiO ₂ multilayered coatings	Plasma spraying	Rockwell scratch test Wear test: ball-on-disc	<ul style="list-style-type: none"> - 200-500 fold increase in wear resistance in bilayered Ti coatings - Increased scratch resistance and adhesion strength in bilayered coatings compared to other coatings 	[386]
TiO ₂ (electrolyte solution: Na ₂ SiO ₃ + NaPO ₃ + NaAlO ₂ with/without Al ₂ O ₃ microparticles)	PEO	Wear test: ball-on-disc (dry friction)	<ul style="list-style-type: none"> - Better wear resistance and increased hardness on coatings with Al₂O₃ 	[387]
TiO ₂	PIII	Wear test: pin-on-disc (dry friction)	<ul style="list-style-type: none"> - Increased hardness on TiO₂ films with higher oxygen partial pressure 	[381]

			-Better wear resistance on coated Ti under a small load.	
--	--	--	----------------------------------------------------------	--

3.4.2 Titanium nitride coatings

Titanium nitride (TiN) is a hard ceramic material used as a coating on Ti and its alloys, steel, and aluminum to improve the material's surface properties. Various techniques are available to produce a TiN coating on a Ti surface, including the direct reaction of Ti, ion implantation, physical vapor deposition, plasma ion nitriding, powder immersion reaction assisted coating (PIRAC) and the Hardion+ nitrogen implantation technique [388–394]. Budzynski et al. [395] investigated the tribological properties of surface modified Ti alloys by nitrogen implantation. Nitrogen ions were implanted with carbon Ti(C, N) and without carbon deposition (TiN) to observe the influence of carbon on the mechanical properties of TiN coatings. The frictional coefficient was reduced by a factor of 3 for the coating with carbon deposition Ti(C, N). Moreover, improved wear resistance and increased hardness were observed on all nitrogen implanted samples. The TiN-coated Ti alloys also showed a high scratch resistance, a low coefficient of friction, improved fretting and improved corrosion resistance compared to uncoated Ti [396,397]. A hip stimulator test was also performed by Gutmanas et al. and Pappas et al. to study the wear mechanism of TiN-coated Ti against an ultra-high molecular weight poly ethylene (UHMWPE) acetabular cup [390,398]. Ti femoral heads with a diameter of 32 mm were coated with several μm thick TiN layers using PIRAC which produced nitriding due to interaction of the Ti alloy with highly reactive monatomic nitrogen. The coated Ti heads were subsequently tested against UHMWPE cups at peak pressures in a constant rotation mode at 37°C. It was observed that the wear rate of the UHMWPE cups articulating against the TiN-coated heads was greatly lowered [390]: the average maximum reduction in thickness of UHMWPE was $< 2 \mu\text{m}$ in the case of the TiN-coated samples [398]. It was also shown that TiN-coated Ti-6Al-4V and commercially pure Ti showed no signs of surface delamination, wear, and coating failure in hip and knee simulator tests [390,398,399]. However, TiN-coated Ti-6Al-4V using PVD was prone to more pitting

and blistering during corrosion testing and exhibited coating adhesion failure [400]. In addition to the preclinical studies mentioned before, clinical studies were also performed to evaluate the survival of TiN-coated orthopedic implants. These studies revealed that loosening of the femoral component occurred in 44 % of the patients who received TiN-coated Ti hip implants [401]. Moreover, TiN coating breakthrough and fretting also occurred in prostheses retrieved at revision surgery [402], and one year after the surgery TiN-coated Ti-6Al-4V femoral heads exhibited circular voids without TiN coating but instead filled with droplets of pure Ti [403]. These adverse effects might be related to the unoptimized coating process of TiN. Therefore, more studies have to be performed to optimize and standardize the used TiN coating techniques. Studies focusing on TiN coatings are summarized in **Table 3.8**.

Table 3.8. Overview of literature on TiN coating son Ti and its alloys not discussed in the main text.

Coating	Technique	Experimental model	Results	References
TiN	Cathodic arc deposition	Nanoindentation scratch tests Wear test: Ball-on-disc & pin-on-disc	- Hardness increased seven times compared to uncoated Ti - <i>In-vitro</i> wear rate was four times lower than for uncoated Ti - <i>In-vitro</i> corrosion resistance increased due to hydrophilicity of the coating	[404]
TiN	PVD-magnetron sputtering	Wear test: pin-on-ring(dry sliding)	- Significant improvement in wear resistance - Increased surface roughness -Reduced frictional coefficient	[405]

TiN	Cathodic arc deposition - PVD	Rockwell scratch test Wear test: ball-on-disc (dry friction) & Nanoindentation	- Worn out of TiN coating during wear test - Reduced frictional coefficient on coated Ti	[406]
TiN	Plasma assisted electron beam PVD	Knoop microhardness test Microindentation, <i>In-vitro</i> corrosion test	- Superior pitting resistance on coated Ti - Improved wear and corrosion performance - Failure of TiN films after cyclic loading	[407]
TiN	PVD	Flat-on-flat fretting fatigue test	- Fretting fatigue life improved on the coated Ti alloy - Reduced frictional coefficient and surface damage	[408]
TiN	Nitrogen ion implantation	Nanoindentation Ball-on-flat fretting test (dry friction & bovine serum lubrication)	- Increased nanohardness (7.7 GPa) - Reduced frictional coefficient in dry friction compared to lubrication - Improved fretting wear resistance both in dry/lubrication conditions	[409]
TiN	Plasma nitriding and magnetron sputtering (duplex treatment)	<i>In-vitro</i> corrosion test (artificial saliva)	- Improved corrosion resistance of treated Ti samples	[410]
TiN and Ti silicon nitride (TiSiN) nanoco	Pulsed DC PACVD	Vickers microhardness test Rockwell scratch test, Wear test: ball-on-disk (SBF lubrication)	- TiN and TiSiN coatings exhibited improved hardness, wear resistance and corrosion	[411]

composite coatings		<i>In-vitro</i> corrosion test (SBF)	resistance while superior anti-wear and anti-corrosion properties were observed for TiSiN due to the presence of Si.	
TiN	Plasma source ion nitriding	Vickers microhardness test Wear test: ball-on-disk(dry sliding) <i>In-vitro</i> corrosion test	- Improved microhardness on nitride Ti samples - Improved wear resistance and pitting corrosion on treated samples	[412]
TiN	Plasma nitriding	Fretting wear test for 50,000 cycles (counter - alumina ball)	- Improved hardness and reduced tangential force coefficient on nitride samples	[413]

3.4.3 Diamond-like carbon (DLC) coatings

DLC is a class of amorphous carbon material composed of diamond and graphite (sp^3 and sp^2) bonds that is applied for surface enhancement of materials used in biomedical applications due to its superior mechanical properties. DLC coatings have superior hemocompatibility, corrosion resistance, wear resistance, hardness, and a low frictional coefficient. Various surface modification techniques have been applied to produce DLC coatings using different carbon-based precursors such as plasma-assisted chemical/physical vapor deposition, magnetron sputtering, ion beam sputtering, pulsed laser deposition and mass-selected ion beam deposition [60,414–416]. Many extensive reviews on carbon-based coatings have already been published in the past years, which have described in detail the different deposition techniques, deposition mechanisms, surface properties, biocompatibility and biomedical applications of DLC-based coatings. Therefore, in this section, only the tribological properties of

DLC-based coatings deposited on Ti implant surfaces and its major influencing factors will be discussed.

The tribological properties of DLC-based coatings depend on various factors such as the sp^3/sp^2 ratio, the presence of hydrogen and carbon in the films, the adhesion mechanism, the used deposition technique, the precursor materials, the deposition rate and the substrate itself.

Saenz de Viteri et al. investigated the tribological properties of Ti-C-N coatings deposited on Ti alloys by PVD using the cathodic arc evaporation (CAE) method [417]. A very pure Ti layer (1 μm thickness) using a very high bias voltage was deposited on a Ti substrate to ensure adhesion. In a next step, five different types of Ti-C-N coatings were deposited using a reactive gas mixture of nitrogen and acetylene. All Ti-C-N coatings exhibited a reduced frictional coefficient and wear; however, the coating with low acetylene content exhibited the best tribological performance. This is due to the larger sp^3/sp^2 ratio on this particular coating which provided the necessary hardness (10 GPa) and a monocrystalline graphite (nc-G) and amorphous carbon (a-C:H) structure, which in turn resulted into the best wear resistance of this coating. Improved tribological performance was thus observed on coatings possessing a higher sp^3 contribution, as sp^2 bonded carbon tend to be relatively soft (as in graphite) while sp^3 bonded carbon are hard (as in diamond). This phenomenon was further investigated by Du et al. who performed a comparative study of the influence of DLC and graphite-like coatings (GLC) deposited by closed field unbalanced magnetron sputtering on the behavior and mechanism of fretting wear and fretting fatigue resistance of Ti alloys. The obtained results revealed that the bonding strength and toughness of the DLC coatings were superior to those of the GLC coatings. While both coatings reduced the friction factor, wear resistance and fatigue resistance was better for the DLC coatings due to the presence of sp^3 bonds [418].

To investigate the effect of carbon on DLC coating behavior, Bayon et al. fabricated different DLC coatings with different carbon content on Ti alloys via cathodic arc evaporation. All DLC coatings exhibited good corrosion resistance, high electrochemical stability, and notably reduced friction and wear compared to untreated Ti. However, the DLC coating with high carbon content exhibited superior tribocorrosion performance compared to the coating with low carbon

content [419]. Despite these positive results, the successful application of DLC coatings has been compromised due to the release of residual stress as high as 10 GPa or more, which inevitably limits the coating thickness and adhesive strength between the coating and the substrate as it leads to coating delamination [420,421]. To combat this problem, various methods have been used to improve the adhesion strength and reduce compressive stress. Firstly, cleaning the surface of the substrates with Ar ion or N₂ ion bombardment prior to coating deposition can improve the interfacial adhesion strength. Secondly, forming an interface between the substrate and the coating can also increase the adhesion strength. Thirdly, doping metal or non-metal elements in the films (Ti, Cr, Si) to reduce its internal stress is also an effective way to obtain a high adhesion strength. Fourthly, a multilayer approach using an alternating soft coating or a nanocomposite coating comprising two interpenetrating a-C:H networks is another effective method to increase the adhesion strength. Finally, functional grading and bias grading methods are also proposed to overcome the residual stress and to improve the adhesion strength. To investigate the influence of bias grading on the coating adhesion strength and tribological behavior, Cai et al. deposited an a-C:H gradient composite coating on a Ti substrate using magnetron sputtering by gradually varying the bias voltage (-20 to -150 V). The results showed that the bias graded coating exhibited excellent tribological performance along with a reduction in residual stress. Compared to the constant bias film (-150 V), the bias graded film had high hardness (19 GPa), a high toughness and a high adhesion strength. Both the frictional coefficient and wear rate decreased with increasing the applied load, and the bias graded coating exhibited a low wear rate in Hank's solution [422]. The observed effect is due to the structure of the coatings obtained at bias graded voltage. At low bias voltage, the graphite-like bonds were dominating in the films, indicating less residual stress and lower hardness, while more diamond-like bonds were produced and the sp³ content reached the maximum value when the bias voltage was increased to -150 V. However, at constant bias voltage (-150 V), the dissipation of the excess heat generated by the impinging of the energetic ions can relax the high compressive stress and loose carbon networks, hence, the sp³ content decreases and graphite-like bonds form in this case. Therefore, when a bias voltage is used to

deposit an a-C:H film from the bottom to the surface, a soft layer will gradually turn into a hard layer, thus increasing the hardness, toughness and adhesion strength. Zhang et al. [421] and Wang et al. [421] reported similar results, as these authors deposited a bias graded diamond-like coating and a Ti-doped a-C:H coating via magnetron sputtering and the cathodic arc method. The aforementioned studies observed that the bias graded coating had the highest sp³ fraction at the surface and this fraction gradually decreased at the interface which in turn facilitated the best adhesion strength.

Improving the surface properties of Ti implants may also improve the tribological properties of the material that it is articulating with. Dong et al. demonstrated that DLC coatings produced by PVD on Ti counterfaces improved the tribological behavior of UHMWPE under water lubricated sliding conditions [423]. Similar results were observed on PECVD DLC-coated stainless steel during a pin-on-flat test, exhibiting a reduced frictional coefficient and a reduced wear rate [424].

Although many studies have reported promising results on the tribological properties of carbon films, some contradictory findings were also reported [425]. Although positive effects of the coating were obtained during pin-on-disk and ball-on disk tribology tests, no significant effect was observed when tested on hip or knee joint simulators [423]. In addition, a Swiss company “Implant design AG” reported the failure of DLC coatings in orthopedic implants: DLC-coated knee joints exhibited excessive wear and spallation when articulated against UHMWPE. Clinical tests performed on DLC-coated implants reported that the failure rate of DLC-coated Ti femoral heads was much higher than in case of alumina femoral heads [426,427]. It is therefore essential to perform more *in-vitro* and *in-vivo* tests to confirm the potential of DLC coatings in prosthetic joints. An overview of additional literature focusing on DLC coatings is given in **Table 3.9**.

Table 3.9. Overview of literature on DLC coatings on Ti and its alloys not discussed in the main text.

Coating	Technique	Experimental model	Results	References
DLC	Ion implantation (Ar + C ₂ H ₂) with and without carbon implantation (CH ₄)	Nanoindentation adhesion tests	- Carbon implantation improved the adhesion strength of DLC coatings to metals	[428]
DLC	Plasma assisted chemical vapor deposition (PACVD)	Nanoindentation Wear test: ball-on-disk (dry sliding)	- 3.5 fold increase in hardness of coated Ti. - Reduced frictional coefficient and wear rate.	[429]
DLC	RF (PACVD)	Cyclic loading test	- Reduced Ti implant loosening	[430]
DLC	Magnetron sputtering	Wear test: ball-on-plate(dry sliding & lubrication)	- Reduced frictional coefficient on DLC coated Ti. - Improved wear resistance under dry friction.	[431]
a-C:H gradient composite coatings	Bias graded magnetron sputtering	Nanoindentation, Scratch test Wear test: ball-on-disk (dry sliding)	- Improved adhesion strength. - Decreased frictional coefficient & decreased wear rate	[422]

a-C/a-C:Ti multilayer composites	Magnetron sputtering	Rockwell test Nanoindentation Wear test: ball-on-disk (dry sliding)	- Improved hardness (26 GPa) & elastic modulus (232 GPa). - Improved adhesion strength. - Decreased frictional coefficient (0.09) & decreased wear rate	[432]
a-C/a-C:Ti multilayer film	Magnetron sputtering	Nanoindentation Scratch test Wear test - ball-on-disk	- Improved adhesion strength due to thin interlayer. - Low frictional coefficient (in humid air) & improved wear resistance	[433]

4 Conclusion

More than 1000 tons of Ti-based devices of every description and function are implanted in patients every year. Ti and its alloys are widely used in biomedical implants such as joint prostheses, fracture fixation devices, dental implants as well as in cardiovascular devices due to their outstanding mechanical properties and excellent corrosion resistance. Even though Ti implants are expected to last for at least a decade or more, they often fail prematurely, resulting in revision surgery that is usually characterized by a higher level of complexity and that forms a heavy burden on the current healthcare systems. Although a large number of coatings have been applied to Ti surfaces using a variety of surface modification techniques, still only a few studied coatings have multi-functions and only very few of them have come into clinical practice. Therefore, immense work should still be done to validate the existing potential coatings and to develop new coating candidates.

Chapter 4. Materials and Methods

4.1 Introduction

In this chapter, an overview of all experimental techniques used in this dissertation will be given. After describing the preparation of Ti test specimens, the different coating deposition techniques used in this study will be presented. Then, a brief overview of the used surface characterization tools used will be given. Finally, the different methodologies used to investigate the *in-vitro* antibacterial and cell-interactive properties of the deposited coatings will be described.

4.2 Preparation of Ti test specimens

Commercially used pure Ti sheets with a thickness of 3 mm were waterjet cut (L&D Techniek NV) into discs with a diameter of 12 mm containing a circular opening of 2 mm diameter with the center of the opening at 3 mm from the top (Figure 4.1). Based on the measured dimensions, the surface area of the disc was calculated and found to be 339 mm².

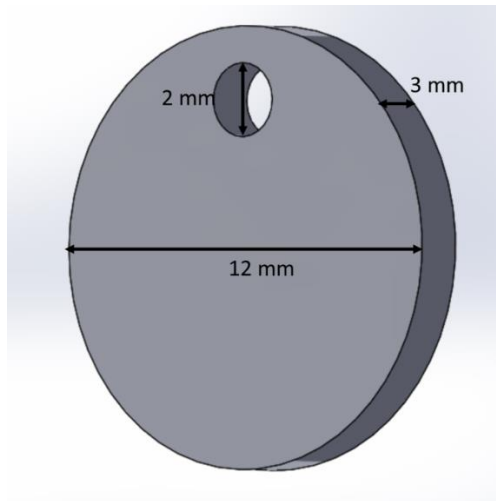


Figure 4.1. Schematic diagram of the titanium disc along with its dimensions.

Prior to coating deposition, all Ti discs were ground with successive 400, 800 and 1200 SiC abrasive papers (Struers) using water as a lubricating agent. After grinding, the samples were polished with MD Largo (Struers) using diamond paste as a lubricating agent to obtain a smooth mirror-like polished surface. After this procedure, all samples

were ultrasonically cleaned with acetone, ethanol, distilled water and air-dried.

4.3 Coating deposition methods

4.3.1 PEO deposition

A laboratory-scale in-house set-up was customized to conduct a PEO deposition process on Ti discs and the set-up is schematically represented in **Figure 4.2**. The main components of the system are a DC power supply (DSC electronics, DP15H-1D), a double-walled cylindrical stainless steel tank with two electrodes (stainless steel acts as a counter electrode and the Ti specimen as an anode) and a water cooling system (Julabo, F250) to maintain the temperature during the deposition process.

4.3.1.1 Deposition of Ag-doped oxide coatings

To deposit oxide coatings (TiO_2) on Ti discs, an electrolyte was prepared by dissolving 0.4 g/L sodium hydroxide (NaOH) and 4.0 g/L sodium dihydrogen phosphate (NaH_2PO_4) in 1L of distilled water. To synthesize microporous TiO_2 surfaces containing AgNPs, different concentrations of AgNPs (concentrations of 0.1 g/L, 0.5 g/L and 1.0 g/L) were dispersed in freshly prepared electrolyte. The particle suspension was then stirred for 3 hours using a magnetic stirrer (500 rpm) for better suspension of the AgNPs in the electrolyte. 150 mL of the electrolyte was added to the double-walled stainless steel electrolytic cell for the synthesis of the coatings.

4.3.1.2 Deposition of Ca/P/Ag-doped oxide coatings

To deposit un-doped and Ag-doped TiO_2 coatings, a second type of electrolyte was also prepared by dissolving 2.0 g of sodium dihydrogen phosphate dihydrate ($\text{NaH}_2\text{PO}_4 \cdot 2\text{H}_2\text{O}$) and 5.0 g of calcium acetate monohydrate ($\text{Ca}(\text{OOCCH}_3)_2 \cdot \text{H}_2\text{O}$) in 1L of distilled water with and without the addition of silver acetate (AgOOCCH_3) (concentrations of 0.1 g/L, 0.5 g/L, 0.8 g/L) respectively. The suspension was then stirred for 1 hour using a magnetic stirrer (500 rpm) for better suspension of the electrolyte. 150 mL of the electrolyte was added to the double-walled stainless steel electrolytic cell for the synthesis of the coatings.

4.3.1.3 PEO deposition process

It is important to note that the following steps used for the synthesis of the PEO coatings are identical for the Ag-doped and the Ca/P/Ag-doped

coatings. The electrolyte was cooled to approximately 5°C by circulating a mixture of water and glycerol through the double walls of the electrolytic cell using a thermostatic water cooling bath. The temperature of the electrolyte was kept at $25 \pm 5^\circ \text{C}$ during the treatment to prevent chemical dissolution of the coating. Subsequently, the PEO synthesis was performed at a fixed voltage of 400 to 500 V for 5 min. After the treatment, the coated Ti samples were washed with ethanol and distilled water and were finally air-dried.

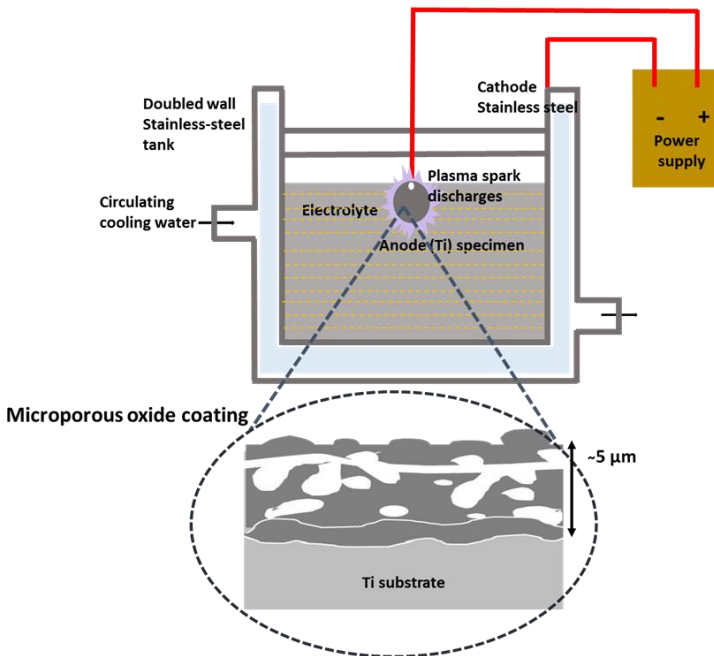


Figure 4.2. Schematic diagram of the PEO experimental device used for the fabrication of microporous oxide coating.

4.3.2 Cluster source deposition

Besides PEO deposition, also cluster source deposition was performed in this dissertation to deposit coatings on Ti discs. This cluster source deposition was conducted at the facilities of the Department of Macromolecular Physics, Charles University, Prague. The used

experimental set-up consisted of two systems, as shown in **Figure 4.3**: a magnetron-based gas aggregation source (GAS) for the deposition of metal NPs and a deposition chamber for the deposition of plasma polymeric thin films. The different deposition processes performed using the cluster source will be given in the following sections.

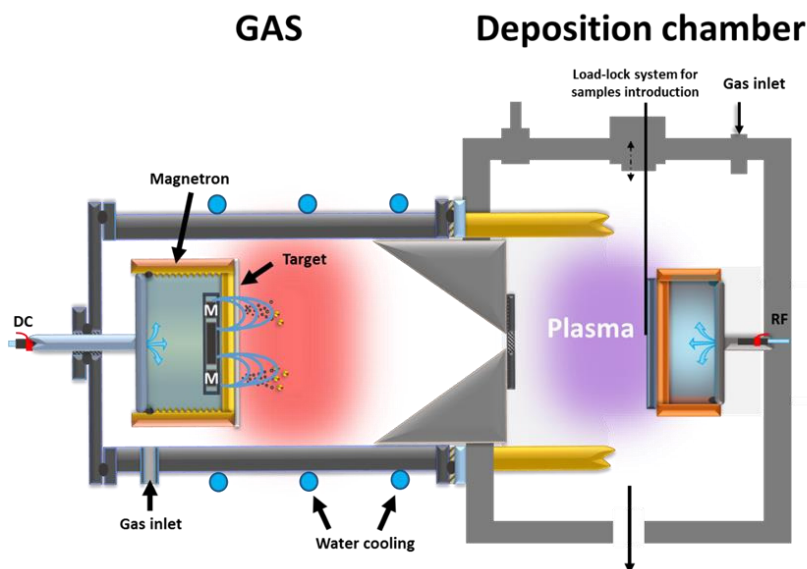


Figure 4.3. Schematic representation of the cluster source utilized for the fabrication of metallic NPs and thin plasma polymeric films.

4.3.2.1 Deposition of amorphous hydrocarbon (a-C:H) plasma polymer thin films

The deposition of amorphous hydrocarbon (a-C:H) plasma polymer films was performed in an high vacuum stainless steel chamber equipped with a planar electrode powered by an RF power supply (Dressler Cesar 133) through a matching box. The schematic representation of the deposition chamber is shown in **Figure 4.4**. The Ti substrates were placed directly on the RF electrode (position 1 in **Figure 4.4**) for the deposition of hard a-C:H coatings. The deposition chamber was pumped using diffusion and rotary pumps up to a base pressure of 10^{-4} Pa. The deposition chamber was equipped with a load-lock system (position 2 in **Figure 4.4**) with additional diffusion and

rotary pumps to enable easy transfer of the substrates. Needle valves were used to ensure a continuous flow of working gas (Ar) and the precursor (n-hexane) into the deposition chamber. A gas mixture of Ar and n-hexane was determined by a 7:1 ratio of partial pressures, with 5.6 Pa of total pressure inside the deposition chamber. The pressure in the deposition chamber was measured by means of a baratron (1 Torr, MKS) connected to a two-channel digital readout (PDR2000A, MKS). The discharge power was set at 70 W with a negative self-bias voltage of 400 V. The deposition rate was 40 nm/min and the thickness of the a-C:H matrix was maintained at 100 nm (treatment time fixed at 2.5 min).

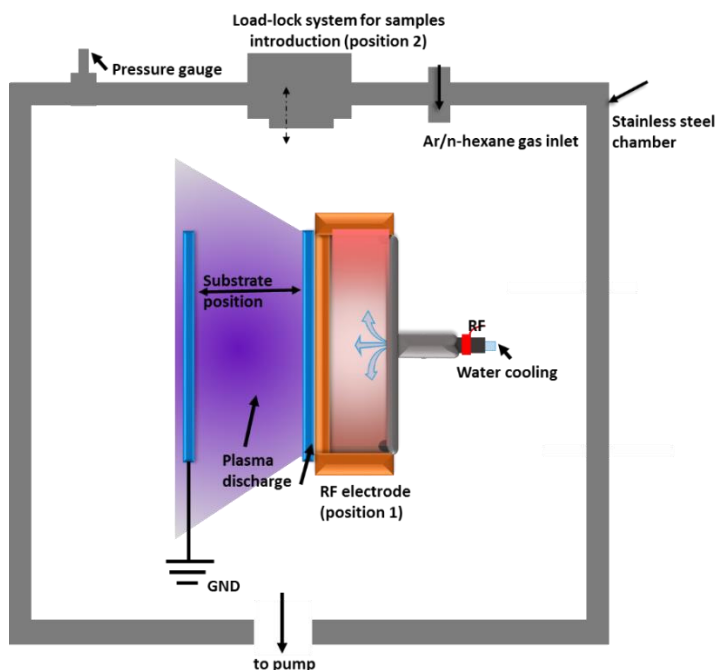


Figure 4.4. Schematic arrangement utilized for the deposition of amorphous hydrocarbon thin films (a-C:H) thin films, plasma activation and plasma etching of as prepared nanocomposite and nanolayered coatings.

4.3.2.2 Deposition of NPs by GAS

The Haberland type GAS was used in this PhD study for the production of NPs and a schematic representation of the GAS system is shown in **Figure 4.5**. The water cooled GAS aggregation chamber consists of a tube-like case that ends with a cone of 2 mm orifice connecting the GAS to the deposition chamber described above. The GAS was equipped with a DC planar magnetron and the pressure difference between both chambers (GAS and deposition chamber) directed a beam of NPs into the deposition chamber, providing a soft landing of the NPs onto the Ti substrate which was placed 18-20 cm away from the orifice.

NPs (AgNPs, CuNPs) were produced in this work using a GAS equipped with an 81 mm planar magnetron covered by a 3 mm thick silver/copper target (Safina, purity 99.99%). The magnetron was powered by an Advanced Energy MDX 500 DC power supply operated in constant current regime. The number of produced NPs was tailored by varying the DC magnetron current from 200 mA to 500 mA. Ar (purity 99.99 %) was used as buffer gas and the pressure in the aggregation chamber was maintained at 100 Pa.

4.3.2.3 Plasma activation

Prior to the deposition process, the mirror-like polished Ti discs were plasma pre-treated in Ar plasma followed by a N₂ plasma to provide good adhesion between the Ti substrates and the functional coatings. The plasma pre-treatment step was performed in the same deposition chamber as mentioned above and the samples were placed on the RF electrode (position 1 in **Figure 4.4**). The discharge was ignited at a power of 70 W with a pressure of 4.5 Pa for Ar and a pressure of 2.5 Pa for N₂. The plasma activation step was performed for 2 min and 10 min respectively.

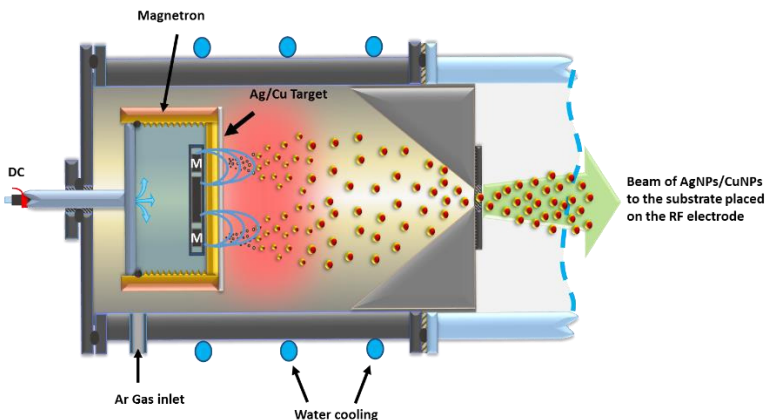


Figure 4.5. Schematic arrangement of the GAS utilized for the fabrication of metallic NPs.

4.3.2.4 Fabrication of functional antibacterial coatings

Deposition of NPs/amorphous hydrocarbon (a-C:H) nanocomposite coatings

Hard nanocomposite coatings incorporating AgNPs/CuNPs were prepared by simultaneous deposition of NPs and plasma polymerization of the monomer n-hexane. As mentioned earlier, the NPs were produced by the GAS and the beam of the NPs was directed onto the Ti substrates placed directly on the RF electrode as it is depicted in **Figure 4.6.A**. The RF discharge was operated in pulsed regime with a frequency of 1 Hz and a duty cycle of 50 %. Under these conditions, the NPs reach the RF electrode (substrate) only during T_{off} . The discharge power was set at 70 W with a negative self-bias voltage of 400 V. The deposition time was kept constant (5 min) which guarantees a similar thickness of the a-C:H matrix (100 nm) (**Figures 4.6.B and C**). The number of NPs incorporated within the a-C:H matrix was tailored by varying the DC magnetron current from 200 mA to 500 mA. This set-up allows independent control of the amount of AgNPs/CuNPs incorporated and the properties of the plasma polymer a-C:H matrix.

Oxygen plasma etching

The effect of oxygen plasma etching on as-prepared nanocomposite coatings was also investigated (**Figures 4.6.C**). The etching step was performed using the same deposition chamber and the Ti samples were placed on the RF electrode. The RF power was set at 16 W with a corresponding negative self-bias of approximately 160 V. The oxygen pressure was set to 2.5 Pa and the etching time was kept constant at 4 min. Using these experimental conditions, the etching rate of the a-C:H matrix was found to be 8 nm/min.

Deposition of nanolayered coating

The deposition of nanolayered coatings was performed using the same parameters as applied for the deposition of the nanocomposite coatings, but instead of simultaneously depositing the NPs and the plasma polymer matrix, a layer-by-layer deposition approach was followed. The thickness of the first a-C:H layer (the reservation layer) was maintained at 60 nm by setting the deposition time to 1.5 min while the thickness of the second a-C:H layer (the barrier layer) was maintained at 10 nm or 20 nm by varying the deposition time to 13 sec and 27 sec respectively (**Figure 4.6.D**). In order to produce coatings with the same amount of incorporated NPs as in the case of the nanocomposite coatings (**Figure 4.6.C and D**), the deposition time of the NPs was maintained at 2.5 min which corresponded to the deposition time of NPs during the fabrication of the nanocomposite coatings.

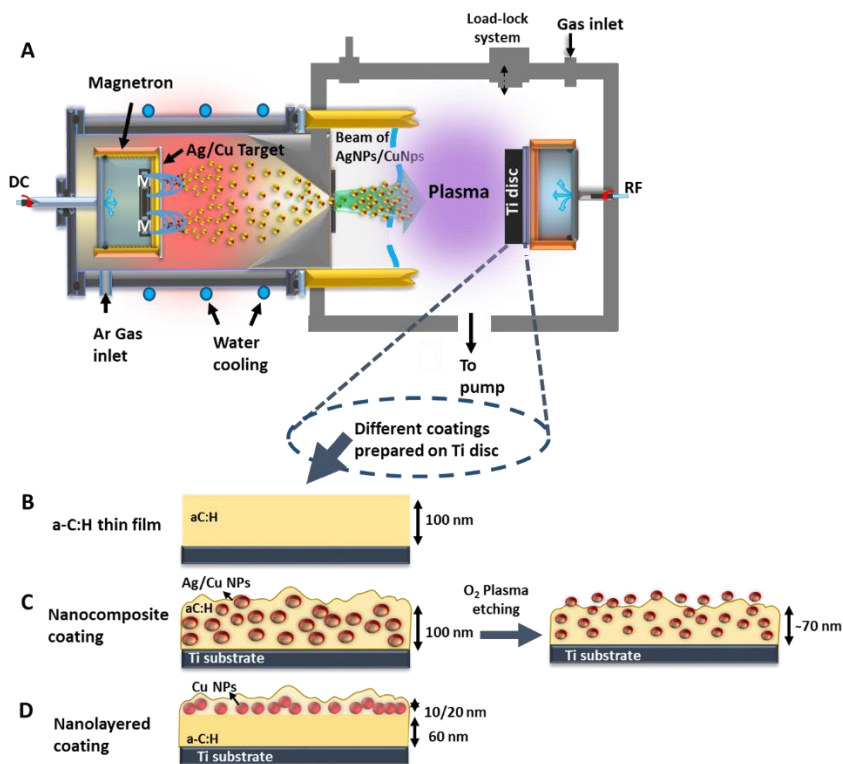


Figure 4.6. Schematic representation of the experimental setup (A) used for the fabrication of a-C:H films (B), nanocomposite (C) and nanolayered (D) coatings.

4.4 Coating characterization techniques

4.4.1 Surface chemical analysis: X-ray photoelectron spectroscopy (XPS)

XPS is one of the most powerful surface analysis techniques that allows determining the elemental composition as well as the chemical bonds present in the near-surface regions. XPS spectra are typically obtained by irradiating the material under investigation with a beam of monochromatic X-rays, after which the photoelectrons escaping from the top 0-10 nm of the material are quantified as a function of their kinetic energy. As the kinetic energy (E_{kin}) of the emitted photoelectrons is subsequently recorded, the binding energy (E_{bin}) of the emitted photoelectrons can be measured using equation 4.1:

$$h\nu = E_{\text{bin}} + E_{\text{kin}} + \Phi \quad (4.1)$$

where ν is the frequency of the X-ray beam, h is Planck's constant and Φ is the work function of the system, which is a small amount of energy used by the electrons to overcome the electron binding energy. The physical principle of XPS is depicted in **Figure 4.7.A**, where an incident X-ray beam with an energy $h\nu$ hits an electron of the inner shells transferring its energy to the target electron. When the transferred energy is higher than the electron binding energy plus the material work function, photoelectrons with specific kinetic energy will be emitted. The binding energy of these emitted electrons can provide information on how strongly the particular electron is bound to the nucleus, which greatly depends on the type of the atom as well as on the interaction with nuclei of the surrounding atoms. As such, an XPS system can be used to identify elements as well as the chemical bonds present on the top surface of a material.

As shown in **Figure 4.7.B**, an XPS system typically consists of a monochromatic X-ray source (Al monochromator: 1486.6 eV), a hemispherical analyzer, an electron detector to convert the emitted electrons into an electric signal and a computer to translate the detector signal into an appropriate XPS spectrum. The XPS system requires a high vacuum or ultra-high vacuum to avoid collisions of photoelectrons with the inner gas and to avoid surface contaminations during the measurements. A typical XPS system consists of an introduction chamber maintained in pre-vacuum, and a main chamber maintained in ultra-high vacuum conditions[434].

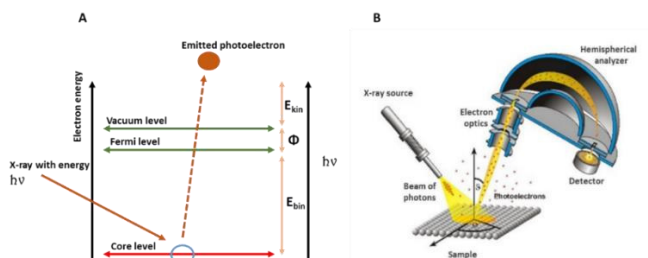


Figure 4.7. Schematic representation of XPS physical principle of photoelectron extraction from atom or molecules electronic orbitals (A) and simplified apparatus (B).

In this dissertation, the chemical composition of all coated and uncoated Ti samples was analyzed using a PHI 5000 Versaprobe II spectrometer. The samples were excited with a monochromatic Al K α X-ray source ($h\nu=1486.6$ eV) operating at a power of 25 W resulting in a beam size of 100 μm . During the analysis, the pressure in the XPS main chamber was maintained at 10^{-6} Pa or lower and the photoelectrons were detected with a hemispherical analyzer positioned at an angle of 45° with respect to the normal of the sample surface. Survey scans and individual high-resolution spectra were recorded with a pass energy of 187.85 eV (eV step = 0.8 eV) and 23.5 eV (eV step = 0.1 eV) respectively. For each condition, 4 randomly chosen spots on a single sample were selected for measurements. The elements present on the Ti samples were identified and quantified from XPS survey scans using Multipak software (Version 9.6.2) and the results are presented as the average of 4 different measurements on a single sample. Calibration of the energy scale (C-C =285 eV) was first performed after which an iterated Shirley background was applied to determine the elemental composition using the relative sensitivity factors supplied by the manufacturer of the XPS device. Curve peak fitting of the high-resolution peaks was also done making use of Multipak software after applying a Savitzky-Golay smoothing procedure. The peaks were deconvoluted using Gaussian-Lorentzian peak shapes, keeping the full width at half-maximum below 1.8 eV and the χ^2 value below 2.

4.4.2 Coating crystallinity: X-ray powder diffraction crystallography (XRD)

XRD is one of the commonly used analytical techniques for the determination of crystalline substances present in a material. The basis of this technique relies on the fact that crystals present in a material contain periodic arrangements of atoms, thus X-ray diffraction is obtained by the constructive interference of monochromatic X-rays and a crystalline material. The schematic of the XRD principle is depicted in **Figure 4.8**. When an incident X-ray beam interacts with a material, it is reflected by different atomic planes and when the reflected beams are in phase (during constructive interference), they will be amplified; otherwise, they will be dismissed (during destructive interference). The relationship between the crystal

lattice plane spacing, the wavelength of the incident X-rays and the incident angle follows Bragg's law is given in equation 4.2:

$$2d\sin\theta = n\lambda \quad (4.2)$$

where d is the crystal lattice spacing, θ is the incident angle and λ is the incident X-ray wavelength. All possible diffraction directions of the lattice can be attained by scanning the sample through a range of 2θ angles. Different crystalline phases present in a material can be identified by converting the obtained diffraction peaks to d -spacings. A typical XRD device contains standard reference patterns which enable to compare the d -spacings.

In this dissertation, the crystalline structure of the different TiO_2 layers deposited by PEO on Ti substrates was studied using a powder X-ray diffraction ARL X'TRA diffractometer (Thermo Scientific) equipped with a $\text{Cu K}\alpha$ ($\lambda = 1.5405 \text{ \AA}$) source and operating at angles in the range of 20 - 80° . The integration time and scan rate were fixed at 1.2 s and 1° min^{-1} respectively. Analysis of the obtained XRD spectra was performed using the American mineralogist crystal structure database.

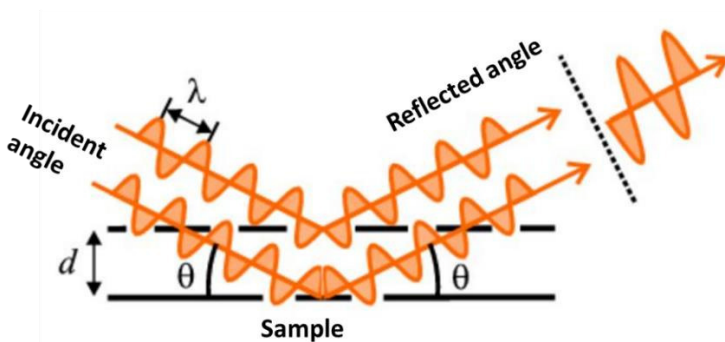


Figure 4.8. Schematic representation of the XRD principle

4.4.3 Surface wettability analysis : water contact angle (WCA)

WCA analysis is an easy and most commonly used method to analyze the wettability of a sample surface. Using this technique, surface wettability is evaluated by measuring the static contact angle formed by small droplets of distilled water on the studied surface. **Figure 4.9** gives a schematic representation of how the contact angle θ is defined:

it is the angle between a solid surface and the tangential line drawn through the three-phase boundary, where a liquid, gas, and solid interact. The contact angle can thus be considered as a quantitative measure of the relative amounts of adhesive (liquid to solid) and cohesive (liquid to liquid) forces counteracting each other and may vary between 0° and 180° . In essence, a low contact angle ($<90^\circ$) corresponds to high wettability (a hydrophilic surface), while a high contact angle ($>90^\circ$) corresponds to low wettability (a hydrophobic surface).

In this dissertation, to investigate the surface wettability of the uncoated and the coated Ti discs, static WCA measurements were performed at room temperature using a commercial Krüss Easy Drop optical system. Distilled water drops of $1\ \mu\text{L}$ were used as test liquid and the contact angles were obtained using Laplace-Young curve fitting. An average WCA value per sample condition was calculated based on WCA analysis of 3 different samples (3 water drops per sample).

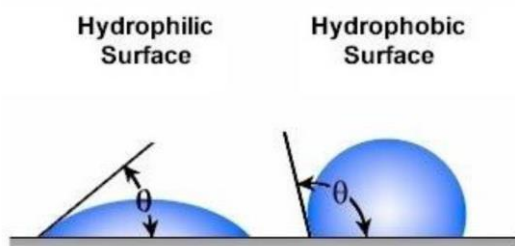


Figure 4.9. Principle of WCA measurements.

4.4.4 Surface morphology analysis : Scanning electron microscopy – Energy dispersive X-ray spectroscopy (SEM-EDS)

A scanning electron microscope is a type of electron microscope, where the beam of primary electrons is focused onto a sample surface resulting in a number of surface interactions (**Figure 4.10.A**):

- The emission of secondary electrons via inelastic scattering
- Reflection of high-energy electrons (backscattered electrons) via elastic scattering
- Absorption of an electron by the sample surface

- Emission of X-rays from the sample surface
- Photo-emission of the sample surface

Most of the occurring absorption and emission processes are interrelated and depend on the chemical composition and the chemical state of the sample and the surface morphology. In **Figure 4.10.B**, a simplified schematic of an SEM device is represented showing that a typical set-up consists of an electron gun, a set of focusing lenses, coils, and a special combination of detectors. An electron beam is generated either by thermionic emission or by a field emission gun, followed by accelerating and focusing of the electron beam using a series of electromagnetic lenses and beams, after which the beam reaches the sample under investigation. When the electron beam impacts onto the sample surface, several signals are generated and the most important ones include secondary electrons (SE), backscattered electrons (BSE) and characteristic X-rays, which are all applied in this dissertation. Secondary electrons that are ejected by inelastic scattering are low-energy electrons, and thus they originate from within the first few nanometers of the sample surface. Therefore, images from the SE detector carry information about the surface topography. BSE electrons consist of high-energy electrons originating from the electron beam, which are back-scattered from the sample surface by elastic scattering. Since high atomic number elements back-scatter more strongly than low atomic number elements, they appear brighter in SEM images. Thus BSEs can be used to detect the contrast between areas of different chemical elements [435]. In addition, the elemental composition of a sample and its distribution can be obtained by the emitted characteristic X-rays as a result of electronic transitions in ionized atoms, in a SEM device equipped with EDS. The size of the interaction volume extends from nm^3 to μm^3 depending on the energy of the incident electrons and the nature of the studied material.

In chapters 5 and 6 the surface morphology of the uncoated and PEO-coated Ti discs was analyzed using a JEOL JSM-6010 PLUS/LV SEM device operated at an accelerating voltage of 7 kV and a working distance of 11 mm. The cross-sectional morphology of the PEO-coated Ti samples was analyzed using a JEOL JSM-7600F field emission gun (FEG)-SEM device operating at an accelerating voltage of 15 kV and a working distance of 8 mm. In addition, cross-sectional elemental

mapping of the coatings was also performed with an energy dispersive spectrometer (EDS) present on the JSM-7600F FEG-SEM device. For each experimental condition, two samples were analyzed using both microscopes.

In chapters 7 and 8 the surface morphology of the Ti discs coated by the cluster source was analyzed using a SEM device (JSM-7200F, JSM-7600F FEG, JEOL) in backscattered electron mode. The microscope was operated under the following conditions: an accelerating voltage of 20 kV and 15 kV and a working distance of 10 mm. For each condition, 2 different samples were examined and all SEM images were analyzed using ImageJ (V 1.48) software.

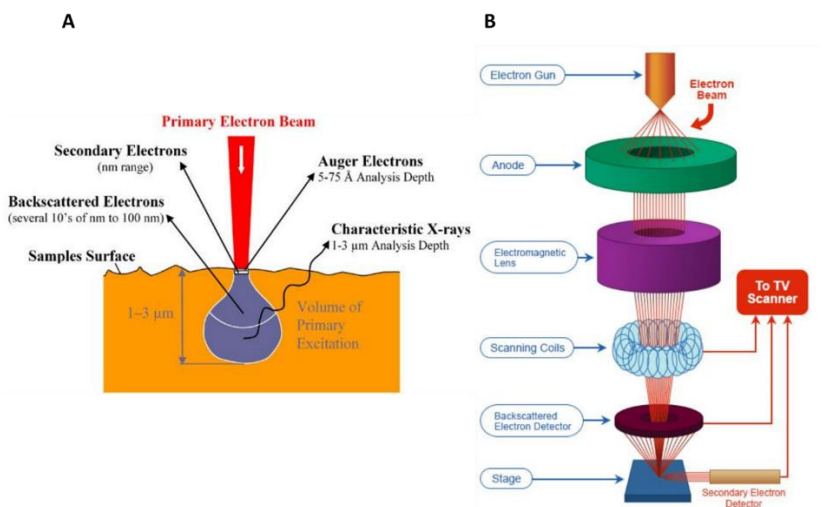


Figure 4.10. Schematic representation of electron beam-surface interactions (A) and a simplified SEM setup(B) [436].

4.4.5 Surface topographical analysis

Surface topography is defined by surface orientation and surface roughness and is characterized by a succession of peaks and valleys. Surface roughness is crucial for a bone implant material, and is dependent on micro-, macro- and nano-roughness. Distinct surface roughness levels result in discrete effects on living tissues. In addition, the surface topography and roughness may also affect protein adsorption and bacterial adhesion [437]. Therefore, in this dissertation,

to successfully characterize the surface topography of the prepared coatings, surface profilometry and atomic force microscopy (AFM) were employed to measure the surface roughness. The surface roughness of the produced samples is characterized by a commonly used parameter to describe surface topography: the R_a value (arithmetic average roughness) which is defined as the mean of the deviations of the surface height from the median line.

4.4.5.1 Stylus profilometer: 2D roughness measurements

Stylus profilometer is the oldest scanning probe technique, where a fine stylus or a probe is moved over a surface in a straight line as schematically represented in **Figure 4.11**. In contact profilometry, the tip is moved vertically in contact with the surface and then moved laterally across the sample for a specified distance and using specified contact force. Thus, this method can evaluate small surface variations in vertical stylus displacement as a function of position and can measure vertical features ranging in sub-micron levels.

In chapters 5 and 6, 2D roughness measurements of uncoated and PEO-coated Ti discs were performed using a computerized Hommel somimetric surface scan profilometer based on stylus line scan measurements. The device was equipped with a stylus pin with a radius of $2\ \mu\text{m}$ and an opening angle of 90° . In this dissertation, for each sample, measurements were done on four random locations and the sample roughness given is the average of the four obtained values.

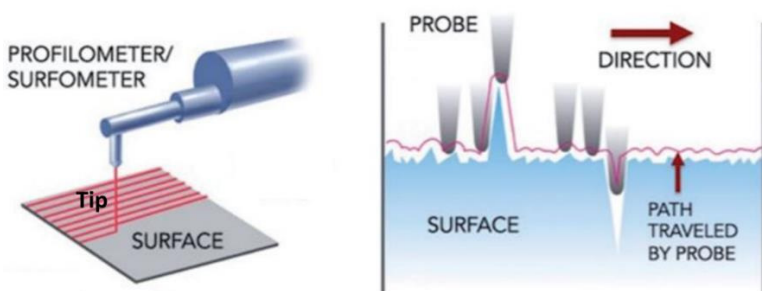


Figure 4.11. Schematic of a surface profilometer and its principle [438].

4.4.5.2 AFM

AFM is a very powerful and modern scanning probe technique for the quantitative measurement of a surface on the nanoscale and can create 3-dimensional topographical images with sub-nanometer resolution. This imaging technique uses a flexible cantilever with a tip attached to the end of the cantilever, and a laser beam reflected from the other side. When the tip approaches a sample surface, it will start interacting with the force fields associated with the surface (**Figure 4.12**). Once the probe is in proximity of the sample surface, a scanning pattern is performed in such a way that the forces between the sample and the probe remain constant. As the force is kept constant, the cantilever moves up and down, depending on the surface topography, which is tracked by the laser optics system connected to a computer.

In chapters 7 and 8, changes in the topography of the nanocomposite/nanolayered coatings prepared by the cluster source were analyzed on a nanoscale using an XE-70 AFM system (Park Systems™). AFM micrographs measuring $3 \times 3 \mu\text{m}^2$ were recorded in non-contact mode using a silicon-based cantilever (Nanosensors™ PPP-NCHR). Micrographs were analyzed using the open source software Gwyddion (V 2.45) and were subjected to plane levelling by mean subtraction prior to roughness determination. In this dissertation, for each condition, measurements were done on three random locations of a single sample and the sample roughness and roughness parameter are presented as the average of these three obtained values.

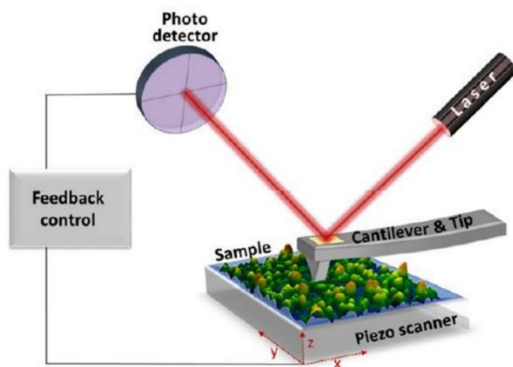


Figure 4.12. Schematic representation of an AFM device.

4.4.6 Silver/copper ion release characteristics of the coating : Inductively coupled plasma mass spectrometry (ICP-MS)

The antibacterial nature of Ag-based and Cu-based coatings is associated with their ability to release Ag^+ and Cu^{2+} when immersed in an aqueous environment. A sustained release of these ions is crucial for the long-term antibacterial effect as a burst release of these ions can have a cytotoxic effect and can only provide short-term antibacterial efficiency. Therefore, it is essential to quantify the amount of silver ions released from the Ag-doped coatings and the amount of copper ions released from the Cu-doped coatings into a surrounding aqueous medium. ICP-MS is an elemental analysis technique capable of detecting metal ions at μg to ng levels per liter. A typical configuration of an ICP-MS is shown in **Figure 4.13**. The ICP is an ionization source that can ionize the sample into its constituents and transform the elements into ions. It is typically composed of argon gas, and the energy is coupled to it using an induction coil to form plasma.

In this dissertation, an ICP-MS device (Perkin Elmer NexION 350) was used to monitor the $\text{Ag}^+/\text{Cu}^{2+}$ release kinetics of the fabricated coatings. Prior to ICP-MS analysis, the coated Ti discs were immersed into 20 mL of distilled water in small bottles at room temperature for different time points (6 h, 1 day, 3 days, 5 days and 7 days). Afterwards, micro-filtration (Chromafil RC-45/25, regenerated cellulose filters, pore size: $0.45\ \mu\text{m}$) followed by ultra-filtration (Amicon ultra centrifugal filters, regenerated cellulose 3 KDa) was performed. Subsequently, the filtered samples were acidified with 1mL of concentrated nitric acid (65%a.r. Chemlab), after which the samples were analyzed with ICP-MS. Each reported $\text{Ag}^+/\text{Cu}^{2+}$ concentration value in this dissertation is the average of 2 independent measurements.

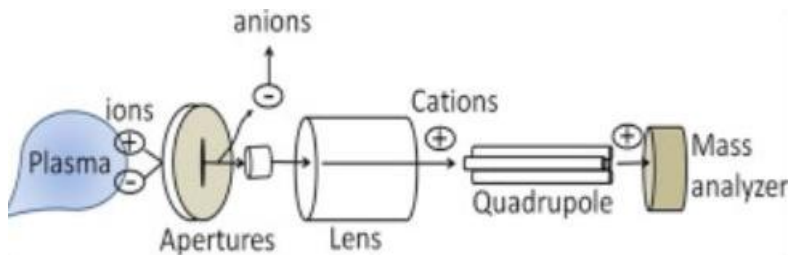


Figure 4.13. Schematic of ICP-MS [439].

4.5 Evaluation of the coating's mechanical properties

As the prepared coatings should possess adequate mechanical properties to be used on implant materials, the mechanical properties of the fabricated coatings have also been examined in this dissertation. To investigate this, hardness and scratch tests were performed on the deposited coatings and the methodologies used will be described in the following sections.

4.5.1 Microhardness test

Micro-indentation tests are characterized by indentation loads and penetration depths and two main tests used in this context are the Vickers and Knoop indentation tests. These indentation hardness tests are used to determine the material resistance to the penetration of a diamond indenter with the shape of a pyramid. The hardness value obtained is correlated with the penetration depth, to which the indenter sinks into a material under an applied load within a specific period of time. In chapters 5 and 6, the surface hardness of the uncoated and PEO-coated Ti samples was measured using a Vickers/Knoop hardness tester (Shimadzu HMV) with an applied load of 5 N and a loading duration of 10 s. The test was performed on 10 random locations distributed over a single sample surface and an average Vickers hardness number (VHN) and Knoop hardness number (HK) per sample were calculated.

4.5.2 Scratch test

The frictional characteristics of the uncoated and PEO-coated Ti discs, discussed in chapter 6, were evaluated by performing single asperity microscale scratch tests as shown in **Figure 4.14**. A diamond indenter corresponding to Rockwell C scale with a 200 μm tip radius and an included angle of 120° was used to experimentally simulate scratches on the prepared specimens. A constant load varying between 1 and 7 N was applied by means of a calibrated dead weight. The sliding velocity for scratch testing was kept constant at 3 mm/s for a 7 mm sliding distance. The tests were carried out at room temperature, which was measured to be between 24 ± 4 °C. Three replicate tests were performed for each sample and the average friction coefficient is reported in this dissertation.

4.5.3 Adhesion tests

The adhesion strength of the nanocomposite coatings deposited on Ti discs, discussed in chapter 7, was evaluated using a CSEM Revetest scratch tester as schematically represented in **Figure 4.14**. A spherical indenter with 200 μm tip radius and an included angle of 120° was used to experimentally simulate scratches on the prepared samples. A varying load ranging between 1 and 50 N with a total scratch length of 2 mm was applied. The scratching speed was kept constant at 0.4 mm/min. The critical load, the load at which the coating delaminated from the Ti disc, is reported in this dissertation.

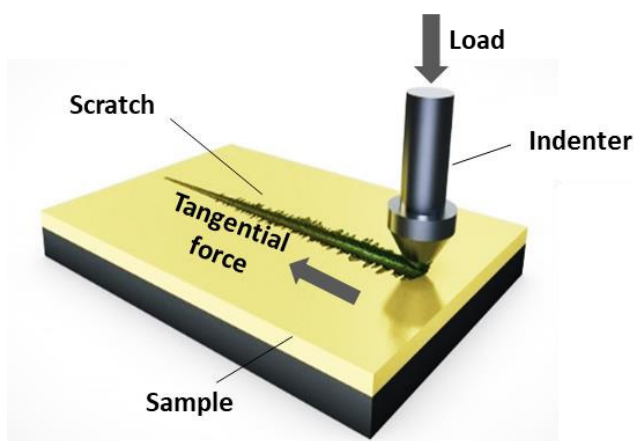


Figure 4.14. Schematic representation of the scratch tester.

4.6 *In-vitro* antibacterial studies

The fabricated coatings on Ti discs are intended to act as antibacterial coatings due to the incorporation of Ag/Cu. Therefore, the antibacterial efficiency needs to be investigated as this characteristic plays an important role in treating implant-associated infections. Thus, in this dissertation, the antibacterial properties of the prepared coatings are investigated against *Escherichia coli* ATCC 25922, *Staphylococcus aureus* ATCC 6538 (methicillin susceptible, MSSA), and *Staphylococcus aureus* Mu50 (methicillin resistant, MRSA). *Escherichia coli* (*E. coli*) and *Staphylococcus aureus* (*S. aureus*) correspond to gram-negative and gram-positive bacteria and are the most common pathogens which have the potential to cause implant-associated infections. In this dissertation, the CFU (colony forming

unit) serial dilution method and resazurin assay were performed to quantify the CFUs and metabolic activity of the bacteria. Additionally, the morphology of the cultured bacteria was visualized using SEM. The used experimental procedures will be described in detail in the following sections.

4.6.1 CFU assay

E. coli ATCC 25922, *S. aureus* ATCC 6538, and *S. aureus* Mu50 were grown on Luria-Bertani (LB) agar or in LB broth at 37°C. An overnight culture was standardized to an optical density (at 590 nm) of 0.05 and subsequently diluted 1:1000 in 2% LB broth. 2 mL of the resulting suspension was added to the wells of a 12-well microtiter plate, each well containing one coated Ti sample. Microtiter plates were subsequently incubated at 37°C for 24 h, with shaking (100 rpm). After 24 h, samples were removed from the microtiter plates and placed in 10 mL physiological saline (0.9% NaCl) after which they were vortexed and sonicated in order to remove all surface-attached bacteria from the samples. Serial dilutions of the resulting suspension were used to determine the number of CFUs by plating on LB agar.

4.6.2 Fluorescent staining (Resazurin assay)

To quantify the metabolic activity of the bacterial strains adhering on the samples, resazurin fluorescent staining was performed. A non-fluorescent blue resazurin dye turns to fluorescent pink resorufin after the mitochondrial reductase of the living bacterial cells. In order to allow the occurrence of this reaction, 100 μ L of the undiluted suspension was mixed with 10 μ L resazurin (CellTiter Blue, Promega), incubated at 37°C for 30 min and the resulting fluorescence (λ_{ex} 535 nm/ λ_{em} 590 nm) was measured using a multilabel microtiter plate reader (Envision, PerkinElmer).

Experiments were performed on 3 independent samples (n=4) and the obtained data are represented as a mean with standard deviation. For statistical analysis, ANOVA was performed followed by a Tukey's HSD post hoc test and a p-value <0.05 was considered to be significant.

4.6.3 Visualization of bacterial cell morphology using SEM

The morphology of *S. aureus* Mu50 was visualized using SEM by fixing the bacterial cells after 24 h of incubation on the samples under investigation. Prior to SEM analysis, the Ti discs were gently removed

from the culture media and rinsed 3 times with phosphate buffered saline (PBS) to remove any non-adhered bacteria. The samples were then immersed in a fixing solution (2.5% glutaraldehyde with cacodylate buffer) for 1 h, washed in a buffer solution (fixing solution without glutaraldehyde) and then dehydrated in increasing concentrations of ethanol (50%, 75%, 85%, 95% and 100%) for 10 min each. After dehydration, the samples were immersed in hexamethyldisilazane (HMDS) twice for 10 min and air-dried. The Ti samples under investigation, with fixed bacteria, were subsequently visualized with the JSM-7600F FEG-SEM device at an accelerating voltage and a working distance of 7.5 kV and 8 mm, respectively.

4.7 *In-vitro* cell studies

In addition to *in-vitro* antibacterial studies, the biocompatibility of the coatings including cell adhesion and proliferation was also investigated as the cellular behavior of the coatings plays a crucial role in the final success of the implant material. Therefore, in this dissertation, cell-material interactions on the fabricated coatings were examined after osteoblast cell seeding using fluorescence microscopy and 3-[4,5-dimethylthiazol-2-yl]-2,5-diphenyl tetrazolium bromide (MTT) assays. Additionally, the morphology of the cultured cells was also visualized using SEM. The used methodologies will be described in detail in the following sections.

4.7.1 Cell culture

In this dissertation, prior to cell seeding, the Ti samples under investigation were sterilized by exposure to UV light (Sylvania; 254 nm wavelength) for 30 min. After sterilization, samples were placed in a 24-well plate. MC3T3 (mouse osteoblastic cell line) cells were seeded onto the samples at a density of 50,000 cells/mL of medium, using a total of 1 mL of medium. Cell culture was performed using a Dulbecco's modified eagle medium (DMEM) supplemented with glutamax (Gibco Invitrogen) and enriched with 15% fetal calf serum (Gibco Invitrogen), 2 mM L-glutamine (Sigma-Aldrich), 10 U/mL penicillin, 10 mg/mL streptomycin and 100 mM sodium-pyruvate (all from Gibco Invitrogen). The cultures were incubated at 37° C under 5% CO₂ for 1 and 7 days (time required for osteoblasts to adhere and proliferate on surfaces). Cell adhesion, proliferation, and

viability were measured for 7 days and tissue culture polystyrene plates (TCPS) were used as a positive control.

4.7.2 Live/dead staining and fluorescent microscopy

Live/dead cell staining was performed to visualize the cell adhesion and proliferation on the Ti substrates 1 and 7 days after cell seeding. In the first step, the supernatant was removed and the samples were rinsed twice with PBS to remove any non-adhered cells after which the samples were stained in 2 μ L (1 mg/mL) of calcein-acetoxymethyl ester and 2 μ L (1 mg/mL) of propidium iodide in 1 mL PBS for 10 min at room temperature in the dark. The samples were then removed from the staining solution and they were observed with a fluorescence microscopy (Olympus, IX 81), using the appropriate filters.

4.7.3 Visualization of cell morphology using SEM

Cell morphology was also observed 1 and 7 days after cell seeding using SEM. Prior to SEM analysis, the Ti disks were gently removed from the culture media and rinsed 3 times with PBS to remove any non-adhered cells. The samples were then immersed in a fixing solution (2.5% glutaraldehyde with cacodylate buffer) for 1 h, washed in a buffer solution (fixing solution without glutaraldehyde) and then dehydrated in increasing concentrations of ethanol (50%, 75%, 85%, 95% and 100%) for 10 min each. After dehydration, the samples were immersed in hexamethyldisilazane (HMDS) twice for 10 min and air-dried. The treated Ti samples with fixed cells were visualized with SEM at an accelerating voltage and a working distance of 7.5 kV and 8 mm, respectively. From these images, the edges of the individual cells were selected and processed using ImageJ software, to quantify the cell morphology by determining the shape factor $[(\text{perimeter})^2 / (4\pi \text{ area})]$ of 25 randomly selected single cells. The shape factor determination was performed on 2 samples per condition and the obtained results are represented as mean \pm standard deviation.

4.7.4 Cell proliferation - MTT assay

The MTT assay is a colorimetric assay to quantify the cell viability by calorimetrically measuring the amount of viable cells. Cell viability was measured 1 and 7 days after cell seeding by replacing the culture medium by 0.5 mL (0.5 mg/mL) MTT reagent. The samples were then incubated at 37°C at 5% CO₂ for 4 h in the MTT solution.

Mitochondrial dehydrogenase enzymes of viable cells reduced the tetrazolium ring to purple formazan crystals. The formazan crystals were dissolved in a lysis buffer (1% Triton-X100 in isopropanol/ 0.04 N HCl) for 30 min, then 200 μ L of this solution was transferred to a 96-well plate and the optical density (OD) was measured at 580 nm using a spectrophotometer (BioTek, USA). Background absorbance at 750 nm was subtracted from the measured absorbance and the obtained optical density of the solution was reported as a percentage compared to the TCPS positive control. Experiments were performed on 3 independent samples (n=3) per sample condition and the cell viability data are represented as a mean with standard deviation. For statistical analysis, ANOVA was performed followed by a Tukey's HSD post hoc test and a p-value < 0.05 was considered to be significant.

4.8 Protein testing

When a foreign material is placed in the body, the first mechanism that takes place is the deposition of a protein layer from the blood and the body fluids onto the surface of the implant [440]. The presence of this film influences the interactions between the material and the cell/bacteria together with the activation of inflammatory reactions. Therefore, it is important to investigate the protein adsorption on the implant material and, for this purpose, FBS (fetal bovine serum) and BSA (bovine serum albumin) were used as model proteins to investigate the *in-vitro* protein interaction with the prepared coatings.

4.8.1 Protein adsorption assay by sodium dodecyl sulfate-polyacrylamide gel electrophoresis (SDS-PAGE)

SDS-PAGE is a gel electrophoresis technique, primarily used to separate proteins based on their polypeptide chain length. In SDS-PAGE, a polyacrylamide (PA) gel is used as a support medium and sodium dodecyl sulfate (SDS) is used to denature the proteins. Under the influence of an applied electric field, the proteins are separated by SDS-PAGE according to the molecular weight (between 5 and 250 kDa) based on their differential rates of migration through the PA gel, i.e. smaller proteins migrate faster due to less resistance from the gel matrix.

To investigate the *in-vitro* protein interactions, the investigated samples were immersed in either a 10% FBS or a 2 mg/mL BSA solution in distilled H₂O for 2 h at 37°C. Afterwards, the samples were washed three times with distilled water and air-dried to remove non-adherent proteins. Subsequently, all strongly adhered proteins were detached from the samples by immersing them in 1 mL of Laemmli buffer (62.5 x 10⁻³ M Tris-HCl, 2% SDS, 0.04 M β-mercapto-ethanol) supplemented with 0.01 % bromophenol blue at 100°C for 4 min after which the supernatants were collected. Next, 10 μL of the above-mentioned supernatants were loaded onto a 10% SDS polyacrylamide gel (Bio-rad, Mini-Protean electrophoresis system, 100 V, 70 mA) to visualize the protein bands. The gels were collected once the bromophenol blue reached the end of the gel. Afterwards, the gels were stained with Coomassie Blue G-250 250 (17% (w/v) (NH₄)₂SO₄, 0.2% (w/v) Coomassie Brilliant blue G-250, 34% (v/v) methanol, and 3% (v/v) phosphoric acid) followed by de-staining of the gel using a 6:3:1 water/methanol/acetic acid mixture. The de-staining procedure was performed until the protein bands were clearly seen. Photographs of the gels were then taken and the protein band intensities were measured using ImageJ software. Three replicate tests were performed for each sample and the average band intensities are reported relative to the control group of the corresponding protein (FBS, BSA).

4.8.2 Protein adsorption by fluorescence microscopy

As an alternative, the investigated samples were also immersed into a 0.5 mg/mL fluorescein isothiocyanate (FITC)-labelled albumin solution in distilled H₂O for 1 h after which protein adsorption was visualized using an Olympus IX 81 fluorescence microscope with appropriate filters.

Chapter 5. Antibacterial activity of a porous silver doped TiO₂ coating on Ti substrates synthesized by PEO

The results of chapter 5 were published in the following international peer-reviewed journal:

Thukkaram M, Cools P, Nikiforov A, Rigole P, Coenye T, Van Der Voort P, Du Laing G, Vercruyssen C, Declercq H, Morent R, De Wilde L, De Baets P, Verbeken K, De Geyter N.

“Antibacterial activity of a porous silver doped TiO₂ coating on titanium substrates synthesized by plasma electrolytic oxidation”.

Applied Surface Science, 500(2019): 144235-144246 (2019).

5.1 Introduction

Despite the success of PEO to fabricate antibacterial coatings, most of the previous work has focused on investigating the influence of PEO operational parameters such as applied voltage, treatment time, and current density on the final properties of the coatings. In contrast, the influence of silver concentration in the electrolyte on the coating properties such as its phase composition, microhardness, roughness, wettability, and silver ion release have not been addressed so far. Therefore, this chapter aims to investigate the above-mentioned properties of the PEO coatings and to perform a comprehensive scanning electron microscopical coating study as a function of varying concentrations of AgNPs in the electrolyte.

The aims of this particular chapter are therefore: (i) the synthesis of porous TiO₂ coatings on Ti substrates with and without bearing AgNPs by PEO; (ii) the assessment of the physical and chemical characteristics of the deposited coatings using different characterization techniques such as scanning electron microscopy-energy dispersive spectroscopy (SEM/EDS), X-ray photoelectron spectroscopy (XPS), X-ray diffraction (XRD), water contact angle (WCA) analysis, surface profilometry, and hardness tests and (iii) evaluation of the silver ion release kinetics and the *in-vitro* antibacterial activity of the coatings against *E. coli* (gram-negative bacterium) and *S. aureus* (gram-positive bacterium).

5.2 Experimental methods

All experimental details can be found in chapter 4. The deposition method, analysis techniques and their parameters that are specifically used in this chapter are summarized in the **Table 5.1**.

Table 5.1. Experimental methods.

Deposition method	PEO
	<ul style="list-style-type: none">• Electrolyte - 0.4 g/L NaOH and 4.0 g/L NaH₂PO₄ , AgNPs with a mean size of 50nm (concentrations of 0.1 g/L, 0.5 g/L and 1.0 g/L)• Voltage - 400 V• Treatment time - 5 min

Titanium specimen	Pre-treatment - Ground and mirror like polished
Characterization techniques	1) SEM <ul style="list-style-type: none"> • Surface SEM-EDS: Accelerating voltage - 7 kV • Cross-sectional SEM-EDS: Accelerating voltage - 15 kV 2) XPS <ul style="list-style-type: none"> • Survey scans and O1s high resolution spectra 3) XRD 4) WCA 5) 2D roughness measurement 6) Hardness test <ul style="list-style-type: none"> • Knoop indenter – load:25 g to 100 g • Duration - 10 s 7) ICP-MS silver ion release
<i>In-vitro</i> antibacterial test	CFU and resazurin assay <ul style="list-style-type: none"> • <i>E. coli</i> ATCC 25922 • <i>S. aureus</i> ATCC 6538 • Incubation time - 24 hours

In this chapter, samples oxidized in the Ag-free electrolyte and the Ag-doped electrolyte containing 0.1 g/L, 0.5 g/L, and 1 g/L will be referred to as the Ag0, Ag1, Ag2 and Ag3 samples, respectively.

5.3 Results and discussions

5.3.1 Coating morphology and distribution of AgNPs

The top surface morphologies of Ag-free (Ag0) and Ag-doped (Ag1, Ag2 and Ag3) coatings and their corresponding EDS spectra can be seen in **Figure 5.1 A, B and C** respectively. It was observed that the surfaces of all coatings under investigation exhibited a microporous morphology and that the pores were homogenously distributed over the entire coating surface. Additionally, no obvious differences could be seen in the top surface morphology between the Ag-free sample on the one

hand and all Ag-doped samples (Ag1, Ag2 and Ag3) on the other hand. This indicated that the incorporation of AgNPs had no significant effect on the top surface morphology of the coating and that in fact AgNP incorporation did not alter the main structural characteristics including porous morphology and distribution of pores. Similar findings were also observed when using different electrolyte concentrations [177,342]. EDS spot analysis also confirmed that no Ag was found on the Ag-free coating while it was present in all three Ag-doped coatings along with Ti and O from the metallic TiO₂ coating, P from the electrolyte and some small amounts of C due to surface contamination (**Figure 5.1.C**).

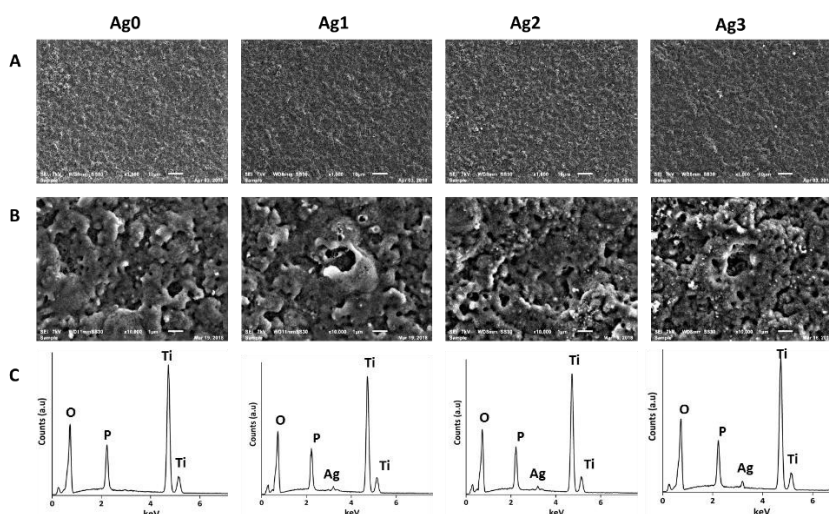


Figure 5.1. Surface SEM micrographs of Ag-free (Ag0) and Ag-doped (Ag1, Ag2, Ag3) TiO₂ coatings at 10 μm (A) and 1 μm (B) and their corresponding EDS spectra (C).

To further investigate the distribution of AgNPs on the coating surface, high resolution SEM images in back scattered electron (BSE) mode were also taken for the Ag-doped samples (Ag1, Ag2 and Ag3) at 1000x and 30,000x magnification and the results are presented in **Figure 5.2 A and B**. High atomic number elements (such as Ag), backscatter electrons more strongly than low atomic number elements such as Ti, O, and P and thus appear brighter in BSE micrographs. At low

magnification (**Figure 5.2.A**), it can be observed that for all Ag-doped samples AgNPs were mainly distributed as clusters of NPs while some stand-alone NPs within the TiO₂ matrix could also be observed. **Figure 5.2.A** also reveals that the clustering of the AgNPs increased with increasing concentration of AgNPs in the electrolyte. SEM-BSE images at high magnification **Figure 5.2.B** also showed that AgNPs were found to be not only fused on the top surface of the TiO₂ coatings, but also inside the pores of the coating (indicated with the arrow marks). Again, also in **Figure 5.2.B**, more AgNPs can be seen when adding higher amounts of AgNPs to the electrolyte.

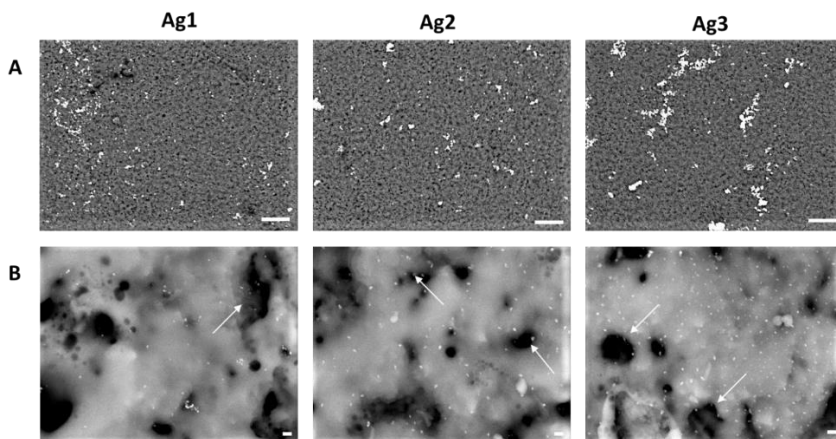


Figure 5.2. SEM-BSE images of the surface of antibacterial coatings (Ag1, Ag2, Ag3) clearly showing the presence of AgNPs (scale bar: 10 μ m (A) and 100 nm (B)). The arrows indicate the incorporation of AgNPs inside the coating pores.

NPs are incorporated into the growing oxide layer when they are added in the PEO electrolyte. Studies have reported the mechanism of incorporation of NPs within the porous TiO₂ matrix during the PEO process [441–444]. The authors of these studies stated that different stages are involved in the incorporation of AgNPs within the porous oxide layer such as the delivery of particles to the sites of oxide matrix, accumulation of particles at the sites of the oxide matrix and preservation of the already embedded particles during coating growth.

Many studies have also investigated the incorporation of NPs like Ag, Cu and Zn within a TiO₂ matrix [38]. These authors have reported that the NPs are delivered into the oxide coating via transport pathways such as pores, cracks and short-circuit channels. Then, these particles are embedded at the sites of coating growth which are preserved during the growth of the oxide layer [441,445].

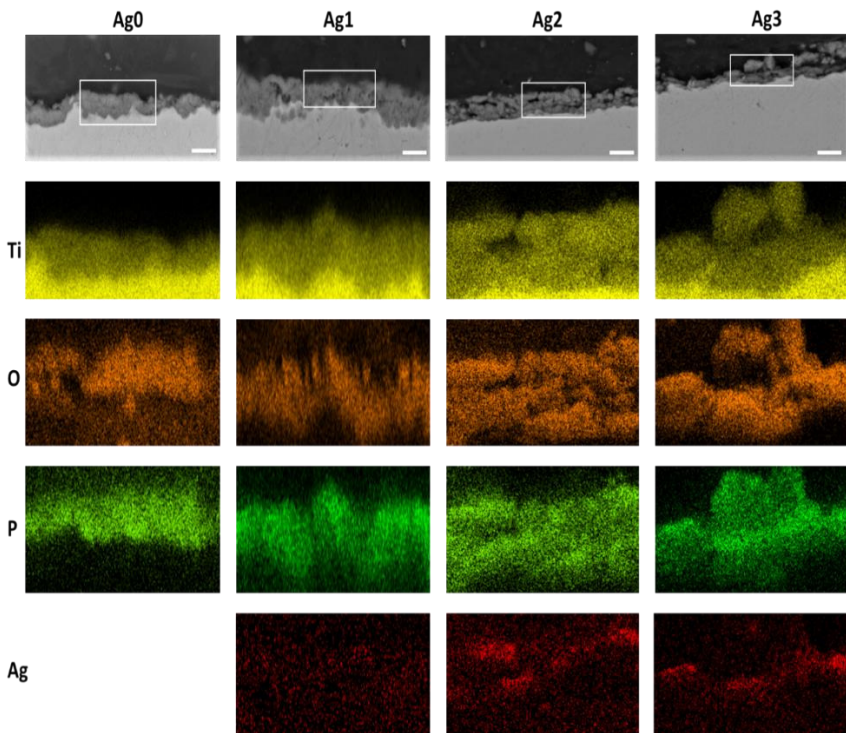


Figure 5.3. Cross-sectional SEM-BSE images and EDS mapping corresponding to the framed area in the upper SEM-BSE images of the Ag0, Ag1, Ag2 and Ag3 coatings (scale bar: 5 μ m).

Figure 5.3 shows the cross-sectional SEM-BSE micrographs of the Ag-free (Ag0) and the Ag-doped coatings (Ag1, Ag2 and Ag3) and their corresponding elemental mapping of Ti, O, P and Ag. Based on these cross-sectional images, the thicknesses of the oxide layers were measured to be $4.7 \pm 0.5 \mu\text{m}$, $5.5 \pm 1.1 \mu\text{m}$, $5.1 \pm 0.6 \mu\text{m}$ and $5.9 \pm 1.9 \mu\text{m}$

μm for the Ag0, Ag1, Ag2 and Ag3 samples respectively. Consequently, adding different amounts of AgNPs to the electrolyte did not affect the final thickness of the created oxide layer. From the EDS elemental mapping, it can also be observed that Ti, O and P were uniformly distributed along the coating surface and coating thickness. From the Ag mapping results it also became apparent that the AgNPs preferably aggregated at the O and P layer in case of the Ag2 and Ag3 samples.

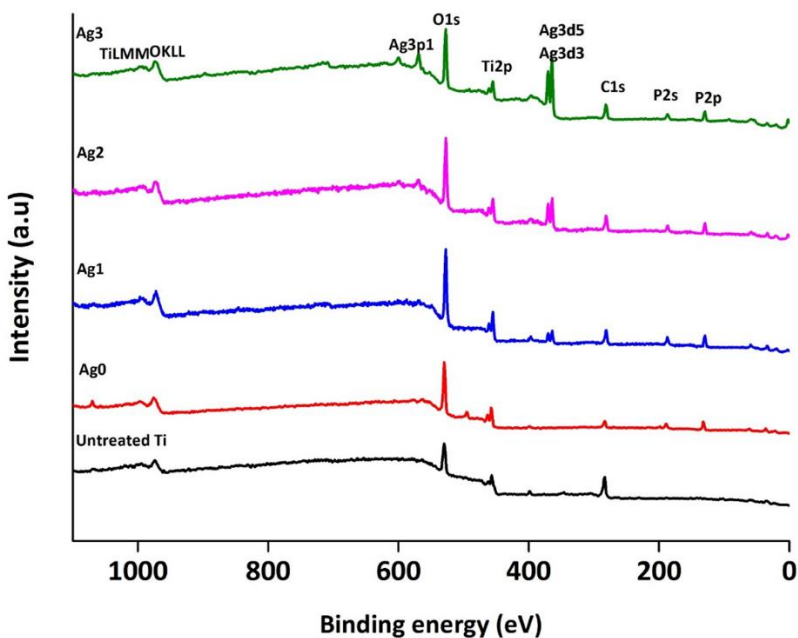


Figure 5.4. XPS survey spectra of the coatings.

In addition to EDS, XPS was also applied to determine the chemical composition of the top coating surface. The XPS survey spectra, depicted in **Figure 5.4**, show that the elements Ti, O, P and C are detected on all coating surfaces. For the Ag-doped coatings (Ag1-Ag3), the Ag element was also detected and the strength of the Ag peaks increased with increasing Ag content in the electrolyte. From these survey spectra, the elemental composition of the coatings can be determined and the obtained results are shown in **Table 5.2**. This table shows that the coatings, besides O, Ti and P, also contain a significant

amount of carbon, which is believed to arise from adventitious carbon contamination at the coating surface. Additionally, this table also reveals that the Ag concentration at the top coating surface increased with increasing silver content in the electrolyte. **Figure 5.5** shows the high resolution O1s spectra of the coating surfaces and its deconvolution into three component peaks [446,447]: the peak located at 530.1 eV is assigned to O1s in TiO₂ [448,449]; the second peak at 531 eV corresponds to O1s in titanium phosphates and the third peak at 532.1 eV can be attributed to the chemical bonds Ti-OH and P-O-H [447]. From the high resolution O1s spectra, it can be observed that the coating surface is mainly composed of TiO₂ groups with a small amount of titanium phosphates and free phosphate groups. However, it is important to mention that the XPS results only provide chemical information of the top 5-10 nm of the coating and therefore does not represent the entire coating thickness which is of the order of μm's.

Table 5.2. Elemental composition of Ag-free and Ag-doped TiO₂ coatings obtained from XPS analysis.

Coated Surface	Ti (at%)	O(at%)	P (at%)	C (at%)	Ag (at%)
Ag0	7.5 ± 1.1	56.6± 2.3	10.2 ± 2.1	25.7 ± 3.5	0
Ag1	7.2 ± 1.3	56.2 ± 1.6	9.8 ± 1.1	25.3 ± 1.6	1.5 ± 0.5
Ag2	7.0 ± 1.2	54.2 ± 2.8	8.9 ± 0.8	26.4 ± 1.9	3.5 ± 0.8
Ag3	6.8 ± 1.6	53.1 ± 1.8	9.1 ± 1.1	25.2 ± 1.7	5.8 ± 0.5

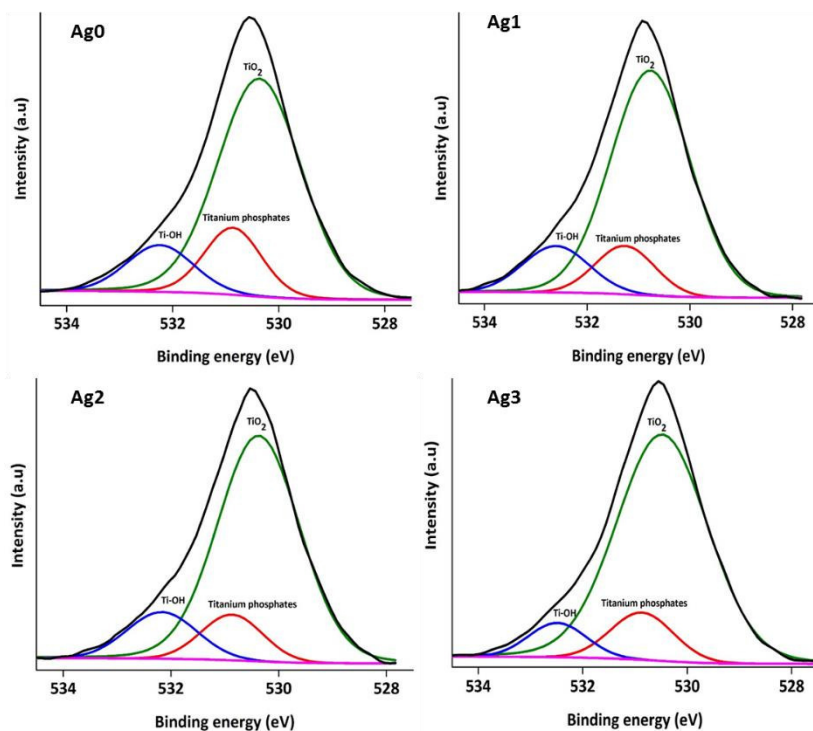


Figure 5.5. XPS deconvoluted high resolution O1s peaks of the coatings.

5.3.2 Surface crystallinity

Figure 5.6 shows the X-ray diffraction patterns of untreated Ti, the Ag-free and different Ag-doped TiO₂ coated Ti substrates. The untreated Ti sample consisted of both the pure Ti phase with characteristic peaks at $2\theta = 39.2^\circ$, 52.6° , 70.1° and 77.4° as well as very small amounts of oxidized Ti phases, which were identified as anatase and rutile TiO₂ [450,451]. As can be seen in **Figure 5.6**, after performing the PEO processes, the peak intensities of these anatase ($2\theta = 25.2^\circ$, 38.5° and 53.8°) and rutile TiO₂ ($2\theta = 28.1^\circ$, 36.2° , 41.3° and 69.2°) phases strongly increased compared to the untreated Ti sample while the intensity of the Ti peaks decreased [217,452]. Nevertheless, Ti peaks were still present on the XRD spectra of the PEO treated samples due to the penetration of the X-ray beam beyond the TiO₂ coating. In addition, there were no obvious differences in crystalline phases

between the Ag-free TiO₂ coatings and the TiO₂ coatings doped with different amounts of AgNPs. This may be due to the low amount of AgNPs incorporated in the coatings fabricated in this work resulting in a total silver content below the detection limit of the XRD system. It should be noted that TiO₂ exists in three different crystal lattices: anatase, rutile and brookite. After PEO treatment, the thickness of the oxide layer increased to approximately 5 μm and the crystallinity of the layer drastically changed exhibiting increased peak intensities of anatase and rutile crystal phases in comparison to untreated Ti (**Figure 5.6**). In this context, studies have reported that a TiO₂ film composed of an anatase crystal structure can attract calcium and phosphate ions from the physiological environment to form a hydroxyapatite-like coating. It was already reported that such a coating can improve the osteogenic properties due to lattice match and superposition of hydrogen bonding grounds in anatase crystal structure. Similarly, a rutile TiO₂ film on Ti was already associated with acidic and basic hydroxyl groups (OH⁻) which are conducive to cell adhesion and growth [217,453,454]. It is therefore believed that the mixture of anatase and rutile phases in the coated Ti samples prepared in this work may positively influence the bioactivity of Ti by enhancing the osteogenic properties of Ti.

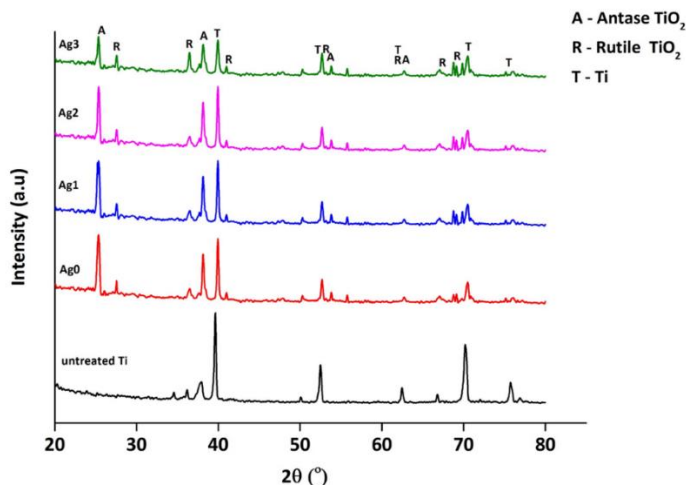


Figure 5.6. XRD spectra of untreated Ti, Ag-free and Ag-doped TiO₂ coatings.

5.3.3 Surface wettability

Besides the surface crystallinity, surface wettability was also found to be another important aspect in improving the bioactivity of Ti surfaces. Consequently, the surface wettability of the coated Ti samples was also investigated in this work and **Figure 5.7.A** shows the results of this WCA analysis. The WCA value of the untreated polished Ti sample was found to be approximately 65°, while after PEO treatment, both Ag-free and Ag-doped TiO₂ samples showed a significant reduction in WCA values. In case of the Ag-free TiO₂ coating, the WCA value decreased to approximately 20°, indicating a change from a moderate to a strong hydrophilic surface. **Figure 5.7.A** also reveals that the presence of AgNPs on/in the porous TiO₂ coating did not result in a significant change in wettability compared to the Ag-free TiO₂ samples. The increase in wettability of the PEO-treated Ti samples may therefore be primarily attributed to the transition from Ti metal to Ti oxide structures, surface crystallinity changes and surface topography variations. The latter parameter could be related to the increased porosity of the oxidized surface allowing the water droplet to better penetrate inside the pores [455].

5.3.4 Surface roughness

The average roughness values Ra for the untreated polished Ti, Ag-free and Ag-doped TiO₂ samples are presented in **Figure 5.7.B**. As mentioned earlier, PEO is a process that is known to increase the surface roughness of the substrate due to the in-depth growth of a porous oxide coating. The results obtained in this work confirm this observation: the surface roughness increased from $0.08 \pm 0.02 \mu\text{m}$ for the untreated polished Ti sample to $1.30 \pm 0.11 \mu\text{m}$ for the Ag-free PEO treated Ti sample. Similar as in case of the surface wettability, no significant differences in surface roughness were observed between the Ag-free and Ag-doped coatings.

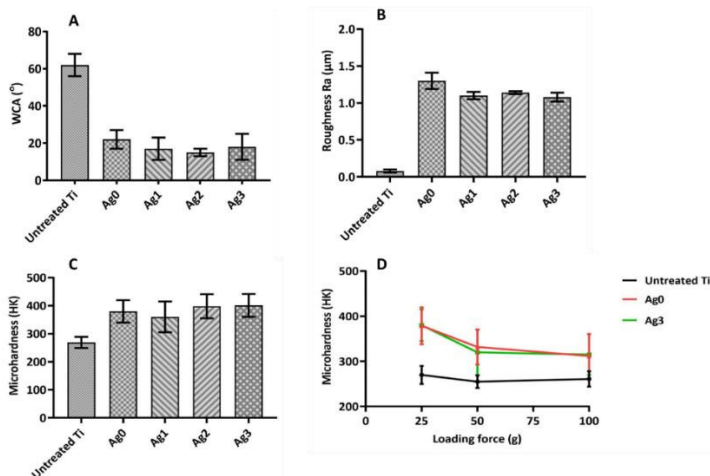


Figure 5.7. WCA (A), roughness (B), microhardness (C) of untreated Ti, Ag0, Ag1, Ag2 and Ag3 samples and evolution of the microhardness as a function of loading force for the untreated Ti, Ag0 and Ag3 samples (D).

5.3.5 Surface microhardness

Figure 5.7.C shows the microhardness of all samples under investigation in this work using a loading force of 25 g, while Figure 5.7.D shows the evolution of the microhardness as a function of loading force for the untreated Ti, Ag-free (Ag0) and Ag-doped (Ag3) samples. The microhardness of the untreated Ti substrate was found to be approximately 269 HK and after PEO treatment, the coating microhardness increased to approximately 380 HK. Again, no significant difference in surface microhardness was observed between the Ag-free and Ag-doped coatings. The increased microhardness may be caused due to the formation of dense oxide layer which is attributed to the formation of thermal micro arcs during PEO. Additionally, the larger standard deviations on the PEO treated samples may also be attributed to their higher surface porosity. Since there was no difference in microhardness after PEO at a loading force of 25 g, only untreated Ti, Ag0 and Ag3 samples were chosen to analyze the microhardness at different loading conditions (Figure 5.7.D). It can be observed that for the untreated Ti the microhardness was constant as a function of the loading force. In contrast, the PEO treated samples

possessed a higher surface hardness compared to the untreated sample but the hardness values slowly decreased with increasing load thus with increasing penetration depth. This observation may be due to the reduced load support from a relatively thin coating. For clinical applications, an increase in Ti surface microhardness could be beneficial, because it increases the resistance to wear of the material, thereby positively contributing to the longevity of a Ti implant [456].

5.3.6 Silver ion release characteristics of the coatings

The antibacterial nature of Ag-based coatings depends on their ability to release silver ions. It has already been demonstrated that AgNPs oxidize to Ag ions while interacting with an aqueous medium [457]. Hence, it is essential to quantify the amount of silver ions released from the Ag-doped TiO₂ coatings into a surrounding aqueous medium. **Figure 5.8.A** presents the cumulative Ag⁺ release profiles of Ag-doped TiO₂ samples in distilled water for up to 7 days. This cumulative Ag⁺ release is observed to increase with immersion time with different release rates, depending on the initial Ag loading. Samples with higher Ag concentration present in the coating exhibited a higher Ag⁺ release at any given point during the 7 days measurement. As shown in **Figure 5.8.B**, the release of Ag⁺ per day (ppb/day) was 20 ppb/day for the Ag1 sample, 78 ppb/day for the Ag2 sample and approximately 97 ppb/day for the Ag3 sample after the first immersion; this Ag⁺ release eventually decreased to 9, 35 and 29 ppb/day after an immersion time of 7 days for the Ag1, Ag2 and Ag3 samples, respectively. Silver ion release profiles of the silver-doped coatings thus show a fast initial release followed by a low level of continuous release (**Figure 5.8.B**) While the rapid release of Ag⁺ ions at the initial periods could be beneficial in preventing implant related infections after the surgical procedure, a slow release rate may contribute to a long-term antibacterial activity. In this respect, Ag⁺ release rates from the examined samples are higher than the reported minimum Ag⁺ concentration of 0.1 ppb required to exhibit an antibacterial activity [457]. In addition, studies have also reported that Ag⁺ concentrations of more than 300 ppb in human blood could cause side effects in the form of liver and kidney damage [51]. In contrast, Tweden et al. [458] reported that an Ag⁺ concentration up to 1200 ppb had no cytotoxic effect on *in-vitro* fibroblast cells. Although a higher Ag content can

provide an excellent antibacterial activity, it is equally important for the coating to exhibit biocompatibility. The highest cumulative silver release after 7 days in this study was 240 ppb (Ag3 sample) meaning that the Ag^+ release is well maintained below 300 ppb, which is considered the normal Ag^+ concentration in human blood [458,459]. However, further studies have to be performed to estimate the long term release kinetics of Ag^+ from the coatings.

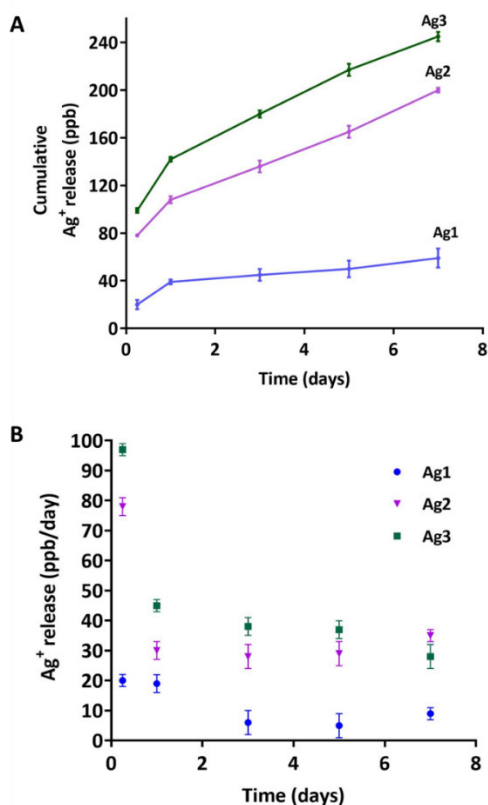


Figure 5.8. Cumulative Ag^+ release (ppb) (A) and Ag^+ release rate (ppb/day)(B) when immersed in water up to 7 days for Ag1, Ag2 and Ag3 samples.

5.3.7 Evaluation of the *in-vitro* antibacterial activity of the coatings

The final step of this chapter was testing the antibacterial potential of the prepared coatings. The antibacterial activity of the coatings was

investigated against *S. aureus* (gram-positive bacterium) and *E. coli* (gram-negative bacterium). From untreated Ti samples, approximately 10^8 CFU are recovered, both for *E. coli* and *S. aureus* (**Figure 5.9.A**). This is also reflected in the high fluorescence after staining with resazurin (**Figure 5.9.B**). No reduction in *E. coli* and *S. aureus* were observed in Ag-free TiO₂ coatings. In contrast, the Ag-doped coatings showed a significant reduction ($p < 0.05$) in cell numbers and metabolic activity. This was most pronounced for *E. coli* and for the samples Ag2 and Ag3 (**Figure 5.9**). Studies have reported that the antibacterial effect was found to be strongly dependent on the amount of AgNPs in the coatings [324], which is also observed in this work. In the case of Ag1, a 4-log reduction of *E. coli* bacteria and a 2-log reduction of *S. aureus* bacteria were observed. Samples with high silver content (Ag2, Ag3) exhibited a complete reduction of *E. coli* and a 6-log reduction of *S. aureus*.

The antibacterial activity of the Ag-doped coatings can be explained by the close contact between bacteria and the AgNPs and/or the release of Ag⁺ ions from the coating to the aqueous medium, as extensively described in literature [324]. It has been reported that direct contact of bacteria with AgNPs can cause physical damage to the bacterial membrane leading to cell death. In addition, it has been proven that the bacterial cell membrane has a negative charge which confers electrostatic attraction to the positively charged AgNPs. This helps the AgNPs to attach onto bacterial cell membranes followed by membrane damage [325,326]. There is also evidence suggesting that the released Ag⁺ ions from AgNPs are also a crucial contributing factor towards the antibacterial activity. From the performed ICP-MS analysis in this work, the Ag⁺ concentration after 1-day incubation of the samples in water was found to be in the range of tens to hundreds of ppb (**Figure 5.8**). The Ag⁺ ions are in this case generated by oxidative dissolution involving protons and dissolved oxygen. Therefore, an increase in antibacterial activity with an increasing amount of AgNPs in the coating was to be expected. In fact, it has also been noted that the Ag⁺ release depends not only on the amount of AgNPs, but also on the ability of water to penetrate through the coating to reach the NPs. From **Figure 5.7.A**, it could be observed that the water permeation through the coating can be high due to the coating's increased hydrophilicity. However, considering the distribution of AgNPs within the TiO₂ coating, it is crucial to note that only two locations are

important in exhibiting the antibacterial activity on the material, i.e AgNPs fused in the walls of open pores and those adherent on the surface of the oxide coating. However, further research is needed to understand the exact mechanism of antibacterial activity of silver-doped TiO₂ coatings and on their *in vitro* cytotoxicity evaluation.

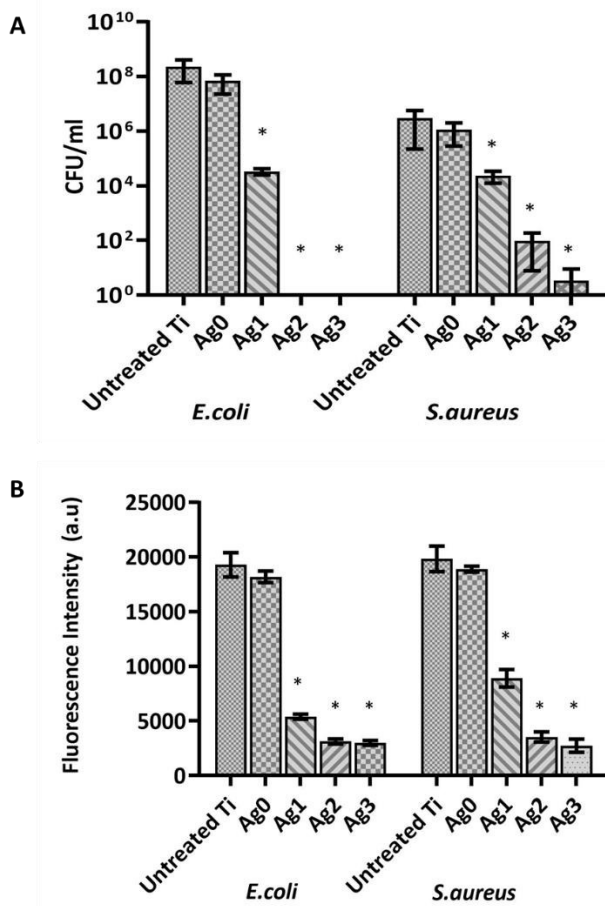


Figure 5.9. Number of CFU (A) and metabolic activity (B) after 24 hours of incubation with different samples. The data are expressed as mean \pm SD of 4 independent experiments ($n=4$). Asterisk (*) denotes significant difference at $p < 0.05$ compared to the control sample (untreated Ti).

5.4 Conclusion

In this chapter, commercially available pure Ti samples were subjected to PEO in sodium dihydrogen phosphate and sodium hydroxide containing base electrolyte with and without the addition of AgNPs (0.1 g/L, 0.5 g/L and 1g/L) at a DC voltage of 400 V for 5 min. In summary, porous TiO₂ coatings and antibacterial silver-containing TiO₂ coatings were prepared on the surface of Ti by plasma electrolytic oxidation without and with the presence of AgNPs respectively. In the latter case, AgNPs were successfully incorporated into the coating and distributed on the coating surface and inside the pores of the coating. Increasing the concentration of AgNPs in the electrolyte increased the amount of Ag in the oxidized coatings from 0.6 wt% to 3.1 wt%. In contrast, the microstructure and phase composition, surface roughness and surface wettability of the TiO₂ coatings were not affected by the incorporation of AgNPs. The silver ion release kinetics of the Ag-doped TiO₂ samples were also examined and showed a fast initial Ag⁺ release followed by a slow continuous release over a period of 7 days. Additionally, the coatings synthesized in alkaline base electrolyte with added AgNPs exhibited excellent antibacterial activity against *E. coli* and *S. aureus* in comparison to the coating formed in Ag-free base electrolyte. Moreover, the antibacterial activity of the coating was found to increase with an increase in AgNPs amount in the electrolyte. The efficient bactericidal effect of the Ag-loaded coatings can be attributed to the release of Ag⁺ ions into the bacterial solution alone or in combination with contact killing.

Chapter 6. Fabrication of microporous coatings on Ti implants with improved mechanical, antibacterial and cell-interactive properties

The results of Chapter 6 were published in the following international peer-reviewed journal:

Thukkaram M, Coryn R, Asadian M, Esbah Tabaei PS, Rigole P, Rajendhran N, Nikiforov A, Sukumaran J, Coenye T, Van Der Voort P, Du Laing G, Morent R, Van Tongel A, De Wilde L, De Baets P, Verbeken K, De Geyter N.

“Fabrication of Microporous Coatings on Titanium Implants with Improved Mechanical, Antibacterial and Cell-Interactive Properties. ACS Applied Materials and Interfaces, 12(27): 30155-30169 (2020).

6.1 Introduction

As already mentioned earlier, AgNPs are widely used as antibacterial agent due to their strong and broad antibacterial spectrum. However, from the study discussed in chapter 5, it was observed that AgNPs have a tendency to aggregate, and this can lead to bacterial resistance towards silver [460]. Therefore, in this chapter, the antibacterial property of silver will be harnessed from Ag^+ without actually using AgNPs but delivering Ag^+ from silver acetate present with a suitable matrix. Besides improving the antibacterial efficacy of the PEO-treated coatings, this chapter is also dedicated to enhancing the osteoconductive performance (by the addition of Ca and P ions) as well as the mechanical properties of the coatings. In the past, most researchers have investigated the influence of PEO operational parameters on the surface characteristics of the coatings, while the possible correlations between the physio-chemical properties of the PEO-treated coatings, and their cellular interaction have not been addressed so far. Also, most of the previous work has investigated either the antibacterial performance or the bioactivity of PEO coatings fabricated in silver-containing or hydroxyapatite (HA) particle-containing electrolytes [332, 461–464]. To the best of our knowledge, no study has ever been reported on the bi-functional character of PEO coatings by incorporating antibacterial Ag^+ ions together with osteoconductive Ca and P ions on Ti implant surfaces.

Therefore, this particular chapter aims to synthesize porous bi-functional oxide coatings on Ti discs employing PEO with a base electrolyte containing calcium acetate monohydrate, sodium dihydrogen phosphate dihydrate with and without the addition of different amounts of silver acetate as a supplier of Ag^+ ions. The physico-chemical characteristics of the deposited coatings are assessed using different characterization techniques such as SEM/EDS, XPS, XRD, WCA analysis, 2D surface profilometry, Vickers hardness test, and scratch tests. In addition, the dose-dependent effect of silver on the *in-vitro* antibacterial performance, protein interactions, and osteoconductivity of the prepared coatings is also investigated.

6.2 Experimental methods

All experimental details can be found in chapter 4. The deposition method, analysis techniques and the corresponding parameters that are specifically used in this chapter are summarized in the **Table 6.1**.

Table 6.1. Experimental methods.

Deposition method	<p>PEO</p> <ul style="list-style-type: none"> • Electrolyte - 2.0 g/L NaH₂PO₄·2H₂O and 5.0 g/L Ca(OOCCH₃)₂·H₂O, AgOOCCH₃ (concentrations of 0.1 g/L, 0.5 g/L and 0.8 g/L) • Voltage - 500 V • Treatment time - 5 min
Ti specimen	Pre-treatment - Ground and mirror-like polished
Characterization techniques	<p>1) SEM</p> <ul style="list-style-type: none"> • Surface SEM-EDS: Accelerating voltage - 7 kV • Cross-sectional SEM-EDS: Accelerating voltage - 15 kV <p>2) XPS</p> <ul style="list-style-type: none"> • Survey scans and Ti2p, O1s, Ca2p, P2p, Ag3d high-resolution spectra <p>3) XRD</p> <p>4) WCA</p> <p>5) 2D roughness measurement</p> <p>6) Hardness test</p> <ul style="list-style-type: none"> • Vickers indenter - load (5N), • Duration - 10 s <p>7) Scratch test</p> <ul style="list-style-type: none"> • Diamond indenter - load (1N-5N),

	8) ICP-MS silver ion release
<i>In-vitro</i> analysis	Antibacterial assay : CFU <ul style="list-style-type: none"> • <i>E. coli</i> ATCC 25922 • <i>S. aureus</i> ATCC 6538 • <i>S. aureus</i> Mu50 • Incubation time - 24 hours Protein interactions : SDS PAGE <ul style="list-style-type: none"> • 10% FBS, 2mg/L BSA • Immersion time - 2 hours Cell culture : MTT, SEM and Fluorescence microscopy <ul style="list-style-type: none"> • MC3T3 cells • Cell seeding time – day 1 and day 7

In this chapter, samples oxidized in the Ag-free electrolyte and the Ag-doped electrolyte containing 0.1 g/L, 0.5 g/L and 0.8 g/L of AgOOCCH_3 will be referred to as the Ag0, Ag1, Ag2 and Ag3 samples, respectively.

6.3 Results and discussions

6.3.1 Influence of the silver acetate concentration on the current density of the PEO process

Figure 6.1 shows the current density of the PEO process when different silver acetate concentrations are used in the electrolyte. As can be seen in **Figure 6.1**, increasing the concentration of silver acetate in the electrolyte caused the PEO process to proceed at higher current density. Although there was a slight increase in the current density for the Ag1 sample compared to the Ag0 sample, the current density characteristics of both samples showed a similar trend as a function of treatment time: after being stable, the current density started to slowly decrease after a treatment time of 3 min. However, when using electrolytes containing high amounts of silver acetate (Ag2, Ag3), the initially very high current density, remained only stable for 1-1.5 min after which it started to strongly decrease.

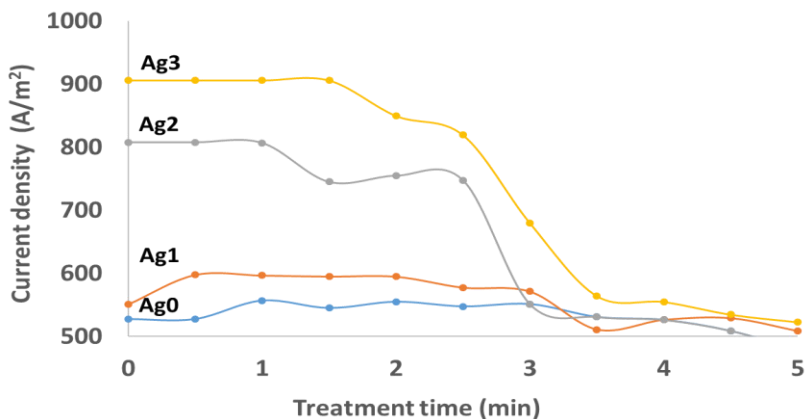


Figure 6.1. Current density characteristics of PEO-treated Ti discs at varying silver concentrations (Ag0, Ag1, Ag2, Ag3).

6.3.2 Morphologies, chemical states and crystalline phases of the coatings

Figure 6.2 A and B shows the top surface morphologies of silver free (Ag0) and silver-doped coatings (Ag1, Ag2, Ag3). It can be seen that irrespective of the silver content all coatings were porous, a typical characteristic of coatings prepared by PEO. Similar findings were also observed when using other electrolytes [441,465]. It can also be seen that the pores were homogeneously distributed over the entire coating surface and these porosities are due to the electrical discharges that are formed on the surface of the samples. Figure 6.3 shows the cross-sectional SEM-BSE (backscattered electrons) micrographs of the Ag-free (Ag0) and Ag-doped coatings (Ag1, Ag2 and Ag3). Based on these cross-sectional images, the thicknesses of the created oxide layers were determined to be $5.0 \pm 0.2 \mu\text{m}$, $5.1 \pm 0.3 \mu\text{m}$, $5.1 \pm 0.6 \mu\text{m}$ and $4.5 \pm 1.9 \mu\text{m}$ for the Ag0, Ag1, Ag2 and Ag3 samples, respectively. Consequently, adding different amounts of silver acetate to the electrolyte did not affect the final thickness of the created oxide layer. From the EDS elemental mapping (Figure 6.4), it can be observed that O, P and Ca were uniformly distributed along the coating surface and the entire coating thickness. It can thus be observed that the deposited oxide coatings were enriched with both Ca and P, suggesting the possible presence of calcium titanates and/or Ti phosphates [462]. From the Ag

mapping, it also becomes apparent that Ag did not form any aggregates in the oxide layer which is commonly observed when incorporating other forms of Ag in the electrolyte [462,465]. This finding is very positive as a uniform deposition of Ag in the oxide layer is essential to have a constant release of Ag⁺ which can in turn provide a better antibacterial performance as aggregates of silver are known to lead to bacterial resistance [460].

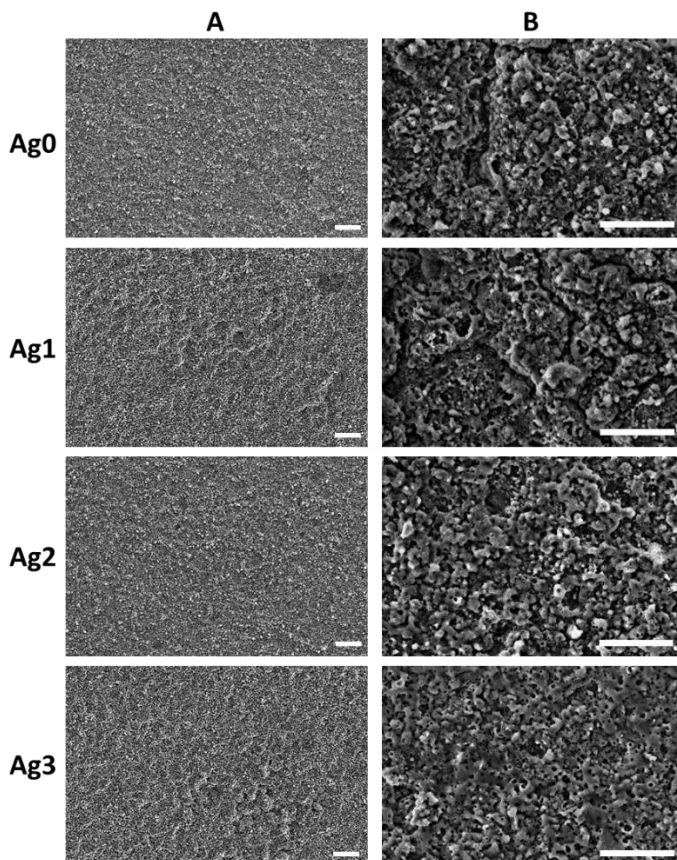


Figure 6.2. Surface SEM micrographs of Ag-free (Ag0) and Ag-doped (Ag1, Ag2, Ag3) TiO₂ coatings (scale bar: 10 μm) (A) and (scale bar: 5 μm) (B).

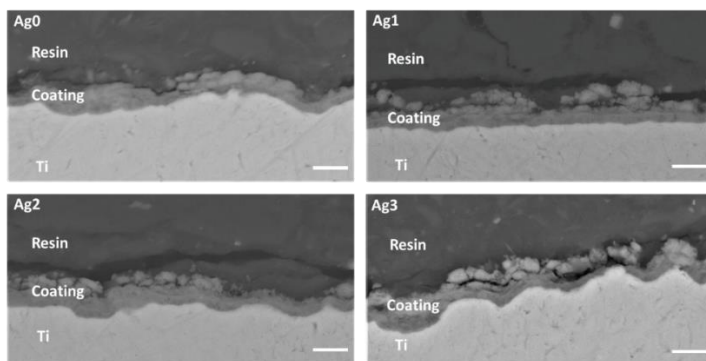


Figure 6.3. Cross-sectional SEM-BSE images of Ag-free (Ag0) and Ag-doped (Ag1, Ag2, Ag3) TiO_2 coatings (scale bar: 5 μm).

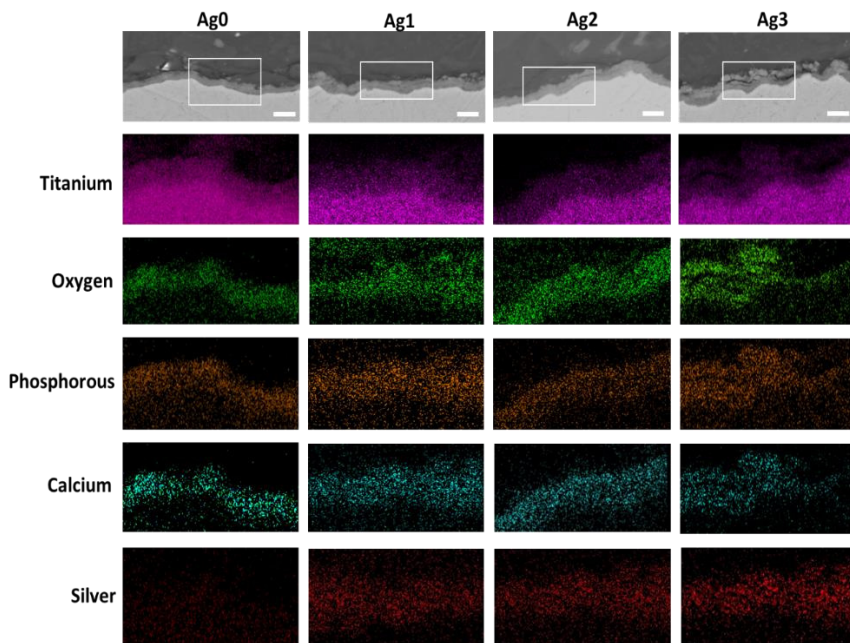


Figure 6.4. Cross-sectional SEM-BSE images and EDS mapping corresponding to the framed area in the upper SEM-BSE images of Ag-free (Ag0) and Ag-doped (Ag1, Ag2, Ag3) TiO_2 coatings (scale bar: 5 μm).

To explore the surface chemical composition of the coatings, the coatings were examined by XPS. **Figure 6.5** shows the XPS survey spectra of silver-free (Ag0) and all silver-doped coatings (Ag1, Ag2, Ag3). The surface of all studied coatings consisted out of Ti, O, Ca, P and C, which is in agreement with the previously shown EDS mapping results. The C peak present in the XPS survey spectra is believed to arise from adventitious carbon surface contamination. For the Ag-doped coatings (Ag1-Ag3), a peak attributed to the element Ag was also detected in the XPS survey spectra and the intensity of these Ag peaks increased with increasing silver acetate content in the electrolyte. The surface elemental composition of the coatings was determined from these survey spectra and the obtained results are shown in **Table 6.1**. The data clearly show that the surface elemental composition of all studied coatings was similar, with the exception of the silver content. As expected, silver was not observed at the surface of the Ag0 sample, in contrast to the samples Ag1, Ag2 and Ag3. A small (though not significantly different) increase in Ag content with increasing silver acetate content in the electrolyte was also observable. This relatively small Ag concentration was the result of the limited penetration depth of XPS as in the case of AlK_{α} radiation, the sampling depth of XPS is typically in the range 3-10 nm while the coating thickness is in the order of μm 's. Consequently, only the Ag that was present in the close proximity of the surface of the oxide films contributed to the XPS signal and Ag that was buried deeper inside the porous layer was thus not detected. **Figure 6.5 (B-F)** shows the high-resolution XPS spectra of the elements titanium (Ti2p), silver (Ag3d), oxygen (O1s), phosphorous (P2p) and calcium (Ca2p) of the coating surface of the sample Ag3. As there was no significant difference in the obtained high-resolution spectra for all Ag-doped samples, only the high-resolution XPS peaks of the sample Ag3 are presented in this work. As can be seen in **Figure 6.5.B**, the Ti2p spectrum contained two well-separated peaks at 464.5 eV for Ti2p_{1/2} and 458.8 eV for Ti2p_{3/2}, a doublet which is known to correspond to titanium dioxide[466]. The Ag3d high-resolution spectrum (**Figure 6.5.C**) also consisted out of 2 well-defined peaks centered at 368.2 eV for Ag3d_{5/2} and 374.2 eV for Ag3d_{3/2} with a binding energy difference of 6 eV between both peaks indicating the presence of metallic silver[467,468]. The broad O1s spectrum (**Figure 6.5.D**) could be deconvoluted into three Gaussian components [447]. The peak located at 530.1 eV was assigned to oxygen in TiO₂ [448,449] and O

atoms bound to other atoms such as Ca and Ag. The second peak at 531 eV corresponded to oxygen present in titanium phosphates while the third peak at 532.2 eV was attributed to oxygen present in the chemical groups Ti-OH and P-OH. The broad P2p spectrum (**Figure 6.5.E**) of the Ag3 coating could be deconvoluted into 2 separate peaks: one at 132.8 eV and one at 133.5 eV which could be assigned to P-O bonds in PO_4^{3-} and HPO_4^{2-} , respectively [469]. Finally, the high-resolution Ca2p spectrum (**Figure 6.5.F**) was deconvoluted into two separated peaks located at 347.1 eV and 350.7 eV, which could be attributed to calcium present in $\text{Ca}_3(\text{PO}_4)_2$ [446,470]. From the high resolution spectra, it can thus be observed that the developed coating surface was composed of TiO_2 containing a small amount of calcium and phosphate groups. The Ca and P elements in the coatings mainly existed as $\text{Ca}_3(\text{PO}_4)_2$, regardless of the degree of Ag incorporation. However, as already stated, the XPS results can only provide chemical information of the top few nm's of the coating, therefore, XRD analysis was also performed to additionally investigate the crystallinity of the developed coatings.

Table 6.2. Elemental composition of Ag-free and Ag-doped TiO_2 coatings obtained from XPS analysis.

Sample	Ti (at%)	O (at%)	Ca (at%)	P (at%)	C (at%)	Ag (at%)
Ag0	5.7 ± 1.1	54.6 ± 2.3	9.7 ± 1.6	6.2 ± 2.1	23.9 ± 3.5	0
Ag1	4.7 ± 1.3	55.2 ± 1.6	10.3 ± 0.6	7.1 ± 1.1	21.9 ± 1.6	0.8 ± 0.5
Ag2	4.2 ± 1.2	54.2 ± 1.8	10.7 ± 1.5	6.5 ± 0.8	22.9 ± 1.9	1.5 ± 0.8
Ag3	4.3 ± 1.6	53.1 ± 1.8	9.6 ± 1.1	6.6 ± 0.9	24.3 ± 1.7	2.2 ± 1.5

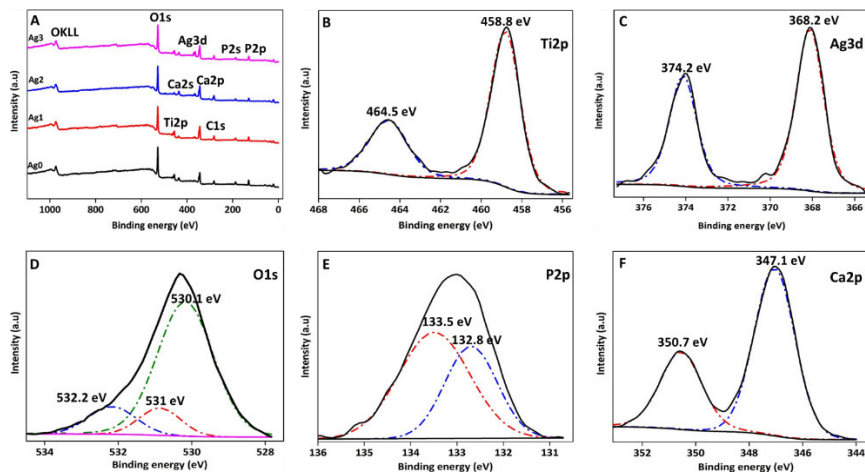


Figure 6.5. XPS survey spectra of the coatings (A), deconvoluted high-resolution Ti2p (B), Ag3d (C), O1s (D), P2p (E) and Ca2p (F) peaks of the Ag3 coating.

XRD patterns of PEO-treated Ti discs were obtained and the gathered results are shown in **Figure 6.6**. The coatings mainly consisted of the rutile and anatase forms of titanium dioxide (TiO_2), hydroxyapatite and calcium titanate (CaTiO_3). The intensities of the peaks changed depending on the silver acetate concentration of the electrolyte utilized during the PEO process. As can be seen in **Figure 6.6**, with an increased silver concentration in the electrolyte, the peak intensities of the rutile phase ($2\theta = 28.1, 35.06, 36.2$) were increased in comparison to the anatase phase ($2\theta = 25.2$) along with an increase in peak intensities of the hydroxyapatite ($2\theta = 27.46, 31.66, 39.7, 44.6$) and CaTiO_3 ($2\theta = 47.04, 49.48$) phases. This effect was more noticeable for the Ag2 and Ag3 samples. Therefore, it can be stated that the Ag2 and Ag3 samples contained more rutile TiO_2 and Ca- and P-containing phases (hydroxyapatite and CaTiO_3) compared to the Ag0 and Ag1 samples. Similar to our findings, Muhaffel et al. [462] also reported more intense hydroxyapatite and rutile phase formation in the coatings when using an increased concentration of AgNO_3 in the electrolyte. Similarly, Song et al. [331] reported the formation of Ca- and P-containing phases such as hydroxyapatite and tricalcium phosphate and observed that the appearance of the hydroxyapatite phases was dependent on the AgNO_3 or CH_3COOAg concentration used in the electrolyte. The observed

differences in crystallinity are due to the fact that increasing the silver content in the electrolyte leads to a PEO process proceeding at higher current density thereby enhancing the crystallinity of the deposited TiO_2 layer (**Figure 6.1**).

Thus, during PEO, different crystalline phases can be obtained by varying the composition of the electrolyte. At the first stage of the PEO process, Ti ions and hydroxyl ions react with one another to form anatase and rutile phases in the microdischarge channels. The anatase phase is formed earlier when the temperature is low in the microdischarge channels hence it is thermodynamically less stable than rutile. Both anatase and rutile phases can form bioactive hydroxyapatite layers and have good biocompatibility towards different cell types [471,472]. At the next stage of the PEO process, calcium and phosphate ions occurring at a higher temperature in the microdischarge channels react with each other to form hydroxyapatite phases in the coating while calcium titanate phases are formed by the reaction of calcium, titanium and hydroxyl ions[473]. Studies have demonstrated that calcium titanate layers can contribute to an increased adhesion strength between Ti and hydroxyapatite and can decrease the progression of hydroxyapatite dissolution in an acidic environment which is produced by osteoclastic resorption in the body [474]. It is therefore presumed that the presence of these crystalline phases in the coated Ti samples prepared in this chapter may positively influence the bioactivity of Ti by enhancing its osteogenic properties.

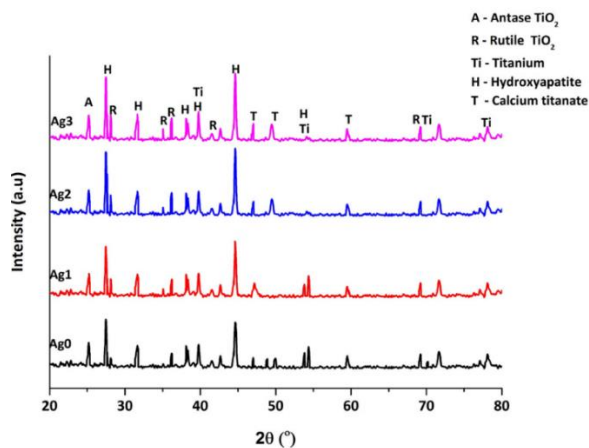


Figure 6.6. XRD spectra of the Ag-doped TiO_2 coatings.

6.3.3 Surface roughness, wettability and microhardness

The average roughness values (R_a) of the pristine polished Ti surface and the Ag0, Ag1, Ag2 and Ag3 coatings are shown in **Figure 6.7.A**. The originally very low surface roughness of the polished Ti disc strongly increased after all conducted PEO processes. The observed increase in surface roughness could be attributed to the formation of porous coatings on top of the smooth Ti substrate during the PEO process. Meanwhile, after the PEO processes, the water contact angle of the samples significantly decreased from 60° for the untreated Ti disc to approximately 22° for all coated samples (**Figure 6.7.B**). The surface roughness and the water contact angles of the silver-doped coatings (Ag1, Ag2, Ag3) were comparable to those of the silver-free coating (Ag0), indicating that the incorporation of Ag in the coatings did not apparently change their surface topography nor wettability. Similar findings were observed by Zhang et al. [342]. The microhardness of the untreated Ti and PEO-treated Ti samples is shown in **Figure 6.7.C**. While the microhardness of the untreated Ti was approximately 200 VHN, the microhardness of the PEO-treated samples was much higher (400-500 VHN). The difference in microhardness between the untreated and coated Ti substrates could be attributed to the porous morphology (hard ceramic oxide layers) and the crystallinity (rutile phase) of the deposited coatings [371]. Although there was no significant difference in microhardness between the different PEO coatings, a slight increase in microhardness was observed for the samples Ag2 and Ag3 in comparison to the samples Ag0 and Ag1. This increase is may be due to the higher amount of rutile phase (as observable in **Figure 6.6**) in the former samples. The observed increase in sample surface hardness is very beneficial for clinical applications, as it decreases the occurrence of wear of an implant and thus contributes to its longevity [475].

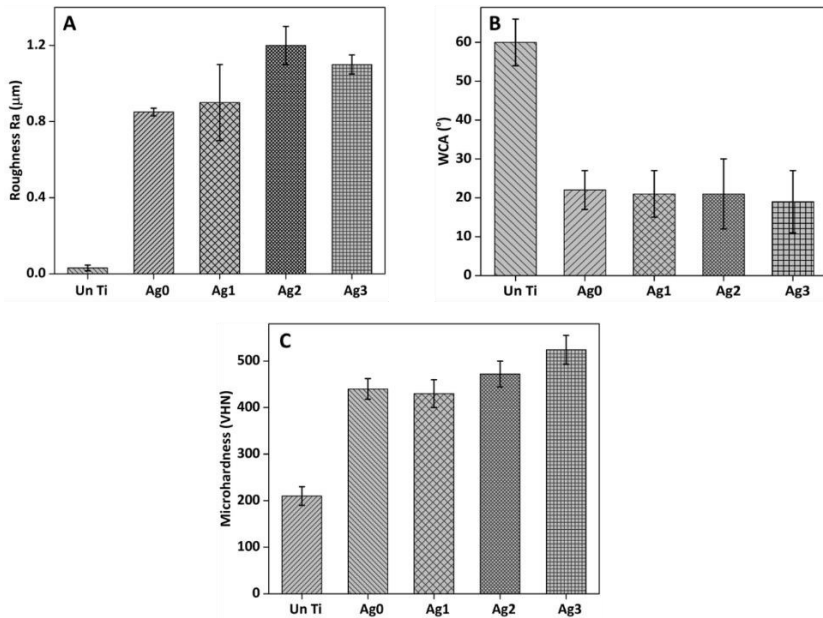


Figure 6.7. Roughness (A), WCA (B) and microhardness (C) of untreated Ti, Ag0, Ag1, Ag2 and Ag3 samples.

6.3.4 Frictional coefficient of the coatings

The frictional coefficient of the untreated and PEO-treated Ti discs measured from scratch tests using a diamond indenter at various loads is illustrated in **Figure 6.8**. As shown, all PEO-treated coatings exhibited a lower coefficient of friction compared to the untreated Ti at all examined loads. This decrease could be explained by the increased hardness of the deposited ceramic-like coatings (see **Figure 6.7.C**). However, the frictional coefficient was also reduced when the Ag concentration in the electrolyte was increased (Ag2, Ag3) and the decrease was more pronounced at higher loads (5 N and 7 N). A similar trend was also observed for coatings containing alumina and silica particles prepared by PEO [476] and for silver tantalate coatings [477]. This frictional coefficient decrease may be either due to the increased crystallinity [478] of the Ag2 and Ag3 coatings or due to lowest contact resistance offered by the Ag containing surface [479]. Moreover, the silver content in the coating may act as a lubricant between the indenter and the Ti substrate, thus reducing the frictional coefficient [387,476,477,480]. Although coatings with high frictional coefficient

are considered to be an advantage in providing primary fixation for implants, the prominent factors causing implant loosening are considered to be particle accumulation and failure in osseointegration [24]. Moreover, coatings with a high frictional coefficient can also generate wear debris, leading to inflammation which is in turn destructive to the bone supporting the implant. The observed decrease in the frictional coefficients of the PEO-treated samples might thus be favorable for implant applications, as the coatings might increase the resistance to wear and consequently decrease the occurrence of implant loosening [481,482].

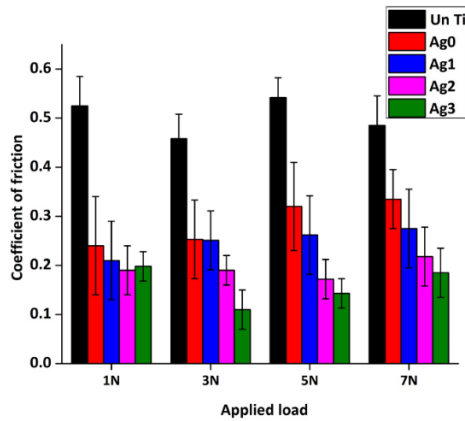


Figure 6.8. Coefficient of friction of untreated and PEO-treated Ti discs evaluated by a pin-on-disc scratch tester at varying loads.

6.3.5 Silver ion release kinetics

To study the Ag^+ release kinetics of the prepared coatings, the silver-doped samples (Ag1, Ag2, Ag3) were incubated in distilled water for up to 7 days and the amount of Ag^+ released from the coatings was analyzed using ICP-MS. The result of this test is summarized in **Figures 6.9 A and B** where the Ag^+ cumulative release profiles and the Ag^+ release per day of Ag1, Ag2 and Ag3 samples are plotted as a function of incubation time in water. As can be seen in **Figure 6.9.A**, the cumulative Ag^+ release was observed to increase with incubation time for all Ag-doped samples. However, the increase was much less pronounced for the Ag1 sample compared to the coatings containing higher amounts of silver (Ag2 and Ag3). Samples with a higher Ag concentration present in the coating (Ag2, Ag3) exhibited a higher Ag^+

release at any given point throughout the total incubation time of 7 days. The maximum amount of Ag^+ released from the Ag1, Ag2 and Ag3 samples in cumulative measurements over 7 days was approximately 264 ppb, 813 ppb and 1110 ppb, respectively. As expected, the actual amount of released Ag^+ was thus strongly affected by the initial silver loading, and also strongly depended on the incubation time. This observation was in agreement with previously reported release results for other oxide coatings[332,462]. As shown in **Figure 6.9.B**, the release of Ag^+ per day (ppb/day) after the first immersion day was 30 ppb/day, 84 ppb/day and 112 ppb/day for the Ag1, Ag2 and Ag3 coatings, respectively. The Ag^+ release per day of the Ag1 sample was observed to increase during the first day of immersion after which a constant level of release was observed followed by a decrease in the Ag^+ release after 7 days of immersion. On the other hand, for the Ag2 and Ag3 samples, the Ag^+ release was found to decrease already after 3 days of immersion. Thus, these samples showed an initially increasing Ag^+ release reaching a peak release after 3 days immersion, followed by a more constant, lower Ag^+ release. Additionally, it can also be observed that the Ag^+ release for the Ag1 and Ag3 samples was lower at day 7 than at day 5, whereas a slight increase in Ag^+ release was observed for the Ag2 sample on day 7 compared to day 5. This opposite trend may be due to the slightly different arrangement of silver within the oxide layer in case of sample Ag2 as the release kinetics of the prepared coatings are known to mainly depend on the diffusion pathway of silver present in the porous coatings. Silver present closer to the surface releases Ag^+ more quickly due to its shorter diffusion path (initial Ag^+ release) while silver present deeper in the porous oxide coating is released at later time as this release is diffusion limited. Consequently, the slight increase in Ag^+ release for the sample Ag2 on day 7 might be due to the particular arrangement of silver within this porous oxide layer, which is unfortunately an uncontrollable factor in the case of PEO.

Concerning the optimal amount of Ag^+ desired to achieve excellent biocompatibility and antibacterial ability, Shi et al. reported that an Ag^+ concentration between 270 ppb and 2200 ppb exhibited 90% antibacterial efficiency against *E. coli* and *S. aureus* and 80% cell viability of fibroblast cells. However, increasing the Ag^+ concentration above 2200 ppb showed an increase in bacterial reduction combined

with a decrease in cell viability [483]. Similarly, no cytotoxic reaction of human mesenchymal stem cells was observed with an Ag^+ concentration below or equal to 1000 ppb [484]. On the other hand, the minimum inhibitory Ag^+ concentrations for *E. coli* and *S. aureus* are 0.3 ppb and 3.5 ppb. In this respect, Ag^+ rates from the coated samples prepared in this work are sufficient for killing bacteria without negatively affecting cells. However, further studies have to be performed to evaluate the long-term release kinetics of Ag^+ from the prepared coatings.

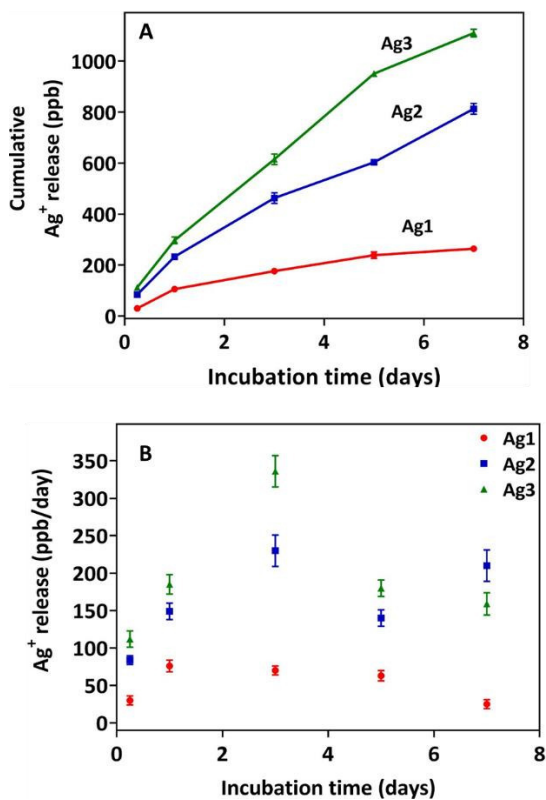


Figure 6.9 Cumulative Ag^+ release (ppb) (a) and Ag^+ release rate (ppb/day) when immersed in water up to 7 days for Ag1, Ag2 and Ag3 samples.

6.3.6 *In-vitro* antibacterial activity of the coatings

The antibacterial assays against *E. coli* (ATCC 25922), MSSA (ATCC 6538) and MRSA (Mu50) were performed on the studied samples and the untreated Ti disc served as control. These bacterial species were selected as representatives of gram-negative and gram-positive bacteria and because they are commonly found in implant associated infections[485]. As can be seen in **Figure 6.10**, no reduction in *E. coli*, MSSA and MRSA was observed when untreated Ti and Ag- free coatings (Ag0) were tested. In both cases, approximately 10^8 CFU were recovered for all three bacterial strains after 24 hours of incubation. In contrast, the Ag-doped (Ag1, Ag2, Ag3) coatings showed a significant reduction ($P < 0.05$) in bacterial cell numbers. The antibacterial efficiency of the coatings was strongly dependent on the concentration of silver acetate in the electrolyte during the PEO treatment process. In the case of samples with low Ag content (Ag1), a 4-log reduction of *E. coli*, a 3-log reduction of MSSA and a 2-log reduction of MRSA were observed. Samples with high Ag content (Ag2, Ag3) exhibited an even superior antibacterial activity showing approx. a 6-log reduction of *E. coli* and a 5-log reduction of MSSA and MRSA after 24 hours of incubation. These findings, i.e. the decrease in bacterial numbers with increasing concentration of silver acetate in the electrolyte corresponded well with the measured Ag^+ release (**Figure 6.9**) and suggested that the Ag^+ ions released from the coatings into the surrounding aqueous medium were the main antibacterial compounds [324,457]. In fact, studies have reported that the mechanism of antibacterial action of Ag^+ is jointly associated with its interface with thiol groups in enzymes and proteins [486]. Sondi et al. observed cells of *S. aureus* and *E. coli* exposed to Ag^+ by means of transmission electron microscopy and observed that after exposure the cellular content of the bacteria was released from the cell wall and consequently the cell wall was degraded [487]. Although the exact mechanisms underlying the antibacterial mechanism of Ag^+ are still not fully understood, many previous studies reported that the interaction between Ag^+ and bacterial membranes can cause structural damage to the membranes and the cell metabolic activity resulting into cell death [486,488–490].

In addition to the antibacterial assays, SEM examination of MRSA was also performed to investigate the effect of Ag incorporation in the coatings on the bacterial adhesion and morphology of MRSA colonies.

From **Figure 6.11**, it can be seen that the adherent *S. aureus* started to form a biofilm as they clustered on the untreated Ti surface and the Ag0 coating, but these bacterial clusters were decreased with increased dose of Ag⁺. MRSA cells displayed a round-shaped morphology and undamaged binary fission (indicated by the blue arrows in the inset SEM images of samples Ti, Ag0 and Ag1) when cultured on the untreated Ti surface (Ti), the Ag-free coating (Ag0) and the coating with the lowest Ag content (Ag1). While the cells look intact and display smooth surfaces on the untreated Ti surface and the Ag0 sample, distinct cell debris and lysed cells (red arrows in the inset SEM images of samples Ag1, Ag2 and Ag3) were also observed on the silver-doped Ag1, Ag2 and Ag3 coatings. In addition, no undamaged binary fission was observed on the Ag2 and Ag3 samples. Combined, these results indicated that the Ag-doped coatings exhibited a greater ability to inhibit both gram-positive and gram-negative bacteria and the coatings with increased Ag content had superior antibacterial efficacy against all investigated bacteria.

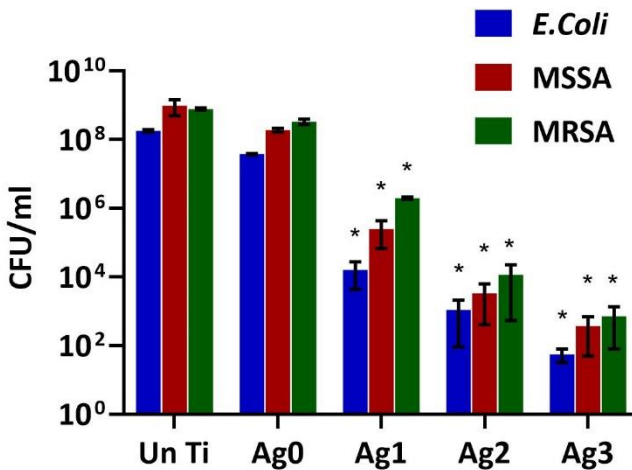


Figure 6.10. Number of CFU after 24 hours of incubation for different samples. Asterisk () denotes a significance difference at $P < 0.05$ compared to the control sample (untreated Ti).*

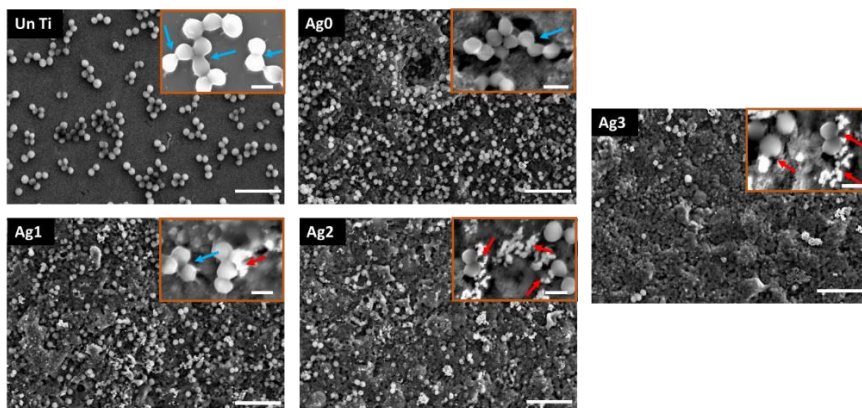


Figure 6.11. SEM images of MRSA strain cultured on uncoated and coated Ti samples (scale bar: 5 μm , insert : 1 μm). Blue arrow indicates bacterial colonies and undamaged binary fission, red arrow indicated distinct cell debris and lysed cells

6.3.7 Protein adsorption to the coatings

When a foreign material is placed in the body, the first mechanism that takes place is the deposition of a protein layer from the blood and the body fluids onto the surface of the implant [440]. The presence of this film influences the interactions between the material and the cell/bacteria together with the activation of inflammatory reactions [491]. Therefore, it is important to investigate the protein adsorption on the implant material and for this purpose, FBS and BSA were used as model proteins. **Figures 6.12 A and B** show the images of the obtained SDS-PAGE gels and the percentage of the band intensities (relative to the control samples FBS and BSA, respectively). As can be seen, in case of FBS, no protein band was present for the untreated Ti whereas a very light band was observed for the samples Ag0, Ag1 and Ag2 and a strong band for the Ag3 sample. This finding thus suggests that FBS adsorption was the most pronounced on the Ag3 sample. A similar trend was seen for samples exposed to BSA, while in this particular case the intensity of the BSA band strongly increased on the samples Ag2 and Ag3. Thus, a preferential adsorption of albumin (molecular weight – 64 kDa) was observed on all PEO-treated samples with the most pronounced adsorption on the Ag2 and Ag3 samples at the early phase of the formation of a protein layer (after 2h immersion). A similar effect was seen on the

fluorescence images of samples incubated in FITC-labelled albumin (**Figure 6.13**). As can be seen in **Figure 6.13**, a strong increase in fluorescence intensity was observed on the PEO-treated coatings (Ag0, Ag1, Ag2 and Ag3) compared to the untreated Ti sample. Additionally, the Ag-doped coatings (Ag1, Ag2, Ag3) also showed a larger amount of protein adsorption than the Ag-free coating (Ag0) and the effect is more pronounced with increasing Ag content (Ag2, Ag3). These results are in agreement with Chen et al., who reported that an Ag⁺ release up to 1.7 ppm did not have any deleterious effect on protein structure or protein adsorption [492].

Albumin adsorption on the surface was observed to be beneficial for biomaterials, as pre-adsorption of albumin inhibits platelet adhesion and hence inhibits inflammatory reactions [491,493]. Between the PEO-treated and the untreated Ti, an increased albumin adsorption observed in the former was mainly related to the surface physico-chemical properties such as changed chemical composition as well as improved wettability, roughness and crystallinity which was in agreement with previously published results [491]. However, among the PEO-treated coatings (Ag0, Ag1, Ag2 and Ag3), the observed difference in albumin adsorption was mainly due to the increased amount of Ag on the coating surface and the increased crystallinity as all coatings exhibited a similar wettability (WCA – 20°) and surface roughness (approximately 1 μm). The observed increase in albumin adsorption on the coatings containing high amounts of silver was due to the fact that these coatings possess more binding sites as disulfide bonds present in the albumin can form strong sulfur-silver complexes [494]. Moreover, the presence of Ca²⁺ and PO₄³⁻ ions in the investigated coatings are also believed to be albumin binding sites and thus provide a major driving force for its adsorption [495,496].

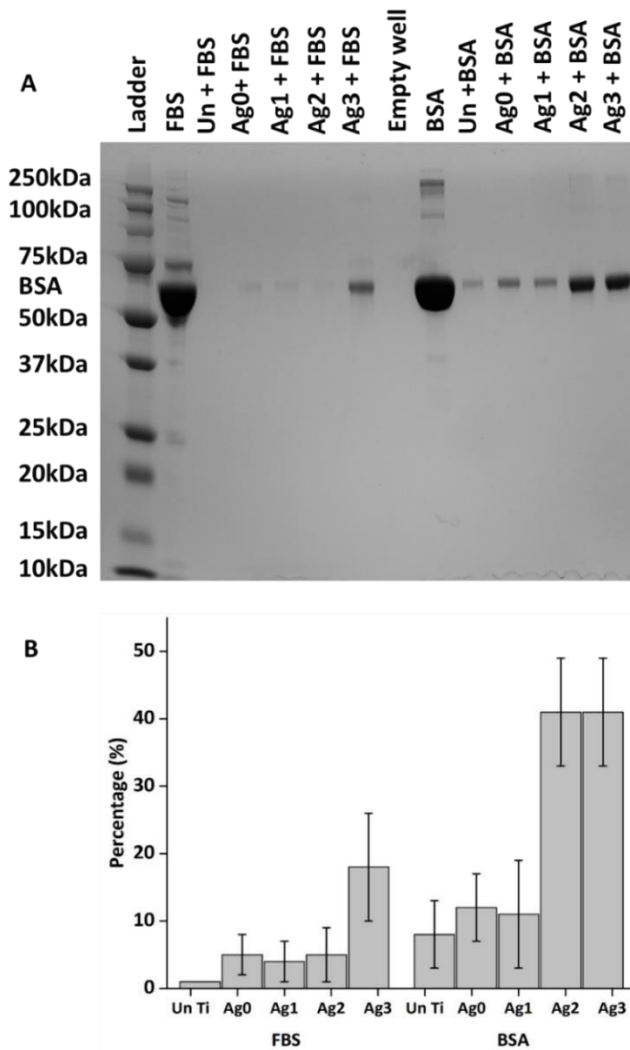


Figure 6.12. SDS-PAGE analysis of FBS and BSA proteins for different investigated Ti samples: (A) gel image of one of the triplicate measurements showing the protein bands (A) and percentage of the intensity of the FBS/BSA bands calculated from the gel images using ImageJ (B).

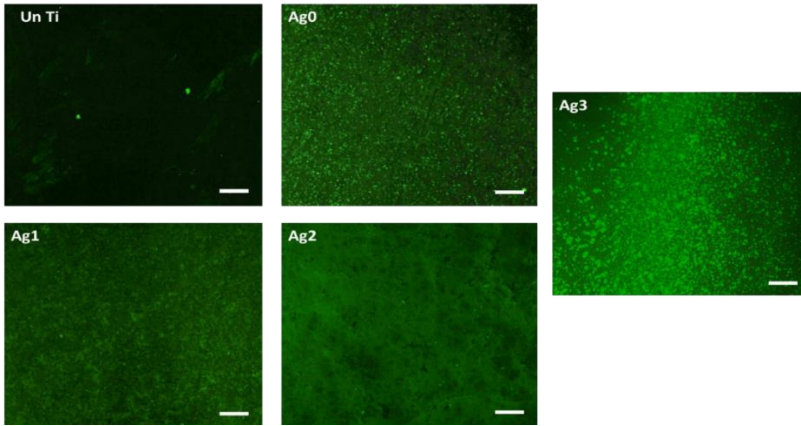


Figure 6.13. Fluorescent images of Ti samples after incubation in FITC-labelled albumin for 1 hour.

6.3.8 Osteoblast cell response

Besides examining the surface characteristics, the *in vitro* antibacterial properties and protein adsorption of the produced coatings, the cellular behavior was also studied in an effort to understand possible correlations between the coating's surface properties, the Ag content of the coatings and their cellular response. In the first step, the morphology and viability of MC3T3 cells cultured on both untreated and PEO-treated Ti samples were examined by SEM and fluorescence microscopy after live/dead staining of the cells. **Figure 6.14** and **Figure 6.15** show the SEM and live/dead images that were obtained on day 1 and day 7 after cell seeding, respectively. These images clearly exhibited differences between the untreated Ti sample, the Ag-free (Ag0) and the Ag-doped (Ag1, Ag2, Ag3) coatings. As it is shown in **Figure 6.14** (1st and 2nd column), one day after cell seeding, the MC3T3 cells adhering to the untreated Ti sample demonstrated a rather round morphology indicating limited cell adhesion. In contrast, the amount of adhered cells was significantly higher on all PEO-treated samples compared to the untreated Ti. Moreover, on these samples, the MC3T3 cells were more elongated and spindle-shaped suggesting excellent cell adhesion. From the fluorescence images (3rd column), it can be observed that one day after cell seeding, nearly no dead cells were observed on the surface of all samples indicating that the coatings deposited on the Ti substrate had no detectable cytotoxicity to

osteoblast cells. In fact, the Ag-free and Ag-doped coatings exhibited a higher cell density with more living cells independently of the Ag content in the coating as compared to the untreated Ti surface.

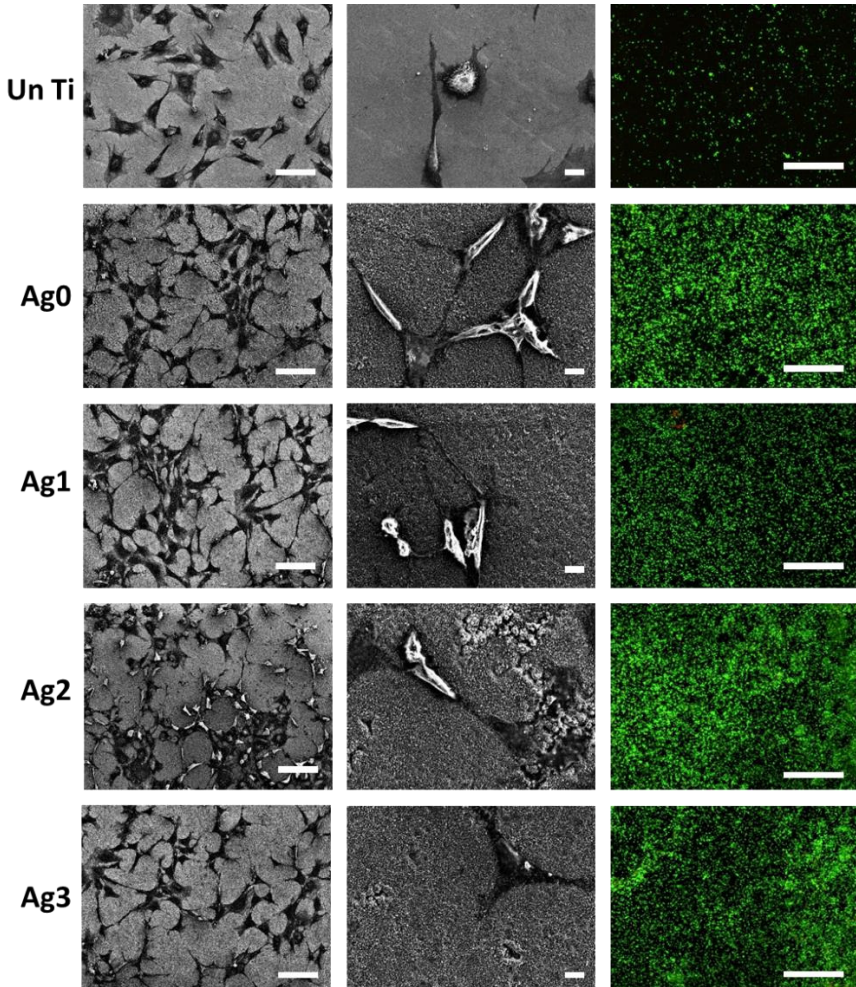


Figure 6.14. Fluorescence and SEM images of MC3T3 cells cultured on uncoated and coated Ti samples 1 day after cell seeding (scale bar: 100 μm (1st column), 10 μm (2nd column) and 500 μm (3rd column)).

Figure 6.15 shows the SEM and live/dead staining images obtained on untreated and PEO-treated Ti substrates seven days after cell seeding.

The SEM images demonstrated similar results as were observed one day after cell seeding: a significantly higher number of MC3T3 cells with a spread out morphology was observed on all PEO-treated samples in contrast to the untreated Ti sample which mainly showed the adherence of more round cells. However, the fluorescence images of PEO-treated samples revealed that the viability of the osteoblast cells reduced when using the highest silver concentration in the coatings (sample Ag3). Although there were no discernible dead cells found on the Ag0, Ag1 and Ag2 coatings, a marked number of dead cells was present on the Ag3 coating suggesting possible cytotoxic effects of this particular coating.

To quantify the cellular response of the different coatings, an MTT assay was also performed and the results are presented in **Figure 6.16**. This figure shows the viability of MC3T3 cells relative to TCPS one day and seven days after cell seeding for all Ti samples. At the first glance, it can be clearly seen that cell viability was higher on all PEO-treated samples than on untreated Ti. One day after cell seeding, there was no significant difference in cell viability between the Ag0 and Ag1 samples, both exhibiting approximately 80% cell viability. However, in the case of the Ag2 and Ag3 samples, the cell viability was slightly higher (around 93%). The obtained MTT results were thus in good agreement with the previously shown fluorescence images. Seven days after cell seeding, the cell viability increased further on all investigated samples with the exception of the Ag3 sample, on which cell viability reduced.

The observed differences in cellular response between the PEO treated and untreated Ti can be correlated to the surface wettability, roughness and surface chemical composition of the samples. The untreated Ti sample was less wettable and very smooth and thus showed poor protein adsorption and consequently a reduced osseointegration [497] compared to the PEO-treated samples. In fact, a very recent study suggested that a moderately hydrophilic (WCA in the range 20-40°) and a roughened Ti surface exhibited the highest level of cell attachment [498,499]. Similar findings were also reported in several *in-vivo* studies where rough surfaces were found to produce better bone fixation than smooth machined surfaces [497,500,501]. Consequently, the rough and more hydrophilic nature of the deposited coatings can thus explain the

observed enhanced cell adhesion and growth. Moreover, the incorporation of Ca and P ions into the coatings also further enhanced the bioactivity of the coating. In fact, studies have reported that stoichiometric HA has a Ca/P ratio of 1.6 and that a lower bioactivity was observed on HA coatings possessing Ca/P ratios below 1.5. From the XPS elemental composition (**Table 6.1**), it can be seen that the Ca/P ratio of the Ag0, Ag1, Ag2 and Ag3 coatings were 1.55, 1.45, 1.64 and 1.62, respectively, values which are close to the target ratio (Ca/P = 1.6). Consequently, an increased bioactivity was seen on all PEO-treated samples irrespective of the silver content in the coating. However, among the PEO-treated coatings (Ag0, Ag1, Ag2 and Ag3), the observed difference in cell viability and proliferation was mainly related to the amount of Ag present on the coating surface and the increased crystalline phases since all coatings exhibited a similar wettability and surface roughness (see **Figure 6.7**). For example, the significant difference in cell viability 1 day after cell seeding between the Ag0/Ag1 samples and the Ag2/Ag3 samples and 7 days after cell seeding between the Ag0 and the Ag2 samples could be mainly attributed due to increased crystalline phases (rutile, hydroxyapatite, CaTiO_3) observed in the coatings with high Ag content (Ag2 and/or Ag3). Similar findings were reported by other researchers where an enhanced osseointegration was observed on a crystallized hydroxyapatite phase in comparison to an amorphous phase or a rutile TiO_2 coated material [454,502,503]. At this point, it is also important to note that the cumulative Ag^+ released from all the Ag-doped coatings during the first day was less than 400 ppb which is very significantly below the toxicity level for cells. However, 7 days after cell seeding, the Ag2 samples showed superior cell viability performance (Ag^+ release approximately 800 ppb), while the Ag3 samples showed lower cell viability. This may be due to the high Ag^+ release from this particular coating (> 1000 ppb) which potentially reduced the cell viability. However, based on our results, it can be seen that even on the Ag3 samples the cell viability was still above 70%, thereby meeting the ISO standards for an implant material to be biocompatible [504]. Hence, it can be stated that coatings with favorable surface properties containing a small amount of silver can provide an implant surface with a bi-functional character (antibacterial activity and tissue integration).

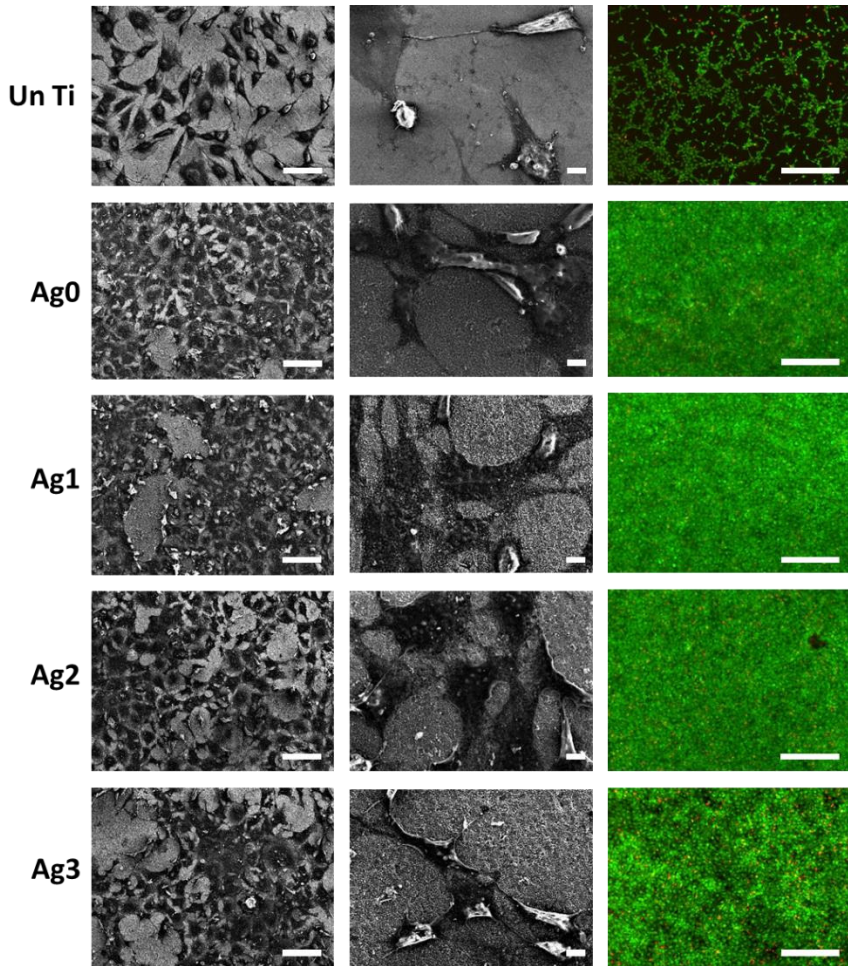


Figure 6.15. Fluorescent and SEM images of MC3T3 cells cultured on uncoated and coated Ti samples 7 days after cell seeding (scale bar: 100 μm (1st column), 10 μm (2nd column) and 500 μm (3rd column)).

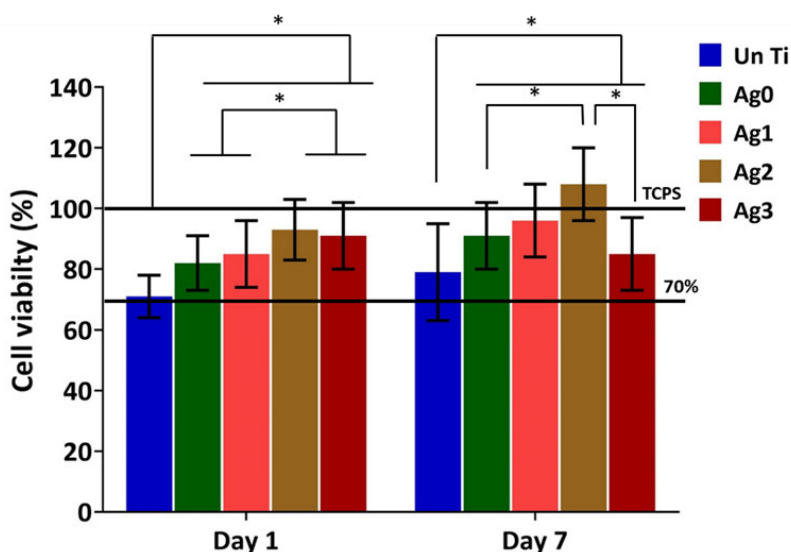


Figure 6.16. Cell viability results 1 day and 7 days after cell seeding on different titanium samples. Asterisk (*) denotes a significant difference at $P < 0.05$.

6.4 Conclusion

In this chapter, the successful synthesis of bi-functional Ti surfaces by PEO has been demonstrated using an electrolyte enriched with calcium, phosphorus and silver acetate. For the first time, it was shown that the amount of crystalline phases such as rutile TiO_2 and Ca- and P-containing phases (hydroxyapatite, CaTiO_3) on the coating can be increased with increasing the silver acetate concentration in the electrolyte. This increased crystallinity was found to be a crucial factor in promoting successful protein adsorption and tissue integration. Increasing the concentration of silver acetate in the electrolyte increased the amount of silver in the coatings from 0.8 at% to 2.2 at%. On the other hand, the porous microstructure of the coatings, their moderate surface roughness (0.8-1 μm) and high wettability (approximately 20°) were not altered by the incorporation of Ag. In addition, all PEO-treated coatings exhibited superior mechanical properties i.e. improved microhardness and reduced frictional coefficient. The silver ion release kinetics of the Ag-doped coatings in

an aqueous environment were also examined and showed that the amount of Ag⁺ released was dependent on the initial silver loading and the total incubation time. Due to this Ag⁺ release, the Ag-doped coatings exhibited excellent antibacterial activity against *E. coli*, MRSA and MSSA in comparison to the Ag-free coatings. Moreover, the antibacterial activity of the coating was found to increase with an increase in silver acetate content in the electrolyte. Besides the very good antibacterial performance of the Ag-doped coatings, all prepared coatings were also able to promote osteoblast adhesion and proliferation in comparison to the untreated Ti surface. Due to their superior mechanical properties, antibacterial efficacy and excellent biocompatibility, the produced coatings may be of significant interest for orthopedic implants. Therefore, future studies should assess interactions of different cells as well as bone formation on PEO-treated Ti surfaces and should focus on a tribocorrosion study to understand the degradation mechanisms of these coatings during implant applications. In addition, clinical trials will be needed to assess the longevity of the PEO-treated implant surfaces.

**Chapter 7. Fabrication of Ag/a-C:H
nanocomposite coatings on Ti implants
with improved mechanical,
antibacterial and cell-interactive
properties**

The results of chapter 7 were published in the following international peer-reviewed journal:

Thukkaram M, Vaidulych M, Kylian O, Hanus J, Rigole P, Aliakbarshirazi S, Asadian M, Nikiforov A, Van Tongel A, Biederman H, Coenye T, Du Laing G, Morent R, De Wilde L, Verbeken K, De Geyter N.

“Investigation of Ag/a-C:H nanocomposite coatings on titanium for orthopedic applications”

ACS Applied Materials and Interfaces, 12(21): 23655-23666 (2020).

7.1 Introduction

Chapters 5 and 6 have focused on the fabrication of microporous oxide coatings using the PEO technique employing two different types of electrolytes. This technique provides a plasma-assisted electrochemical conversion of metal surfaces into oxide layers in the presence of an electrolyte. Thus, the deposited oxide coating contains both the elements of the metal substrate and the elements of the electrolyte. The PEO deposited coatings, as discussed in chapters 5 and 6, improved the surface properties, mechanical, antibacterial and cell-interactive properties via the incorporation of several ions and particles present in the electrolyte. However, the drawback of this technique is the limited ability to independently control the properties of the oxide matrix and the amount and size of the antibacterial agents embedded inside the matrix. In contrast, using a cluster technique (combining a magnetron based gas aggregation source (GAS) system and PE-CVD technology), it is possible to independently control the size distribution and the flux of NPs that depends solely on the parameters in the GAS and the properties of the matrix material that can be adjusted by the parameters employed for PE-CVD (e.g. applied power, type of precursor, working gas mixture, bias on the substrate). Within this context, it is very desirable to generate a-C:H (amorphous hydrocarbon) nanocomposites embedding AgNPs using a cluster technique, as the a-C:H matrix can serve as a reservoir for the continuous out-diffusion of silver ions formed during contact of AgNPs with an aqueous environment by an oxidation mechanism involving protons and dissolved oxygen [488]. In addition, a-C:H films can elicit a more favorable biological response and possess superior mechanical properties, essential for implant applications. For instance, earlier studies have shown that this technique allows for the production of metal/amorphous hydrocarbon (a-C:H) nanocomposites on glass or silicon substrates with tailor-made metal filling factors and controllable mechanical properties of the a-C:H matrix [505,506]. However, the reported studies have focused mainly on the technological aspects of the production of metal/a-C:H nanocomposites and on the determination of their chemical structure and morphology. In contrast, a detailed investigation of the physico-chemical properties and its influence on the bi-functional character of the coatings (i.e. a coating with the combination of antibacterial ability and biocompatibility) have not been addressed so far. Taking this lack of experimental data into

account, in the present chapter, Ag/a-C:H nanocomposites possessing a variable amount of AgNPs have been deposited directly onto medical grade Ti substrates to investigate the relationship between various AgNPs contents in the nanocomposite coatings and the physio-chemical properties, antibacterial activity and osteoblast viability of the coatings.

7.2 Experimental methods

All experimental details can be found in chapter 4. The deposition method, analysis techniques and the corresponding parameters that are specifically used in this chapter are summarized in the **Table 7.1** and **Table 7.2**

Table 7.1. Experimental methods

Deposition method	GAS + PECVD Parameters (see Table 7.2)
Ti specimen	Pre-treatment - Ground and mirror like polished - Ar plasma : Power (70W), pressure (4.5 Pa) treatment time (2 min) - N ₂ plasma : Power (70W), pressure (2.5 Pa) treatment time (10 min)
Characterization techniques	1) Surface -SEM <ul style="list-style-type: none"> • SE mode and BSE mode - accelerating voltage : 20 kV • SE mode (titled at 30°) - accelerating voltage : 2 kV 2) XPS <ul style="list-style-type: none"> • Survey scans and high resolution C1s spectra 3) AFM 4) WCA 5) Scratch tests <ul style="list-style-type: none"> • Load : 10 - 50 N • Scratch length - 2mm

	<ul style="list-style-type: none"> • Indenter radius - 200 μm 6) ICP-MS silver ion release
<i>In-vitro</i> analysis	Antibacterial assay : CFU <ul style="list-style-type: none"> • <i>E. coli</i> ATCC 25922 • <i>S. aureus</i> ATCC 6538 • Incubation time - 24 hours Cell culture : MTT assay, SEM and Fluorescence microscopy <ul style="list-style-type: none"> • MC3T3 cells • Cell seeding time – day 1 and day 7

Table 7.2. Operational parameters used for the deposition of Ag/a-C:H nanocomposites.

RF power	DC magnetron current	Duty cycle	Pressure deposition chamber	Pressure aggregation chamber	Deposition time
70 W	200 mA - 500 mA	50%	5.6 Pa (Ar/n-hexane)	100 Pa (Ar)	5 min (100 nm)

7.3 Results and discussions

7.3.1 Characterization of AgNPs

As a first step, the AgNPs deposited in this work at a pressure of 100 Pa in the aggregation chamber using a DC magnetron current in the range 200 mA-500 mA are characterized using SEM and UV-Vis spectroscopy. **Figure 7.1.A** shows the size distribution of the AgNPs and **Figure 7.1.B** shows the evolution of the number of deposited AgNPs and their size as a function of DC magnetron current for a fixed deposition time (2.5 min). It was observed that the produced NPs were spherical

with a mean diameter of 24 ± 6 nm (**Figure 7.1.A**) independently of the used magnetron current (**Figure 7.1.B**). On the other hand, the DC magnetron current strongly influenced the deposition rate of the AgNPs: the number of NPs detected on the Ti substrates after 2.5 mins of deposition increased from 60 NPs/ μm^2 at 200 mA to 600 NPs/ μm^2 at 500 mA (**Figure 7.1.B**).

As can be seen in **Figure 7.2.A**, the acquired UV-Vis spectra were characterized by an intense localized surface plasmon resonance (LSPR) peak of silver at 390 nm and the intensity of this peak, which is correlated to the number of AgNPs, increased with magnetron current. In addition, to check the spatial homogeneity of the deposited AgNPs, UV-Vis spectra were also recorded at different positions on the treated samples (**Figure 7.2.B**). The fact that no variation in the LSPR peak intensity was observed on different positions of the treated samples clearly proves the very good homogeneity of the AgNPs deposition.

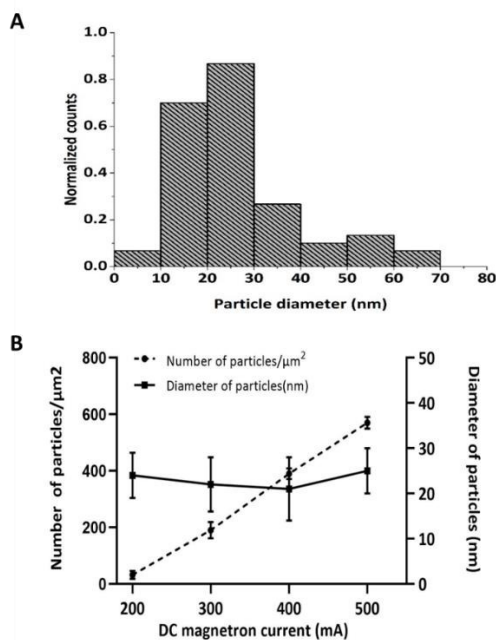


Figure 7.1. Histogram of the diameter of the AgNPs (A) and evolution of the number of deposited AgNPs and their size as a function of DC magnetron current(B). The deposition time was fixed at 2.5 mins.

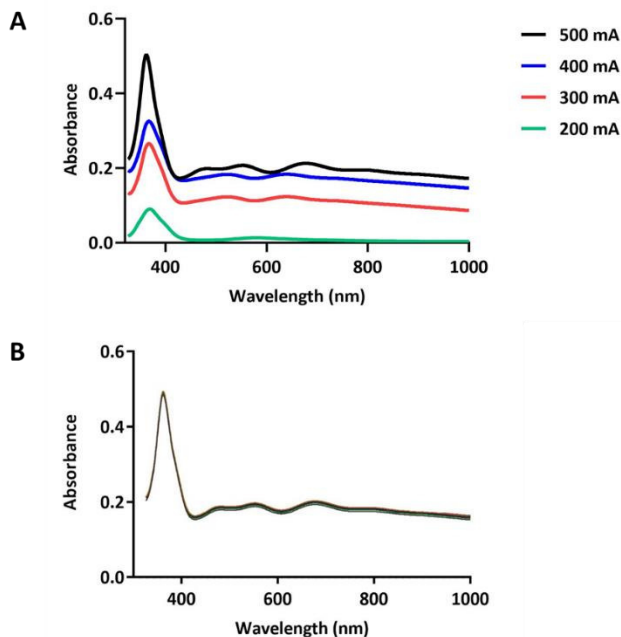


Figure 7.2. UV-Vis spectra of Ag monolayer films for different applied DC magnetron currents (A) and UV-Vis spectra recorded at different positions on the sample (magnetron current: 500 mA) (B).

7.3.2 Physico-chemical properties of Ag/a-C:H nanocomposites

As a next step, the physical and chemical characterization of the different nanocomposite coatings developed in this work was conducted. As previously mentioned, the amount of AgNPs embedded in the a-C:H matrices was changed by varying the magnetron current between 200 and 500 mA, while all other experimental parameters were fixed. **Table 7.3** shows the influence of the applied magnetron current on the surface chemical composition of the coatings, as determined from XPS. As expected, the silver content in the Ag/a-C:H nanocomposite films increased with increasing magnetron current, which is consistent with the results shown in **Figure 7.1.B** indicating the deposition of more AgNPs with increasing magnetron current. **Table 7.3** also indicates that this increase in silver content was accompanied by a relative decrease in carbon content, while no clear

trend in oxygen content was found with applied magnetron current. The oxygen content in the coatings can be explained by post-oxidation processes taking place during exposure of the coatings to ambient air prior to XPS analysis or partially by the unavoidable presence of impurities in the deposition chamber [506]. Besides determining the surface chemical composition, XPS was also used to reveal more information on the type of carbon functional groups present at the surface of the nanocomposite coatings by deconvolution of the high resolution C1s spectra. These deconvoluted C1s spectra are represented in **Figure 7.3** for the a-C:H matrix as well as for the Ag/a-C:H coatings prepared using a magnetron current of 200 and 500 mA. As shown in **Figure 7.3**, 2 components were used to deconvolute all C1s spectra: a peak at 284.8 eV which could be attributed to C-C/C-H functional groups as well as a peak at 286.0 eV which can be assigned to C-O functional groups. These results thus suggest that post-plasma oxidation mainly resulted in the incorporation of C-O functionalities at the coating surface. **Figure 7.3** also reveals no significant changes in all depicted C1s spectra suggesting that the matrix had a comparable chemical composition for the a-C:H sample and the Ag/a-C:H samples prepared with a magnetron current of 200 and 500 mA. It is important to note that the post-plasma oxidation may also affect the AgNPs and may result in oxidation of silver. However, the high resolution XPS spectra of silver did not confirm the presence of silver oxides. This is due to the limited penetration depth of the XPS technique that enables to analyze only the AgNPs in the close vicinity of the surface of the Ag/a-C:H films, i.e. only the small fraction of NPs presented in the coatings, which results in a low intensity of the Ag peaks and in turn does not allow for a reliable deconvolution of the peak. Consequently, these high-resolution Ag XPS peaks are not presented in this work.

Table 7.3. Surface elemental composition of Ag-free and Ag-incorporated a-C:H films.

Nanocomposite coating	C (at%)	O (at%)	Ag (at%)
a-C:H	91.2 ± 0.6	9.8 ± 0.4	-
Ag/a-C:H (200 mA)	87.5 ± 0.5	11.2 ± 0.7	1.3 ± 0.1
Ag/a-C:H (300 mA)	86.4 ± 0.9	10.2 ± 0.8	3.4 ± 0.2
Ag/a-C:H (400 mA)	85.1 ± 0.6	10.3 ± 0.9	4.1 ± 0.2
Ag/a-C:H (500 mA)	85.6 ± 0.2	9.0 ± 0.3	5.4 ± 0.2

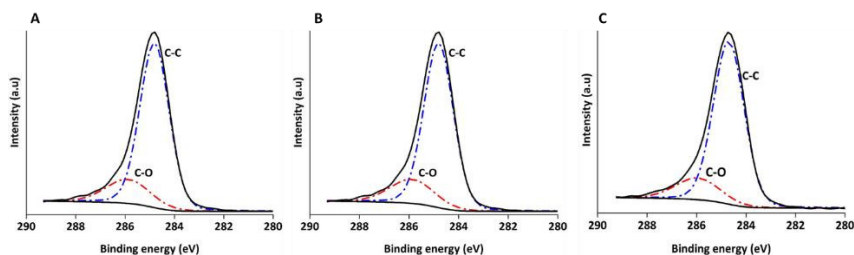


Figure 7.3. Deconvoluted high resolution C1s spectra measured on an a-C:H coating (A) and on Ag/a-C:H nanocomposites prepared at a DC magnetron current of 200 mA (B) and 500 mA (C).

Besides the surface chemical composition, also the surface morphology of the coatings under study was examined using AFM as it is to be expected that the increasing number of AgNPs would result in an alteration of the surface morphology of the produced samples. **Figure 7.4** shows the obtained 3 x 3 μm² AFM images of the a-C:H coating and Ag/a-C:H nanocomposite coatings deposited at different magnetron currents. It can be clearly seen that the a-C:H coating was relatively smooth, while in case of the Ag/a-C:H coatings, besides the smooth matrix, also different small spots appeared which can be attributed to the presence of the AgNPs. With increasing magnetron current, more spots were visible indicating the increasing amount of AgNPs in the coatings at higher magnetron current. From these images, the surface roughness (R_a value) was determined and the results are also presented

in **Figure 7.5.A**. As expected from the AFM images, the R_a values were significantly higher for the nanocomposite coatings than for the a-C:H matrix, which showed an R_a value < 1 nm. **Figure 7.5.A** also reveals that the roughness of the nanocomposite coatings increased with an increase in DC magnetron current, i.e. with an increase in the number of AgNPs incorporated into the a-C:H matrix. The R_a roughness increased from 0.6 nm for a plain a-C:H film to 25 nm for an Ag/a-C:H film deposited at the highest magnetron current (500 mA) resulting in an increase in roughness parameter r from 1 to 1.1.

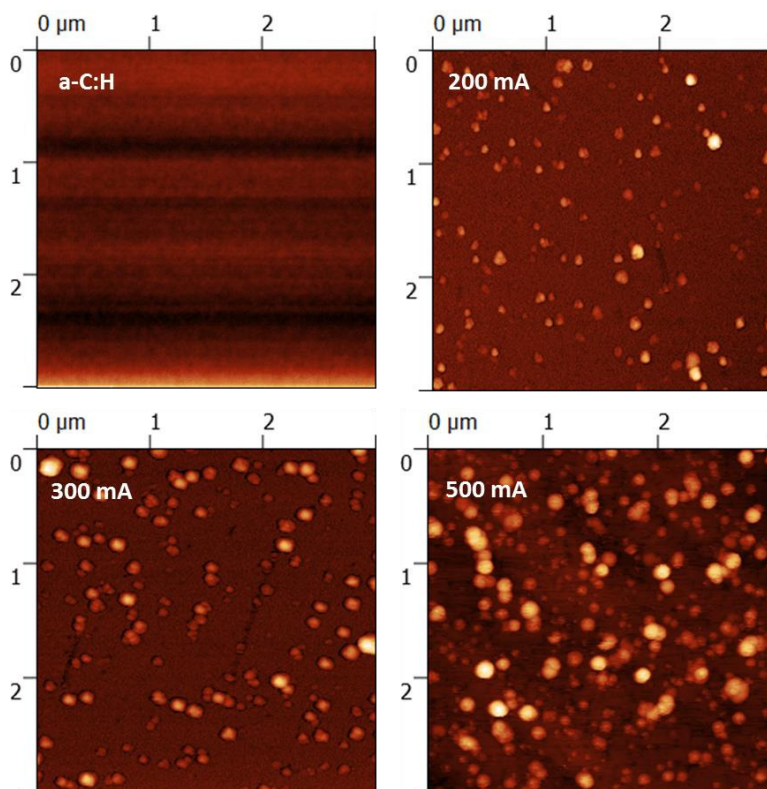


Figure 7.4. AFM images of the a-C:H coating and different Ag/a-C:H nanocomposite coatings.

The wettability of the coatings was also investigated for the coatings under study as the observed changes in surface roughness might in turn also affect the wettability of the samples. The obtained results of the performed WCA analysis are shown in **Figure 7.5.A**. The a-C:H

coating, i.e. the coating without any incorporated AgNPs, had a WCA value of $80 \pm 3^\circ$ which is common for a-C:H films prepared by PECVD[507]. Slightly higher WCA values ($90\text{-}100^\circ$) were observed for the Ag/a-C:H nanocomposites which reflects both the alterations of the surface nanoroughness and the increasing chemical heterogeneity of the sample surfaces with increasing number of embedded AgNPs. However, the experimentally observed variations in the wettability of the produced samples are relatively small and thus it can be presumed that such changes should not influence the biological performance of the coatings.

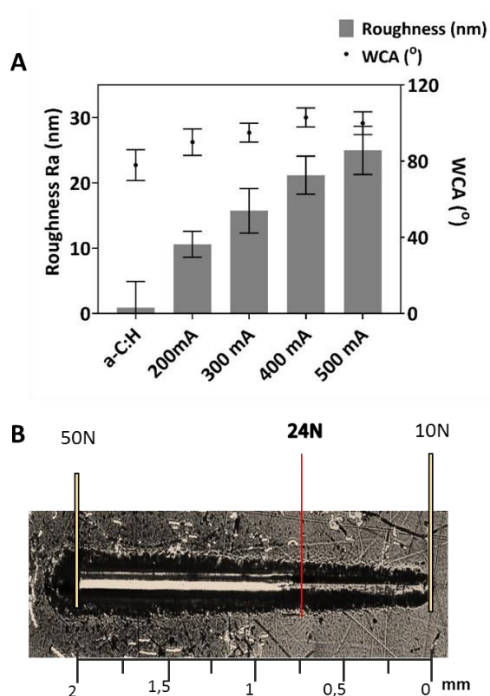


Figure 7.5. R_a and WCA values of the a-C:H coating and Ag/a-C:H films (A) and photography of the Ag/a-C:H coating (500 mA) after the scratch test (B).

Finally, the adhesion strength of the Ti-Ag/a-C:H interface has also been evaluated using a scratch test for the Ag/a-C:H coating deposited

at the highest magnetron current (500 mA). Based on this measurement, the critical load, i.e. the load at which the Ag/a-C:H coating delaminated from the Ti disk, was found to be 24 N. This is demonstrated in **Figure 7.5.B**, where an optical micrograph of a scratch created by the indenter in the coating is presented.

7.3.3 Silver ion release of the nanocomposite coatings

The antibacterial efficacy of the Ag based nanocomposite coating is associated with their ability to release Ag⁺ ions when submerged in an aqueous environment[508]. Hence, to evaluate the Ag⁺ ion release kinetics of the differently prepared nanocomposite coatings, the coated Ti substrates were immersed in distilled water for up to 7 days and the amount of Ag⁺ released from the coatings was analyzed using ICP-MS. The results of these tests are summarized in **Figure 7.6**, where the cumulative silver ion release is plotted as a function of water immersion time for coatings prepared at different DC magnetron current. As can be seen in this figure, an increase in released silver ions with immersion time was observed for all silver containing coatings. However, as expected and in agreement with reported results for other silver/plasma polymer nanocomposites[509,510], the actual amount of released silver ions was strongly linked to the number of AgNPs embedded in the matrix and also depended on the immersion time. Related to the latter, a faster release of Ag⁺ ions was observed during the first 6 hours of immersion. In this time period, an almost 10 times higher amount of Ag⁺ ions was released from the samples prepared at 500 mA (a release rate of 0.5 µg/cm²/hour) as compared to the samples deposited at a DC magnetron current of 200 mA (a release rate of approximately 0.05 µg/cm²/hour). This initial burst release of Ag⁺ was followed by a slower, but temporary stable release of silver ions from the coatings. However, also in this phase, the release rate remained considerably higher for the samples fabricated at higher DC magnetron currents. For instance, the release rate was 0.017 µg/cm²/hour for the samples prepared at 200 mA, while samples deposited at 500 mA exhibited a release rate of 0.037 µg/cm²/hour.

In addition, it is also worth stressing that the AgNPs were strongly fixed into the a-C:H matrix as the NPs did not migrate from the coatings into the water even after prolonged immersion times. As such, the undesirable release of AgNPs into the aqueous environment was prevented in case of the nanocomposite coatings developed in this

study. This conclusion is documented in **Figure 7.7**, where SEM images of the nanocomposite coatings after 7 days immersion in water and phosphate buffered saline (PBS), used as a common model of a physiological environment, are compared with SEM images of the corresponding as-deposited coated Ti samples. These images clearly show that the surface morphology determined from SE images did not change and the AgNPs were still present in the coatings after 7 days of water and PBS immersion as can be seen from the SEM images acquired in the BSE mode. Therefore, it can be presumed that the silver amount detected in the water by ICP-MS is not due to the release of AgNPs from the coatings, but due to the penetration of water through the a-C:H matrix. This latter process facilitates the surface oxidation of the incorporated AgNPs owing to the oxygen dissolved in the water. After that, Ag⁺ ions are hydrated and can diffuse through the matrix into the liquid. In other words, the release of Ag⁺ from the nanocomposites is supposed to be strongly influenced by the ability of water to penetrate through the a-C:H matrix to reach the embedded AgNPs. However, since the chemical composition of the a-C:H matrix was not varied in this study (**Figure 7.3**) and all fabricated coatings had a similar wettability (**Figure 7.5.A**), it may be expected that the permeation of water towards the embedded AgNPs is for all samples the same and thus the different release rates have to be solely linked with the amount of AgNPs present in the coatings.

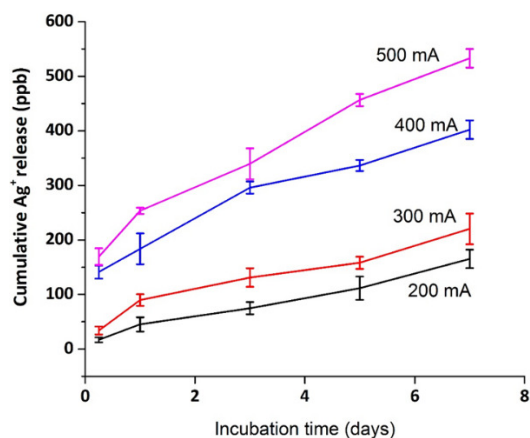


Figure 7.6. Cumulative silver ion release (ppb) of the Ag/a-C:H nanocomposite coatings as a function of water immersion time.

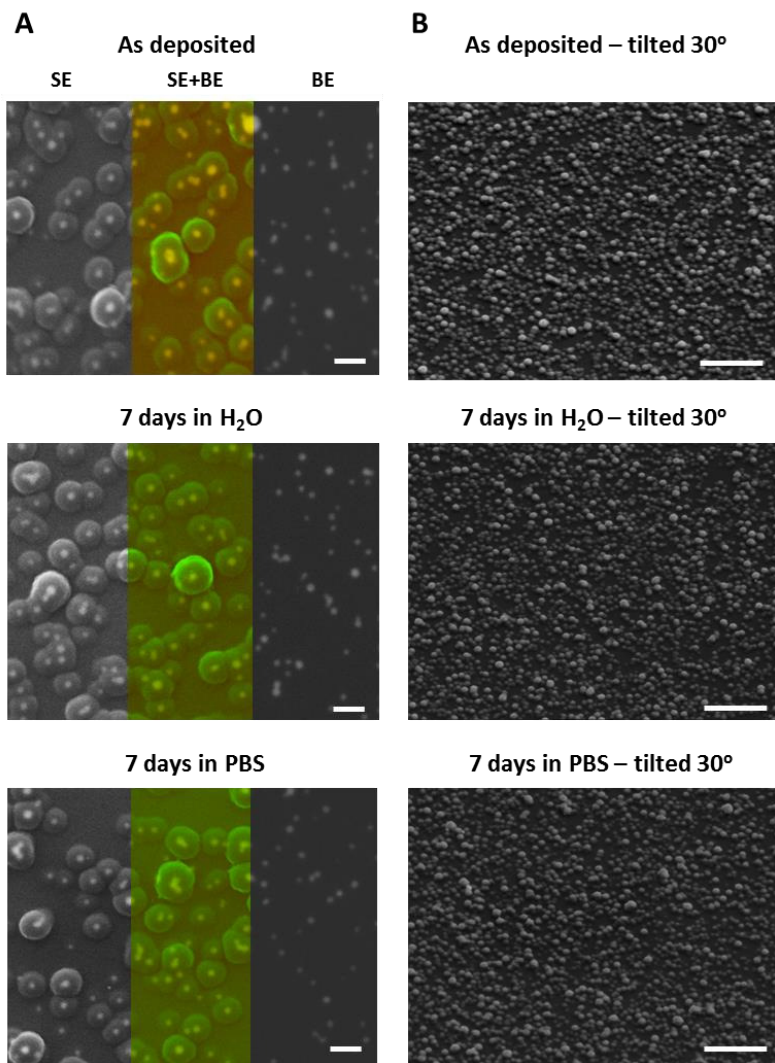


Figure 7.7. SEM images of Ag/a-C:H nanocomposite coatings deposited at 500 mA before and after 7 days of immersion in water and PBS: comparison of SEM images acquired in SE and BSE imaging modes (scale bar = 100 nm) (A) and SE images of Ag/a-C:H coatings acquired at 30° tilt (scale bar = 1 μm) (B).

7.3.4 Antibacterial efficiency of the Ag/a-C:H coatings

Antibacterial assays against *E. coli* and *S. aureus* were performed on different Ag/a-C:H coatings as well as on the Ag-free coating and polished Ti to serve as controls. The used bacterial species were selected as they are the two most common pathogens associated with implant associated infections and they are known to be resistant to antibiotics [103,105,511]. As can be seen in **Figure 7.8 A and B**, no reduction in *E. coli* and *S. aureus* was observed when uncoated Ti and a silver free a-C:H coating deposited on a Ti substrate were tested. In both cases, approximately 10^8 CFU were recovered, both for *E. coli* and *S. aureus*, after 24 hours of incubation. In contrast, the Ag/a-C:H nanocomposite coatings showed a significant reduction ($P < 0.05$) in bacterial cell numbers. The antibacterial efficiency of the nanocomposites was however strongly dependent on the DC magnetron current used for AgNPs deposition. In the case of samples with low Ag content (200 mA, 300 mA) a 2-log reduction of *E. coli* bacteria and a 1.5-log reduction of *S. aureus* bacteria were observed. In contrast, samples with high silver content (400 mA, 500 mA) exhibited superior bactericidal efficacy showing a 5-log reduction of *E. coli* and a 4-log reduction of *S. aureus* after 6 hours of incubation. These findings, i.e. the decreases in the amount of bacteria with increasing number of AgNPs, correspond well to the measured silver ion release discussed in the section 7.3.3 and suggests that the main antibacterial action is performed by the Ag^+ ions released from the nanocomposites to the aqueous medium [324]. **Figure 7.8** also reveals that the antibacterial efficiency further increased at 24 hours of incubation. However, as the main portion of silver ions was already released from the Ag/a-C:H nanocomposites during the first 6 hours (**Figure 7.6**), the additional decrease in bacteria count after a prolonged incubation of 24 h instead of 6 h was relatively small.

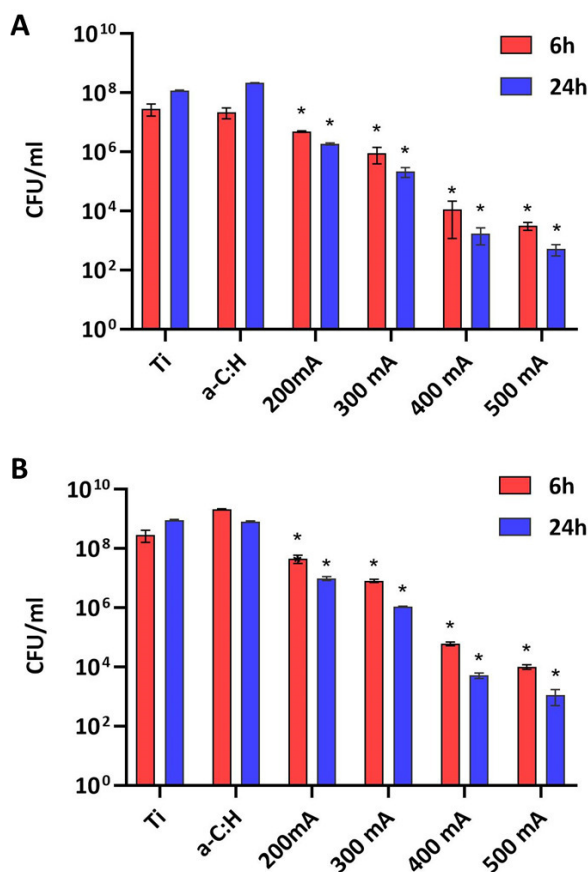


Figure 7.8. CFU assay of gram negative *E. coli* (A) and gram positive *S. aureus* (B) after 6 and 24 hours of incubation. The data are reported as mean \pm SD of 3 independent experiments ($n=3$). Asterisk (*) represents a significant difference at $P < 0.05$ compared to the control (untreated Ti).

7.3.5 Cytocompatibility of the Ag/a-C:H coatings

After performing the coating surface characterization and investigating the antibacterial properties of the deposited films in the previous sections, the cytotoxicity of the prepared coatings was also examined in this part of the study. First, the viability of the MC3T3 cells seeded on different samples (uncoated Ti, a-C:H coating and Ag/a-C:H coatings prepared at 200, 300, 400 and 500 mA) was examined by

fluorescence microscopy 1 and 7 days after cell seeding and the results are presented in **Figure 7.9**. One day after cell seeding, nearly no dead cells were observed on the surface of all samples indicating that the coatings possessed no significant cytotoxicity to osteoblasts. In fact, Ag free and Ag incorporated a-C:H films even exhibited a higher cell density with more living cells independently of the Ag content in the coating as compared to the uncoated polished Ti surface. This result is similar to what was already observed in literature[161,512]. The situation however slightly changed 7 days after cell seeding. Whereas almost no dead cells were found on the coatings with low Ag content (200 mA, 300 mA), a notable number of dead cells was present on the coatings possessing high amounts of AgNPs (400 mA, 500 mA). Nevertheless, the uncoated Ti surface was still covered with less cells compared to all Ag/a-C:H coatings under study.

To quantify the number of viable cells present on the different samples 1 day and 7 days after cell seeding, an MTT assay was also conducted. As can be seen in **Figure 7.10**, where the results of this MTT assay are presented, there was an increase in cell viability with time on all samples. In addition, Ag-free and Ag incorporated a-C:H coatings exhibited a cell viability $\geq 90 \pm 10 \%$ 7 days after cell seeding, which was a considerably higher cell viability than in case of the uncoated Ti disks ($70 \pm 10 \%$). This conclusion is thus in close accordance with the previously shown fluorescence images (**Figure 7.9**). In fact, previous studies have also reported that diamond like-amorphous carbon coatings are non-toxic to osteoblast cells and other cell types[513]. At this point, it is also important to note that according to the ISO standards, any material is considered to be biocompatible if the cell viability is higher than 70 %[514]. Thus, the cytotoxicity tests performed in this work clearly showed that all coatings under study meet the ISO standards as they exhibited a cell viability $\geq 90 \pm 10 \%$. This shows that the Ag/a-C:H nanocomposite coatings possessing an appropriate amount of AgNPs are beneficial for osteoblast adhesion and proliferation. Nevertheless, one has to consider though that an excess of AgNPs may induce some cytotoxicity, as evidenced from **Figure 7.9**.

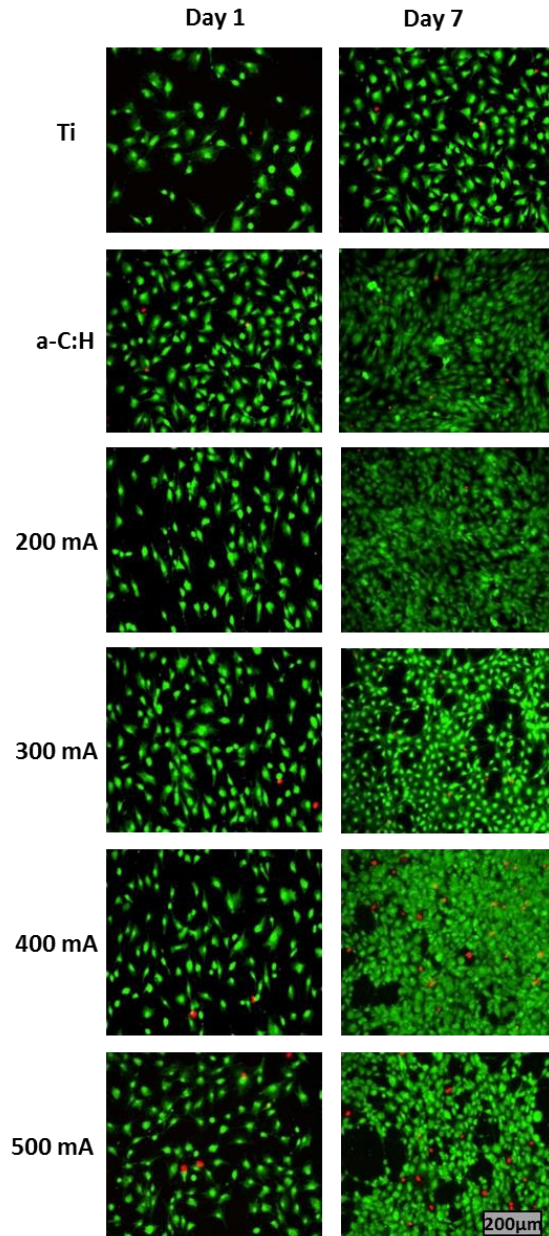


Figure 7.9. Fluorescence images of live/dead stained MC3T3 cells 1 and 7 days after cell seeding on a bare Ti substrate and different coated Ti samples (scale bar = 200 μ m).

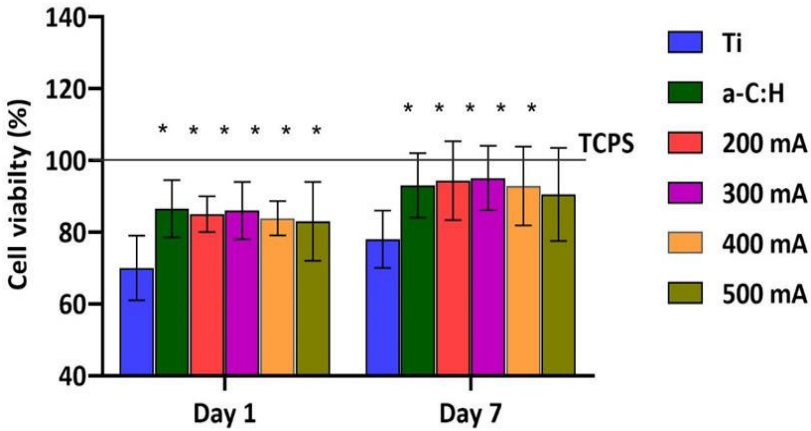


Figure 7.10. Cell viability 1 day and 7 days after cell seeding on different Ti samples. The data are reported as mean \pm SD of 3 independent experiments ($n=3$). Asterisk (*) represents significant difference at $P < 0.05$ compared to the control sample (untreated Ti).

To further characterize the bio adhesive properties of the developed Ag/a-C:H nanocomposite coatings, the morphology of the MC3T3 cells cultured on different samples 1 day and 7 days after cell seeding was also visualized by means of SEM imaging. As it is depicted in **Figure 7.11**, 1 day after cell seeding, the adherent cells were elongated and spindle shaped on all samples. After 7 days, the cells however displayed a more spread out morphology on all coated Ti substrates and more cells proliferated on both Ag-free and Ag-incorporated a-C:H coatings as compared to the uncoated Ti disks. This observation showed that independently of the Ag content in the coating, the a-C:H coatings result in better cell proliferation than the pure Ti surface. Similar findings were also reported for fibroblasts seeded on carbon-based coatings deposited onto stainless steel substrates [515]. No adverse effects on the morphology of osteoblast-like macrophages and fibroblasts seeded on diamond-like carbon coated polystyrene well plates were also reported in [55]. In contrast, a negative biological effect, i.e. attenuation of the osteoblast cell activity, was observed when Ti disks were coated with a hydrocarbon film in [516]. These opposing findings together with the results obtained in this work thus clearly show that the applied deposition method of a carbon-based coating may

have an important influence on the final biological activity of seeded cells.

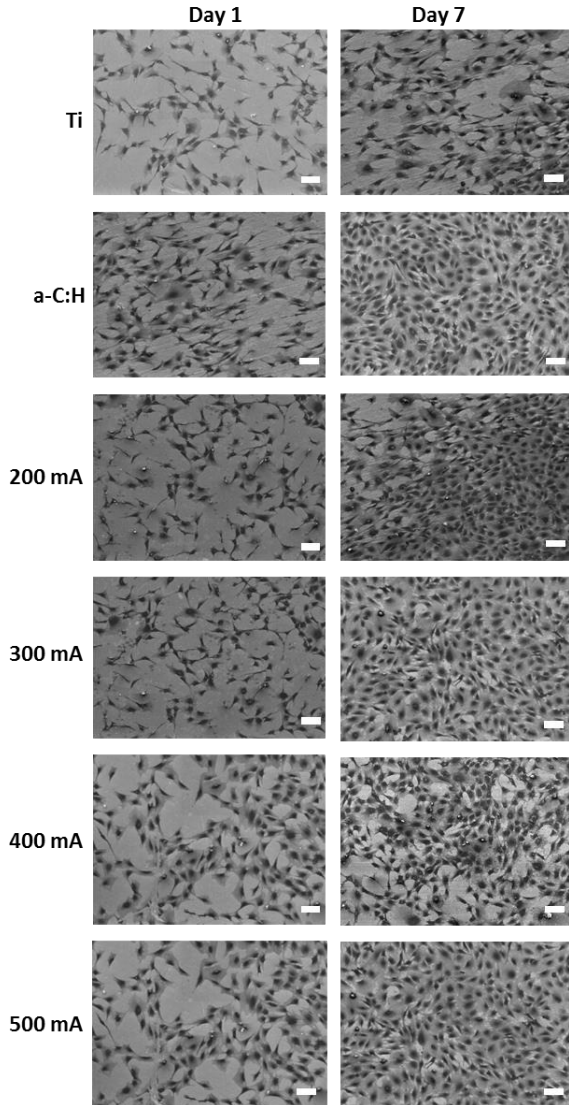


Figure 7.11. SEM images of MC3T3 cells 1 and 7 days after cell seeding on different Ti samples(scale bar = 100 μm).

7.4 Conclusions

In this chapter, we have investigated the properties of Ag/a-C:H nanocomposite coatings deposited onto Ti disks by means of a vacuum-based deposition technique that combines a gas aggregation source for AgNPs production and a PE-CVD process to deposit the matrix material (a-C:H). As it was shown, this deposition strategy for the production of Ag/a-C:H coatings made it possible to tune the silver content in the nanocomposites independently of the properties of the matrix material. This in turn also allowed to precisely control the antibacterial efficiency of the produced coatings which was connected with their ability to release silver ions into an aqueous environment. Presented results showed that the coatings with the highest silver content exhibited superior antibacterial efficacy with a 6-log reduction of *E. coli* and a 4-log reduction of *S. aureus* after 24 hours of incubation. Besides the very good antibacterial performance of the produced Ag/a-C:H films, all silver-containing coatings were also able to promote osteoblast adhesion and proliferation that was higher than on the uncoated Ti surfaces. This property, together with the excellent antibacterial efficacy of the produced nanocomposite coatings, makes them highly interesting materials for orthopedic implants.

Chapter 8. Biological activity and antimicrobial properties of Cu/a-C:H nanocomposites and nanolayered coatings on titanium substrates

The results of chapter 8 were published in the following international peer-reviewed journal:

Thukkaram M, Vaidulych M, Kylian O, Hanus J, Rigole P, Aliakbarshirazi S, Asadian M, Nikiforov A, Van Tongel A, Biederman H, Coenye T, Du Laing G, Morent R, De Wilde L, Verbeken K, De Geyter N.

“Biological activity and antimicrobial properties of Cu/a-C:H nanocomposites and nanolayered coatings on titanium substrates”

Material Science and Engineering: C (2020)

8.1 Introduction

The previous chapter focused on the synthesis of Ag containing amorphous hydrocarbon (Ag/a-C:H) nanocomposites making use of a fully vacuum-based cluster technique. As the Ag rich a-C:H films developed in Chapter 7 showed promising results, the bi-functional character of an a-C:H matrix loaded with CuNPs on Ti substrates will be examined in this final experimental part of this dissertation, an approach which has not yet been explored in the past. CuNPs will be used in this chapter because apart from their use as an antibacterial agent, Cu ions released from CuNPs are also beneficial to the cardiovascular system by stimulating the proliferation and differentiation of endothelial cells, and a sustained release of trace amounts of Cu ions could also promote osteogenesis. As such, this chapter will focus on examining the potential of using a vacuum-based strategy that combines the cluster beam deposition of CuNPs with PECVD of a-C:H thin films for the fabrication of three different types of Cu/a-C:H coatings with approximately the same amount of embedded CuNPs but with a different arrangement of the NPs inside the a-C:H matrix. A detailed analysis of the physical and chemical properties of the obtained coatings will be conducted. Additionally, the copper ion release characteristics of the coatings up to 7 days of immersion in water will be examined. In the final section of this chapter, the *in-vitro* antibacterial efficiency and the biological response of the coated Ti samples will be analysed to examine if the coated samples can be used for implant applications.

8.2 Experimental methods

All experimental details can be found in chapter 4. The deposition method and analysis techniques that are specifically used in this chapter are summarized in the **Table 8.1**. In this chapter, three strategies for the deposition of Cu/a-C:H nanocomposite coatings were employed as schematically depicted in **Figure 8.1**. The parameters used for the different deposition procedures are summarized in **Table 8.2**.

Table 8.1. *Experimental methods.*

Deposition method	GAS + PECVD Parameters (see Table 8.2)
Ti specimen	Pre-treatment <ul style="list-style-type: none"> - Ground and mirror like polished - Ar plasma : Power (70W), pressure (4.5 Pa) treatment time (2 min) - N₂ plasma : Power (70W), pressure (2.5 Pa) treatment time (10 min)
Characterization techniques	<ol style="list-style-type: none"> 1) Surface-SEM <ul style="list-style-type: none"> • BSE mode - accelerating voltage : 20 kV 2) XPS <ul style="list-style-type: none"> • Survey scans and high resolution Cu2p, C1s spectra 3) AFM 4) WCA 5) ICP-MS copper ion release
<i>In-vitro</i> analysis	<p>Antibacterial assay : CFU</p> <ul style="list-style-type: none"> • <i>E. coli</i> ATCC 25922 • <i>S. aureus</i> ATCC 6538 • Incubation time - 24 hours <p>Cell culture : MTT, SEM and fluorescence microscopy</p> <ul style="list-style-type: none"> • MC3T3 cells • Cell seeding time - day 1 and day 7

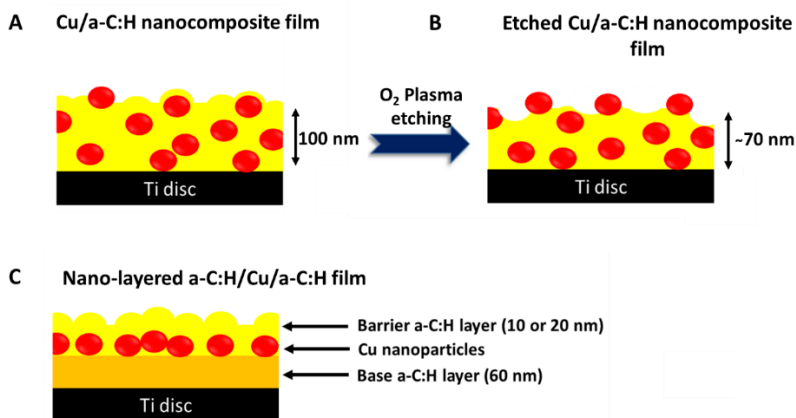


Figure 8.1. Schematic representation of the produced samples: Cu/a-C:H nanocomposites (A), O₂ plasma etched Cu/a-C:H nanocomposites (B) and nano-layered a-C:H/Cu/a-C:H films (C).

Table 8.2. Operational parameters used for the deposition of Cu/a-C:H nanocomposites and nano-layered a-C:H/Cu/a-C:H coatings.

Cu/a-C:H						
	RF power	DC magnetron current	Duty cycle	Pressure deposition chamber	Pressure aggregation chamber	Deposition time
Cu/a-C:H deposition	70 W	600 mA	50%	5.6 Pa (Ar/n-hexane)	100 Pa (Ar)	5 min (100 nm)
Cu/a-C:H etched						
	RF power	DC magnetron current	Duty cycle	Pressure deposition chamber	Pressure aggregation chamber	Deposition time
Cu/a-C:H deposition	70 W	600 mA	50%	5.6 Pa (Ar/n-hexane)	100 Pa (Ar)	5 min (100 nm)
Etching	16 W	-	100 %	2.5 Pa (oxygen)	-	4 min

Cu/a-C:H-10nm and Cu/a-CH-20nm						
	RF power	DC magnetron current	Duty cycle	Pressure deposition chamber	Pressure aggregation chamber	Deposition time
Deposition of the base layer	70 W	-	100 %	5.6 Pa (Ar/n-hexane)	-	1.5 min (60 nm)
Deposition of Cu NPs	-	600 mA	-	-	100 Pa (Ar)	2.5 min
Deposition of the barrier layer	70 W	-	100 %	5.6 Pa (Ar/n-hexane)	-	13 sec (10 nm) 27 sec (20 nm)

8.3 Results and discussions

8.3.1 Physico-chemical characterization of the coatings

The first step of this study was a detailed characterization of all three types of produced Cu/a-C:H coatings. As can be seen from the SEM images presented in **Figure 8.2**, the mean size of the CuNPs was approximately 20 nm and the number of NPs that were present in the coatings was for all samples comparable and in the range 130-160 NPs/ μm^2 . A slightly higher number of CuNPs was observed for the Cu/a-C:H and Cu/a-C:H etched samples as compared to the Cu/a-C:H-10nm and Cu/a-C:H-20nm nano-layered structures. This suggests that during the simultaneous deposition of Cu/a-C:H and Cu/a-C:H etched samples, some CuNPs may still reach the substrate when the RF plasma is used during the a-C:H matrix deposition causing slight increase in the number of NPs deposited [506].

Table 8.3 presents the values of the Ra roughness of the different coatings under study as measured by AFM. As can be seen, the Ti disks coated with a-C:H matrix were smooth with a Ra roughness of 3.8 ± 1.5 nm. The incorporation of CuNPs to the a-C:H matrix led to further increases in Ra roughness: for Cu/a-C:H and both types of nano-layered coatings, the Ra roughness was found to be close to 20 nm. This result is in agreement with the SEM images, which showed approximately the same number of copper NPs in the films which contributed to the surface roughening. Finally, the plasma etching step caused a slight smoothing of the Cu/a-C:H coatings: in this case, the Ra roughness

was 12.2 ± 1.5 nm, which is still considerably higher when compared to Cu-free a-C:H films due to the presence of the CuNPs in the coatings.

With respect to the wettability, all coated Ti disks exhibited higher water contact angles as compared to uncoated Ti samples (WCA – 65°) (**Table 8.3**). However, no significant differences in WCA values were observed between the plain a-C:H matrix and all three types of Cu-containing coatings: in all cases, the WCA values were in the range 70 – 80° , which is in a good agreement with WCA results reported in literature [517,518].

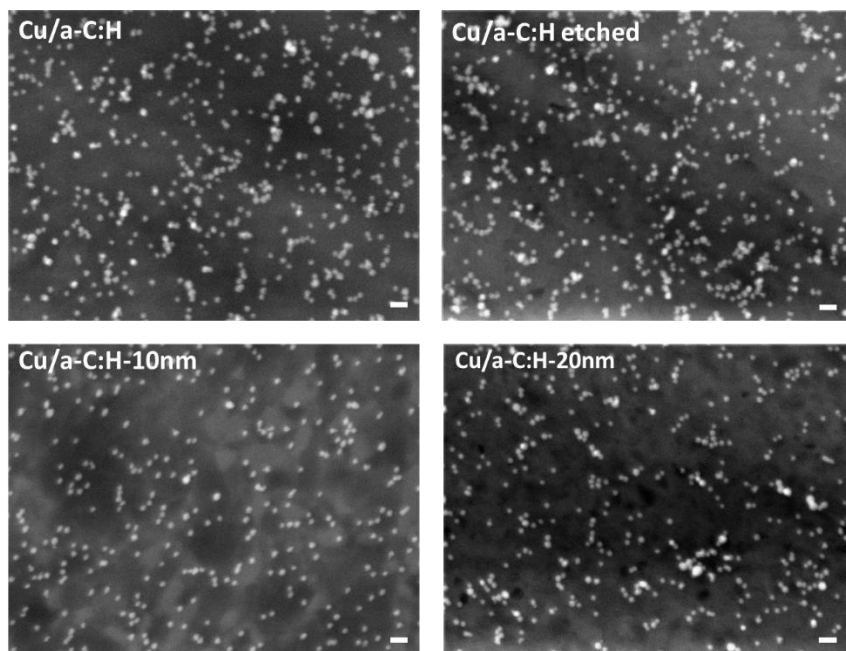


Figure 8.2. SEM-BSE images of the coated Ti samples (scale bar: 100 nm).

Table 8.3. R_a roughness, WCA and elemental surface composition of coated Ti disks.

Samples	R_a (nm)	WCA ($^\circ$)	C (at%)	O (at%)	Cu (at%)
a-C:H	3.8 ± 1.5	80 ± 5	91.0 ± 0.6	9.0 ± 0.4	-
Cu/a-C:H	21.2 ± 0.7	85 ± 6	88.9 ± 0.5	9.9 ± 0.3	1.2 ± 0.3
Cu/a-C:H etched	12.2 ± 1.5	70 ± 9	77.2 ± 0.6	18.2 ± 0.5	4.6 ± 0.4
Cu/a-C:H-10nm	18.9 ± 1.8	81 ± 10	89.2 ± 0.8	9.9 ± 0.4	0.9 ± 0.4
Cu/a-C:H-20nm	19.9 ± 1.2	78 ± 9	88.9 ± 0.8	10.5 ± 0.6	0.6 ± 0.5

The surface elemental composition of the (un)coated Ti samples was also determined by XPS (**Table 8.3**). The samples coated with only the a-C:H matrix were composed of 91.0 at% C and 9.0 at% O, which is in good agreement with previously reported results [519]. The presence of oxygen in the coating may be explained by the post-oxidation of the samples occurring during their transfer into the XPS device. For the samples that contained CuNPs, Cu peaks became detectable in the XPS detailed spectra (Cu2p_{1/2} and Cu2p_{3/2} centred at 952.7 eV and 933.0 eV, respectively, with a spin-orbit separation of 19.7 eV; see **Figure 8.3**) alongside with the peaks of carbon and oxygen. The Cu/a-C:H nanocomposite samples were composed of 88.9 at% C, 9.9 at% O and only 1.2 at% Cu. This relatively small concentration of copper was the result of the limited penetration depth of XPS: in case of AlK α radiation, the sampling depth of XPS is typically in the range 3-10 nm [507]. As a consequence, only copper close to the surface of the nanocomposite coating contributed to the XPS signal and CuNPs that were buried deeper in the films were thus not detected by XPS. This phenomenon may also explain the obtained elemental composition of the samples with CuNPs over coated by an a-C:H barrier layer: the presence of the barrier layer reduced the surface Cu concentration to 0.9 at% and 0.6 at% in case of a 10 and 20 nm thick barrier layer, respectively. The concentration of copper in the top surface layer of the Cu/a-C:H coatings was, however, substantially enhanced when the samples were etched by oxygen plasma which removed the topmost a-C:H layer. In fact, the Cu atomic concentration went up to 4.6 at% after the plasma

etching of the Cu/a-C:H nanocomposites. This was accompanied by an increase in the surface concentration of oxygen which was due to the oxidation of both the a-C:H matrix and the surface of the CuNPs which were easily accessible by the oxygen plasma due to its etching behaviour. The latter was confirmed by XPS high-resolution spectra of the Cu2p peak (**Figure 8.3**). As can be seen in this figure, a clear shake-up satellite peak appeared in the XPS spectra in the binding energy range 939-946 eV in the case of the Cu/a-C:H etched sample. This additional peak indicated the presence of Cu²⁺ [520] and thus confirmed the partial oxidation of the CuNPs in the top surface layers.

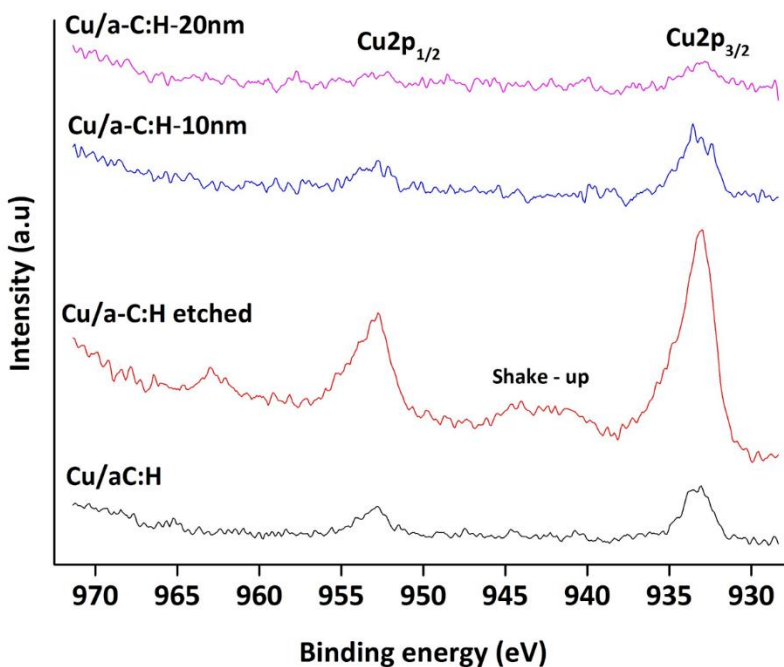


Figure 8.3. High-resolution XPS spectra of the Cu_{2p} peak of uncoated and coated Ti disks.

To test the stability of the coated samples in aqueous media, an additional test was performed in which the samples were immersed into distilled water for 1, 3, 5 and 7 days, air-dried in vacuum and subsequently analysed by means of XPS. As presented in **Figure 8.4**,

the Cu surface concentration showed almost negligible fluctuations at all-time points in the case of samples covered with a 10 nm and 20 nm thick barrier layer. This suggests that a 10 nm thick film of the a-C:H matrix used as a homogeneous overcoat of the CuNPs was already sufficient to protect the CuNPs from water. This finding is in agreement with the results reported previously for Cu/C:F nanocomposites [521].

In contrast, for the Cu/a-C:H and the Cu/a-C:H etched samples, their immersion into water caused substantial variations in the amount of Cu detected by XPS, i.e. the amount of Cu on the surface of the coatings or in its close vicinity. For both sample types, the surface atomic concentration of copper initially increased after water immersion followed by a gradual decrease in copper concentration for longer immersion times. This effect may be explained by two opposing processes that act simultaneously. First of all, the water may wash out or partially dissolve the topmost layer of the a-C:H film that covers the CuNPs thereby increasing the amount of copper in the top surface layers. Here it is important to note that unlike the nano-layered structures, in which the CuNPs were covered by a homogeneous protective film of a-C:H, the simultaneous deposition of CuNPs and a-C:H led to the occurrence of a population of CuNPs that were covered by a considerably thinner a-C:H layer which was consequently more prone to damage. The fraction of CuNPs that were not sufficiently coated by a-C:H was even enhanced after the plasma etching step which completely removed the topmost layer of a-C:H. Alongside with the washing out or damage of the protective a-C:H layer that increased the Cu XPS signal, the water penetrating into the nanocomposite layer initiated the process of a gradual release of Cu ions from the coatings or oxidation of the CuNPs. These latter effects consequently resulted in a steady lowering of the amount of copper in the topmost layer of the Cu/a-C:H nanocomposites detectable by XPS. Naturally, the rate of this effect was higher for the situation in which a higher amount of CuNPs was accessible by water. This may explain the differences observed between the Cu/a-C:H and the Cu/a-C:H etched samples: as the number of CuNPs accessible by water was much higher for the Cu/a-C:H etched samples, their dissolution and oxidation was more effective as compared to the Cu/a-C:H samples thereby resulting in a faster onset of the phase in which the Cu surface concentration started to decrease.

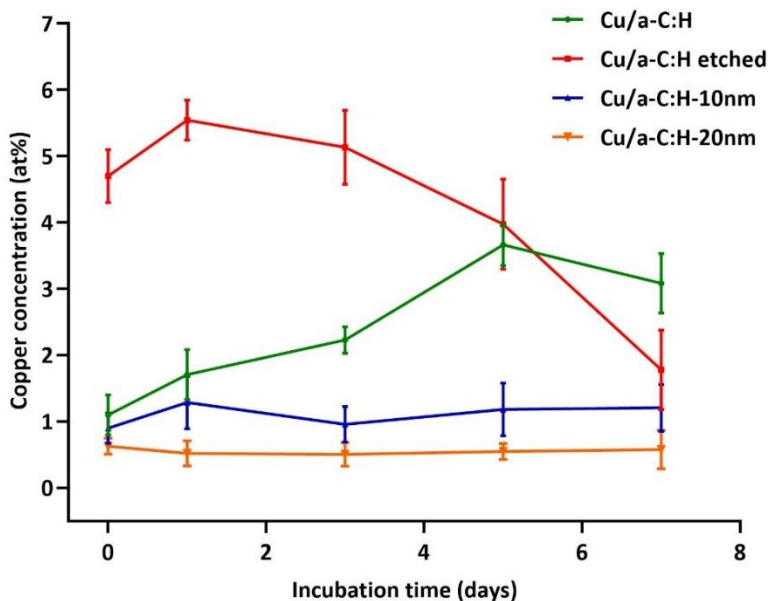


Figure 8.4. Evolution of the copper surface concentration as a function of water incubation time for the coated Ti samples under study (XPS surface analysis).

8.3.2 Cu ion release study

An important characteristic of copper-based materials is their ability to release Cu^{2+} ions which are responsible for the antibacterial action and bioactivity of the coating as these ions may induce the death of bacteria, enhance differentiation of osteoblast and mesenchymal stem cells, and/or promote osteostimulation[522,523]. Hence, the release kinetics of Cu^{2+} from the fabricated coatings were analysed using ICP-MS. **Figure 8.5.A** presents the cumulative release profiles of Cu^{2+} from all three types of Cu-containing composites in distilled water up to 7 days. These results can be summarized as follows. First, it is clear that the samples differed in the total amount of released Cu^{2+} : the cumulative amount of released Cu^{2+} from Cu/a-C:H, Cu/a-C:H etched, Cu/a-C:H-10nm and Cu/a-C:H-20nm samples after 7 days was 418 ppb, 513 ppb, 92 ppb and 44 ppb, respectively. Taking into account the

comparable number of CuNPs in all tested samples as well as their similar wettability, the obtained large difference in the amount of released Cu^{2+} ions clearly showed the importance of the structure of the Cu/a-C:H coatings, i.e. the way how the CuNPs were arranged in the coatings. Naturally, the coatings, for which the CuNPs were in direct contact with water or were present closer to the surface, released Cu^{2+} more easily due to the shorter diffusion path as compared to the coatings in which the CuNPs were separated from the aqueous environment by a barrier a-C:H layer.

Furthermore, the structure of the samples not only influenced the total amount of released Cu^{2+} ions but also affected the kinetics of their release as is demonstrated in **Figure 8.5.B**, where the kinetics of the Cu^{2+} release measured at different immersion times is depicted. The Cu/a-C:H etched coatings reached the highest release rate on the third day of the immersion in distilled water. This initial and relatively fast release stage was due to the direct contact of the topmost CuNPs with the aqueous medium that allowed the fast release of Cu^{2+} . This effect was even enhanced as the uppermost CuNPs were in the oxidized state (**Figure 8.3**) which further facilitated the formation of Cu^{2+} . However, for longer immersion times, the dissolution of NPs reduced the amount of copper in the surface layer as shown by XPS (**Figure 8.4**). As a result of this, the release from the surface CuNPs started to decay and more importantly became the release of ions from CuNPs that were buried deeper in the coating which is a diffusion-limited and thus considerably slower process. A similar trend, i.e. two-phases kinetics of the Cu^{2+} ion release, was also observed for the Cu/a-C:H nanocomposites in which CuNPs were randomly distributed over the whole volume of the a-C:H matrix. However, the maximal release rate was observed, in agreement with the XPS results presented in **Figure 8.4**, at a longer immersion time – 5 days. **Figure 8.5.B** also showed that the nano-layered structure with the 10 nm thick a-C:H barrier exhibited negligible Cu^{2+} release rates until day 5, after which the Cu^{2+} release rate suddenly increased. This may be due to the breakage of the barrier layer thereby facilitating the Cu^{2+} production. Finally, for the samples with the 20 nm thick barrier, the release rate of Cu^{2+} stayed very low and even temporally stable in the time period of 7 days.

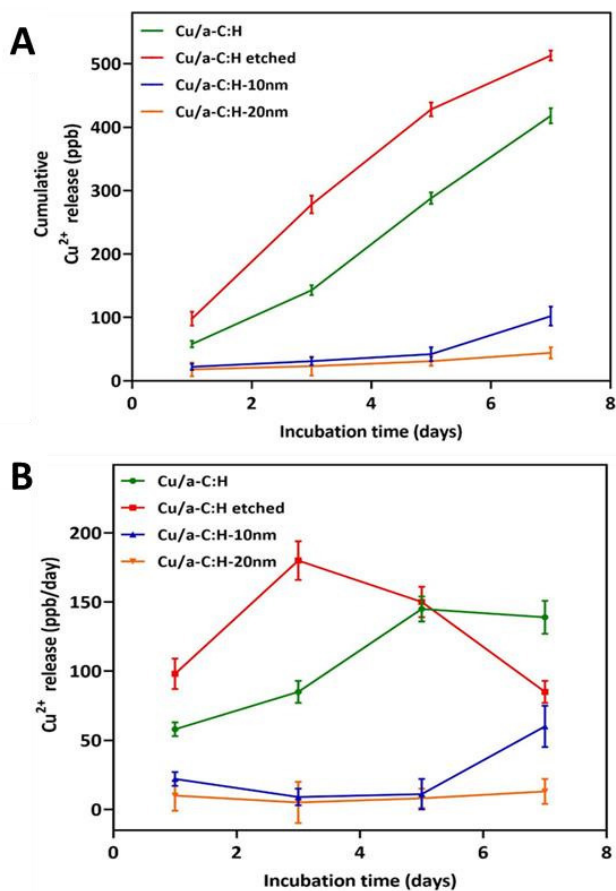


Figure 8.5. Cumulative Cu²⁺ release (ppb) (A) and Cu²⁺ release rate (ppb/day) (B) when immersed in water up to 7 days for Cu/a-C:H, Cu/a-C:H etched, 10 nm and 20 nm barrier samples.

8.3.3 Antimicrobial efficiency of the produced coatings

The antimicrobial efficiency of the coated Ti disks was tested against *Escherichia coli* (*E. coli*, gram-negative) and *Staphylococcus aureus* (*S. aureus*, gram-positive). These bacteria were selected as they are the most common pathogens causing implant-associated infections[103]. The antimicrobial properties of the as-deposited samples were tested after 24 hours of incubation in bacteria-containing medium and uncoated Ti disks were used as controls. From **Figure 8.6 A and B** it is observed that approximately 10⁸ CFU were recovered from the

uncoated Ti disks and Ti disks coated solely with the a-C:H film both for *E. coli* and *S. aureus*, i.e. no bacterial reduction was observed for the Cu-free disks for both types of bacteria. In contrast, all Ti disks coated with copper-containing coatings showed measurable antibacterial activity that was furthermore strongly dependent on the architecture of the coatings. The Cu/a-C:H and Cu/a-C:H etched samples without any barrier showed the highest reduction (nearly 4- and 5-log, respectively) for both tested bacteria. On the other hand, the presence of the 10 nm thick barrier layer resulted in a 3 log reduction of *E. coli* and a 2 log reduction of *S. aureus*. An increase of the barrier thickness to 20 nm caused a further decrease of the antimicrobial efficiency showing approximately a 2 log reduction of *E. coli* and a 1 log reduction of *S. aureus*. Taking into account the results of the Cu²⁺ release measurements, a clear correlation between the antibacterial activity of the tested samples and the amount of released Cu²⁺ ions (**Figure 8.5**) was observed in this study: the higher the amount of released Cu²⁺, the higher the antibacterial activity of the coatings. In fact, the samples without an a-C:H barrier (Cu/a-C:H and Cu/a-C:H etched coatings) were able to provide a fast and sufficient release of Cu²⁺ into the bacteria-containing medium and consequently exhibited superior antibacterial activity against both tested microorganisms. On the other hand, when an a-C:H barrier film was present, the direct contact between the CuNPs and the medium was obstructed and the release of Cu²⁺ from the CuNPs was reduced which in turn lowered the antibacterial potential of the coatings. Moreover, this lowering effect was more pronounced in case of a thicker barrier layer. Similar findings were reported when a hydrophobic C:F barrier layer was used to immobilize either CuNPs or AgNPs [521,524]. It was found that the antibacterial effect for both Ag/C:F and Cu/C:F dramatically decreased with increasing thickness of the C:F barrier layer up to 40 nm. However, it is worth noting that the decay of the antibacterial activity with increasing thickness of a barrier layer deposited over Ag or Cu NPs has no universal validity. For instance, Kuzminova et al. [525] and Alisawi et al. [526] reported a different behaviour for hydrophobic (C:H):SiO_x and hydrophilic SiO_x matrices and Ploux et al. [527] reported that the thickness of the barrier layer, plasma polymerized n-heptylamine in their case, had no significant influence on the antibacterial activity of AgNPs against planktonic bacteria up to 18 nm. These results show that also the structure of the barrier film,

namely its ability to be hydrated, has to be taking into account for the design of antibacterial coatings with desired properties.

To investigate the long-term antibacterial efficiency of the produced coatings, in a next step, the coated Ti disks were prior to the measurements of their antibacterial activity pre-incubated in 20 mL of distilled water in small bottles in a shaking water bath at 37°C for different times up to 7 days. After these time points, disks were washed with distilled water, air dried and finally incubated for 24 hours in the bacteria-containing medium. The results of these tests are presented in **Figures 8.7 A and B** for both *E. coli* and *S. aureus*. For the samples without the barrier layer (Cu/a-C:H and Cu/a-C:H etched), a difference in their antibacterial activity was observed at all examined incubation times in comparison to the non-pre-incubated samples. In case of the Cu/a-C:H samples, the antibacterial efficacy slightly increased after 5 days and 7 days of pre-incubation, which could be explained by the higher Cu²⁺ release rates at these time points, as evidenced from **Figure 8.5.B**. On the other hand, for the etched samples, the opposite trend was found: the antibacterial efficiency strongly reduced when the samples were pre-incubated in water for longer times. This result can again be correlated with the Cu²⁺ release rate shown in **Figure 8.5.B**: longer incubations times resulted in a decrease in the Cu²⁺ release rate and, consequently a lower antibacterial performance of the etched samples. For the samples covered by the barrier layer, no difference in antibacterial activity was observed for all incubation times in comparison to the non-pre-incubated samples. **Figure 8.7** also revealed that for all examined samples, the overall antimicrobial activity remained superior for the samples without the barrier layer due to the higher amount of CuNPs on the surface of these samples which was consistent with the higher Cu²⁺ release rate from these samples even after 7 days of pre-incubation in water (**Figure 8.7.B**).

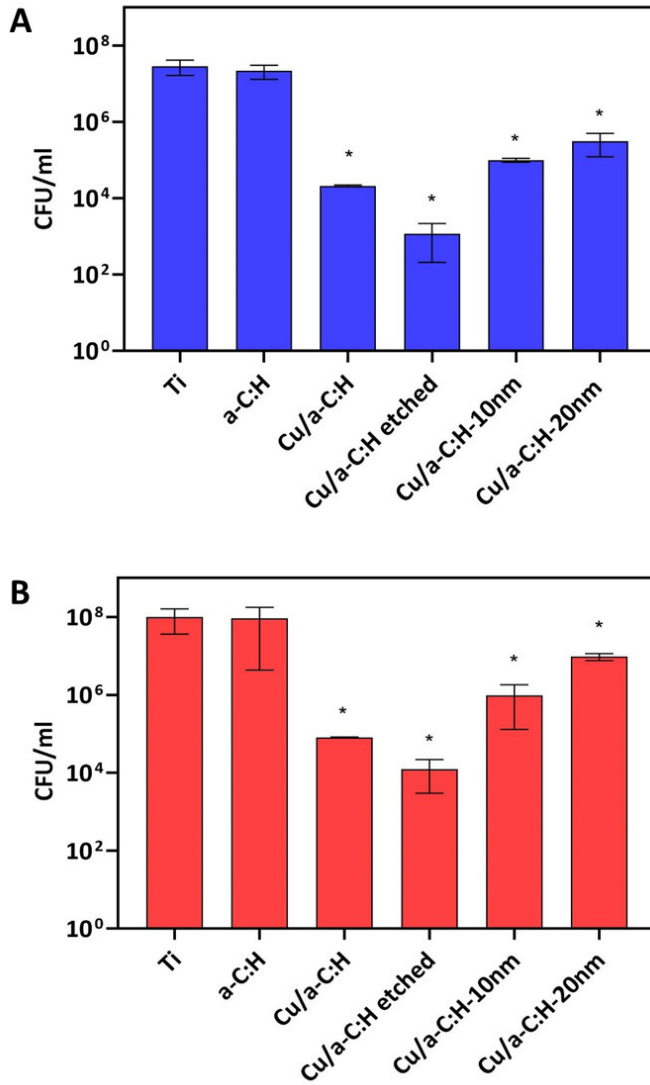


Figure 8.6. CFU assay of gram-negative *E. coli* (A) and gram-positive *S. aureus* (B) after 24 hours of incubation. Asterisk (*) denotes significant difference at $P < 0.05$ compared to the control (untreated Ti).

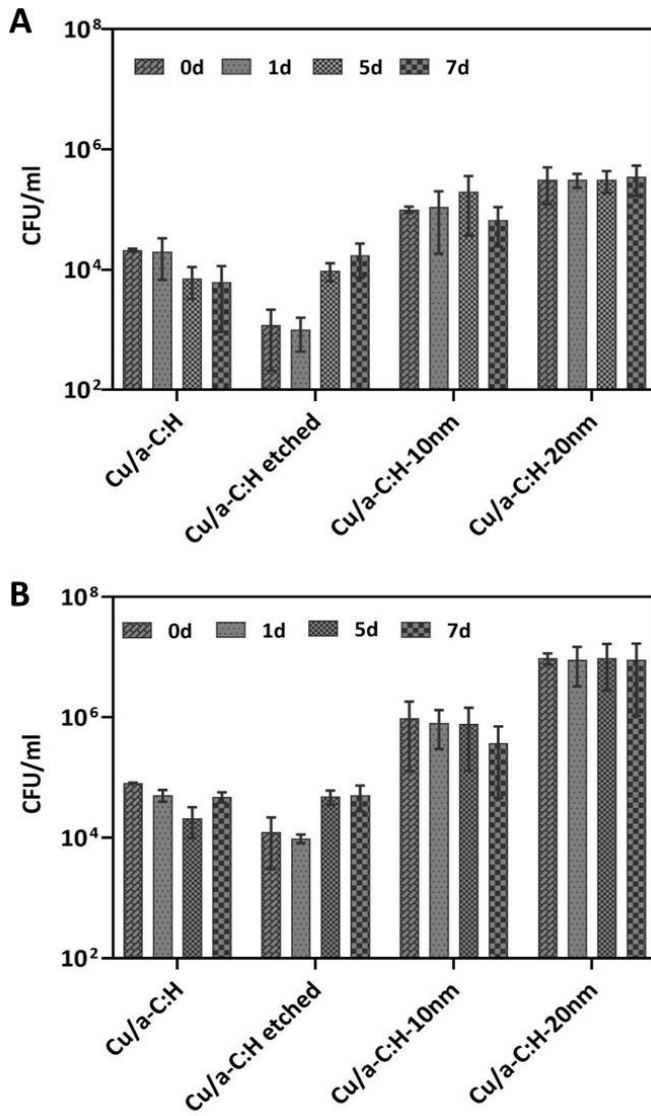


Figure 8.7. CFU assay of gram-negative *E. coli* (A) and gram-positive *S. aureus* (B) after pre-incubation (up to 7 days) of coated Ti samples.

8.3.4 Cytotoxicity study

For a material to be biocompatible, it is important to completely avoid any direct interaction between CuNPs and mammalian cells. Studies have reported that CuNPs induce oxidative stress in cells in a dose-dependent manner resulting in many physiological and cellular events causing DNA damage and apoptosis [528]. To initiate these harmful effects, CuNPs have to be in direct contact with a cell membrane which enables them to interfere with cellular organelles (such as mitochondria, lysosomes, nuclei and some enzymes) which are involved in metabolism, detoxification and damage repair. In our study, CuNPs were fixed on Ti disks by a a-C:H matrix which prevented NPs–cell interactions thereby limiting possible intracellular damage[529]. Therefore, we presume that the cytotoxicity of the produced Cu-containing coatings induced by direct interactions between CuNPs and cells should be insignificant. The second cause of cytotoxicity may be the Cu²⁺ ions released from the studied coatings. With respect to the amount of Cu²⁺, Zhuang et al. [530] have reported that a Cu²⁺ concentration up to 450 ppb had no toxic effect during *in-vitro* histological examination. In addition, Cao et al. [531] reported that the percentage relative growth factor (%RGF) was 77% in the presence of 26000 ppb of Cu ions, which implies that this Cu dose had caused cytotoxicity according to ISO standards. However, the highest cumulative Cu²⁺ release from the coatings prepared in this study was 513 ppb after 7 days which is much lower than the aforementioned amount and thus none of studied Cu/a-C:H coatings should exhibit cytotoxic effects due to the measured Cu²⁺ release. To confirm our presumption, cytotoxicity studies using a live/dead staining assay and an MTT assay were performed in this chapter.

In a first step, the morphology of MC3T3 cells seeded on different Ti samples and their viability were examined by fluorescence microscopy after life/dead staining and SEM microscopy after cell dehydration and fixation 1 day after cell seeding and the results are presented in **Figure 8.8**. It is clear that fewer cells adhered on the uncoated Ti sample whereas more cells adhered on all other samples examined in this study. From the SEM images, it can also be observed that the cells exhibited a spherical-shaped morphology on all samples, however, in the case of samples covered by a 10 nm or 20 nm thick a-C:H barrier layer, a more spread out cell morphology was seen. This visual observation was confirmed by the analysis of the shape factor of the

cells seeded on uncoated and coated Ti disks (**Figure 8.9**): cells grown on uncoated Ti disks had a shape factor of 1.7, whereas those grown on a-C:H and Cu incorporated samples had a shape factor of approximately 2.6. Furthermore, this shape factor increased to 3 for both samples covered with the barrier layer.

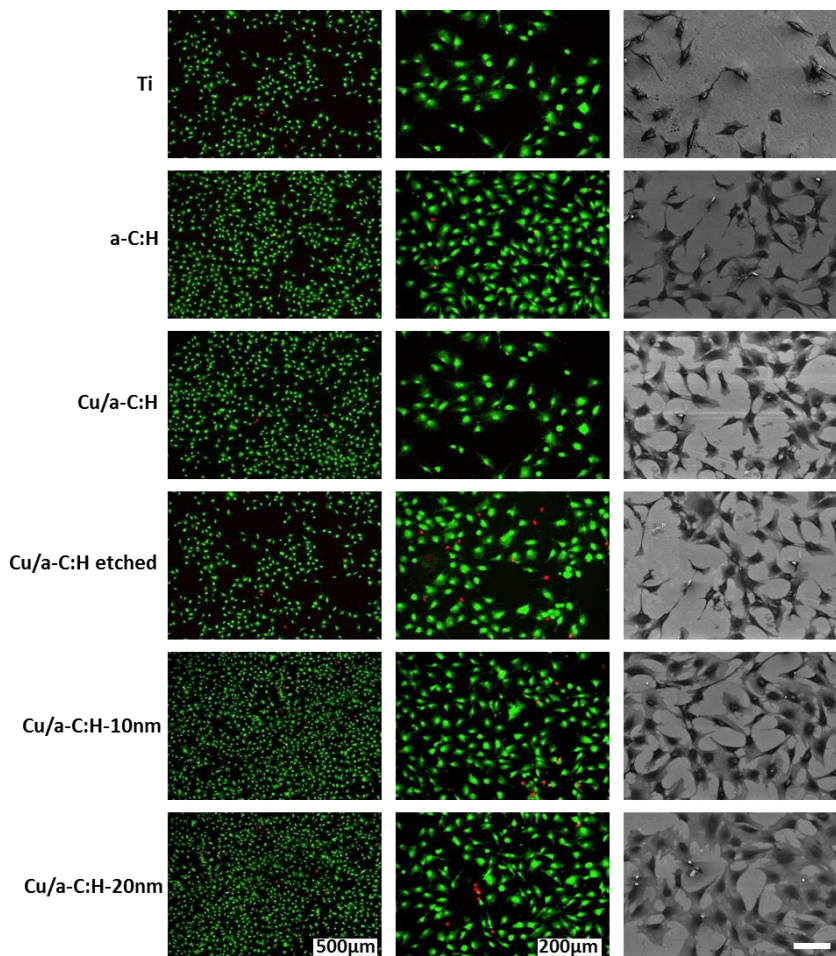


Figure 8.8. Fluorescence (scale bar : 500 μm & 200 μm) and SEM images (scale bar: 100 μm) of MC3T3 cells 1 day after cell seeding on uncoated and coated Ti samples.

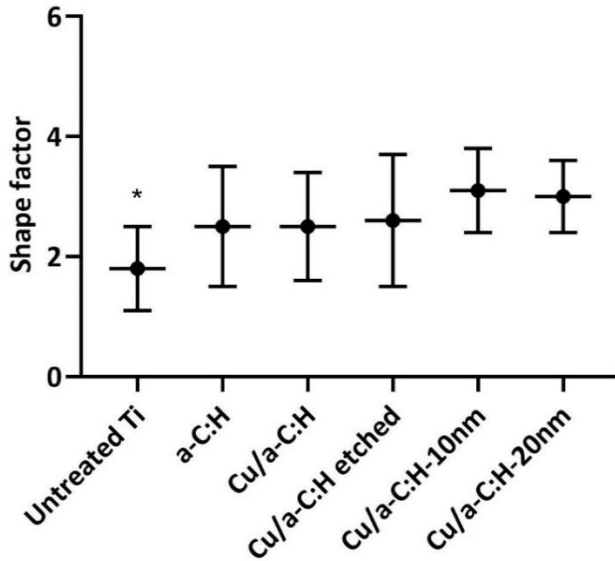


Figure 8.9. Quantification of the cell shape factor 1 day after cell seeding on uncoated and coated Ti disks. Asterisk () denotes a significantly different sample ($P < 0.05$).*

Considerable differences in cell proliferation between the uncoated and coated Ti disks were also seen 7 days after cell seeding (**Figure 8.10**): both fluorescent and SEM images indicated the higher cell surface density and higher spread out cell morphology on all coated surfaces as compared to uncoated Ti disks. Furthermore, it should be mentioned that for samples with the a-C:H barrier (10 nm/20 nm), almost 100% cell confluence was reached. To quantify the number of viable cells present on the different samples, an MTT assay was also performed 1 day and 7 days after cell seeding. As can be seen in **Figure 8.11**, all coated samples induced a strong improvement in cell adhesion and proliferation as they all exhibited cell viability values above 90% viability which are considerably higher viability values as compared to uncoated Ti disks (approximately 70%). Furthermore, the number of viable cells for both 1 day and 7 days after cell seeding followed the order: Cu/a-C:H-20nm > Cu/a-C:H-10nm > Cu/a-C:H > Cu/a-C:H

etched $a\text{-C:H}$, i.e. all coatings that contained CuNPs showed enhanced cell viability as compared to Cu-free $a\text{-C:H}$ films.

It is well-known that the bioactivity of any material is governed by its surface characteristics: wettability, roughness, and chemical composition. Therefore, it can be stated that a material with appropriate surface characteristics can have an improved performance in biomedical applications. Regarding the wettability, Bacakova et al.[56] reported that a moderately wettable surface (WCA: 70° to 80°) enables the adsorption of cell adhesion mediated extracellular matrix (ECM) molecules at an optimal amount. Another important factor contributing to cell adhesion is a nanostructured surface. Human osteoblast-like cells cultured on monocrystalline diamond layers showed increased cellular activity with increasing surface roughness in a certain range (from 11 nm to 39 nm)[532]. Many studies have also reported the superior biocompatibility of nanocrystalline diamond-like and carbon-like coatings on osteoblast-like cells[533,534]. Improved cell adhesion, proliferation and differentiation were observed on all diamond-like coatings regardless of their nanoscale topographies[57].

Taking into account the aforementioned reports and the wettability, roughness and surface chemical composition results obtained in this chapter (see **Table 8.3**), all fabricated Cu/ $a\text{-C:H}$ coatings were very similar and posed surface characteristics favourable for the growth of osteoblast-like cells, namely a slightly hydrophobic character and a moderate surface roughness.

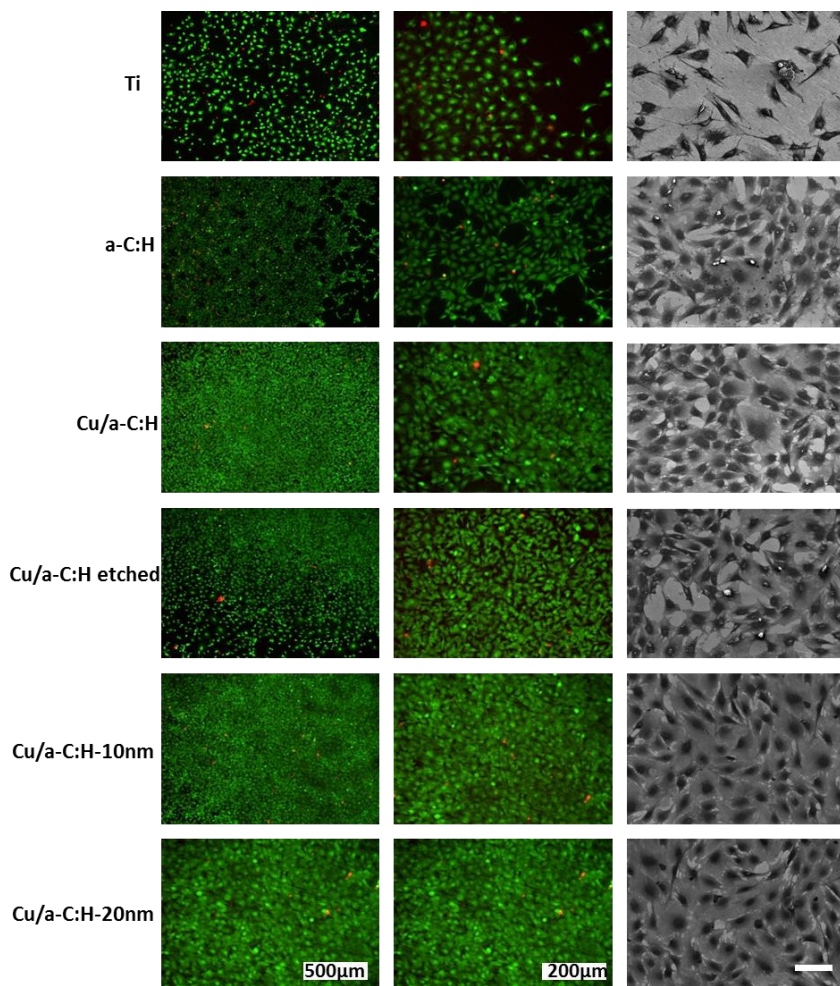


Figure 8.10. Fluorescence scale bar : (500 μm & 200 μm) and SEM images (scale bar: 100 μm) of MC3T3 cells 7 days after cell seeding on uncoated and coated Ti.

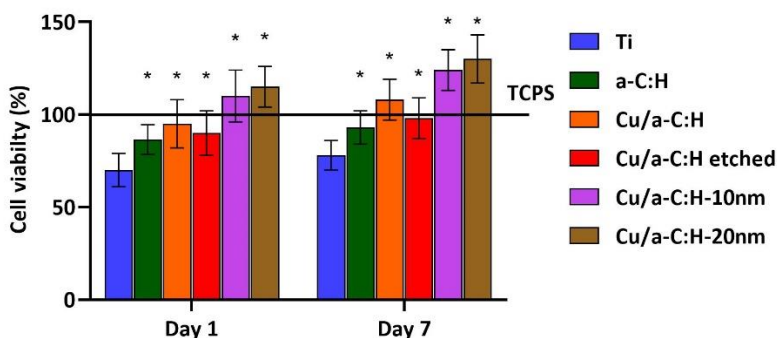


Figure 8.11. Cell viability results 1 day and 7 days after cell seeding on different titanium samples. Asterisk (*) denotes a significant difference at $P < 0.05$ compared to the control sample (uncoated Ti).

This may explain their superior bioactivity as compared to uncoated Ti disks. Furthermore, the bioactivity of the produced Cu/a-C:H coatings may also be promoted by the released Cu ions as cell spreading and viability was higher for all Cu-containing coatings as compared to the Cu-free a-C:H film. In fact, it has been reported that Cu^{2+} could possibly positively influence osteoblast cell activity and proliferation [177,342]. It was also previously demonstrated that Cu^{2+} ions play a crucial role in stimulating alkaline phosphatase (ALP) activity and osteogenic gene expression of osteoblasts which are important indicators for bone differentiation and mineralization [46,47,338,535,536]. In addition, an *in-vivo* study showed that Cu^{2+} are also responsible for the promotion of osteoconduction, osteoinduction and osseointegration [338]. Nonetheless, several studies have also reported that when the copper content in the biomaterial is above a certain limit, possible toxic effects can be observed [177,537]. However, based on our results, it can be seen that even for the coatings that are characterized by the highest release rate of Cu ions (Cu-a/C:H etched), the cell viability was still higher than 90% thereby meeting the ISO standards for a biocompatible material [514]. However, for the Cu-containing samples, the cell viability was found to increase with a decreasing release rate of Cu^{2+} showing that this parameter has to be carefully considered when designing and optimizing the performance of bio-active coatings on biomedical implants.

8.4 Conclusion

In summary, in this chapter, the properties of Cu/a-C:H nanocomposite coatings deposited onto Ti disks by means of a vacuum-based strategy that combined cluster beam deposition of CuNPs, plasma-enhanced chemical vapour deposition of an a-C:H matrix and plasma etching have been investigated. The combination of these deposition techniques allowed for the production of Cu/a-C:H coatings with approximately the same amount of embedded CuNPs but with a different arrangement of the NPs inside the a-C:H matrix. As was shown, different structures of the produced coatings resulted in significantly different release rates of copper ions from the coatings in aqueous media and consequently also different antibacterial efficiencies. According to the results presented in this study, the highest antibacterial effect (nearly a 5- and 4-log reduction of *E. coli* and a 2-log reduction of *S. aureus* within 24 hours) was observed for the samples with the highest number of CuNPs on or the presence of CuNPs close to the surface of the Cu/a-C:H nanocomposites, i.e. for the Cu/a-C:H and the Cu/a-C:H etched coatings. However, even for the layered coatings in which the CuNPs were covered by a thin a-C:H barrier film, the antibacterial effect was still measurable and in the worst case (*S. aureus* and a 20 nm thick a-C:H barrier layer) a 1-log reduction of viable bacteria was still detected. From the cytocompatibility study, it was observed that in spite of the substantial antibacterial activity of the fabricated Cu/a-C:H coatings, all investigated coatings with incorporated CuNPs were able to enhance osteoblast adhesion, proliferation and viability as compared to the uncoated Ti surfaces and Ti disks coated with copper-free a-C:H films. These results are of high importance as they clearly show that by a careful material design it is possible to generate bi-functional nanocomposite coatings that can inhibit planktonic bacteria while still favour the adhesion and growth of osteoblast cells, i.e. properties required for the excellent performance of Ti-based implants.

Chapter 9. Conclusions and outlook

9.1 Conclusions

The constant threat posed by bacterial colonization on implant surfaces has led to a rise of a new paradigm in preventing infections, with antibacterial coatings taking a significant role. Therefore, this dissertation was undertaken to develop antibacterial coatings on Ti implant surfaces to prevent implant-associated infections while also mimicking the properties of the bone to provide implant durability and longevity. To achieve this, a combinatorial approach by functionalizing the Ti surface with specific topographic and biochemical cues was adopted in the design of novel microporous and nanoporous composite coatings using two different non-thermal plasma-based techniques (PEO and cluster technique).

A profound and well-defined step-by-step approach was followed all the way through this dissertation to reach the ultimate goal of fabricating functional coatings on Ti implant surfaces for bone implant applications. The first objective of this dissertation was to study the effect of PEO treatment on the surface properties of Ti (**Chapters 5 and 6**). To do so, In **Chapter 5**, Ti discs were subjected to a PEO process in a sodium dihydrogen phosphate and sodium hydroxide containing base electrolyte with and without the addition of AgNPs. Taking into account all acquired results, it was proven that PEO treatment was suitable for Ti surface enhancement, resulting in improving its surface microstructure, roughness, wettability, and microhardness by the formation of a dense porous oxide layer. This was attributed to the formation of thermal micro arcs that occurred during the PEO process and the incorporation of rutile and anatase crystalline phases of TiO₂. In addition, the silver ion release profiles of the Ag-doped coatings exhibited a fast initial release followed by a slow continuous release over a period of 7 days. The results also revealed the superior antibacterial efficacy of the Ag-doped coatings against gram-negative and gram-positive bacteria. Despite exhibiting superior antibacterial efficacy, the incorporated AgNPs were observed to aggregate as clusters on the coating surface and the clustering effect was more pronounced at increased Ag content. This finding is unfavorable as aggregates of silver are known to lead to bacterial resistance and may cause a potential cytotoxic effect on cell lines. In fact, the coatings fabricated in **Chapter 5** were not sufficient to achieve the near-perfect implant surface without functionalizing the Ti surface with specific

biochemical cues to attain sufficient bone ingrowth and osteoconductive performance.

Therefore, in the next step of this dissertation, the focus was shifted to harness the antibacterial properties of Ag ions without actually using AgNPs but delivering Ag ions from AgOOCCH_3 together with incorporating osteoconductive Ca and P ions (from $\text{NaH}_2\text{PO}_4 \cdot 2\text{H}_2\text{O}$ and $\text{Ca}(\text{OOCCH}_3)_2 \cdot \text{H}_2\text{O}$) in the porous oxide matrix (**Chapter 6**). Although the formation of a micro-rough surface and the incorporation of anatase and rutile TiO_2 can enhance the bone ingrowth, incorporation of HA onto the implant material improves osseointegration, bone formation and reduces bone loss due to its structural resemblance to bone minerals. Hence, the composition of the electrolyte was chosen in such a way to attain the ratio characteristic for stoichiometric HA (Ca/P = 1.6), which mimics the bone apatite properties. The attained results revealed that the surface of Ti was converted to anatase and rutile TiO_2 , hydroxyapatite, and calcium titanate phases. The presence of these crystalline phases was further increased with increased silver content in the coatings. This increased crystallinity was, in fact, found to be a crucial factor in promoting successful protein adsorption and osseointegration. The developed coatings also exhibited a more porous morphology with an improved surface wettability, roughness, microhardness, and frictional coefficient. The silver ion release profiles of the Ag-doped coatings were found to be strongly affected by the initial silver loading in the electrolyte and also on the immersion time. Besides the beneficial surface modification and the excellent *in-vitro* biological response, it became also apparent that the use of silver acetate did not form any aggregates in the oxide layer, which was observed when incorporating AgNPs in the electrolyte (**Chapter 5**). This finding is very positive as a uniform deposition of Ag in the oxide layer is essential to have a constant release of Ag^+ , which can in turn provide a better antibacterial performance and biocompatibility.

As an alternative approach to enhance the properties of Ti implants, setting the same objectives, the cluster technology (a combination of magnetron sputtering and plasma-enhanced chemical vapor deposition) was used in the second half of the dissertation (**Chapters 7 and 8**). This technology, in contrast to PEO, enables to control the properties of the matrix, the amount of antibacterial agents loaded into

the matrix as well as its release rate independently. Within this work, it was opted to work with n-hexane as precursor to deposit an a-C:H film, as this class of film can elicit a more favorable biological response and possesses superior mechanical properties, which are essential for implant applications. Similar to the previously mentioned PEO studies, the physico-chemical, *in-vitro* antibacterial, and cell-interactive properties were studied. The obtained results revealed that all the prepared coatings exhibited good antibacterial efficacy against gram-positive and gram-negative bacteria, and the effect was more pronounced in case of the coatings with the highest amount of Ag content (**Chapter 7**). Besides the very good antibacterial performance, all coatings were also able to promote osteoblast adhesion and proliferation independent of the Ag content in the coating. While the antibacterial effect of the fabricated coatings was found to be proportional to the number of embedded AgNPs and with it connected, the rate of silver ion release, the enhanced growth of osteoblast cells was primarily the result of the increased nanoroughness of the coatings induced by the presence of the AgNPs. In addition to this dual-function of the developed Ag/a-C:H films, these coatings also exhibited a remarkably high adhesion to the Ti surface as demonstrated by scratch tests (critical load of 24 N) and also showed long-term stability in aqueous environments (both distilled water and PBS). As the Ag- rich amorphous hydrocarbon thin films (Ag/a-C:H) developed in **Chapter 7** showed promising results, the bi-functional character of a thin a-C:H matrix loaded with CuNPs on Ti substrates has also been examined, an approach which has not yet been explored in the past (**Chapter 8**). CuNPs are used in this study because apart from their use as an antibacterial agent, Cu ions released from CuNPs are also beneficial to the cardiovascular system by stimulating the proliferation and differentiation of endothelial cells, and a sustained release of trace amounts of Cu ions could also promote osteogenesis. The obtained results revealed that different structures of the produced coatings possess significantly different release rates of Cu ions from the coatings into the aqueous media. This, in fact, is connected to the antibacterial efficiency and osteoblast cell viability of the treated coatings. Even the coatings with the highest amount of CuNPs resulted in excellent antibacterial efficiency and osteoblast cell adhesion and proliferation. Consequently, the coating, formed with a properly tailored number of

CuNPs and a-C:H structure, offers a strong antibacterial effect without any harm to osteoblast cells.

Next to the conclusion, it is also crucial to discuss the advantages and disadvantages of each of these techniques. It is evident that both PEO and cluster source techniques were able to inhibit bacterial adhesion as well as promote osteoblast adhesion and proliferation with the improved mechanical property. However, each of these techniques has its own merits and demerits and hence a careful choice has to be made in selecting the right technique depending on the end application. For instance, the PEO technique is simple, economical, and easy to build and enables treatment of 3D substrate while the cluster technique, a vacuum-based process is too expensive to build to be able to treat on 3D substrates. Furthermore, in cluster technique, all pretreatment and deposition steps are performed in a single deposition system and it requires no washing/ cleanings steps in contrast to PEO that utilize chemical synthesis for the production of bi-functional coatings. Additionally, in the case of the PEO technique, the content of antibacterial and bioactive elements on the PEO treated surface surfaces cannot be tuned independently whereas cluster technique enables to independently control the properties of the matrix, the amount of antibacterial agents loaded into the matrix as well as their release rate. Moreover, using the cluster technique it is possible to control the size of the NPs, unlike the PEO technique. The final noteworthy difference between these two techniques is the morphology of the produced coatings. PEO coatings can produce a microporous and adhesive coating which improves the adhesion between the Ti substrate and the matrix while the cluster technique produces nanoporous coating and it challenging to improve the adhesion between the Ti substrate and the matrix.

Overall, this PhD work has proven that both surface modification technologies (PEO, PECVD+GAS) have a great potential in fabricating functional coatings as the deposited coatings exhibited sufficient osseointegration and antibacterial properties, thus making them highly interesting materials for implant applications. The results obtained in this dissertation thus prove that favourable surface properties such as surface wettability, surface roughness and surface chemical composition together with a controlled release of Ag ions or

Cu ions are the determining factors for the success of an implant material.

9.2 Outlook and future work

The findings of this dissertation revealed that the employed non-thermal plasma-assisted surface modification techniques (PEO, PECVD+GAS) have a great potential in functionalizing Ti implant surfaces with appropriate topographical and biochemical cues to achieve a near-perfect implant material. i.e. an antibacterial coating with controlled release of the antibacterial agent, a surface promoting tissue integration, and a coating with superior mechanical properties. Although we have achieved the objectives of this dissertation, there are still some unanswered questions that need to be addressed before transferring to *in-vivo* experiments or pre-clinical studies to check our hypotheses.

1) Antibacterial efficacy of the coatings on various bacterial strains:

E. coli and *S. aureus* were selected in this dissertation as they are the commonly found bacterial strains in implant-associated infections. However, a thorough investigation of various types of bacteria such as *Staphylococcus epidermidis*, *Pseudomonas aeruginosa*, *Corynebacterium xerosis*, *Mycobacterium avium* on the implant surfaces is important to provide a comprehensive understanding of the bacterial response.

2) Long-term release kinetics of the antibacterial agent: The silver ion and copper ion release kinetics of the coatings developed in this dissertation exhibited a fast initial release followed by a slow continuous release over a period of 7 days. In fact, the release kinetics were dependent on the structure of the coatings, the arrangement of the antibacterial agents within the coatings, and the initial loading of the antibacterial agents. Therefore, the antibacterial agents released from the prepared coatings were well maintained below the toxicity levels of human blood. However, the observed release kinetics were not guaranteed for the whole implantation period, and it is crucial to investigate the long-term release kinetics as the implants are supposed to be present in the body for a period of weeks/months (in case of temporary fracture fixation devices) or even years (in case of permanent implants).

3) **Co-culturing of bacterial and osteoblast cells:** The *in-vivo* fate of an implant can be depicted as a race between bacterial adhesion and biofilm formation on the implant surface versus tissue integration. The prepared coatings in this dissertation were able to inhibit initial bacterial adhesion meaning that they prevent biofilm formation; thus, it is presumed that successful tissue integration would occur before bacterial adhesion takes place owing to the favorable surface properties of the coatings. However, *in-vivo*, the processes occurring at an implant surface are quite complicated and involve multiple cell types, cytokines, macrophages and secretion of both bacterial and cellular substances. Therefore, it is essential to address the simultaneous effects of the presence of bacteria and osteoblast cells on an implant surface *in-vitro* by co-culturing both cell types before transferring to expensive *in-vivo* experiments to determine the ultimate fate of the material.

4) **Investigating different cell types:** Cell-interactive properties of the prepared coatings were investigated using osteoblast cells as this dissertation was mainly focused on orthopedic applications. However, it would be of great value to conduct studies with other cell types which would provide more knowledge on how surface functionalities could steer cell interactions. These studies would also confirm if this methodology could be an alternative for other implant materials such as oral implants, cardiovascular implants, surgical meshes and vascular grafts where bacterial infection occurs.

4) **Assessing the efficacy of coating in an *in vivo* animal model:** The next crucial step is to test the ability of the coated Ti disc to reduce the bacterial infection in an *in vivo* animal model. The best performance coatings in terms of silver ion release, biocompatibility and antibacterial performance have to be selected for this study. Ti disc can be subcutaneously inserted into the animal and bacterial contamination with a *s. aureus* or *s. epidermis* strain following insertion can be conducted on the insertion area. After an initial incubation of 48 hours after surgery, daily evaluation of the insertion area could be conducted to assess the infection. In addition, toxicity in the animal model could be investigated by taking blood samples and testing for silver levels, liver function and kidney function. This would be helpful in optimising the silver release in the deposited coatings.

References

- [1] Musculoskeletal conditions, (n.d.). <https://www.who.int/news-room/fact-sheets/detail/musculoskeletal-conditions> (accessed February 24, 2020).
- [2] S. Bose, S. Tarafder, A. Bandyopadhyay, Hydroxyapatite coatings for metallic implants, in: *Hydroxyapatite Biomed. Appl.*, Elsevier, 2015: pp. 143–157. doi:10.1016/b978-1-78242-033-0.00007-9.
- [3] R. Gheno, J.M. Cepparo, C.E. Rosca, A. Cotten, R. Salengro, *Musculoskeletal Disorders in the Elderly*, *J. Clin. Imaging Sci.* | 2 (n.d.). doi:10.4103/2156-7514.99151.
- [4] Facts and Statistics | International Osteoporosis Foundation, (n.d.). <https://www.iofbonehealth.org/facts-statistics> (accessed February 24, 2020).
- [5] E. Hernlund, A. Svedbom, M. Ivergård, J. Compston, C. Cooper, J. Stenmark, E. V. McCloskey, B. Jönsson, J.A. Kanis, Osteoporosis in the European Union: Medical management, epidemiology and economic burden: A report prepared in collaboration with the International Osteoporosis Foundation (IOF) and the European Federation of Pharmaceutical Industry Associations (EFPIA), *Arch. Osteoporos.* 8 (2013). doi:10.1007/s11657-013-0136-1.
- [6] A. Svedbom, E. Hernlund, M. Ivergård, J. Compston, C. Cooper, J. Stenmark, E. V. McCloskey, B. Jönsson, J.A. Kanis, Osteoporosis in the European Union: A compendium of country-specific reports, *Arch. Osteoporos.* 8 (2013) 137. doi:10.1007/s11657-013-0137-0.
- [7] Orthopedic Devices Market by device type and region 2017-2022 | Lucintel, (n.d.). <https://www.lucintel.com/orthopedic-device-industry-2017-2022.aspx> (accessed February 24, 2020).
- [8] A. Woolf, B.P.-B. of the world health organization, undefined 2003, Burden of major musculoskeletal conditions, *SciELO Public Heal.* (n.d.). <https://www.scielosp.org/article/bwho/2003.v81n9/646-656/> (accessed April 18, 2020).
- [9] R. Marsell, T.A. Einhorn, *THE BIOLOGY OF FRACTURE HEALING*, (2011). doi:10.1016/j.injury.2011.03.031.
- [10] A history of orthopaedics | LimBO Products, (n.d.). <https://limboproducts.co.uk/news/history-orthopaedics> (accessed February 24, 2020).

- [11] S.F. Hulbert, J.J. Klawitter, L.S. Bowman, History of ceramic orthopedic implants, *Mater. Res. Bull.* 7 (1972) 1239–1246. doi:10.1016/0025-5408(72)90103-1.
- [12] J. Bartoníbek, Early history of operative treatment of fractures, *Arch Orthop Trauma Surg.* 130 (2010) 1385–1396. doi:10.1007/s00402-010-1082-7.
- [13] K. Markatos, G. Tsoucalas, M. Sgantzios, Hallmarks in the history of orthopaedic implants for trauma and joint replacement., *Acta Med. Hist. Adriat.* 14 (2016) 161–76. <http://www.ncbi.nlm.nih.gov/pubmed/27598960> (accessed February 24, 2020).
- [14] L.C. Jones, L.D. Timmie Topoleski, A.K. Tsao, Biomaterials in orthopaedic implants, in: *Mech. Test. Orthop. Implant.*, Elsevier, 2017: pp. 17–32. doi:10.1016/B978-0-08-100286-5.00002-0.
- [15] J.T. Evans, J.P. Evans, R.W. Walker, A.W. Blom, M.R. Whitehouse, A. Sayers, How long does a hip replacement last? A systematic review and meta-analysis of case series and national registry reports with more than 15 years of follow-up, *Lancet* (London, England). 393 (2019) 647–654. doi:10.1016/S0140-6736(18)31665-9.
- [16] G. Labek, M. Thaler, W. Janda, M. Agreiter, B. Stöckl, O. Surgeon, Revision rates after total joint replacement CUMULATIVE RESULTS FROM WORLDWIDE JOINT REGISTER DATASETS, *J Bone Jt. Surg [Br.]*. (2011) 93–293. doi:10.1302/0301-620X.93B3.
- [17] A. Postler, C. Lützner, F. Beyer, E. Tille, J. Lützner, Analysis of Total Knee Arthroplasty revision causes, *BMC Musculoskelet. Disord.* 19 (2018). doi:10.1186/s12891-018-1977-y.
- [18] S.M. Jafari, C. Coyle, S.M.J. Mortazavi, P.F. Sharkey, J. Parvizi, Revision hip arthroplasty: Infection is the most common cause of failure, in: *Clin. Orthop. Relat. Res.*, Springer New York, 2010: pp. 2046–2051. doi:10.1007/s11999-010-1251-6.
- [19] T. Jennison, M. McNally, H. Pandit, Prevention of infection in external fixator pin sites, *Acta Biomater.* 10 (2014) 595–603. doi:10.1016/j.actbio.2013.09.019.
- [20] H. Qu, C. Knabe, S. Radin, J. Garino, P. Ducheyne, Percutaneous external fixator pins with bactericidal micron-thin sol-gel films for the prevention of pin tract infection,

- Biomaterials. 62 (2015) 95–105.
doi:10.1016/j.biomaterials.2015.05.041.
- [21] S. Esposito, S. Leone, Prosthetic joint infections: microbiology, diagnosis, management and prevention, *Int. J. Antimicrob. Agents.* 32 (2008) 287–293.
doi:10.1016/j.ijantimicag.2008.03.010.
- [22] S.J. McConoughey, R. Howlin, J.F. Granger, M.M. Manring, J.H. Calhoun, M. Shirtliff, S. Kathju, P. Stoodley, Biofilms in periprosthetic orthopedic infections, *Future Microbiol.* 9 (2014) 987–1007. doi:10.2217/fmb.14.64.
- [23] N. Høiby, T. Bjarnsholt, C. Moser, ... G.B.-C. microbiology, undefined 2015, ESCMID guideline for the diagnosis and treatment of biofilm infections 2014, Elsevier. (n.d.).
<https://www.sciencedirect.com/science/article/pii/S1198743X14000901> (accessed June 6, 2019).
- [24] Y. Abu-Amer, I. Darwech, J.C. Clohisy, Aseptic loosening of total joint replacements: Mechanisms underlying osteolysis and potential therapies, *Arthritis Res. Ther.* 9 (2007) S6.
doi:10.1186/ar2170.
- [25] S.D. Ulrich, T.M. Seyler, D. Bennett, R.E. Delanois, K.J. Saleh, I. Thongtrangan, M. Kuskowski, E.Y. Cheng, P.F. Sharkey, J. Parvizi, J.B. Stiehl, M.A. Mont, M.A. Mont, K.J. Saleh, I. Thongtrangan, M. Kuskowski, E.Y. Cheng, P.F. Sharkey, J. Parvizi, J.B. Stiehl, Total hip arthroplasties: What are the reasons for revision?, (n.d.). doi:10.1007/s00264-007-0364-3.
- [26] B.J. Nelson, M. Morra, C. Cassinelli, G. Cascardo, A. Carpi, M. Fini, G. Giavaresi, R. Giardino, A. Kozlovsky, Z. Artzi, O. Moses, N. Kamin-Belsky, R.B.-N. Greenstein, W.H. Kim, S.B. Lee, K.T. Oh, S.K. Moon, K.M.K.N. Kim, K.M.K.N. Kim, The release behavior of CHX from polymer-coated titanium surfaces, *Surf. Interface Anal.* 58 (2004) 1194–1200. doi:10.1002/sia.2809.
- [27] A. Kozlovsky, Z. Artzi, O. Moses, N. Kamin-Belsky, R.B.-N. Greenstein, Interaction of Chlorhexidine With Smooth and Rough Types of Titanium Surfaces, *J. Periodontol.* 77 (2006) 1194–1200. doi:10.1902/jop.2006.050401.
- [28] M. Morra, C. Cassinelli, G. Cascardo, A. Carpi, M. Fini, G. Giavaresi, R. Giardino, Adsorption of cationic antibacterial on collagen-coated titanium implant devices, *Biomed. Pharmacother.* 58 (2004) 418–422.

doi:10.1016/j.biopha.2004.08.002.

- [29] M.E. Barbour, D.J. O'Sullivan, D.C. Jagger, Chlorhexidine adsorption to anatase and rutile titanium dioxide, *Colloids Surfaces A Physicochem. Eng. Asp.* 307 (2007) 116–120. doi:10.1016/j.colsurfa.2007.05.010.
- [30] E.I. Alarcon, K. Udekwu, M. Skog, N.L. Pacioni, K.G. Stamplecoskie, M. González-Béjar, N. Poliseti, A. Wickham, A. Richter-Dahlfors, M. Griffith, J.C. Scaiano, The biocompatibility and antibacterial properties of collagen-stabilized, photochemically prepared silver nanoparticles, *Biomaterials*. 33 (2012) 4947–4956. doi:10.1016/j.biomaterials.2012.03.033.
- [31] R. Suntornnond, J. An, C.K. Chua, Effect of gas plasma on polycaprolactone (PCL) membrane wettability and collagen type I immobilized for enhancing cell proliferation, *Mater. Lett.* 171 (2016) 293–296. doi:10.1016/j.matlet.2016.02.059.
- [32] S. Mei, H. Wang, W. Wang, L. Tong, H. Pan, C. Ruan, Q. Ma, M. Liu, H. Yang, L. Zhang, Y. Cheng, Y. Zhang, L. Zhao, P.K. Chu, Antibacterial effects and biocompatibility of titanium surfaces with graded silver incorporation in titania nanotubes, *Biomaterials*. 35 (2014) 4255–4265. doi:10.1016/j.biomaterials.2014.02.005.
- [33] H. Wu, X. Zhang, X. He, M. Li, X. Huang, R. Hang, B. Tang, Wear and corrosion resistance of anti-bacterial Ti-Cu-N coatings on titanium implants, *Appl. Surf. Sci.* 317 (2014) 614–621. doi:10.1016/j.apsusc.2014.08.163.
- [34] X. Zhang, Y. Ma, N. Lin, X. Huang, R. Hang, A. Fan, B. Tang, Microstructure, antibacterial properties and wear resistance of plasma Cu-Ni surface modified titanium, *Surf. Coatings Technol.* 232 (2013) 515–520. doi:10.1016/j.surfcoat.2013.06.012.
- [35] X. Zhang, X. Huang, L. Jiang, Y. Ma, A. Fan, B. Tang, Surface microstructures and antimicrobial properties of copper plasma alloyed stainless steel, *Appl. Surf. Sci.* 258 (2011) 1399–1404. doi:10.1016/j.apsusc.2011.09.091.
- [36] G. Jin, H. Qin, H. Cao, S. Qian, Y. Zhao, X. Peng, X. Zhang, X. Liu, P.K. Chu, Synergistic effects of dual Zn/Ag ion implantation in osteogenic activity and antibacterial ability of titanium, *Biomaterials*. 35 (2014) 7699–7713. doi:10.1016/j.biomaterials.2014.05.074.

- [37] G. Jin, H. Qin, H. Cao, Y. Qiao, Y. Zhao, X. Peng, X. Zhang, X. Liu, P.K. Chu, Zn/Ag micro-galvanic couples formed on titanium and osseointegration effects in the presence of S.aureus, *Biomaterials*. 65 (2015) 22–31. doi:10.1016/j.biomaterials.2015.06.040.
- [38] K. Huo, X. Zhang, H. Wang, L. Zhao, X. Liu, P.K. Chu, Osteogenic activity and antibacterial effects on titanium surfaces modified with Zn-incorporated nanotube arrays, *Biomaterials*. 34 (2013) 3467–3478. doi:10.1016/j.biomaterials.2013.01.071.
- [39] R. Dastjerdi, M. Montazer, A review on the application of inorganic nano-structured materials in the modification of textiles: Focus on anti-microbial properties, *Colloids Surfaces B Biointerfaces*. 79 (2010) 5–18. doi:10.1016/j.colsurfb.2010.03.029.
- [40] M.J. Hajipour, K.M. Fromm, A. Akbar Ashkarran, D. Jimenez de Aberasturi, I.R. de Larramendi, T. Rojo, V. Serpooshan, W.J. Parak, M. Mahmoudi, Antibacterial properties of nanoparticles, *Trends Biotechnol.* 30 (2012) 499–511. doi:10.1016/j.tibtech.2012.06.004.
- [41] R.O. Darouiche, Anti-Infective Efficacy of Silver-Coated Medical Prostheses, *Clin. Infect. Dis.* 29 (1999) 1371–1377. doi:10.1086/313561.
- [42] U. Samuel, J. Guggenbichler, Prevention of catheter-related infections: the potential of a new nano-silver impregnated catheter, *Int. J. Antimicrob. Agents*. 23 (2004) 75–78. doi:10.1016/J.IJANTIMICAG.2003.12.004.
- [43] L.M. Coester, J. V Nepola, J. Allen, J.L. Marsh, The effects of silver coated external fixation pins., *Iowa Orthop. J.* 26 (2006) 48–53. <http://www.ncbi.nlm.nih.gov/pubmed/16789449> (accessed September 30, 2019).
- [44] M. Bosetti, A. Massè, E. Tobin, M. Cannas, Silver coated materials for external fixation devices: In vitro biocompatibility and genotoxicity, *Biomaterials*. 23 (2002) 887–892. doi:10.1016/S0142-9612(01)00198-3.
- [45] J. Harges, H. Ahrens, C. Gebert, A. Streitbuenger, H. Buerger, M. Erren, A. Gunsel, C. Wedemeyer, G. Saxler, W. Winkelmann, G. Gosheger, Lack of toxicological side-effects in silver-coated megaprotheses in humans, *Biomaterials*. 28 (2007) 2869–2875.

doi:10.1016/J.BIOMATERIALS.2007.02.033.

- [46] A. Ewald, C. Käppel, E. Vorndran, C. Moseke, M. Gelinsky, U. Gbureck, The effect of Cu(II)-loaded brushite scaffolds on growth and activity of osteoblastic cells, *J. Biomed. Mater. Res. - Part A*. 100 A (2012) 2392–2400. doi:10.1002/jbm.a.34184.
- [47] M.M. Erol, V. Mouriño, P. Newby, X. Chatzistavrou, J.A. Roether, L. Hupa, A.R. Boccaccini, Copper-releasing, boron-containing bioactive glass-based scaffolds coated with alginate for bone tissue engineering, *Acta Biomater.* 8 (2012) 792–801. doi:10.1016/j.actbio.2011.10.013.
- [48] I. Burghardt, F. Lüthen, C. Prinz, B. Kreikemeyer, C. Zietz, H.G. Neumann, J. Rychly, A dual function of copper in designing regenerative implants, *Biomaterials.* 44 (2015) 36–44. doi:10.1016/j.biomaterials.2014.12.022.
- [49] N.J. Lakhkar, I.H. Lee, H.W. Kim, V. Salih, I.B. Wall, J.C. Knowles, Bone formation controlled by biologically relevant inorganic ions: Role and controlled delivery from phosphate-based glasses, *Adv. Drug Deliv. Rev.* 65 (2013) 405–420. doi:10.1016/j.addr.2012.05.015.
- [50] T. Zhang, L. Wang, Q. Chen, C. Chen, Cytotoxic potential of silver nanoparticles., *Yonsei Med. J.* 55 (2014) 283–91. doi:10.3349/ymj.2014.55.2.283.
- [51] J. Hardes, H. Ahrens, C. Gebert, A. Streitbuerger, H. Buerger, M. Erren, A. Günsel, C. Wedemeyer, G. Saxler, W. Winkelmann, G. Gosheger, Lack of toxicological side-effects in silver-coated megaprotheses in humans, *Biomaterials.* 28 (2007) 2869–2875. doi:10.1016/j.biomaterials.2007.02.033.
- [52] A. Allion-Maurer, C. Saulou-Bérion, R. Briandet, S. Zanna, N. Lebleu, P. Marcus, P. Raynaud, B. Despax, M. Mercier-Bonin, Plasma-deposited nanocomposite polymer-silver coating against *Escherichia coli* and *Staphylococcus aureus*: Antibacterial properties and ageing, *Surf. Coatings Technol.* 281 (2015) 1–10. doi:10.1016/j.surfcoat.2015.09.025.
- [53] F. Faupel, V. Zaporozhchenko, H. Greve, U. Schürmann, V.S.K. Chakravadhanula, C. Hanisch, A. Kulkarni, A. Gerber, E. Quandt, R. Podschun, Deposition of nanocomposites by plasmas, in: *Contrib. to Plasma Phys.*, 2007: pp. 537–544. doi:10.1002/ctpp.200710069.
- [54] C. Damm, H. Münstedt, Kinetic aspects of the silver ion release

- from antimicrobial polyamide/silver nanocomposites, *Appl. Phys. A Mater. Sci. Process.* 91 (2008) 479–486. doi:10.1007/s00339-008-4434-1.
- [55] M. Allen, B. Myer, N. Rushton, In vitro and in vivo investigations into the biocompatibility of diamond-like carbon (DLC) coatings for orthopedic applications, *J. Biomed. Mater. Res.* 58 (2001) 319–328. doi:10.1002/1097-4636(2001)58:3<319::AID-JBM1024>3.0.CO;2-F.
- [56] L. Bacakova, H. Koshelyev, L. Noskova, A. Choukourov, O. Benada, A. Mackova, V. Lisa, H. Biederman, Vascular endothelial cells in cultures on nanocomposite silver/hydrocarbon plasma polymer films with antimicrobial activity, *J. Optoelectron. Adv. Mater.* 10 (2008) 2082–2087.
- [57] S.A. Skoog, G. Kumar, J. Zheng, A. V. Sumant, P.L. Goering, R.J. Narayan, Biological evaluation of ultrananocrystalline and nanocrystalline diamond coatings, *J. Mater. Sci. Mater. Med.* 27 (2016). doi:10.1007/s10856-016-5798-y.
- [58] N. Harrasser, S. Jüssen, A. Obermeier, R. Kmeth, B. Stritzker, H. Gollwitzer, R. Burgkart, Antibacterial potency of different deposition methods of silver and copper containing diamond-like carbon coated polyethylene, *Biomater. Res.* 20 (2016) 1–10. doi:10.1186/s40824-016-0062-6.
- [59] G. Dearnaley, J.H. Arps, Biomedical applications of diamond-like carbon (DLC) coatings: A review, *Surf. Coatings Technol.* 200 (2005) 2518–2524. doi:10.1016/j.surfcoat.2005.07.077.
- [60] A. Grill, Diamond-like carbon coatings as biocompatible materials - An overview, *Diam. Relat. Mater.* 12 (2003) 166–170. doi:10.1016/S0925-9635(03)00018-9.
- [61] F.Z. Cui, D.J. Li, A review of investigations on biocompatibility of diamond-like carbon and carbon nitride films, *Surf. Coatings Technol.* 131 (2000) 481–487. doi:10.1016/S0257-8972(00)00809-4.
- [62] W.E. Brown, L.C. Chow, CHEMICAL PROPERTIES OF BONE MINERAL!, 1976. www.annualreviews.org (accessed April 14, 2020).
- [63] Physical properties and physiology of bone 2.1 THE NATURE OF BONE, n.d.
- [64] Anatomy & Physiology Gross Anatomy of Bones, (n.d.).
- [65] S. Bone, C. Bone, Difference between Spongy Bone and Compact

- Bone Spongy Bone Compact Bone Further Readings : Teaching Resources, (2017) 2–3.
- [66] Types of Bones | Learn Skeleton Anatomy, (n.d.). <https://www.visiblebody.com/learn/skeleton/types-of-bones> (accessed April 14, 2020).
- [67] Bone type Medical Definition of All Four Shape Types, (n.d.). <https://www.medicinenet.com/script/main/art.asp?articlekey=24396> (accessed April 14, 2020).
- [68] D.M.L. Cooper, C.E. Kawalilak, & K. Harrison, B.D. Johnston, J.D. Johnston, Cortical Bone Porosity: What Is It, Why Is It Important, and How Can We Detect It?, (1914). doi:10.1007/s11914-016-0319-y.
- [69] J.D. Currey, R. Shahar, Cavities in the compact bone in tetrapods and fish and their effect on mechanical properties, *J. Struct. Biol.* 183 (2013) 107–122. doi:10.1016/j.jsb.2013.04.012.
- [70] F.G. Evans, Mechanical properties and histology of cortical bone from younger and older men, *Anat. Rec.* 185 (1976) 1–11. doi:10.1002/ar.1091850102.
- [71] C. Xie, H. Lu, W. Li, F.M. Chen, Y.M. Zhao, The use of calcium phosphate-based biomaterials in implant dentistry, *J. Mater. Sci. Mater. Med.* 23 (2012) 853–862. doi:10.1007/s10856-011-4535-9.
- [72] G. Heimke, D.S.-O.C. Implants, undefined 1984, Clinical application of ceramic osseo-or soft tissue-integrated implants, (n.d.).
- [73] S. Parithimarkalaigan, T. V Padmanabhan, Osseointegration: An Update, (n.d.). doi:10.1007/s13191-013-0252-z.
- [74] P. (eds. . Brunette, D.M., Tengvall, P., Textor, M., Thomsen, Titanium in Medicine, Material Science, Surface Science, Engineering, Biological Responses and Medical Applications, Springer- Verlag Heidelb. Berlin. (2000) 704–737. doi:10.1007/978-3-642-56486-4.
- [75] V. Migonney, History of Biomaterials, in: Biomaterials, John Wiley & Sons, Inc., Hoboken, NJ, USA, 2014: pp. 1–10. doi:10.1002/9781119043553.ch1.
- [76] M. Saini, Implant biomaterials: A comprehensive review, *World J. Clin. Cases.* 3 (2015) 52. doi:10.12998/wjcc.v3.i1.52.
- [77] Titanium: A Technical Guide, 2nd Edition - ASM International, (n.d.). <https://www.asminternational.org/search/>

/journal_content/56/10192/06112G/PUBLICATION (accessed January 14, 2020).

- [78] F.H. Froes, Titanium: Alloying, in: *Encycl. Mater. Sci. Technol.*, Elsevier, 2001: pp. 9361–9364. doi:10.1016/b0-08-043152-6/01690-9.
- [79] I. Polmear, D. StJohn, J.-F. Nie, M. Qian, Titanium Alloys, in: *Light Alloy.*, Elsevier, 2017: pp. 369–460. doi:10.1016/b978-0-08-099431-4.00007-5.
- [80] A. Shah, S.N.F. Ismail, M.A. Hasan, R. Daud, Surface Modification on Titanium Alloy for Biomedical Application ☆, in: *Ref. Modul. Mater. Sci. Mater. Eng.*, Elsevier, 2018. doi:10.1016/b978-0-12-803581-8.10484-9.
- [81] K. Jayaraj, A. Pius, Biocompatible coatings for metallic biomaterials, in: *Fundam. Biomater. Met.*, Elsevier, 2018: pp. 323–354. doi:10.1016/b978-0-08-102205-4.00016-7.
- [82] K.K. Sankaran, R.S. Mishra, Titanium Alloys, in: *Metall. Des. Alloy. with Hierarchical Microstruct.*, Elsevier, 2017: pp. 177–288. doi:10.1016/b978-0-12-812068-2.00005-9.
- [83] P. Chakraborty Banerjee, S. Al-Saadi, L. Choudhary, S.E. Harandi, R. Singh, materials Magnesium Implants: Prospects and Challenges, (n.d.). doi:10.3390/ma12010136.
- [84] H.S. Brar, M.O. Platt, M. Sarntinoranont, P.I. Martin, M. V. Manuel, Magnesium as a biodegradable and bioabsorbable material for medical implants, *JOM*. 61 (2009) 31–34. doi:10.1007/s11837-009-0129-0.
- [85] T. Imwinkelried, Testing the mechanical properties of surface-modified magnesium and magnesium alloys for biomedical applications, in: *Surf. Modif. Magnes. Its Alloy. Biomed. Appl.*, Elsevier Ltd, 2015: pp. 311–329. doi:10.1016/B978-1-78242-077-4.00010-3.
- [86] M. Peron, J. Torgersen, F. Berto, Mg and Its Alloys for Biomedical Applications: Exploring Corrosion and Its Interplay with Mechanical Failure, *Metals (Basel)*. 7 (2017) 252. doi:10.3390/met7070252.
- [87] Y.T. Konttinen, I. Milošev, R. Trebše, P. Rantanen, R. Linden, V.M. Tiainen, S. Virtanen, Metals for joint replacement, in: *Jt. Replace. Technol.*, Elsevier Ltd., 2008: pp. 115–162. doi:10.1533/9781845694807.2.115.
- [88] D. Cristea, I. Ghiuță, D. Munteanu, TANTALUM BASED

MATERIALS FOR IMPLANTS AND PROSTHESES APPLICATIONS, 2015.

- [89] V. Balla, S. Bodhak, S. Bose, A.B.-A. biomaterialia, undefined 2010, Porous tantalum structures for bone implants: fabrication, mechanical and in vitro biological properties, Elsevier. (n.d).
<https://www.sciencedirect.com/science/article/pii/S1742706110000619> (accessed January 14, 2020).
- [90] M.D. Budge, M.D. Kurdziel, K.C. Baker, J.M. Wiater, A biomechanical analysis of initial fixation options for porous-tantalum-backed glenoid components, *J. Shoulder Elb. Surg.* 22 (2013) 709–715. doi:10.1016/j.jse.2012.07.001.
- [91] R. Köster, D. Vieluf, M. Kiehn, M. Sommerauer, J. Kahler, S. Baldus, T. Meinertz, C.W. Hamm, Nickel and molybdenum contact allergies in patients with coronary in-stent restenosis, *Lancet.* 356 (2000) 1895–1897. doi:10.1016/S0140-6736(00)03262-1.
- [92] I.A. Neacșu, A.I. Nicoară, O.R. Vasile, B.Ș. Vasile, Inorganic micro- and nanostructured implants for tissue engineering, in: *Nanobiomaterials Hard Tissue Eng. Appl. Nanobiomaterials*, Elsevier Inc., 2016: pp. 271–295. doi:10.1016/B978-0-323-42862-0.00009-2.
- [93] P. Sahoo, S.K. Das, J. Paulo Davim, Tribology of materials for biomedical applications, in: *Mech. Behav. Biomater.*, Elsevier, 2019: pp. 1–45. doi:10.1016/b978-0-08-102174-3.00001-2.
- [94] R.O. Darouiche, Infections Associated with Surgical Implants, *N. Engl. J. Med.* 351 (2004) 193–195. doi:10.1056/nejm200407083510220.
- [95] S. Veerachamy, T. Yarlagadda, G. Manivasagam, P.K. Yarlagadda, Bacterial adherence and biofilm formation on medical implants: A review, *Proc. Inst. Mech. Eng. Part H J. Eng. Med.* 228 (2014) 1083–1099. doi:10.1177/0954411914556137.
- [96] G.A. Melcher, B. Claudi, U. Schlegel, S.M. Perren, G. Printzen, J. Munzinger, Influence of type of medullary nail on the development of local infection. An experimental study of solid and slotted nails in rabbits., *J. Bone Joint Surg. Br.* 76 (1994) 955–9. <http://www.ncbi.nlm.nih.gov/pubmed/7983127> (accessed January 15, 2020).

- [97] B. Hu, Y. Pan, Z. Li, W. Yuan, L. Deng, EmPis-1L, an Effective Antimicrobial Peptide Against the Antibiotic-Resistant VBNC State Cells of Pathogenic Bacteria, *Probiotics Antimicrob. Proteins*. 11 (2019) 667–675. doi:10.1007/s12602-018-9446-3.
- [98] S. Arens, U. Schlegel, G. Printzen, W.J. Ziegler, S.M. Perren, M. Hansis, Influence of materials for fixation implants on local infection. An experimental study of steel versus titanium DCP in rabbits, *J. Bone Jt. Surg. - Ser. B*. 78 (1996) 647–651. doi:10.1302/0301-620X.78B4.0780647.
- [99] A.G. - Science, undefined 1987, Biomaterial-centered infection: microbial adhesion versus tissue integration, *Science*. Science.ScienceMag.Org. (n.d.). <https://science.sciencemag.org/content/237/4822/1588.short> (accessed January 15, 2020).
- [100] L.G. Harris, R.G. Richards, Staphylococci and implant surfaces: a review, *Injury*. 37 (2006). doi:10.1016/j.injury.2006.04.003.
- [101] D.O. Meredith, L. Eschbach, M.A. Wood, M.O. Riehle, A.S.G. Curtis, R.G. Richards, Human fibroblast reactions to standard and electropolished titanium and Ti-6Al-7Nb, and electropolished stainless steel, *J. Biomed. Mater. Res. - Part A*. 75 (2005) 541–555. doi:10.1002/jbm.a.30457.
- [102] E. Gracia, A. Fernández, P. Conchello, A. Laclériga, L. Paniagua, F. Seral, B. Amorena, Adherence of *Staphylococcus aureus* slime-producing strain variants to biomaterials used in orthopaedic surgery, *Int. Orthop.* 21 (1997) 46–51. doi:10.1007/s002640050116.
- [103] B.G. Pfang, J. García-Cañete, J. García-Lasheras, A. Blanco, Á. Auñón, R. Parron-Camero, A. Macías-Valcayo, J. Esteban, Orthopedic Implant-Associated Infection by Multidrug Resistant Enterobacteriaceae, *J. Clin. Med.* 8 (2019) 220. doi:10.3390/jcm8020220.
- [104] W. Zimmerli, Clinical presentation and treatment of orthopaedic implant-associated infection, *J. Intern. Med.* 276 (2014) 111–119. doi:10.1111/joim.12233.
- [105] A. Papadopoulos, A. Ribera, A.F. Mavrogenis, D. Rodriguez-Pardo, E. Bonnet, M.J. Salles, M. Dolores del Toro, S. Nguyen, A. Blanco-García, G. Skaliczki, A. Soriano, N. Benito, S. Petersdorf, M.B. Pasticci, P. Tattevin, Z.K. Tufan, M. Chan, N. O'Connell, N. Pantazis, A. Kyprianou, C. Pigrau, P.D.

- Megaloikonomos, E. Senneville, J. Ariza, P.J. Papagelopoulos, E. Giannitsioti, Multidrug-resistant and extensively drug-resistant Gram-negative prosthetic joint infections: Role of surgery and impact of colistin administration, *Int. J. Antimicrob. Agents.* 53 (2019) 294–301. doi:10.1016/j.ijantimicag.2018.10.018.
- [106] L. Crémet, S. Corvec, P. Bémer, L. Bret, C. Lebrun, B. Lesimple, A.F. Miegerville, A. Reynaud, D. Lepelletier, N. Caroff, Orthopaedic-implant infections by *Escherichia coli*: Molecular and phenotypic analysis of the causative strains, *J. Infect.* 64 (2012) 169–175. doi:10.1016/j.jinf.2011.11.010.
- [107] W. Zimmerli, P. Sendi, Orthopaedic biofilm infections, *APMIS.* 125 (2017) 353–364. doi:10.1111/apm.12687.
- [108] F. Liu, J. Fisher, Z. Jin, Wear prediction of orthopaedic implants, in: *Wear Orthop. Implant. Artif. Joints*, Elsevier, 2013: pp. 403–418. doi:10.1533/9780857096128.1.403.
- [109] G. Dearnaley, Adhesive, abrasive and oxidative wear in ion-implanted metals, *Mater. Sci. Eng.* 69 (1985) 139–147. doi:10.1016/0025-5416(85)90384-2.
- [110] K. Kato, Abrasive wear of metals, *Tribol. Int.* 30 (1997) 333–338. doi:10.1016/S0301-679X(96)00063-1.
- [111] D.W. Hoepfner, V. Chandrasekaran, Fretting in orthopaedic implants: A review, *Wear.* 173 (1994) 189–197. doi:10.1016/0043-1648(94)90272-0.
- [112] S.H. Teoh, Fatigue of biomaterials: A review, *Int. J. Fatigue.* 22 (2000) 825–837. doi:10.1016/S0142-1123(00)00052-9.
- [113] B. Aksakal, Ö.S. Yildirim, H. Gul, Metallurgical failure analysis of various implant materials used in orthopedic applications, *J. Fail. Anal. Prev.* 4 (2004) 17–23. doi:10.1007/s11668-996-0007-9.
- [114] J.L. Gilbert, C.A. Buckley, J.J. Jacobs, K.C. Bertin, M.R. Zernich, Intergranular corrosion-fatigue failure of cobalt-alloy femoral stems. A failure analysis of two implants, *J. Bone Jt. Surg. - Ser. A.* 76 (1994) 110–115. doi:10.2106/00004623-199401000-00014.
- [115] B.F. Shahgaldi, J. Compson, Wear and corrosion of sliding counterparts of stainless-steel hip screw-plates., *Injury.* 31 (2000) 85–92. doi:10.1016/s0020-1383(99)00241-7.
- [116] M. Khan, R. Williams, D.W.- Biomaterials, undefined 1999,

- Conjoint corrosion and wear in titanium alloys, Elsevier. (n.d.).
<https://www.sciencedirect.com/science/article/pii/S0142961298002294> (accessed January 15, 2020).
- [117] N. Aebli, J. Krebs, H. Stich, P. Schawalder, M. Walton, D. Schwenke, H. Gruner, B. Gasser, J.-C. Theis, In vivo comparison of the osseointegration of vacuum plasma sprayed titanium- and hydroxyapatite-coated implants, *J. Biomed. Mater. Res.* 66A (2003) 356–363. doi:10.1002/jbm.a.10508.
- [118] Y. Wang, K.A. Khor, P. Cheang, Thermal spraying of functionally graded calcium phosphate coatings for biomedical implants, *J. Therm. Spray Technol.* 7 (1998) 50–57. doi:10.1007/s11666-006-5003-9.
- [119] L. Sun, Thermal Spray Coatings on Orthopedic Devices: When and How the FDA Reviews Your Coatings, *J. Therm. Spray Technol.* 27 (2018) 1280–1290. doi:10.1007/s11666-018-0759-2.
- [120] L. Sun, C.C. Berndt, C.P. Grey, Phase, structural and microstructural investigations of plasma sprayed hydroxyapatite coatings, *Mater. Sci. Eng. A.* 360 (2003) 70–84. doi:10.1016/S0921-5093(03)00439-8.
- [121] S. Kweh, K. Khor, P.C. Biomaterials, undefined 2002, An in vitro investigation of plasma sprayed hydroxyapatite (HA) coatings produced with flame-spheroidized feedstock, Elsevier. (n.d.).
<https://www.sciencedirect.com/science/article/pii/S0142961201001831> (accessed February 5, 2020).
- [122] Plasma spraying - Engineered Performance Coatings, (n.d.).
<https://www.ep-coatings.com/processes/plasma-spraying/> (accessed February 5, 2020).
- [123] K. Balani, R. Anderson, T. Laha, M. Andara, J.T. Biomaterials, undefined 2007, Plasma-sprayed carbon nanotube reinforced hydroxyapatite coatings and their interaction with human osteoblasts in vitro, Elsevier. (n.d.).
<https://www.sciencedirect.com/science/article/pii/S0142961206008088> (accessed February 5, 2020).
- [124] V.F. Shamray, V.P. Sirotinkin, I. V. Smirnov, V.I. Kalita, A.Y. Fedotov, S.M. Barinov, V.S. Komlev, Structure of the hydroxyapatite plasma-sprayed coatings deposited on pre-heated titanium substrates, *Ceram. Int.* 43 (2017) 9105–9109. doi:10.1016/j.ceramint.2017.04.057.

- [125] J. Ann Gan, C.C. Berndt, Thermal spray forming of titanium and its alloys, in: *Titan. Powder Metall. Sci. Technol. Appl.*, Elsevier Inc., 2015: pp. 425–446. doi:10.1016/B978-0-12-800054-0.00023-X.
- [126] M.F. Smith, Comparing cold spray with thermal spray coating technologies, in: *Cold Spray Mater. Depos. Process Fundam. Appl.*, Elsevier Ltd., 2007: pp. 43–61. doi:10.1533/9781845693787.1.43.
- [127] S.G. Ullattil, P. Periyat, Sol-Gel Synthesis of Titanium Dioxide, in: 2017: pp. 271–283. doi:10.1007/978-3-319-50144-4_9.
- [128] M. Kakihana, “Sol-Gel” preparation of high temperature superconducting oxides, *J. Sol-Gel Sci. Technol.* 6 (1996) 7–55. doi:10.1007/BF00402588.
- [129] A. Ochsenbein, F. Chai, S. Winter, M. Traisnel, J. Breme, H.F. Hildebrand, Osteoblast responses to different oxide coatings produced by the sol-gel process on titanium substrates, *Acta Biomater.* 4 (2008) 1506–1517. doi:10.1016/j.actbio.2008.03.012.
- [130] E. Milella, F. Cosentino, A. Licciulli, C. Massaro, Preparation and characterisation of titania/hydroxyapatite composite coatings obtained by sol-gel process, *Biomaterials.* 22 (2001) 1425–1431. doi:10.1016/S0142-9612(00)00300-8.
- [131] P. Li, K. De Groot, T. Kokubo, Bioactive Ca₁₀(PO₄)₆(OH)₂·TiO₂ composite coating prepared by sol-gel process, *J. Sol-Gel Sci. Technol.* 7 (1996) 27–34. doi:10.1007/BF00401880.
- [132] R.I.M. Asri, W.S.W. Harun, M.A. Hassan, S.A.C. Ghani, Z. Buyong, A review of hydroxyapatite-based coating techniques: Sol-gel and electrochemical depositions on biocompatible metals, *J. Mech. Behav. Biomed. Mater.* 57 (2016) 95–108. doi:10.1016/j.jmbbm.2015.11.031.
- [133] A.S.H. Makhlof, Current and advanced coating technologies for industrial applications, in: *Nanocoatings Ultra-Thin Film.*, Elsevier, 2011: pp. 3–23. doi:10.1533/9780857094902.1.3.
- [134] A. Mubarak, ... E.H.-J., undefined 2005, Review of physical vapour deposition (PVD) techniques for hard coating, *Jurnalmekanikal.Utm.My.* (n.d.). <https://jurnalmekanikal.utm.my/index.php/jurnalmekanikal/article/download/191/190> (accessed February 6, 2020).
- [135] B. Moore, E. Asadi, G. Lewis, *Deposition Methods for Microstructured and Nanostructured Coatings on Metallic Bone*

- Implants: A Review, (2017). doi:10.1155/2017/5812907.
- [136] I.H. Han, I.S. Lee, J.H. Song, M.H. Lee, J.C. Park, G.H. Lee, X.D. Sun, S.M. Chung, Characterization of a silver-incorporated calcium phosphate film by RBS and its antimicrobial effects, in: *Biomed. Mater.*, 2007. doi:10.1088/1748-6041/2/3/S01.
- [137] D. Sanders, A.A.-S. and C. Technology, undefined 2000, Review of cathodic arc deposition technology at the start of the new millennium, Elsevier. (n.d.). <https://www.sciencedirect.com/science/article/pii/S025789720008793> (accessed February 6, 2020).
- [138] S. Onder, F.N. Kok, K. Kazmanli, M. Urgan, Magnesium substituted hydroxyapatite formation on (Ti,Mg)N coatings produced by cathodic arc PVD technique, *Mater. Sci. Eng. C*. 33 (2013) 4337–4342. doi:10.1016/j.msec.2013.06.027.
- [139] M.M. Hassan, Antimicrobial Coatings for Textiles, in: *Handb. Antimicrob. Coatings*, Elsevier, 2018: pp. 321–355. doi:10.1016/b978-0-12-811982-2.00016-0.
- [140] J. Scholz, G. Nocke, F. Hollstein, A. Weissbach, Investigations on fabrics coated with precious metals using the magnetron sputter technique with regard to their anti-microbial properties, *Surf. Coatings Technol.* 192 (2005) 252–256. doi:10.1016/j.surfcoat.2004.05.036.
- [141] X. Liu, P.K. Chu, C. Ding, Surface modification of titanium, titanium alloys, and related materials for biomedical applications, *Mater. Sci. Eng. R Reports*. 47 (2004) 49–121. doi:10.1016/j.mser.2004.11.001.
- [142] E.P. Ivanova, V.K. Truong, J.Y. Wang, C.C. Bemdt, R.T. Jones, I.I. Yusuf, I. Peake, H.W. Schmidt, C. Fluke, D. Barnes, R.J. Crawford, Impact of nanoscale roughness of titanium thin film surfaces on bacterial Retention, *Langmuir*. 26 (2010) 1973–1982. doi:10.1021/la902623c.
- [143] U. Brohede, S. Zhao, F. Lindberg, ... A.M.-A.S., undefined 2009, A novel graded bioactive high adhesion implant coating, Elsevier. (n.d.). <https://www.sciencedirect.com/science/article/pii/S0169433209005303> (accessed February 6, 2020).
- [144] M.A. Surmeneva, R.A. Surmenev, M. V. Chaikina, A.A. Kachaev, V.F. Pichugin, M. Epple, Phase and elemental composition of silicon-containing hydroxyapatite-based coatings

- fabricated by RF-magnetron sputtering for medical implants, *Inorg. Mater. Appl. Res.* 4 (2013) 227–235. doi:10.1134/S2075113313030131.
- [145] J.A. Juhasz, S.M. Best, Surface modification of biomaterials by calcium phosphate deposition, in: *Surf. Modif. Biomater. Methods Anal. Appl.*, Elsevier Inc., 2011: pp. 143–169. doi:10.1533/9780857090768.1.143.
- [146] Z. Hong, A. Mello, T. Yoshida, L. Luan, P.H. Stern, A. Rossi, D.E. Ellis, J.B. Ketterson, Osteoblast proliferation on hydroxyapatite coated substrates prepared by right angle magnetron sputtering, *J. Biomed. Mater. Res. - Part A*. 93 (2010) 878–885. doi:10.1002/jbm.a.32556.
- [147] E.S. Puchi-Cabrera, M.H. Staia, E.A. Ochoa-Pérez, D.G. Teer, Y.Y. Santana-Méndez, J.G. La Barbera-Sosa, D. Chicot, J. Lesage, Fatigue behavior of a 316L stainless steel coated with a DLC film deposited by PVD magnetron sputter ion plating, *Mater. Sci. Eng. A*. 527 (2010) 498–508. doi:10.1016/j.msea.2009.09.030.
- [148] K. Ozeki, T. Yuhta, Y. Fukui, H. Aoki, I. Nishimura, A functionally graded titanium/hydroxyapatite film obtained by sputtering, *J. Mater. Sci. Mater. Med.* 13 (2002) 253–258. doi:10.1023/A:1014002732373.
- [149] S.D.- Biomaterials, undefined 2003, Properties and immersion behavior of magnetron-sputtered multi-layered hydroxyapatite/titanium composite coatings, Elsevier. (n.d.). <https://www.sciencedirect.com/science/article/pii/S014296120303156> (accessed February 6, 2020).
- [150] X. Liu, P.K. Chu, C. Ding, Surface modification of titanium, titanium alloys, and related materials for biomedical applications, *Mater. Sci. Eng. R Reports*. 47 (2004) 49–121. doi:10.1016/j.mser.2004.11.001.
- [151] J. Wood, G. Majumdar, Ion Implantation, in: *Ref. Modul. Mater. Sci. Mater. Eng.*, Elsevier, 2016. doi:10.1016/B978-0-12-803581-8.03724-3.
- [152] J. Wood, Ion Implantation, in: *Encycl. Mater. Sci. Technol.*, Elsevier, 2001: pp. 4284–4286. doi:10.1016/B0-08-043152-6/00751-8.
- [153] Z.A. Uwais, M.A. Hussein, · M Abdul Samad, N. Al-Aqeeli, B.M.A. Samad, Surface Modification of Metallic Biomaterials for

- Better Tribological Properties: A Review, *Arab. J. Sci. Eng.* 42 (2017) 4493–4512. doi:10.1007/s13369-017-2624-x.
- [154] T.R. Rautray, R. Narayanan, T.-Y. Kwon, K.-H. Kim, Surface modification of titanium and titanium alloys by ion implantation, *J. Biomed. Mater. Res. Part B Appl. Biomater.* 93B (2010) 581–591. doi:10.1002/jbm.b.31596.
- [155] T. Sawase, A. Wennerberg, K. Baba, Y. Tsuboi, L. Sennerby, C.B. Johansson, T. Albrektsson, Application of oxygen ion implantation to titanium surfaces: Effects on surface characteristics, corrosion resistance, and bone response, *Clin. Implant Dent. Relat. Res.* 3 (2001) 221–229. doi:10.1111/j.1708-8208.2001.tb00144.x.
- [156] P. O'Brien, Chemical Vapor Deposition, in: *Encycl. Mater. Sci. Technol.*, Elsevier, 2001: pp. 1173–1176. doi:10.1016/B0-08-043152-6/00219-9.
- [157] J.O. Carlsson, P.M. Martin, Chemical Vapor Deposition, in: *Handb. Depos. Technol. Film. Coatings*, Elsevier Inc., 2010: pp. 314–363. doi:10.1016/B978-0-8155-2031-3.00007-7.
- [158] P. Sahoo, S.K. Das, J. Paulo Davim, Surface Finish Coatings, in: *Compr. Mater. Finish.*, Elsevier Inc., 2017: pp. 38–55. doi:10.1016/B978-0-12-803581-8.09167-0.
- [159] J. Mungkalasiri, L. Bedel, F. Emieux, J. Doré, F.N.R. Renaud, F. Maury, DLI-CVD of TiO₂-Cu antibacterial thin films: Growth and characterization, *Surf. Coatings Technol.* 204 (2009) 887–892. doi:10.1016/j.surfcoat.2009.07.015.
- [160] Y. Sasikumar, K. Indira, N. Rajendran, Surface Modification Methods for Titanium and Its Alloys and Their Corrosion Behavior in Biological Environment: A Review, *J. Bio-Tribo-Corrosion.* 5 (2019). doi:10.1007/s40735-019-0229-5.
- [161] C.C. Wachesk, C.A.F. Pires, B.C. Ramos, V.J. Trava-Airoldi, A.O. Lobo, C. Pacheco-Soares, F.R. Marciano, N.S. Da-Silva, Cell viability and adhesion on diamond-like carbon films containing titanium dioxide nanoparticles, *Appl. Surf. Sci.* 266 (2013) 176–181. doi:10.1016/j.apsusc.2012.11.124.
- [162] O. Kylián, A. Kuzminova, J. Hanuš, D. Slavínská, H. Biederman, Super-hydrophilic SiO_x coatings prepared by plasma enhanced chemical vapor deposition combined with gas aggregation source of nanoparticles, *Mater. Lett.* 227 (2018) 5–8. doi:10.1016/j.matlet.2018.04.104.

- [163] L. ye Huang, K. wei Xu, J. Lu, B. Guelorget, H. Chen, Nano-scratch and fretting wear study of DLC coatings for biomedical application, *Diam. Relat. Mater.* 10 (2001) 1448–1456. doi:10.1016/S0925-9635(00)00501-X.
- [164] E.J. Szili, S. Kumar, R.S.C. Smart, N.H. Voelcker, Generation of a stable surface concentration of amino groups on silica coated onto titanium substrates by the plasma enhanced chemical vapour deposition method, *Appl. Surf. Sci.* 255 (2009) 6846–6850. doi:10.1016/j.apsusc.2009.02.092.
- [165] G.L. Song, Z. Shi, Anodization and corrosion of magnesium (Mg) alloys, in: *Corros. Prev. Magnes. Alloy. A Vol.* Woodhead Publ. Ser. *Met. Surf. Eng.*, Elsevier Ltd, 2013: pp. 232–281. doi:10.1533/9780857098962.2.232.
- [166] L.M. Muresan, Corrosion Protective Coatings for Ti and Ti Alloys Used for Biomedical Implants, in: *Intell. Coatings Corros. Control*, Elsevier Inc., 2015: pp. 585–602. doi:10.1016/B978-0-12-411467-8.00017-9.
- [167] M.G. Blamire, Anodization Spectrometry, in: *Encycl. Mater. Sci. Technol.*, Elsevier, 2001: pp. 323–325. doi:10.1016/b0-08-043152-6/00067-x.
- [168] J.C.M. Souza, L. Bins-Ely, M.B. Sordi, R.S. Magini, C. Aparicio, T. Shokuhfar, L. Cooper, Nanostructured surfaces of cranio-maxillofacial and dental implants, in: *Nanostructured Biomater. Cranio-Maxillofacial Oral Appl.*, Elsevier Inc., 2018: pp. 13–40. doi:10.1016/B978-0-12-814621-7.00002-0.
- [169] Y. Fu, A. Mo, A Review on the Electrochemically Self-organized Titania Nanotube Arrays: Synthesis, Modifications, and Biomedical Applications, *Nanoscale Res. Lett.* 13 (2018). doi:10.1186/s11671-018-2597-z.
- [170] D. Gong, C.A. Grimes, O.K. Varghese, W. Hu, R.S. Singh, Z. Chen, E.C. Dickey, Titanium oxide nanotube arrays prepared by anodic oxidation, *J. Mater. Res.* 16 (2001) 3331–3334. doi:10.1557/JMR.2001.0457.
- [171] P.K. Chu, Progress in direct-current plasma immersion ion implantation and recent applications of plasma immersion ion implantation and deposition, *Surf. Coatings Technol.* 229 (2013) 2–11. doi:10.1016/j.surfcoat.2012.03.073.
- [172] H. Cao, X. Liu, F. Meng, P.K. Chu, Biological actions of silver nanoparticles embedded in titanium controlled by micro-

- galvanic effects, *Biomaterials*. 32 (2011) 693–705. doi:10.1016/j.biomaterials.2010.09.066.
- [173] J.H. Sui, W. Cai, Effect of diamond-like carbon (DLC) on the properties of the NiTi alloys, *Diam. Relat. Mater.* 15 (2006) 1720–1726. doi:10.1016/j.diamond.2006.03.004.
- [174] X. He, X. Zhang, X. Wang, L. Qin, Review of Antibacterial Activity of Titanium-Based Implants' Surfaces Fabricated by Micro-Arc Oxidation, *Coatings*. 7 (2017) 45. doi:10.3390/coatings7030045.
- [175] M. Echeverry-Rendón, O. Galvis, R. Aguirre, S. Robledo, J.G. Castaño, F. Echeverría, Modification of titanium alloys surface properties by plasma electrolytic oxidation (PEO) and influence on biological response, *J. Mater. Sci. Mater. Med.* 28 (2017). doi:10.1007/s10856-017-5972-x.
- [176] M. Thukkaram, P. Cools, A. Nikiforov, P. Rigole, T. Coenye, P. Van Der Voort, G. Du Laing, C. Vercruyssen, H. Declercq, R. Morent, L. De Wilde, P. De Baets, K. Verbeken, N. De Geyter, Antibacterial activity of a porous silver doped TiO₂ coating on titanium substrates synthesized by plasma electrolytic oxidation, *Appl. Surf. Sci.* (2019) 144235. doi:10.1016/j.apsusc.2019.144235.
- [177] X. Zhang, J. Li, X. Wang, Y. Wang, R. Hang, X. Huang, B. Tang, P.K. Chu, Effects of copper nanoparticles in porous TiO₂ coatings on bacterial resistance and cytocompatibility of osteoblasts and endothelial cells, *Mater. Sci. Eng. C*. 82 (2018) 110–120. doi:10.1016/j.msec.2017.08.061.
- [178] R. Asmawi, M.H.I. Ibrahim, A.M. Amin, N. Mustafa, Z. Noranai, Development of Bioactive Ceramic Coating on Titanium Alloy substrate for Biomedical Application Using Dip Coating Method, *IOP Conf. Ser. Mater. Sci. Eng.* 226 (2017). doi:10.1088/1757-899X/226/1/012179.
- [179] D.F. Williams, On the mechanisms of biocompatibility, *Biomaterials*. 29 (2008) 2941–2953. doi:10.1016/j.biomaterials.2008.04.023.
- [180] T.K.- Biomaterials, undefined 1991, Bioactive glass ceramics: properties and applications, Elsevier. (n.d.). <https://www.sciencedirect.com/science/article/pii/014296129190194F> (accessed April 14, 2020).
- [181] T. Kokubo, H. Takadama, How useful is SBF in predicting in

- vivo bone bioactivity?, *Biomaterials*. 27 (2006) 2907–2915. doi:10.1016/j.biomaterials.2006.01.017.
- [182] M.A.E. Cruz, G.C.M. Ruiz, A.N. Faria, D.C. Zancanela, L.S. Pereira, P. Ciancaglini, A.P. Ramos, Calcium carbonate hybrid coating promotes the formation of biomimetic hydroxyapatite on titanium surfaces, *Appl. Surf. Sci.* 370 (2016) 459–468. doi:10.1016/j.apsusc.2015.12.250.
- [183] Y. Liu, T. Jiang, Y. Zhou, Z. Zhang, Z. Wang, H. Tong, X. Shen, Y. Wang, Evaluation of the attachment, proliferation, and differentiation of osteoblast on a calcium carbonate coating on titanium surface, *Mater. Sci. Eng. C*. 31 (2011) 1055–1061. doi:10.1016/j.msec.2011.03.003.
- [184] C. García, S. Ceré, A. Durán, Bioactive coatings deposited on titanium alloys, *J. Non. Cryst. Solids*. 352 (2006) 3488–3495. doi:10.1016/j.jnoncrysol.2006.02.110.
- [185] A. Rad, M. Solati-Hashjin, N. Osman, S.F.-C. International, undefined 2014, Improved bio-physical performance of hydroxyapatite coatings obtained by electrophoretic deposition at dynamic voltage, Elsevier. (n.d.). <https://www.sciencedirect.com/science/article/pii/S0272884214006671> (accessed March 16, 2020).
- [186] C. Liu, J. Zhang, S. Zhang, P. Wang, Y. Lian, S. Deng, Y. He, Preparation and properties of ceramic coatings by cathode plasma electrolytic deposition on titanium alloy, *Surf. Coatings Technol.* 325 (2017) 708–714. doi:10.1016/j.surfcoat.2017.04.033.
- [187] K. De Groot, R. Geesink, C.P.A.T. Klein, P. Serekian, Plasma sprayed coatings of hydroxylapatite, *J. Biomed. Mater. Res.* 21 (1987) 1375–1381. doi:10.1002/jbm.820211203.
- [188] R.J. Furlong, J.F. Osborn, Fixation of hip prostheses by hydroxyapatite ceramic coatings, *J. Bone Jt. Surg. - Ser. B*. 73 (1991) 741–745. doi:10.1302/0301-620x.73b5.1654336.
- [189] H. Sayed Hedia, H.S. Hedia, Effect of Coating thickness and its Material on the Stress distribution for Dental Implant Improving the Performance of Cementless Knee Prosthesis Coating through Functionally Graded Material View project Candida View project Effect of coating thickness and its material on the stress distribution for dental implants, (n.d.). doi:10.1080/03091900600861616.

- [190] a K. Lynn, D.L. DuQuesnay, Hydroxyapatite-coated Ti-6Al-4V part 1: the effect of coating thickness on mechanical fatigue behaviour., *Biomaterials*. 23 (2002) 1937–46. <http://www.ncbi.nlm.nih.gov/pubmed/11996034> (accessed January 22, 2020).
- [191] C.M. De Assis, L.C.D.O. Vercik, M.L. Dos Santos, M.V.L. Fook, A.C. Guastaldi, Comparison of crystallinity between natural hydroxyapatite and synthetic cp-Ti /HA coatings, in: *Mater. Res.*, 2005: pp. 207–211. doi:10.1590/s1516-14392005000200022.
- [192] S. Overgaard, Calcium phosphate coatings for fixation of bone implants. Evaluated mechanically and histologically by stereological methods, *Acta Orthop. Scand.* 71 (2001) 1–74. doi:10.1080/000164702760300297.
- [193] L. Montanaro, C.R. Arciola, D. Campoccia, M. Cervellati, In vitro effects on MG63 osteoblast-like cells following contact with two roughness-differing fluorohydroxyapatite-coated titanium alloys., *Biomaterials*. 23 (2002) 3651–9. doi:10.1016/s0142-9612(02)00098-4.
- [194] D.D. Deligianni, N.D. Katsala, P.G. Koutsoukos, Y.F. Missirlis, Effect of surface roughness of hydroxyapatite on human bone marrow cell adhesion, proliferation, differentiation and detachment strength, *Biomaterials*. 22 (2000) 87–96. doi:10.1016/S0142-9612(00)00174-5.
- [195] M.C. Kuo, S.K. Yen, The process of electrochemical deposited hydroxyapatite coatings on biomedical titanium at room temperature, *Mater. Sci. Eng. C*. 20 (2002) 153–160. doi:10.1016/S0928-4931(02)00026-7.
- [196] N. Isa, Y. Mohd, N.Y.-A. Procedia, undefined 2012, Electrochemical deposition and characterization of hydroxyapatite (HAp) on titanium substrate, Elsevier. (n.d.). <https://www.sciencedirect.com/science/article/pii/S2212670812001157> (accessed March 17, 2020).
- [197] M.K.-H. (HAp) for B. Applications, undefined 2015, Hydroxyapatite coating on biodegradable magnesium and magnesium-based alloys, Elsevier. (n.d.). <https://www.sciencedirect.com/science/article/pii/B9781782420330000134> (accessed April 14, 2020).
- [198] S. Sobieszczyk, Hydroxyapatite coatings on porous ti and ti

- alloys, *Adv. Mater. Sci.* 10 (2010). doi:10.2478/v10077-010-0002-4.
- [199] B. Yang, M. Uchida, H. Kim, X. Zhang, T.K.- Biomaterials, undefined 2004, Preparation of bioactive titanium metal via anodic oxidation treatment, Elsevier. (n.d.). <https://www.sciencedirect.com/science/article/pii/S0142961203006264> (accessed April 14, 2020).
- [200] Y. Huang, X. Zhang, R. Zhao, H. Mao, Y. Yan, X. Pang, Antibacterial efficacy, corrosion resistance, and cytotoxicity studies of copper-substituted carbonated hydroxyapatite coating on titanium substrate, *J. Mater. Sci.* 50 (2015) 1688–1700. doi:10.1007/s10853-014-8730-1.
- [201] R. Roest, B. Latella, G. Heness, B.B.-N.-S. and Coatings, undefined 2011, Adhesion of sol–gel derived hydroxyapatite nanocoatings on anodised pure titanium and titanium (Ti6Al4V) alloy substrates, Elsevier. (n.d.). <https://www.sciencedirect.com/science/article/pii/S0257897210012806> (accessed March 16, 2020).
- [202] C. Massaro, M.A. Baker, F. Cosentino, P.A. Ramires, S. Klose, E. Milella, Surface and biological evaluation of hydroxyapatite-based coatings on titanium deposited by different techniques, *J. Biomed. Mater. Res.* 58 (2001) 651–657. doi:10.1002/jbm.1065.
- [203] H.W. Kim, Y.H. Koh, L.H. Li, S. Lee, H.E. Kim, Hydroxyapatite coating on titanium substrate with titania buffer layer processed by sol-gel method, *Biomaterials.* 25 (2004) 2533–2538. doi:10.1016/j.biomaterials.2003.09.041.
- [204] L.H. Li, H.W. Kim, S.H. Lee, Y.M. Kong, H.E. Kim, Biocompatibility of titanium implants modified by microarc oxidation and hydroxyapatite coating, *J. Biomed. Mater. Res. - Part A.* 73 (2005) 48–54. doi:10.1002/jbm.a.30244.
- [205] Y. Han, S.H. Hong, K. Xu, Structure and in vitro bioactivity of titania-based films by micro-arc oxidation, *Surf. Coatings Technol.* 168 (2003) 249–258. doi:10.1016/S0257-8972(03)00016-1.
- [206] I.C. Lavos-Valereto, S. Woly nec, M.C.Z. Deboni, B. König, *In vitro* and *in vivo* biocompatibility testing of Ti-6Al-7Nb alloy with and without plasma-sprayed hydroxyapatite coating, *J. Biomed. Mater. Res.* 58 (2001) 727–733. doi:10.1002/jbm.1072.
- [207] S.A. Alves, R. Bayón, V.S. de Viteri, M.P. Garcia, A. Igartua,

- M.H. Fernandes, L.A. Rocha, Tribocorrosion Behavior of Calcium- and Phosphorous-Enriched Titanium Oxide Films and Study of Osteoblast Interactions for Dental Implants, *J. Bio-Tribo-Corrosion*. 1 (2015). doi:10.1007/s40735-015-0023-y.
- [208] M. Catauro, Cronicon Human Cells to Hydroxyapatite Coatings on Titanium Substrates Synthesized by Sol-Gel Process, n.d.
- [209] G. Ciobanu, M. Harja, Investigation on hydroxyapatite coatings formation on titanium surface, (2018). doi:10.1088/1757-899X/444/3/032007.
- [210] B.D. Hahn, J.M. Lee, D.S. Park, J.J. Choi, J. Ryu, W.H. Yoon, J.H. Choi, B.K. Lee, J.W. Kim, H.E. Kim, S.G. Kim, Enhanced bioactivity and biocompatibility of nanostructured hydroxyapatite coating by hydrothermal annealing, *Thin Solid Films*. 519 (2011) 8085–8090. doi:10.1016/j.tsf.2011.07.008.
- [211] C. Prakash, M.S. Uddin, Surface modification of β -phase Ti implant by hydroxyapatite mixed electric discharge machining to enhance the corrosion resistance and in-vitro bioactivity, *Surf. Coatings Technol.* 326 (2017) 134–145. doi:10.1016/j.surfcoat.2017.07.040.
- [212] A. Carradò, N. Viart, Nanocrystalline spin coated sol-gel hydroxyapatite thin films on Ti substrate: Towards potential applications for implants, *Solid State Sci.* 12 (2010) 1047–1050. doi:10.1016/j.solidstatesciences.2010.04.014.
- [213] P. Tengvall, I. Lundström, Physico-chemical considerations of titanium as a biomaterial, *Clin. Mater.* 9 (1992) 115–134. doi:10.1016/0267-6605(92)90056-Y.
- [214] Y. Okazaki, E. Gotoh, Comparison of metal release from various metallic biomaterials in vitro, *Biomaterials*. 26 (2005) 11–21. doi:10.1016/j.biomaterials.2004.02.005.
- [215] B. Yang, M. Uchida, H.M. Kim, X. Zhang, T. Kokubo, Preparation of bioactive titanium metal via anodic oxidation treatment, *Biomaterials*. 25 (2004) 1003–1010. doi:10.1016/S0142-9612(03)00626-4.
- [216] N.K. Kuromoto, R.A. Simão, G.A. Soares, Titanium oxide films produced on commercially pure titanium by anodic oxidation with different voltages, *Mater. Charact.* 58 (2007) 114–121. doi:10.1016/j.matchar.2006.03.020.
- [217] G. Wang, J. Li, K. Lv, W. Zhang, X. Ding, G. Yang, X. Liu, X. Jiang, Surface thermal oxidation on titanium implants to

- enhance osteogenic activity and in vivo osseointegration, *Sci. Rep.* 6 (2016) 1–13. doi:10.1038/srep31769.
- [218] M.C. Advincula, F.G. Rahemtulla, R.C. Advincula, E.T. Ada, J.E. Lemons, S.L. Bellis, Osteoblast adhesion and matrix mineralization on sol-gel-derived titanium oxide, *Biomaterials*. 27 (2006) 2201–2212. doi:10.1016/j.biomaterials.2005.11.014.
- [219] H. Cao, X. Liu, Activating titanium oxide coatings for orthopedic implants, *Surf. Coatings Technol.* 233 (2013) 57–64. doi:10.1016/j.surfcoat.2013.01.043.
- [220] P. Santiago-Medina, P.A. Sundaram, N. Diffoot-Carlo, Titanium Oxide: A Bioactive Factor in Osteoblast Differentiation, (2015). doi:10.1155/2015/357653.
- [221] M. Vandrovcova, J. Hanus, M. Drabik, O. Kylian, H. Biederman, V. Lisa, L. Bacakova, Effect of different surface nanoroughness of titanium dioxide films on the growth of human osteoblast-like MG63 cells, *J. Biomed. Mater. Res. Part A*. 100A (2012) 1016–1032. doi:10.1002/jbm.a.34047.
- [222] S. Popescu, I. Demetrescu, V. Mitran, A.N. Gleizes, Fabricated TiO₂ Thin Films: Influence of Growth Conditions on Fibroblast Cells Culture, *Mol. Cryst. Liq. Cryst.* 483 (2008) 266–274. doi:10.1080/15421400801914301.
- [223] T. Popescu, A.R. Lupu, L. Diamandescu, D. Tarabasanu-Mihaila, V.S. Teodorescu, V. Raditoiu, V. Purcar, A.M. Vlaicu, Effects of TiO₂ nanoparticles on the NO₂⁻ Levels in cell culture media analysed by Griess colorimetric methods, *J. Nanoparticle Res.* 15 (2013). doi:10.1007/s11051-013-1449-0.
- [224] A. Majeed, J. He, L. Jiao, X. Zhong, Z. Sheng, Surface properties and biocompatibility of nanostructured TiO₂ film deposited by RF magnetron sputtering, *Nanoscale Res. Lett.* 10 (2015) 1–9. doi:10.1186/s11671-015-0732-7.
- [225] N. Tsukimura, N. Kojima, K. Kubo, W. Att, K. Takeuchi, Y. Kameyama, H. Maeda, T. Ogawa, The effect of superficial chemistry of titanium on osteoblastic function, *J. Biomed. Mater. Res. Part A*. 84A (2008) 108–116. doi:10.1002/jbm.a.31422.
- [226] Y.-T. Sul, B.-S. Kang, C. Johansson, H.-S. Um, C.-J. Park, T. Albrektsson, The roles of surface chemistry and topography in the strength and rate of osseointegration of titanium implants in bone, *J. Biomed. Mater. Res. Part A*. 89A (2009) 942–950.

doi:10.1002/jbm.a.32041.

- [227] O. Akhavan, Lasting antibacterial activities of Ag-TiO₂/Ag/a-TiO₂nanocomposite thin film photocatalysts under solar light irradiation, *J. Colloid Interface Sci.* 336 (2009) 117–124. doi:10.1016/j.jcis.2009.03.018.
- [228] C. Volpato, ... L.G.-A. in ceramics, undefined 2011, Application of zirconia in dentistry: biological, mechanical and optical considerations, Books.Google.Com. (n.d.). https://books.google.be/books?hl=en&lr=&id=e-GdDwAAQBAJ&oi=fnd&pg=PA397&dq=1+Application+of+zirconia+in+dentistry:+biological,+mechanical+and+optical+considerations&ots=jVernqovSi&sig=dwGSImQcOxXb2cafjRfk_cB4wFo (accessed March 17, 2020).
- [229] S. Zhang, J. Sun, Y. Xu, S. Qian, B. Wang, F. Liu, X. Liu, Biological Behavior of Osteoblast-like Cells on Titania and Zirconia Films Deposited by Cathodic Arc Deposition, (n.d.). doi:10.1007/s13758-012-0060-8.
- [230] M.T. Tsai, Y.Y. Chang, H.L. Huang, Y.H. Wu, T.M. Shieh, Micro-arc oxidation treatment enhanced the biological performance of human osteosarcoma cell line and human skin fibroblasts cultured on titanium–zirconium films, *Surf. Coatings Technol.* 303 (2016) 268–276. doi:10.1016/j.surfcoat.2016.03.001.
- [231] A.R. Rafieerad, A.R. Bushroa, B. Nasiri-Tabrizi, S. Baradaran, S. Shahtalebi, S. Khanahmadi, M. Afshar-Mohajer, J. Vadivelu, F. Yusof, W.J. Basirun, *In-vitro* bioassay of electrophoretically deposited hydroxyapatite–zirconia nanocomposite coating on Ti–6Al–7Nb implant, *Adv. Appl. Ceram.* 116 (2017) 293–306. doi:10.1080/17436753.2017.1313626.
- [232] W. Han, Y. Wang, Y.Z.-A.M. Research, undefined 2008, In Vitro Biocompatibility Study of Nano TiO₂ Materials, *Trans Tech Publ.* (2008). doi:10.4028/www.scientific.net/AMR.47-50.1438.
- [233] K. Alagarsamy, V. Vishwakarma, G. Saravanan Kaliaraj, Synthesis and Characterization of bioactive composite coating on Titanium by PVD for biomedical application, (n.d.). doi:10.1088/1757-899X/561/1/012027.
- [234] J. anne N. Oliver, Y. Su, X. Lu, P.H. Kuo, J. Du, D. Zhu, Bioactive glass coatings on metallic implants for biomedical applications, *Bioact. Mater.* 4 (2019) 261–270.

doi:10.1016/j.bioactmat.2019.09.002.

- [235] K.S.K. Lin, Y.-H. Tseng, Y. Mou, Y.-C. Hsu, C.-M. Yang, J.C.C. Chan, Mechanistic Study of Apatite Formation on Bioactive Glass Surface Using ^{31}P Solid-State NMR Spectroscopy, *Chem. Mater.* 17 (2005) 4493–4501. doi:10.1021/cm050654c.
- [236] S. Mondal, G. Hoang, P. Manivasagan, M.S. Moorthy, T.P. Nguyen, T.T. Vy Phan, H.H. Kim, M.H. Kim, S.Y. Nam, J. Oh, Nano-hydroxyapatite bioactive glass composite scaffold with enhanced mechanical and biological performance for tissue engineering application, *Ceram. Int.* 44 (2018) 15735–15746. doi:10.1016/j.ceramint.2018.05.248.
- [237] A. Sola, D. Bellucci, V. Cannillo, A. Cattini, Bioactive glass coatings: A review, *Surf. Eng.* 27 (2011) 560–572. doi:10.1179/1743294410Y.0000000008.
- [238] G. Koller, A.E. Richard, J.C. Ae, I.D. Thompson, T.F. Watson, A.E. Lucy, D. Silvio, Surface modification of titanium implants using bioactive glasses with air abrasion technologies, (n.d.). doi:10.1007/s10856-007-3137-z.
- [239] A. Braem, T. Mattheys, B. Neirinck, M. Čeh, S. Novak, J. Schrooten, O. Van Der Biest, J. Vleugels, Bioactive glass-ceramic coated titanium implants prepared by electrophoretic deposition, *Mater. Sci. Eng. C.* 32 (2012) 2267–2273. doi:10.1016/j.msec.2012.06.013.
- [240] G.E. Stan, D.A. Marcov, I. Pasuk, F. Miculescu, S. Pina, D.U. Tulyaganov, J.M.F. Ferreira, Bioactive glass thin films deposited by magnetron sputtering technique: The role of working pressure, *Appl. Surf. Sci.* 256 (2010) 7102–7110. doi:10.1016/j.apsusc.2010.05.035.
- [241] R. Teghil, D. Ferro, S.M. Barinov, View project Research on Phoenician in Northern Africa and Atlantic Area: archaeology, numismatics and economic history and Archaeological mission Prospezioni archeologiche nel Medio Atlas per la ricostruzione dei contesti archeometallurgici punici del Maghreb View project, (n.d.). doi:10.1023/A:1014903117057.
- [242] R. Teghil, L. D'Alessio, D. Ferro, S.M. Barinov, Hardness of bioactive glass film deposited on titanium alloy by pulsed laser ablation, *J. Mater. Sci. Lett.* 21 (2002) 379–382. doi:10.1023/A:1014903117057.
- [243] D. Stojanovic, B. Jokic, D. Veljovic, R. Petrovic, P.S. Uskokovic,

- D. Janackovic, Bioactive glass-apatite composite coating for titanium implant synthesized by electrophoretic deposition, *J. Eur. Ceram. Soc.* 27 (2007) 1595–1599. doi:10.1016/j.jeurceramsoc.2006.04.111.
- [244] E. Verné, M. Ferraris, A. Ventrella, L. Paracchini, A. Krajewski, A. Ravaglioli, Sintering and Plasma Spray Deposition of Bioactive Glass-Matrix Composites for Medical Applications, *J. Eur. Ceram. Soc.* 18 (1998) 363–372. doi:10.1016/S0955-2219(97)00134-9.
- [245] C. Domínguez-Trujillo, F. Ternero, J.A. Rodríguez-Ortiz, S. Heise, A.R. Boccaccini, J. Lebrato, Y. Torres, Bioactive coatings on porous titanium for biomedical applications, *Surf. Coatings Technol.* 349 (2018) 584–592. doi:10.1016/j.surfcoat.2018.06.037.
- [246] X. Liu, C. Ding, Plasma sprayed wollastonite/TiO₂ composite coatings on titanium alloys, *Biomaterials.* 23 (2002) 4065–4077. doi:10.1016/S0142-9612(02)00143-6.
- [247] X. Liu, C. Ding, Z. Wang, Apatite formed on the surface of plasma-sprayed wollastonite coating immersed in simulated body fluid, *Biomaterials.* 22 (2001) 2007–2012. doi:10.1016/S0142-9612(00)00386-0.
- [248] K.J.J. Pajamäki, T.S. Lindholm, O.H. Andersson, K.H. Karlsson, E. Vedel, A. Yli-Urpo, R.P. Happonen, Bioactive glass and glass-ceramic-coated hip endoprosthesis: experimental study in rabbit, *J. Mater. Sci. Mater. Med.* 6 (1995) 14–18. doi:10.1007/BF00121240.
- [249] N. Moritz, S. Rossi, E. Vedel, T. Tirri, H. Ylänen, H. Aro, T. Närhi, Implants coated with bioactive glass by CO₂-laser, an in vivo study, *J. Mater. Sci. Mater. Med.* 15 (2004) 795–802. doi:10.1023/B:JMSM.0000032820.50983.c1.
- [250] J.P. Borrajo AE Julia Serra AE Pío González AE Betty León AE Fernando M Muñoz AE M López, In vivo evaluation of titanium implants coated with bioactive glass by pulsed laser deposition, (n.d.). doi:10.1007/s10856-007-3153-z.
- [251] S. Mistry, D. Kundu, S. Datta, D. Basu, Comparison of bioactive glass coated and hydroxyapatite coated titanium dental implants in the human jaw bone, *Aust. Dent. J.* 56 (2011) 68–75. doi:10.1111/j.1834-7819.2010.01305.x.
- [252] S. Mistry, R. Roy, B. Kundu, S. Datta, M. Kumar, A. Chanda, D.

- Kundu, Clinical outcome of hydroxyapatite coated, bioactive glass coated, and machined Ti6Al4V threaded dental implant in human jaws: A short-term comparative study, *Implant Dent.* 25 (2016) 252–260. doi:10.1097/ID.0000000000000376.
- [253] N. Moritz, E. Vedel, H. Yla È Nen, M. Jokinen, M. Hupa, A. Yli-Urpo, Characterisation of bioactive glass coatings on titanium substrates produced using a CO₂ laser, n.d.
- [254] N. Drnovšek, S. Novak, U. Dragin, M. Čeh, M. Gorenšek, M. Gradišar, Bioactive glass enhances bone ingrowth into the porous titanium coating on orthopaedic implants, (n.d.). doi:10.1007/s00264-012-1520-y.
- [255] C. Covarrubias, M. Mattmann, A. Von Marttens, P. Caviades, C. Arriagada, F. Valenzuela, J.P. Rodríguez, C. Corral, Osseointegration properties of titanium dental implants modified with a nanostructured coating based on ordered porous silica and bioactive glass nanoparticles, *Appl. Surf. Sci.* 363 (2016) 286–295. doi:10.1016/j.apsusc.2015.12.022.
- [256] C.C. Mardare, A.I. Mardare, J.R.F. Fernandes, E. Joanni, S.C.A. Pina, M.H.V. Fernandes, R.N. Correia, Deposition of bioactive glass-ceramic thin-films by RF magnetron sputtering, *J. Eur. Ceram. Soc.* 23 (2003) 1027–1030. doi:10.1016/S0955-2219(02)00278-9.
- [257] C. Soundrapandian, S. Bharati, D. Basu, S. Datta, Studies on novel bioactive glasses and bioactive glass-nano-HAp composites suitable for coating on metallic implants, *Ceram. Int.* 37 (2011) 759–769. doi:10.1016/j.ceramint.2010.10.025.
- [258] Y. Xiao, L. Song, X. Liu, Y. Huang, T. Huang, Y. Wu, J. Chen, F. Wu, Nanostructured bioactive glass-ceramic coatings deposited by the liquid precursor plasma spraying process, *Appl. Surf. Sci.* 257 (2011) 1898–1905. doi:10.1016/j.apsusc.2010.09.023.
- [259] X. Chen, M. Zhang, X. Pu, G. Yin, X. Liao, Z. Huang, Y. Yao, Characteristics of heat-treated plasma-sprayed CaO-MgO-SiO₂-based bioactive glass-ceramic coatings on Ti-6Al-4V alloy, *Surf. Coatings Technol.* 249 (2014) 97–103. doi:10.1016/j.surfcoat.2014.03.056.
- [260] M. Stigter, J. Bezemer, K. De Groot, P. Layrolle, Incorporation of different antibiotics into carbonated hydroxyapatite coatings on titanium implants, release and antibiotic efficacy, *J. Control. Release.* 99 (2004) 127–137. doi:10.1016/j.jconrel.2004.06.011.

- [261] M. Stigter, K. De Groot, P. Layrolle, Incorporation of tobramycin into biomimetic hydroxyapatite coating on titanium, *Biomaterials*. 23 (2002) 4143–4153. doi:10.1016/S0142-9612(02)00157-6.
- [262] H. Chourifa, H. Bouloussa, V. Migonney, C. Falentin-Daudré, Review of titanium surface modification techniques and coatings for antibacterial applications, *Acta Biomater.* 83 (2019) 37–54. doi:10.1016/j.actbio.2018.10.036.
- [263] D. Jahoda, O. Nyc, D. Pokorný, ... I.L.-A. chirurgiae, undefined 2006, Antibiotic treatment for prevention of infectious complications in joint replacement, *Europepmc.Org.* (n.d.). <https://europepmc.org/abstract/med/16735008> (accessed January 16, 2020).
- [264] L.B. Engesæter, S.A. Lie, B. Espehaug, O. Furnes, S.E. Vollset, L.I. Havelin, Antibiotic prophylaxis in total hip arthroplasty: Effects of antibiotic prophylaxis systemically and in bone cement on the revision rate of 22,170 primary hip replacements followed 0-14 years in the Norwegian Arthroplasty Register, *Acta Orthop. Scand.* 74 (2003) 644–651. doi:10.1080/00016470310018135.
- [265] V. Alt, A. Bitschnau, J. Österling, A. Sewing, C. Meyer, R. Kraus, S.A. Meissner, S. Wenisch, E. Domann, R. Schnettler, The effects of combined gentamicin-hydroxyapatite coating for cementless joint prostheses on the reduction of infection rates in a rabbit infection prophylaxis model, *Biomaterials*. 27 (2006) 4627–4634. doi:10.1016/j.biomaterials.2006.04.035.
- [266] S. Radin, J.T. Campbell, P. Ducheyne, J.M. Cuckler, Calcium phosphate ceramic coatings as carriers of vancomycin, *Biomaterials*. 18 (1997) 777–782. doi:10.1016/S0142-9612(96)00190-1.
- [267] K. Yamamura, H. Iwata, T. Yotsuyanagi, Synthesis of antibiotic-loaded hydroxyapatite beads and in vitro drug release testing, *J. Biomed. Mater. Res.* 26 (1992) 1053–1064. doi:10.1002/jbm.820260807.
- [268] H. Shintani, Modification of Medical Device Surface to Attain Anti-Infection, (2004).
- [269] P. Basak, B. Adhikari, I. Banerjee, T.K. Maiti, Sustained release of antibiotic from polyurethane coated implant materials, in: *J. Mater. Sci. Mater. Med.*, 2009. doi:10.1007/s10856-008-3521-3.

- [270] M. Lucke, G. Schmidmaier, S. Sadoni, B. Wildemann, R. Schiller, N.P. Haas, M. Raschke, Gentamicin coating of metallic implants reduces implant-related osteomyelitis in rats, *Bone*. 32 (2003) 521–531. doi:10.1016/S8756-3282(03)00050-4.
- [271] S. Radin, P. Ducheyne, Controlled release of vancomycin from thin sol-gel films on titanium alloy fracture plate material, *Biomaterials*. 28 (2007) 1721–1729. doi:10.1016/j.biomaterials.2006.11.035.
- [272] K.C. Popat, M. Eltgroth, T.J. LaTempa, C.A. Grimes, T.A. Desai, Decreased Staphylococcus epidermis adhesion and increased osteoblast functionality on antibiotic-loaded titania nanotubes, *Biomaterials*. 28 (2007) 4880–4888. doi:10.1016/j.biomaterials.2007.07.037.
- [273] K. Popat, L. Leoni, C. Grimes, T.D. - Biomaterials, undefined 2007, Influence of engineered titania nanotubular surfaces on bone cells, Elsevier. (n.d.). <https://www.sciencedirect.com/science/article/pii/S0142961207002347> (accessed January 16, 2020).
- [274] O.P. Edupuganti, V. Antoci, S.B. King, B. Jose, C.S. Adams, J. Parvizi, I.M. Shapiro, A.R. Zeiger, N.J. Hickok, E. Wickstrom, Covalent bonding of vancomycin to Ti6Al4V alloy pins provides long-term inhibition of Staphylococcus aureus colonization, *Bioorganic Med. Chem. Lett.* 17 (2007) 2692–2696. doi:10.1016/j.bmcl.2007.03.005.
- [275] B. Jose, V. Antoci, A.R. Zeiger, E. Wickstrom, N.J. Hickok, Vancomycin covalently bonded to titanium beads kills Staphylococcus aureus, *Chem. Biol.* 12 (2005) 1041–1048. doi:10.1016/j.chembiol.2005.06.013.
- [276] M.M. Tunney, G. Ramage, S. Patrick, J.R. Nixon, P.G. Murphy, S.P. Gorman, Antimicrobial Susceptibility of Bacteria Isolated from Orthopedic Implants following Revision Hip Surgery, 1998. <http://aac.asm.org/> (accessed January 16, 2020).
- [277] J.X. Liu, D. Bravo, J. Buza, T. Kirsch, O. Kennedy, A. Rokito, J.D. Zuckerman, M.S. Virk, Topical vancomycin and its effect on survival and migration of osteoblasts, fibroblasts, and myoblasts: An in vitro study, *J. Orthop.* 15 (2018) 53–58. doi:10.1016/j.jor.2018.01.032.
- [278] V.P. Mantripragada, A.C. Jayasuriya, Effect of dual delivery of antibiotics (vancomycin and cefazolin) and BMP-7 from chitosan

- microparticles on *Staphylococcus epidermidis* and pre-osteoblasts in vitro, *Mater. Sci. Eng. C.* 67 (2016) 409–417. doi:10.1016/j.msec.2016.05.033.
- [279] A. Ince, N. Schütze, C. Hendrich, R. Thull, J. Eulert, J.F. Löhr, In Vitro Investigation of Orthopedic Titanium-Coated and Brushite-Coated Surfaces Using Human Osteoblasts in the Presence of Gentamycin, *J. Arthroplasty.* 23 (2008) 762–771. doi:10.1016/j.arth.2007.06.018.
- [280] F.D. Naal, G.M. Salzmann, F. von Knoch, J. Tuebel, P. Diehl, R. Gradinger, J. Schauwecker, The effects of clindamycin on human osteoblasts in vitro, *Arch. Orthop. Trauma Surg.* 128 (2008) 317–323. doi:10.1007/s00402-007-0561-y.
- [281] S. Radin, V. Antoci, N. Hickok, C.S. Adams, J. Parvizi, I. Shapiro, P. Ducheyne, In Vitro and In Vivo Bactericidal Effect of Sol-Gel/Antibiotic Thin Films on Fixation Devices, (2007). doi:10.4028/www.scientific.net/KEM.330-332.1323.
- [282] V. Antoci, C.S. Adams, J. Parvizi, H.M. Davidson, R.J. Composto, T.A. Freeman, E. Wickstrom, P. Ducheyne, D. Jungkind, I.M. Shapiro, N.J. Hickok, The inhibition of *Staphylococcus epidermidis* biofilm formation by vancomycin-modified titanium alloy and implications for the treatment of periprosthetic infection, *Biomaterials.* 29 (2008) 4684–4690. doi:10.1016/j.biomaterials.2008.08.016.
- [283] M.C. Lawson, C.N. Bowman, K.S. Anseth, Vancomycin Derivative Photopolymerized to Titanium Kills *S. Epidermidis*, *Clin. Orthop. Relat. Res. PAP* (2007). doi:10.1097/BLO.0b013e3180986706.
- [284] V. Antoci, S.B. King, B. Jose, J. Parvizi, A.R. Zeiger, E. Wickstrom, T.A. Freeman, R.J. Composto, P. Ducheyne, I.M. Shapiro, N.J. Hickok, C.S. Adams, Vancomycin covalently bonded to titanium alloy prevents bacterial colonization, *J. Orthop. Res.* 25 (2007) 858–866. doi:10.1002/jor.20348.
- [285] C.-P. Chen, E. Wickstrom, Self-Protecting Bactericidal Titanium Alloy Surface Formed by Covalent Bonding of Daptomycin Bisphosphonates, (n.d.). doi:10.1021/bc100136e.
- [286] M.E. Barbour, N. Gandhi, A. El-Turki, D.J. O’Sullivan, D.C. Jagger, Differential adhesion of *Streptococcus gordonii* to anatase and rutile titanium dioxide surfaces with and without functionalization with chlorhexidine, *J. Biomed. Mater. Res. -*

- Part A. 90 (2009) 993–998. doi:10.1002/jbm.a.32170.
- [287] W. Chen, S. Li, L. Li, X. Wu, W. Zhang, Effects of daily bathing with chlorhexidine and acquired infection of methicillin-resistant *Staphylococcus aureus* and vancomycin-resistant *Enterococcus*: a meta-analysis., *J. Thorac. Dis.* 5 (2013) 518–51824. doi:10.3978/j.issn.2072-1439.2013.08.30.
- [288] L. Zhang, C. Ning, T. Zhou, X. Liu, K.K. Yeung, T. Zhang, Z. Xu, X. Wang, S. Wu, P.K. Chu, Polymeric Nanoarchitectures on Ti-Based Implants for Antibacterial Applications, (2014). doi:10.1021/am5045604.
- [289] L.G. Harris, L. Mead, E. Müller-Oberländer, R.G. Richards, Bacteria and cell cytocompatibility studies on coated medical grade titanium surfaces, *J. Biomed. Mater. Res. - Part A.* 78 (2006) 50–58. doi:10.1002/jbm.a.30611.
- [290] M.C. Cortizo, T.G. Oberti, M.S. Cortizo, A.M. Cortizo, M.A. Fernández Lorenzo De Mele, Chlorhexidine delivery system from titanium/polybenzyl acrylate coating: Evaluation of cytotoxicity and early bacterial adhesion, *J. Dent.* 40 (2012) 329–337. doi:10.1016/j.jdent.2012.01.008.
- [291] R. Chen, M.D.P. Willcox, K.K.K. Ho, D. Smyth, N. Kumar, Antimicrobial peptide melimine coating for titanium and its in vivo antibacterial activity in rodent subcutaneous infection models, *Biomaterials.* 85 (2016) 142–151. doi:10.1016/j.biomaterials.2016.01.063.
- [292] M. Kazemzadeh-Narbat, B.F.L. Lai, C. Ding, J.N. Kizhakkedathu, R.E.W. Hancock, R. Wang, Multilayered coating on titanium for controlled release of antimicrobial peptides for the prevention of implant-associated infections, *Biomaterials.* 34 (2013) 5969–5977. doi:10.1016/j.biomaterials.2013.04.036.
- [293] X. Wang, L. Tan, X. Liu, Z. Cui, X. Yang, K.W.K. Yeung, P.K. Chu, S. Wu, Construction of perfluorohexane/IR780@liposome coating on Ti for rapid bacteria killing under permeable near infrared light, *Biomater. Sci.* 6 (2018) 2460–2471. doi:10.1039/c8bm00602d.
- [294] R. Lehrer, T.G.-C. opinion in immunology, undefined 1999, Antimicrobial peptides in mammalian and insect host defence, Elsevier. (n.d.).
<https://www.sciencedirect.com/science/article/pii/S09527915998>

- 00053 (accessed January 17, 2020).
- [295] M. Zasloff, Antimicrobial peptides of multicellular organisms, *Nature*. 415 (2002) 389–395. doi:10.1038/415389a.
- [296] P. Bulet, R. Stöcklin, L. Menin, Anti-microbial peptides: From invertebrates to vertebrates, *Immunol. Rev.* 198 (2004) 169–184. doi:10.1111/j.0105-2896.2004.0124.x.
- [297] K. Glinel, P. Thebault, V. Humblot, C.P.-A. biomaterialia, undefined 2012, Antimicrobial surfaces developed from bio-inspired approaches, Elsevier. (n.d.). <https://www.sciencedirect.com/science/article/pii/S1742706112000189> (accessed January 17, 2020).
- [298] M. Kazemzadeh-Narbat, J. Kindrachuk, K.D.- Biomaterials, undefined 2010, Antimicrobial peptides on calcium phosphate-coated titanium for the prevention of implant-associated infections, Elsevier. (n.d.). <https://www.sciencedirect.com/science/article/pii/S0142961210010574> (accessed January 17, 2020).
- [299] X. Chen, H. Hirt, Y. Li, S.U. Gorr, C. Aparicio, Antimicrobial GL13K peptide coatings killed and ruptured the wall of streptococcus gordonii and prevented formation and growth of biofilms, *PLoS One*. 9 (2014). doi:10.1371/journal.pone.0111579.
- [300] M. Godoy-Gallardo, C. Mas-Moruno, ... K.Y.-, undefined 2015, Antibacterial properties of hLf1–11 peptide onto titanium surfaces: a comparison study between silanization and surface initiated polymerization, *ACS Publ.* (n.d.). <https://pubs.acs.org/doi/abs/10.1021/bm501528x> (accessed January 17, 2020).
- [301] D. Rodriguez, Antibacterial Properties of hLf1-11 Peptide onto Titanium Surfaces: A Comparison Study Between Silanization and Surface Initiated Polymerization, (2014). doi:10.1021/bm501528x.
- [302] M. Bagheri, M. Beyermann, M. Dathe, Immobilization reduces the activity of surface-bound cationic antimicrobial peptides with no influence upon the activity spectrum, *Antimicrob. Agents Chemother.* 53 (2009) 1132–1141. doi:10.1128/AAC.01254-08.
- [303] P. Appendini, J.H.-J. of applied polymer science, undefined 2001, Surface modification of poly (styrene) by the attachment of an antimicrobial peptide, *Wiley Online Libr.* (n.d.).

<https://onlinelibrary.wiley.com/doi/abs/10.1002/app.1476>
(accessed January 17, 2020).

- [304] M. Gabriel, K. Nazmi, E.C. Veerman, A.V.N. Amerongen, A. Zentner, Preparation of LL-37-grafted titanium surfaces with bactericidal activity, *Bioconjug. Chem.* 17 (2006) 548–550. doi:10.1021/bc050091v.
- [305] S.A. Onaizi, S.S.J. Leong, Tethering antimicrobial peptides: Current status and potential challenges, *Biotechnol. Adv.* 29 (2011) 67–74. doi:10.1016/j.biotechadv.2010.08.012.
- [306] S.M. Shiels, M. Bouchard, H. Wang, J.C. Wenke, CHLORHEXIDINE-RELEASING IMPLANT COATING ON INTRAMEDULLARY NAIL REDUCES INFECTION IN A RAT MODEL, *Eur. Cells Mater.* 35 (2018) 178–194. doi:10.22203/eCM.v035a13.
- [307] A.A. Campbell, L. Song, X.S. Li, B.J. Nelson, C. Bottoni, D.E. Brooks, E.S. Dejong, Development, characterization, and antimicrobial efficacy of hydroxyapatite-chlorhexidine coatings produced by surface-induced mineralization, *J. Biomed. Mater. Res.* 53 (2000) 400–407. doi:10.1002/1097-4636(2000)53:4<400::AID-JBM14>3.0.CO;2-Z.
- [308] W.H. Kim, S.B. Lee, K.T. Oh, S.K. Moon, K.M. Kim, K.N. Kim, The release behavior of CHX from polymer-coated titanium surfaces, in: *Surf. Interface Anal.*, 2008: pp. 202–204. doi:10.1002/sia.2809.
- [309] R.O. Darouiche, G. Green, M.D. Mansouri, Antimicrobial activity of antiseptic-coated orthopaedic devices, *Int. J. Antimicrob. Agents.* 10 (1998) 83–86. doi:10.1016/S0924-8579(98)00017-X.
- [310] M. Riool, A.J. Dirks, V. Jaspers, L. de Boer, T.J. A Loontjens, C.M. van der Loos, S. Florquin, I. Apachitei, L.N. D Rijk, H.A. Keul, S.A. J Zaat, A chlorhexidine-releasing epoxy-based coating on titanium implants prevents *Staphylococcus aureus* experimental biomaterial-associated infection, 2017. https://pure.uva.nl/ws/files/16051896/Chapter_4.pdf (accessed September 30, 2019).
- [311] G. Gao, D. Lange, K. Hilpert, J. Kindrachuk, Y. Zou, J.T.J. Cheng, M. Kazemzadeh-Narbat, K. Yu, R. Wang, S.K. Straus, D.E. Brooks, B.H. Chew, R.E.W. Hancock, J.N. Kizhakkedathu, The biocompatibility and biofilm resistance of implant coatings

- based on hydrophilic polymer brushes conjugated with antimicrobial peptides, *Biomaterials*. 32 (2011) 3899–3909. doi:10.1016/j.biomaterials.2011.02.013.
- [312] D. Xu, W. Yang, Y. Hu, Z. Luo, J. Li, Y. Hou, Y. Liu, K. Cai, Surface functionalization of titanium substrates with cecropin B to improve their cytocompatibility and reduce inflammation responses, *Colloids Surfaces B Biointerfaces*. 110 (2013) 225–235. doi:10.1016/j.colsurfb.2013.04.050.
- [313] U.F. Gunpath, H. Le, R.D. Handy, C. Tredwin, Anodised TiO₂ nanotubes as a scaffold for antibacterial silver nanoparticles on titanium implants, *Mater. Sci. Eng. C*. 91 (2018) 638–644. doi:10.1016/j.msec.2018.05.074.
- [314] A. Ewald, S.K. Glückermann, R. Thull, U. Gbureck, Antimicrobial titanium/silver PVD coatings on titanium, (n.d.). doi:10.1186/1475-925X-5-22.
- [315] N. Xu, H. Cheng, J. Xu, F. Li, B. gao, Z. li, C. gao, K. huo, J. Fu, W. Xiong, silver-loaded nanotubular structures enhanced bactericidal efficiency of antibiotics with synergistic effect in vitro and in vivo, *Int. J. Nanomedicine*. (2017) 12–731. doi:10.2147/IJN.S123648.
- [316] A. Gao, R. Hang, L. Bai, B. Tang, P.K. Chu, Electrochemical surface engineering of titanium-based alloys for biomedical application, *Electrochim. Acta*. 271 (2018) 699–718. doi:10.1016/j.electacta.2018.03.180.
- [317] K.D. Secinti, M. Ayten, G. Kahilogullari, G. Kaygusuz, H.C. Ugur, A. Attar, Antibacterial effects of electrically activated vertebral implants, *J. Clin. Neurosci*. 15 (2008) 434–439. doi:10.1016/j.jocn.2007.03.010.
- [318] S. Cometa, M.A. Bonifacio, F. Baruzzi, S. De Candia, M.M. Giangregorio, L.C. Giannossa, M. Dicarolo, M. Mattioli-Belmonte, L. Sabbatini, E. De Giglio, Silver-loaded chitosan coating as an integrated approach to face titanium implant-associated infections: analytical characterization and biological activity, (n.d.). doi:10.1007/s00216-017-0685-z.
- [319] E. De Giglio, S. Cometa, N. Cioffi, L. Torsi, L. Sabbatini, Analytical investigations of poly(acrylic acid) coatings electrodeposited on titanium-based implants: a versatile approach to biocompatibility enhancement, (n.d.). doi:10.1007/s00216-007-1299-7.

- [320] A. Roguska, A. Belcarz, T. Piersiak, M. Pisarek, G. Ginalska, M. Lewandowska, Evaluation of the Antibacterial Activity of Ag-Loaded TiO₂ Nanotubes, *Eur. J. Inorg. Chem.* 2012 (2012) 5199–5206. doi:10.1002/ejic.201200508.
- [321] L. Zhao, H. Wang, K. Huo, L. Cui, W. Zhang, H. Ni, Y. Zhang, Z. Wu, P.K. Chu, Antibacterial nano-structured titania coating incorporated with silver nanoparticles, *Biomaterials.* 32 (2011) 5706–5716. doi:10.1016/j.biomaterials.2011.04.040.
- [322] H. Cheng, Y. Li, K. Huo, B. Gao, W. Xiong, Long-lasting *in vivo* and *in vitro* antibacterial ability of nanostructured titania coating incorporated with silver nanoparticles, *J. Biomed. Mater. Res. Part A.* 102 (2014) 3488–3499. doi:10.1002/jbm.a.35019.
- [323] A. Gao, R. Hang, X. Huang, L. Zhao, X. Zhang, L.W.-Biomaterials, undefined 2014, The effects of titania nanotubes with embedded silver oxide nanoparticles on bacteria and osteoblasts, Elsevier. (n.d.). <https://www.sciencedirect.com/science/article/pii/S014296121400088X> (accessed February 4, 2020).
- [324] M. Rai, A. Yadav, A. Gade, Silver nanoparticles as a new generation of antimicrobials, *Biotechnol. Adv.* 27 (2009) 76–83. doi:10.1016/j.biotechadv.2008.09.002.
- [325] Y. Qing, L. Cheng, R. Li, G. Liu, Y. Zhang, X. Tang, J. Wang, H. Liu, Y. Qin, Potential antibacterial mechanism of silver nanoparticles and the optimization of orthopedic implants by advanced modification technologies, *Int. J. Nanomedicine.* 13 (2018) 3311–3327. doi:10.2147/IJN.S165125.
- [326] J.R. Morones, J.L. Elechiguerra, A. Camacho, K. Holt, J.B. Kouri, J.T. Ramírez, M.J. Yacaman, The bactericidal effect of silver nanoparticles, *Nanotechnology.* 16 (2005) 2346–2353. doi:10.1088/0957-4484/16/10/059.
- [327] A. Shivaram, S. Bose, A. Bandyopadhyay, Understanding long-term silver release from surface modified porous titanium implants, *Acta Biomater.* 58 (2017) 550–560. doi:10.1016/j.actbio.2017.05.048.
- [328] Z. Geng, Z. Li, Y.-C. Huang, R. Wang, X. Zhuo, Y. Huang, L. Ma, Z. Cui, S. Zhu, Y. Liang, Y. Liu, H. Bao, X. Li, Q. Huo, Z. Liu, X. Yang, Incorporation of silver and strontium in hydroxyapatite coating on titanium surface for enhanced antibacterial and

- biological properties Intervertebral disc transplantation and regeneration; mesenchymal stem cells for tissue regeneration View project Incorporation of silver and strontium in hydroxyapatite coating on titanium surface for enhanced antibacterial and biological properties, (2016). doi:10.1016/j.msec.2016.10.079.
- [329] A. Besinis, S.D. Hadi, H.R. Le, C. Tredwin, R.D. Handy, Antibacterial activity and biofilm inhibition by surface modified titanium alloy medical implants following application of silver, titanium dioxide and hydroxyapatite nanocoatings, (2017). doi:10.1080/17435390.2017.1299890.
- [330] J.L. Endrino, A. Anders, J.M. Albella, J.A. Horton, T.H. Horton, P.R. Ayyalasomayajula, M. Allen, Antibacterial efficacy of advanced silver-amorphous carbon coatings deposited using the pulsed dual cathodic arc technique Related content Antibacterial efficacy of advanced silver-amorphous carbon coatings deposited using the pulsed dual cathodic arc technique, *J. Phys. Conf. Ser. OPEN ACCESS*. (n.d.). doi:10.1088/1742-6596/252/1/012012.
- [331] W.-H. Song, H.S. Ryu, S.-H. Hong, Antibacterial properties of Ag (or Pt)-containing calcium phosphate coatings formed by micro-arc oxidation, *J. Biomed. Mater. Res. Part A*. 88A (2009) 246–254. doi:10.1002/jbm.a.31877.
- [332] C. Chang, X. Huang, Y. Liu, L. Bai, X. Yang, R. Hang, B. Tang, P.K. Chu, High-current anodization: A novel strategy to functionalize titanium-based biomaterials, *Electrochim. Acta*. 173 (2015) 345–353. doi:10.1016/j.electacta.2015.05.075.
- [333] F.J. Saubade, S. Hughes, D.J. Wickens, J. Wilson-Nieuwenhuis, N. Dempsey-Hibbert, G.S. Crowther, G. West, P. Kelly, C.E. Banks, K.A. Whitehead, Effectiveness of titanium nitride silver coatings against *Staphylococcus* spp. in the presence of BSA and whole blood conditioning agents, *Int. Biodeterior. Biodegrad.* 141 (2019) 44–51. doi:10.1016/j.ibiod.2018.06.016.
- [334] Z. Geng, R. Wang, X. Zhuo, Z. Li, Y. Huang, L. Ma, Z. Cui, S. Zhu, Y. Liang, Y. Liu, H. Bao, X. Li, Q. Huo, Z. Liu, X. Yang, Incorporation of silver and strontium in hydroxyapatite coating on titanium surface for enhanced antibacterial and biological properties, *Mater. Sci. Eng. C*. 71 (2017) 852–861. doi:10.1016/j.msec.2016.10.079.

- [335] T. Ishida, Immunology Journal Mechanism of Antibacterial Activities of Cu (II) Ions against Staphylococcus aureus and Escherichia coli on the Ground of Results Obtained from Dilution Medium Method Mechanism of Antibacterial Activities of Cu (II) Ions against Staphyloc, Virol Immunol J . 1 (2017) 000117. <https://medwinpublishers.com/VIJ/VIJ16000117.pdf>.
- [336] X. Wu, L. Ye, K. Liu, W. Wang, J. Wei, F. Chen, C. Liu, Antibacterial properties of mesoporous copper-doped silica xerogels, Biomed. Mater. 4 (2009). doi:10.1088/1748-6041/4/4/045008.
- [337] S. Mallick, S. Sharma, M. Banerjee, S.S. Ghosh, A. Chattopadhyay, A. Paul, Iodine-stabilized Cu nanoparticle chitosan composite for antibacterial applications, ACS Appl. Mater. Interfaces. 4 (2012) 1313–1323. doi:10.1021/am201586w.
- [338] L. Ren, H.M. Wong, C.H. Yan, K.W.K. Yeung, K. Yang, Osteogenic ability of Cu-bearing stainless steel, J. Biomed. Mater. Res. - Part B Appl. Biomater. 103 (2015) 1433–1444. doi:10.1002/jbm.b.33318.
- [339] S.N. Rath, A. Brandl, D. Hiller, A. Hoppe, U. Gbureck, R.E. Horch, A.R. Boccaccini, U. Kneser, Bioactive Copper-Doped Glass Scaffolds Can Stimulate Endothelial Cells in Co-Culture in Combination with Mesenchymal Stem Cells, PLoS One. 9 (2014) e113319. doi:10.1371/journal.pone.0113319.
- [340] S. Li, H. Xie, S. Li, Y.J. Kang, Copper stimulates growth of human umbilical vein endothelial cells in a vascular endothelial growth factor-independent pathway, Exp. Biol. Med. 237 (2012) 77–82. doi:10.1258/ebm.2011.011267.
- [341] G. Hu, Copper stimulates proliferation of human endothelial cells under culture, J. Cell. Biochem. 69 (1998) 326–335. doi:10.1002/(SICI)1097-4644(19980601)69:3<326::AID-JCB10>3.0.CO;2-A.
- [342] L. Zhang, J. Guo, X. Huang, Y. Zhang, Y. Han, The dual function of Cu-doped TiO₂ coatings on titanium for application in percutaneous implants, J. Mater. Chem. B. 4 (2016) 3788–3800. doi:10.1039/C6TB00563B.
- [343] X.B. Tian, Z.M. Wang, S.Q. Yang, Z.J. Luo, R.K.Y. Fu, P.K. Chu, Antibacterial copper-containing titanium nitride films produced by dual magnetron sputtering, Surf. Coatings Technol. 201 (2007) 8606–8609. doi:10.1016/j.surfcoat.2006.09.322.

- [344] J. Fiedler, A. Kolitsch, B. Kleffner, D. Henke, S. Stenger, R.E. Brenner, Copper and silver ion implantation of aluminium oxide-blasted titanium surfaces: Proliferative response of osteoblasts and antibacterial effects, *Int. J. Artif. Organs*. 34 (2011) 882–888. doi:10.5301/ijao.5000022.
- [345] Y.Z. Wan, G.Y. Xiong, H. Liang, S. Raman, F. He, Y. Huang, Modification of medical metals by ion implantation of copper, *Appl. Surf. Sci.* 253 (2007) 9426–9429. doi:10.1016/j.apsusc.2007.06.031.
- [346] T. Shirai, H. Tsuchiya, T. Shimizu, K. Ohtani, Y. Zen, K. Tomita, Prevention of pin tract infection with titanium-copper alloys, *J. Biomed. Mater. Res. Part B Appl. Biomater.* 91B (2009) 373–380. doi:10.1002/jbm.b.31412.
- [347] Y.Z. Wan, S. Raman, F. He, Y. Huang, Surface modification of medical metals by ion implantation of silver and copper, *Vacuum*. 81 (2007) 1114–1118. doi:10.1016/j.vacuum.2006.12.011.
- [348] F. Hempel, B. Finke, C. Zietz, R. Bader, K.D. Weltmann, M. Polak, Antimicrobial surface modification of titanium substrates by means of plasma immersion ion implantation and deposition of copper, *Surf. Coatings Technol.* 256 (2014) 52–58. doi:10.1016/j.surfcoat.2014.01.027.
- [349] K. Rokosz, T. Hryniewicz, S. Raaen, P. Chapon, F. Prima, Development of copper-enriched porous coatings on ternary Ti-Nb-Zr alloy by plasma electrolytic oxidation, *Int. J. Adv. Manuf. Technol.* 89 (2017) 2953–2965. doi:10.1007/s00170-016-9206-z.
- [350] A. Hoene, C. Prinz, U. Walschus, S. Lucke, M. Patrzyk, L. Wilhelm, H.G. Neumann, M. Schlosser, In vivo evaluation of copper release and acute local tissue reactions after implantation of copper-coated titanium implants in rats, *Biomed. Mater.* 8 (2013). doi:10.1088/1748-6041/8/3/035009.
- [351] W. Zhu, Z. Zhang, B. Gu, J. Sun, L. Zhu, Biological Activity and Antibacterial Property of Nano-structured TiO₂Coating Incorporated with Cu Prepared by Micro-arc Oxidation, *J. Mater. Sci. Technol.* 29 (2013) 237–244. doi:10.1016/j.jmst.2012.12.015.
- [352] B. Nablo, M.S.- Biomaterials, undefined 2005, In vitro cytotoxicity of nitric oxide-releasing sol-gel derived materials, Elsevier. (n.d.).

- <https://www.sciencedirect.com/science/article/pii/S0142961204009974> (accessed January 20, 2020).
- [353] S. Deupree, M.S.-A. biomaterialia, undefined 2009, Morphological analysis of the antimicrobial action of nitric oxide on Gram-negative pathogens using atomic force microscopy, Elsevier. (n.d.).
<https://www.sciencedirect.com/science/article/pii/S1742706109000361> (accessed January 20, 2020).
- [354] E.M. Hetrick, H.L. Prichard, B. Klitzman, M.H. Schoenfisch, Reduced foreign body response at nitric oxide-releasing subcutaneous implants, *Biomaterials*. 28 (2007) 4571–4580. doi:10.1016/j.biomaterials.2007.06.036.
- [355] B.J. Nablo, M.H. Schoenfisch, Poly(vinyl chloride)-coated sol-gels for studying the effects of nitric oxide release on bacterial adhesion, *Biomacromolecules*. 5 (2004) 2034–2041. doi:10.1021/bm049727w.
- [356] B.J. Nablo, M.H. Schoenfisch, Antibacterial properties of nitric oxide-releasing sol-gels, *J. Biomed. Mater. Res.* 67A (2003) 1276–1283. doi:10.1002/jbm.a.20030.
- [357] B.J. Nablo, H.L. Prichard, R.D. Butler, B. Klitzman, M.H. Schoenfisch, Inhibition of implant-associated infections via nitric oxide release, *Biomaterials*. 26 (2005) 6984–6990. doi:10.1016/j.biomaterials.2005.05.017.
- [358] N. Naghavi, A. de Mel, O.S. Alavijeh, B.G. Cousins, A.M. Seifalian, Nitric Oxide Donors for Cardiovascular Implant Applications, *Small*. 9 (2013) 22–35. doi:10.1002/sml.201200458.
- [359] B.J. Nablo, A.R. Rothrock, M.H. Schoenfisch, Nitric oxide-releasing sol-gels as antibacterial coatings for orthopedic implants, *Biomaterials*. 26 (2005) 917–924. doi:10.1016/j.biomaterials.2004.03.031.
- [360] J. Holt, B. Hertzberg, P. Weinhold, W. Storm, M. Schoenfisch, L. Dahners, Decreasing bacterial colonization of external fixation pins via nitric oxide release coatings, *J Orthop Trauma*. 25 (2011) 432–437. doi:10.1097/BOT.0b013e3181f9ac8a.
- [361] P.A. Dearnley, K.L. Dahm, H. Çimenoğlu, The corrosion-wear behaviour of thermally oxidised CP-Ti and Ti-6Al-4V, *Wear*. 256 (2004) 469–479. doi:10.1016/S0043-1648(03)00557-X.
- [362] F. Borgioli, E. Galvanetto, F. Iozzelli, G. Pradelli, Improvement

- of wear resistance of Ti-6Al-4V alloy by means of thermal oxidation, *Mater. Lett.* 59 (2005) 2159–2162. doi:10.1016/j.matlet.2005.02.054.
- [363] H. Guleryuz, H. Cimenoglu, Surface modification of a Ti-6Al-4V alloy by thermal oxidation, *Surf. Coatings Technol.* 192 (2005) 164–170. doi:10.1016/j.surfcoat.2004.05.018.
- [364] J. Xia, C.X. Li, H. Dong, T. Bell, Nanoindentation and nanoscratch properties of a thermal oxidation treated γ -TiAl based alloy, *Surf. Coatings Technol.* 200 (2006) 4755–4762. doi:10.1016/j.surfcoat.2005.04.031.
- [365] D. Siva Rama Krishna, Y.L. Brama, Y. Sun, Thick rutile layer on titanium for tribological applications, *Tribol. Int.* 40 (2007) 329–334. doi:10.1016/j.triboint.2005.08.004.
- [366] M.C. García-Alonso, L. Saldaña, G. Vallés, J.L. González-Carrasco, J. González-Cabrero, M.E. Martínez, E. Gil-Garay, L. Munuera, In vitro corrosion behaviour and osteoblast response of thermally oxidised Ti6Al4V alloy., *Biomaterials.* 24 (2003) 19–26. doi:10.1016/s0142-9612(02)00237-5.
- [367] K. Aniołek, The influence of thermal oxidation parameters on the growth of oxide layers on titanium, *Vacuum.* 144 (2017) 94–100. doi:10.1016/j.vacuum.2017.07.023.
- [368] C.A.H. Laurindo, C.M. Lepienski, F.L. Amorim, R.D. Torres, P. Soares, Tribology Transactions Mechanical and Tribological Properties of Ca/ P-Doped Titanium Dioxide Layer Produced by Plasma Electrolytic Oxidation: Effects of Applied Voltage and Heat Treatment Mechanical and Tribological Properties of Ca/P-Doped Titanium Dioxide Layer Produced by Plasma Electrolytic Oxidation: Effects of Applied Voltage and Heat Treatment, (2018). doi:10.1080/10402004.2017.1404176.
- [369] Bertuccioli, Garzoni, Martini, Morri, Rondelli, Plasma Electrolytic Oxidation (PEO) Layers from Silicate/Phosphate Baths on Ti-6Al-4V for Biomedical Components: Influence of Deposition Conditions and Surface Finishing on Dry Sliding Behaviour, *Coatings.* 9 (2019) 614. doi:10.3390/coatings9100614.
- [370] A.F. Yetim, Investigation of wear behavior of titanium oxide films, produced by anodic oxidation, on commercially pure titanium in vacuum conditions, *Surf. Coatings Technol.* 205 (2010) 1757–1763. doi:10.1016/j.surfcoat.2010.08.079.

- [371] D. Siva Rama Krishna, Y.L. Brama, Y. Sun, Thick rutile layer on titanium for tribological applications, *Tribol. Int.* 40 (2007) 329–334. doi:10.1016/j.triboint.2005.08.004.
- [372] K. Aniolek, M. Kupka, A.B.- Wear, undefined 2016, Sliding wear resistance of oxide layers formed on a titanium surface during thermal oxidation, Elsevier. (n.d.). <https://www.sciencedirect.com/science/article/pii/S004316481600079X> (accessed April 14, 2020).
- [373] C. Fei, Z. Hai, C. Chen, X. Yangjian, Study on the tribological performance of ceramic coatings on titanium alloy surfaces obtained through microarc oxidation, *Prog. Org. Coatings.* 64 (2009) 264–267. doi:10.1016/j.porgcoat.2008.08.034.
- [374] S. Durdu, M.U.-C. International, undefined 2014, The tribological properties of bioceramic coatings produced on Ti6Al4V alloy by plasma electrolytic oxidation, Elsevier. (n.d.). <https://www.sciencedirect.com/science/article/pii/S0272884213011656> (accessed April 14, 2020).
- [375] L. Ceschini, E. Lanzoni, C. Martini, D. Prandstraller, G. Sambogna, Comparison of dry sliding friction and wear of Ti6Al4V alloy treated by plasma electrolytic oxidation and PVD coating, *Wear.* 264 (2008) 86–95. doi:10.1016/j.wear.2007.01.045.
- [376] J.X. Liu, D.Z. Yang, F. Shi, Y.J. Cai, Sol-gel deposited TiO₂ film on NiTi surgical alloy for biocompatibility improvement, *Thin Solid Films.* 429 (2003) 225–230. doi:10.1016/S0040-6090(03)00146-9.
- [377] W. Zhang, W. Liu, Y. Liu, C.W.-C. International, undefined 2009, Tribological behaviors of single and dual sol–gel ceramic films on Ti–6Al–4V, Elsevier. (n.d.). <https://www.sciencedirect.com/science/article/pii/S0272884208002678> (accessed January 29, 2020).
- [378] W. Zhang, C. Wang, W. Liu, Characterization and tribological investigation of sol-gel ceramic films on Ti-6Al-4V, *Wear.* 260 (2006) 379–386. doi:10.1016/j.wear.2005.05.006.
- [379] W. Zhang, W. Liu, B. Li, G. Mai, Characterization and Tribological Investigation of Sol-Gel Titania and Doped Titania Thin Films, *J. Am. Ceram. Soc.* 85 (2004) 1770–1776. doi:10.1111/j.1151-2916.2002.tb00351.x.
- [380] L. Mohan, M. Chakraborty, S. Viswanathan, C. Mandal, P.

- Bera, S.T. Aruna, C. Anandan, Corrosion, wear, and cell culture studies of oxygen ion implanted Ni-Ti alloy, *Surf. Interface Anal.* 49 (2017) 828–836. doi:10.1002/sia.6229.
- [381] Y.X. Leng, J.Y. Chen, Z.M. Zeng, X.B. Tian, P. Yang, N. Huang, Z.R. Zhou, P.K. Chu, Properties of titanium oxide biomaterials synthesized by titanium plasma immersion ion implantation and reactive ion oxidation, *Thin Solid Films.* 377–378 (2000) 573–577. doi:10.1016/S0040-6090(00)01306-7.
- [382] L. Mohan, C. Anandan, Wear and corrosion behavior of oxygen implanted biomedical titanium alloy Ti-13Nb-13Zr, *Appl. Surf. Sci.* 282 (2013) 281–290. doi:10.1016/j.apsusc.2013.05.120.
- [383] X. Tian, C. Gong, S. Yang, Z. Luo, R.K.Y. Fu, P.K. Chu, Oxygen plasma ion implantation of biomedical titanium alloy, *IEEE Trans. Plasma Sci.* 34 (2006) 1235–1240. doi:10.1109/TPS.2006.879002.
- [384] M. Fazel, H.R. Salimijazi, M.A. Golozar, M.R. Garsivaz Jazi, A comparison of corrosion, tribocorrosion and electrochemical impedance properties of pure Ti and Ti6Al4V alloy treated by micro-arc oxidation process, *Appl. Surf. Sci.* 324 (2015) 751–756. doi:10.1016/j.apsusc.2014.11.030.
- [385] Y. Wang, T. Lei, L. Guo, B. Jiang, Fretting wear behaviour of microarc oxidation coatings formed on titanium alloy against steel in unlubrication and oil lubrication, *Appl. Surf. Sci.* 252 (2006) 8113–8120. doi:10.1016/j.apsusc.2005.10.032.
- [386] S. Sathish, M. Geetha, S.T. Aruna, N. Balaji, K.S. Rajam, R. Asokamani, Sliding wear behavior of plasma sprayed nanoceramic coatings for biomedical applications, *Wear.* 271 (2011) 934–941. doi:10.1016/j.wear.2011.03.023.
- [387] S. Wang, Q. Zhao, D. Liu, N. Du, Microstructure and elevated temperature tribological behavior of TiO₂/Al₂O₃ composite ceramic coating formed by microarc oxidation of Ti6Al4V alloy, *Surf. Coatings Technol.* 272 (2015) 343–349. doi:10.1016/j.surfcoat.2015.03.044.
- [388] A.M. Maurer, S.A. Brown, J.H. Payer, K. Merritt, J.S. Kawalec, Reduction of fretting corrosion of Ti-6Al-4V by various surface treatments, *J. Orthop. Res.* 11 (1993) 865–873. doi:10.1002/jor.1100110613.
- [389] K.W.K. Yeung, R.W.Y. Poon, P.K. Chu, C.Y. Chung, X.Y. Liu, W.W. Lu, D. Chan, S.C.W. Chan, K.D.K. Luk, K.M.C. Cheung,

- Surface mechanical properties, corrosion resistance, and cytocompatibility of nitrogen plasma-implanted nickel-titanium alloys: A comparative study with commonly used medical grade materials, *J. Biomed. Mater. Res. - Part A*. 82 (2007) 403–414. doi:10.1002/jbm.a.31154.
- [390] E.Y. Gutmanas, I. Gotman, PIRAC Ti nitride coated Ti-6Al-4V head against UHMWPE acetabular cup-hip wear simulator study., *J. Mater. Sci. Mater. Med.* 15 (2004) 327–30. doi:10.1023/b:jmsm.0000021096.77850.c5.
- [391] D.M. Gordin, T. Gloriant, V. Chane-Pane, D. Busardo, V. Mitran, D. Höche, C. Vasilescu, S.I. Drob, A. Cimpean, Surface characterization and biocompatibility of titanium alloys implanted with nitrogen by Hardion+ technology, *J. Mater. Sci. Mater. Med.* 23 (2012) 2953–2966. doi:10.1007/s10856-012-4750-z.
- [392] W. Dawihl, *Transition Metal Carbides and Nitrides*. Von L. E. Toth. Academic Press, New York–London 1971. 1. Aufl., XIII, 279 S., zahlr. Abb. u. Tab., geb. \$ 16.50, *Angew. Chemie*. 84 (1972) 960–960. doi:10.1002/ange.19720841920.
- [393] R.P. Van Hove, I.N. Sierevelt, B.J. Van Royen, P.A. Nolte, Titanium-Nitride Coating of Orthopaedic Implants: A Review of the Literature, *Biomed Res. Int.* 2015 (2015). doi:10.1155/2015/485975.
- [394] J. Narayan, W.D. Fan, R.J. Narayan, P. Tiwari, H.H. Stadelmaier, Diamond, diamond-like and titanium nitride biocompatible coatings for human body parts, *Mater. Sci. Eng. B*. 25 (1994) 5–10. doi:10.1016/0921-5107(94)90193-7.
- [395] P. Budzynski, A.A. Youssef, J. Sielanko, Surface modification of Ti-6Al-4V alloy by nitrogen ion implantation, *Wear*. 261 (2006) 1271–1276. doi:10.1016/j.wear.2006.03.008.
- [396] R. Venugopalan, J.J. Weimer, M.A. George, L.C. Lucas, The effect of nitrogen diffusion hardening on the surface chemistry and scratch resistance of Ti-6Al-4V alloy, *Biomaterials*. 21 (2000) 1669–1677. doi:10.1016/S0142-9612(00)00049-1.
- [397] J.A. Hendry, R.M. Pilliar, The fretting corrosion resistance of PVD surface-modified orthopedic implant alloys., *J. Biomed. Mater. Res.* 58 (2001) 156–66. doi:10.1002/1097-4636(2001)58:2<156::aid-jbm1002>3.0.co;2-h.
- [398] P. MJ, M. G, B. FF, Titanium Nitride Ceramic Films Against

- Polyethylene, *Clin. Orthop. Relat. Res.* 317 (1995) 64–70. <http://www.ncbi.nlm.nih.gov/pubmed/7671497> (accessed January 30, 2020).
- [399] C.D. Peterson, B.M. Hillberry, D.A. Heck, Component wear of total knee prostheses using Ti-6Al-4V, titanium nitride coated Ti-6Al-4V, and cobalt-chromium-molybdenum femoral components, *J. Biomed. Mater. Res.* 22 (1988) 887–903. doi:10.1002/jbm.820221005.
- [400] J. Komotori, B.J. Lee, H. Dong, P.A. Dearnley, Corrosion response of surface engineered titanium alloys damaged by prior abrasion, *Wear.* 250 (2001) 1239–1249. doi:10.1016/S0043-1648(01)00753-0.
- [401] S.N. Massoud, J.B. Hunter, B.J. Holdsworth, W.A. Wallace, R. Juliusson, EARLY FEMORAL LOOSENING IN ONE DESIGN OF CEMENTED HIP REPLACEMENT, 1997.
- [402] M.K. Harman, S.A. Banks, W.A. Hodge, Wear analysis of a retrieved hip implant with titanium nitride coating., *J. Arthroplasty.* 12 (1997) 938–45. doi:10.1016/s0883-5403(97)90164-9.
- [403] M. Raimondi, R.P.- Biomaterials, undefined 2000, The in-vivo wear performance of prosthetic femoral heads with titanium nitride coating, Elsevier. (n.d.). <https://www.sciencedirect.com/science/article/pii/S014296129900246X> (accessed January 30, 2020).
- [404] S. Datta, M. Das, V.K. Balla, S. Bodhak, V.K. Murugesan, Mechanical, wear, corrosion and biological properties of arc deposited titanium nitride coatings, *Surf. Coatings Technol.* 344 (2018) 214–222. doi:10.1016/j.surfcoat.2018.03.019.
- [405] Danişman, D. Odabas, M. Teber, The Effect of Coatings on the Wear Behavior of Ti6Al4V Alloy Used in Biomedical Applications, in: *IOP Conf. Ser. Mater. Sci. Eng.*, Institute of Physics Publishing, 2018. doi:10.1088/1757-899X/295/1/012044.
- [406] M. Łępicka, M. Grądzka-Dahlke, D. Pieniak, K. Pasierbiewicz, K. Kryńska, A. Niewczas, Tribological performance of titanium nitride coatings: A comparative study on TiN-coated stainless steel and titanium alloy, *Wear.* 422–423 (2019) 68–80. doi:10.1016/j.wear.2019.01.029.
- [407] C. Liu, Q. Bi, A. Matthews, Tribological and electrochemical performance of PVD TiN coatings the femoral head of Ti-6Al-4V

- artificial joints, *Surf. Coatings Technol.* 163–164 (2003) 597–604. doi:10.1016/S0257-8972(02)00630-8.
- [408] A. Vadiraj, M. Kamaraj, Characterization of fretting fatigue damage of PVD TiN coated biomedical titanium alloys, *Surf. Coatings Technol.* 200 (2006) 4538–4542. doi:10.1016/j.surfcoat.2005.03.036.
- [409] Y. Luo, S. Ge, Fretting wear behavior of nitrogen ion implanted titanium alloys in bovine serum lubrication, *Tribol. Int.* 42 (2009) 1373–1379. doi:10.1016/j.triboint.2009.04.009.
- [410] X. Wang, S. Bai, F. Li, D. Li, J. Zhang, M. Tian, Q. Zhang, Y. Tong, Z. Zhang, G. Wang, T. Guo, C. Ma, Effect of plasma nitriding and titanium nitride coating on the corrosion resistance of titanium, *J. Prosthet. Dent.* 116 (2016) 450–456. doi:10.1016/j.prosdent.2016.01.016.
- [411] F. Movassagh-Alanagh, A. Abdollah-zadeh, M. Aliofkhazraei, M. Abedi, Improving the wear and corrosion resistance of Ti–6Al–4V alloy by deposition of TiSiN nanocomposite coating with pulsed-DC PACVD, *Wear.* 390–391 (2017) 93–103. doi:10.1016/j.wear.2017.07.009.
- [412] M.K. Lei, Y.X. Ou, K.S. Wang, L. Chen, Wear and corrosion properties of plasma-based low-energy nitrogen ion implanted titanium, *Surf. Coatings Technol.* 205 (2011) 4602–4607. doi:10.1016/j.surfcoat.2011.03.141.
- [413] M. Mubarak Ali, S. Ganesh Sundara Raman, S.D. Pathak, R. Gnanamoorthy, Influence of plasma nitriding on fretting wear behaviour of Ti-6Al-4V, *Tribol. Int.* 43 (2010) 152–160. doi:10.1016/j.triboint.2009.05.020.
- [414] R.H.-D. and related materials, undefined 2003, A review of modified DLC coatings for biological applications, Elsevier. (n.d.).
<https://www.sciencedirect.com/science/article/pii/S0925963503000815> (accessed January 31, 2020).
- [415] N. Sanchez, C. Rincon, G. Zambrano, H.G.-T.S. Films, undefined 2000, Characterization of diamond-like carbon (DLC) thin films prepared by rf magnetron sputtering, Elsevier. (n.d.).
<https://www.sciencedirect.com/science/article/pii/S004060900010907> (accessed January 31, 2020).
- [416] R. Kalish, Y. Lifshitz, K. Nugent, S. Praver, Thermal stability and relaxation in diamond-like-carbon. A Raman study of films

- with different sp³ fractions (ta-C to a-C), *Appl. Phys. Lett.* 74 (1999) 2936–2938. doi:10.1063/1.123971.
- [417] V.S. De Viteri, M.G. Barandika, U.R. De Gopegui, R. Bayón, C. Zubizarreta, X. Fernández, A. Igartua, F. Agullo-Rueda, Characterization of Ti-C-N coatings deposited on Ti6Al4V for biomedical applications, in: *J. Inorg. Biochem.*, 2012: pp. 359–366. doi:10.1016/j.jinorgbio.2012.09.012.
- [418] D. Du, D. Liu, Z. Ye, X. Zhang, F. Li, Z. Zhou, L. Yu, Fretting wear and fretting fatigue behaviors of diamond-like carbon and graphite-like carbon films deposited on Ti-6Al-4V alloy, *Appl. Surf. Sci.* 313 (2014) 462–469. doi:10.1016/j.apsusc.2014.06.006.
- [419] R. Bayón, A. Igartua, J.J. González, U. Ruiz De Gopegui, Influence of the carbon content on the corrosion and tribocorrosion performance of Ti-DLC coatings for biomedical alloys, *Tribol. Int.* 88 (2015) 115–125. doi:10.1016/j.triboint.2015.03.007.
- [420] S. Zhang, X.L. Bui, Y. Fu, D.L. Butler, H. Du, Bias-graded deposition of diamond-like carbon for tribological applications, *Diam. Relat. Mater.* 13 (2004) 867–871. doi:10.1016/j.diamond.2003.10.043.
- [421] P. Wang, X. Wang, Y. Chen, G. Zhang, W. Liu, J. Zhang, The effect of applied negative bias voltage on the structure of Ti-doped a-C:H films deposited by FCVA, *Appl. Surf. Sci.* 253 (2007) 3722–3726. doi:10.1016/j.apsusc.2006.08.003.
- [422] J.B. Cai, X.L. Wang, W.Q. Bai, X.Y. Zhao, T.Q. Wang, J.P. Tu, Bias-graded deposition and tribological properties of Ti-contained a-C gradient composite film on Ti6Al4V alloy, *Appl. Surf. Sci.* 279 (2013) 450–457. doi:10.1016/j.apsusc.2013.04.136.
- [423] H. Dong, W. Shi, T. Bell, Potential of improving tribological performance of UHMWPE by engineering the Ti6Al4V counterfaces, *Wear.* 225–229 (1999) 146–153. doi:10.1016/S0043-1648(98)00356-1.
- [424] B. Shi, O.O. Ajayi, G. Fenske, A. Erdemir, H. Liang, Tribological performance of some alternative bearing materials for artificial joints, *Wear.* 255 (2003) 1015–1021. doi:10.1016/S0043-1648(03)00276-X.
- [425] R.K. Roy, K.-R. Lee, Biomedical applications of diamond-like carbon coatings: A review, *J. Biomed. Mater. Res. Part B Appl. Biomater.* 83B (2007) 72–84. doi:10.1002/jbm.b.30768.

- [426] G. Taeger, L.E. Podleska, B. Schmidt, M. Ziegler, D. Nast-Kolb, Comparison of Diamond-Like-Carbon and Alumina-Oxide articulating with Polyethylene in Total Hip Arthroplasty, *Materwiss. Werksttech.* 34 (2003) 1094–1100. doi:10.1002/mawe.200300717.
- [427] D. Sheeja, B.K. Tay, S.P. Lau, L.N. Nung, Tribological characterisation of diamond-like carbon coatings on Co-Cr-Mo alloy for orthopaedic applications, *Surf. Coatings Technol.* 146–147 (2001) 410–416. doi:10.1016/S0257-8972(01)01425-6.
- [428] K.C. Walter, M. Nastasi, C. Munson, Adherent diamond-like carbon coatings on metals via plasma source ion implantation, *Surf. Coatings Technol.* 93 (1997) 287–291. doi:10.1016/S0257-8972(97)00062-5.
- [429] A. Granek, M. Monika, D. Ozimina, Diamond-like carbon films for use in medical implants ARTICLES YOU MAY BE INTERESTED IN The influence of non-toxic cutting fluid on the diamond-like carbon coatings AIP Conference Impedance-based method of transverse fault location in medium voltage cables AIP Conference Diamond-Like Carbon Films for Use in Medical Implants, (2017) 20001. doi:10.1063/1.5056269.
- [430] S.K. KIM, J.B. LEE, J.Y. KOAK, S.J. HEO, K.R. LEE, L.R. CHO, S.S. LEE, An abutment screw loosening study of a Diamond Like Carbon-coated CP titanium implant, *J. Oral Rehabil.* 32 (2005) 346–350. doi:10.1111/j.1365-2842.2004.01475.x.
- [431] D. He, S. Zheng, J. Pu, G. Zhang, L. Hu, Improving tribological properties of titanium alloys by combining laser surface texturing and diamond-like carbon film, *Tribol. Int.* 82 (2015) 20–27. doi:10.1016/j.triboint.2014.09.017.
- [432] W.Q. Bai, J.B. Cai, X.L. Wang, D.H. Wang, C.D. Gu, J.P. Tu, Mechanical and tribological properties of a-C/a-C:Ti multilayer films with various bilayer periods, *Thin Solid Films.* 558 (2014) 176–183. doi:10.1016/j.tsf.2014.03.039.
- [433] J.B. Cai, X.L. Wang, W.Q. Bai, D.H. Wang, C.D. Gu, J.P. Tu, Microstructure, mechanical and tribological properties Of A-C/A-C:Ti nanomultilayer film, *Surf. Coatings Technol.* 232 (2013) 403–411. doi:10.1016/j.surfcoat.2013.05.042.
- [434] J.F. Watts, J. Wolstenholme, *An Introduction to Surface Analysis by XPS and AES*, John Wiley & Sons, Ltd, Chichester,

- UK, 2003. doi:10.1002/0470867930.
- [435] J.I. Goldstein, D.E. Newbury, P. Echlin, D.C. Joy, C. Fiori, E. Lifshin, J.I. Goldstein, D.E. Newbury, P. Echlin, D.C. Joy, C. Fiori, E. Lifshin, Introduction, in: *Scanning Electron Microsc. X-Ray Microanal.*, Springer US, 1981: pp. 1–18. doi:10.1007/978-1-4613-3273-2_1.
- [436] Scanning Electron Microscopy (SEM) Technology Overview, (n.d.). <https://www.nanoimages.com/sem-technology-overview/> (accessed April 22, 2020).
- [437] V. Goriainov, R. Cook, J.M. Latham, D.G. Dunlop, R.O.C. Oreffo, Bone and metal: An orthopaedic perspective on osseointegration of metals, *Acta Biomater.* 10 (2014) 4043–4057. doi:10.1016/j.actbio.2014.06.004.
- [438] A. Mendonça Munhoz, F. Santanelli di Pompeo, R. De Mezerville, Nanotechnology, nanosurfaces and silicone gel breast implants: current aspects, *Case Reports Plast. Surg. Hand Surg.* 4 (2017) 99–113. doi:10.1080/23320885.2017.1407658.
- [439] A.K. Singh, Experimental Methodologies for the Characterization of Nanoparticles, in: *Eng. Nanoparticles*, Elsevier, 2016: pp. 125–170. doi:10.1016/b978-0-12-801406-6.00004-2.
- [440] M. Lorenzetti, G. Bernardini, T. Luxbacher, A. Santucci, S. Kobe, S. Novak, Surface properties of nanocrystalline TiO₂ coatings in relation to the in vitro plasma protein adsorption., *Biomed. Mater.* 10 (2015) 045012. doi:10.1088/1748-6041/10/4/045012.
- [441] B.S. Necula, I. Apachitei, F.D. Tichelaar, L.E. Fratila-Apachitei, J. Duszczyk, An electron microscopical study on the growth of TiO₂-Ag antibacterial coatings on Ti6Al7Nb biomedical alloy, *Acta Biomater.* 7 (2011) 2751–2757. doi:10.1016/j.actbio.2011.02.037.
- [442] K.M. Lee, K.R. Shin, S. Namgung, B. Yoo, D.H. Shin, Electrochemical response of ZrO₂-incorporated oxide layer on AZ91 Mg alloy processed by plasma electrolytic oxidation, *Surf. Coatings Technol.* 205 (2011) 3779–3784. doi:10.1016/j.surfcoat.2011.01.033.
- [443] X. Lu, C. Blawert, M.L. Zheludkevich, K.U. Kainer, Insights into plasma electrolytic oxidation treatment with particle addition,

Corros. Sci. 101 (2015) 201–207.
doi:10.1016/j.corsci.2015.09.016.

- [444] E. Matykina, R. Arrabal, P. Skeldon, G.E. Thompson, Transmission electron microscopy of coatings formed by plasma electrolytic oxidation of titanium, *Acta Biomater.* 5 (2009) 1356–1366. doi:10.1016/j.actbio.2008.10.007.
- [445] K. Rokosz, T. Hryniewicz, D. Matysek, S. Raaen, J. Valíček, Ł. Dudek, M. Harničárová, SEM, EDS and XPS analysis of the coatings obtained on titanium after plasma electrolytic oxidation in electrolytes containing copper nitrate, *Materials (Basel)*. 9 (2016) 9–16. doi:10.3390/ma9050318.
- [446] Y. Han, D. Chen, J. Sun, Y. Zhang, K. Xu, UV-enhanced bioactivity and cell response of micro-arc oxidized titania coatings, *Acta Biomater.* 4 (2008) 1518–1529. doi:10.1016/J.ACTBIO.2008.03.005.
- [447] T.K. Sham, M.S. Lazarus, X-ray photoelectron spectroscopy (XPS) studies of clean and hydrated TiO₂ (rutile) surfaces, *Chem. Phys. Lett.* 68 (1979) 426–432. doi:10.1016/0009-2614(79)87231-0.
- [448] T. Kasuga, H. Kondo, M. Nogami, Apatite formation on TiO₂ in simulated body fluid, *J. Cryst. Growth.* 235 (2002) 235–240. doi:10.1016/S0022-0248(01)01782-1.
- [449] F.M.F. de Groot, M. Grioni, J.C. Fuggle, J. Ghijsen, G.A. Sawatzky, H. Petersen, Oxygen 1 *s* x-ray-absorption edges of transition-metal oxides, *Phys. Rev. B.* 40 (1989) 5715–5723. doi:10.1103/PhysRevB.40.5715.
- [450] M. Drabik, A. Choukourov, A. Artemenko, O. Polonskyi, O. Kylian, J. Kousal, L. Nichtova, V. Cimrova, D. Slavinska, H. Biederman, Structure and composition of titanium nanocluster films prepared by a gas aggregation cluster source, *J. Phys. Chem. C.* 115 (2011) 20937–20944. doi:10.1021/jp2059485.
- [451] T.A. Al-Dhahir, Quantitative Phase Analysis for Titanium Dioxide From X-Ray Powder. Diffraction Data Using The Rietveld Method Quantitative Phase Analysis for Titanium Dioxide From X-Ray Powder Diffraction Data Using The Rietveld Method, 9 (2013). <https://www.iasj.net/iasj?func=fulltext&aId=73258> (accessed July 29, 2019).
- [452] J. Li, X. Liu, Y. Qiao, H. Zhu, C. Ding, Antimicrobial activity and

- cytocompatibility of Ag plasma-modified hierarchical TiO₂ film on titanium surface, *Colloids Surfaces B Biointerfaces*. 113 (2014) 134–145. doi:10.1016/J.COLSURFB.2013.08.030.
- [453] J.E. Collazos-Castro, A.M. Cruz, M. Carballo-Vila, M. Lira-Cantú, L. Abad, Á.P. del Pino, J. Fraxedas, A.S. Juan, C. Fonseca, A.P. Pêgo, N. Casañ-Pastor, *Thin solid films.*, Elsevier, n.d.
https://www.academia.edu/14229076/Neural_cell_growth_on_TiO2_anatase_nanostructured_surfaces (accessed June 4, 2019).
- [454] H.-K. Tsou, P.-Y. Hsieh, M.-H. Chi, C.-J. Chung, J.-L. He, Improved osteoblast compatibility of medical-grade polyetheretherketone using arc ionplated rutile/anatase titanium dioxide films for spinal implants, *J Biomed Mater Res Part A*. 100 (2012) 2787–2792. doi:10.1002/jbm.a.34215.
- [455] J. Bico, U. Thiele, D. Quéré, Wetting of textured surfaces, *Colloids Surfaces A Physicochem. Eng. Asp.* 206 (2002) 41–46. doi:10.1016/S0927-7757(02)00061-4.
- [456] P. Soares, A. Mikowski, C.M. Lepiński, E. Santos, G.A. Soares, V. Swinka Filho, N.K. Kuromoto, Hardness and elastic modulus of TiO₂ anodic films measured by instrumented indentation, *J. Biomed. Mater. Res. - Part B Appl. Biomater.* 84 (2008) 524–530. doi:10.1002/jbm.b.30900.
- [457] R. Kumar, H. Münstedt, Silver ion release from antimicrobial polyamide/silver composites, *Biomaterials*. 26 (2005) 2081–2088. doi:10.1016/j.biomaterials.2004.05.030.
- [458] K. Tweden, J. Cameron, ... A.R.-T.J. of heart, undefined 1997, Biocompatibility of silver-modified polyester for antimicrobial protection of prosthetic valves., *Europepmc.Org.* (n.d.). <https://europepmc.org/abstract/med/9330181> (accessed June 4, 2019).
- [459] A. de la R. Brutel, ... K.D.-T.J. of heart, undefined 2000, First clinical experience with a mechanical valve with silver coating., *Europepmc.Org.* (n.d.). <https://europepmc.org/abstract/med/10678384> (accessed June 4, 2019).
- [460] A. Panáček, L. Kvítek, M. Smékalová, R. Večeřová, M. Kolář, M. Röderová, F. Dyčka, M. Šebela, R. Pucek, O. Tomanec, R. Zbořil, Bacterial resistance to silver nanoparticles and how to overcome it, *Nat. Nanotechnol.* 13 (2018) 65–71.

doi:10.1038/s41565-017-0013-y.

- [461] D. Teker, F. Muhaffel, M. Menekse, N.G. Karaguler, M. Baydogan, H. Cimenoglu, Characteristics of multi-layer coating formed on commercially pure titanium for biomedical applications, *Mater. Sci. Eng. C.* 48 (2015) 579–585. doi:10.1016/j.msec.2014.12.058.
- [462] F. Muhaffel, G. Cempura, M. Menekse, A. Czyska-Filemonowicz, N. Karaguler, H. Cimenoglu, Characteristics of multi-layer coatings synthesized on Ti6Al4V alloy by micro-arc oxidation in silver nitrate added electrolytes, *Surf. Coatings Technol.* 307 (2016) 308–315. doi:10.1016/j.surfcoat.2016.09.002.
- [463] H. Cimenoglu, M. Gunyuz, G.T. Kose, M. Baydogan, F. Uğurlu, C. Sener, Micro-arc oxidation of Ti6Al4V and Ti6Al7Nb alloys for biomedical applications, *Mater. Charact.* 62 (2011) 304–311. doi:10.1016/j.matchar.2011.01.002.
- [464] S. Durdu, M. Usta, A.S. Berkem, Bioactive coatings on Ti6Al4V alloy formed by plasma electrolytic oxidation, *Surf. Coatings Technol.* 301 (2016) 85–93. doi:10.1016/j.surfcoat.2015.07.053.
- [465] M. Thukkaram, P. Cools, A. Nikiforov, P. Rigole, T. Coenye, P. Van Der Voort, G. Du Laing, C. Vercruyssen, H. Declercq, R. Morent, L. De Wilde, P. De Baets, K. Verbeken, N. De Geyter, Antibacterial activity of a porous silver doped TiO₂ coating on titanium substrates synthesized by plasma electrolytic oxidation, *Appl. Surf. Sci.* 500 (2020). doi:10.1016/j.apsusc.2019.144235.
- [466] H. Hu, W. Zhang, Y. Qiao, X. Jiang, X. Liu, C. Ding, Antibacterial activity and increased bone marrow stem cell functions of Zn-incorporated TiO₂ coatings on titanium, *Acta Biomater.* 8 (2012) 904–915. doi:10.1016/j.actbio.2011.09.031.
- [467] R.B. Shalvoy, G.B. Fisher, P.J. Stiles, Bond ionicity and structural stability of some average-valence-five materials studied by x-ray photoemission, *Phys. Rev. B.* 15 (1977) 1680–1697. doi:10.1103/PhysRevB.15.1680.
- [468] Y. Liu, R.G. Jordan, S.L. Qiu, Electronic structures of ordered Ag-Mg alloys, *Phys. Rev. B.* 49 (1994) 4478–4484. doi:10.1103/PhysRevB.49.4478.
- [469] J.F. Moulder, W.F. Stickle, P.E. Sobol, K.D. Bomben, J. Chastain, *Handbook of X-ray Photoelectron Spectroscopy*

A Reference Book of Standard Spectra for Identification and Interpretation of XPS Data, n.d. <https://www.cnyn.unam.mx/~wencil/XPS/MANXPS.pdf> (accessed September 24, 2019).

- [470] X. Zhu, J. Chen, L. Scheideler, R. Reichl, J. Geis-Gerstorfer, Effects of topography and composition of titanium surface oxides on osteoblast responses, *Biomaterials*. 25 (2004) 4087–4103. doi:10.1016/J.BIOMATERIALS.2003.11.011.
- [471] F. López-Huerta, B. Cervantes, O. González, J. Hernández-Torres, L. García-González, R. Vega, A.L. Herrera-May, E. Soto, Biocompatibility and surface properties of TiO₂ thin films deposited by DC magnetron sputtering, *Materials (Basel)*. 7 (2014) 4105–4117. doi:10.3390/ma7064105.
- [472] M. Carballo-Vila, B. Moreno-Burriel, E. Chinarro, J.R. Jurado, N. Casañ-Pastor, J.E. Collazos-Castro, Titanium oxide as substrate for neural cell growth, *J. Biomed. Mater. Res. - Part A*. 90 (2009) 94–105. doi:10.1002/jbm.a.32058.
- [473] S. Durdu, Ö.F. Deniz, I. Kutbay, M. Usta, Characterization and formation of hydroxyapatite on Ti6Al4V coated by plasma electrolytic oxidation, *J. Alloys Compd*. 551 (2013) 422–429. doi:10.1016/j.jallcom.2012.11.024.
- [474] A. V. Stanishevsky, S. Holliday, Mechanical properties of sol-gel calcium titanate bioceramic coatings on titanium, *Surf. Coatings Technol*. 202 (2007) 1236–1241. doi:10.1016/j.surfcoat.2007.07.091.
- [475] W.C. Oliver, R. Hutchings, J.B. Pethica, WEAR BEHAVIOR OF NITROGEN-IMPLANTED METALS., *Metall. Trans. A, Phys. Metall. Mater. Sci*. 15 A (1984) 2221–2229. doi:10.1007/BF02647105.
- [476] H. Nasiri Vatan, R. Ebrahimi-Kahrizsangi, M. Kasiri-Asgarani, Wear and corrosion performance of peo-synthesized sic nanocomposite coatings: Effect of processing time and current density, *Int. J. Electrochem. Sci*. 11 (2016) 5631–5654. doi:10.20964/2016.07.17.
- [477] J. Li, X. Zhang, J. Wang, H. Li, J. Huang, D. Xiong, Frictional properties of silver over-coated on surface textured tantalum interlayer at elevated temperatures, *Surf. Coatings Technol*. 365 (2019) 189–199. doi:10.1016/j.surfcoat.2018.10.067.
- [478] C.A.V. Kumar, J.S. Rajadurai, Influence of rutile (TiO₂) content

- on wear and microhardness characteristics of aluminium-based hybrid composites synthesized by powder metallurgy, *Trans. Nonferrous Met. Soc. China (English Ed.)* 26 (2016) 63–73. doi:10.1016/S1003-6326(16)64089-X.
- [479] V. Arash, K. Anoush, S.M. Rabiee, M. Rahmatei, S. Tavanafar, The effects of silver coating on friction coefficient and shear bond strength of steel orthodontic brackets, *Scanning*. 37 (2015) 294–299. doi:10.1002/sca.21212.
- [480] J. Zhu, M. Xu, W. Yang, D. Li, L. Zhou, L. Fu, Friction and Wear Behavior of an Ag–Mo Co-Implanted GH4169 Alloy via Ion-Beam-Assisted Bombardment, *Coatings*. 7 (2017) 191. doi:10.3390/coatings7110191.
- [481] N.B. Damm, M.M. Morlock, N.E. Bishop, Friction coefficient and effective interference at the implant-bone interface, *J. Biomech.* 48 (2015) 3517–3521. doi:10.1016/j.jbiomech.2015.07.012.
- [482] Z. Abdullaeva, Nano-and biomaterials: Compounds, properties, characterization, and applications, 2017. https://books.google.be/books?hl=en&lr=&id=wEpGDwAAQBAJ&oi=fnd&pg=PR11&dq=Nano-and+Biomaterials:+Compounds,+Properties,+Characterization,+and+...&ots=eNqE0hzjg1&sig=puCuOYLzqG1dzLWNLJZ1m2_80Nw (accessed May 15, 2020).
- [483] C. Shi, J. Gao, M. Wang, J. Fu, D. Wang, Y. Zhu, Ultra-trace silver-doped hydroxyapatite with non-cytotoxicity and effective antibacterial activity, *Mater. Sci. Eng. C*. 55 (2015) 497–505. doi:10.1016/J.MSEC.2015.05.078.
- [484] C. Greulich, S. Kittler, M. Epple, G. Muhr, M. Köller, Studies on the biocompatibility and the interaction of silver nanoparticles with human mesenchymal stem cells (hMSCs), *Langenbeck's Arch. Surg.* 394 (2009) 495–502. doi:10.1007/s00423-009-0472-1.
- [485] M. Ribeiro, F.J. Monteiro, M.P. Ferraz, Infection of orthopedic implants with emphasis on bacterial adhesion process and techniques used in studying bacterial-material interactions., *Biomater.* 2 (2012) 176–94. doi:10.4161/biom.22905.
- [486] W.K. Jung, H.C. Koo, K.W. Kim, S. Shin, S.H. Kim, Y.H. Park, Antibacterial activity and mechanism of action of the silver ion in *Staphylococcus aureus* and *Escherichia coli.*, *Appl. Environ. Microbiol.* 74 (2008) 2171–8. doi:10.1128/AEM.02001-07.

- [487] I. SonDI, B. Salopek-SonDI, Silver nanoparticles as antimicrobial agent: a case study on *E. coli* as a model for Gram-negative bacteria, *J. Colloid Interface Sci.* 275 (2004) 177–182. doi:10.1016/j.jcis.2004.02.012.
- [488] J. Liu, H.R. Hurt, Ion Release Kinetics and Particle Persistence in Aqueous Nano-Silver Colloids, *Environ. Sci. Technol.* 44 (2010) 2169–2175. doi:10.1021/es9035557.
- [489] G. McDonnell, A.D. Russell, Antiseptics and disinfectants: activity, action, and resistance., *Clin. Microbiol. Rev.* 12 (1999) 147–79. <http://www.ncbi.nlm.nih.gov/pubmed/9880479> (accessed September 24, 2019).
- [490] S. Pal, Y.K. Tak, J.M. Song, Does the Antibacterial Activity of Silver Nanoparticles Depend on the Shape of the Nanoparticle? A Study of the Gram-Negative Bacterium *Escherichia coli*, *Appl. Environ. Microbiol.* 73 (2007) 1712–1720. doi:10.1128/AEM.02218-06.
- [491] Y. Takami, S. Yamane, K. Makinouchi, G. Otsuka, J. Glueck, R. Benkowski, Y. Nosé, Protein adsorption onto ceramic surfaces, *J. Biomed. Mater. Res.* 40 (1998) 24–30. doi:10.1002/(SICI)1097-4636(199804)40:1<24::AID-JBM3>3.0.CO;2-T.
- [492] K. Chen, P. Ustriyana, F. Moore, N. Sahai, Biological Response of and Blood Plasma Protein Adsorption on Silver-Doped Hydroxyapatite, (2019). doi:10.1021/acsbiomaterials.8b00996.
- [493] Z.L. Sun, L. Bai, G.P. Guan, K.H. Zhuan, H.Q. Dai, Protein adsorption and biocompatibility of porous silk fibroin films, in: *Proc. 2009 2nd Int. Conf. Biomed. Eng. Informatics, BMEI 2009, 2009*. doi:10.1109/BMEI.2009.5305691.
- [494] X. Wang, G. Herting, I. Odnevall Wallinder, E. Blomberg, Adsorption of bovine serum albumin on silver surfaces enhances the release of silver at pH neutral conditions, *Phys. Chem. Chem. Phys.* 17 (2015) 18524–18534. doi:10.1039/c5cp02306h.
- [495] H. Zeng, K.K. Chittur, W.R. Lacefield, Analysis of bovine serum albumin adsorption on calcium phosphate and titanium surfaces, 1999.
- [496] X.C. Shen, H. Liang, J.H. Guo, C. Song, X.W. He, Y.Z. Yuan, Studies on the interaction between Ag⁺ and human serum albumin, *J. Inorg. Biochem.* 95 (2003) 124–130. doi:10.1016/S0162-0134(03)00094-1.
- [497] T. Hara, K. Matsuoka, K. Matsuzaka, M. Yoshinari, T. Inoue,

Effect of surface roughness of titanium dental implant placed under periosteum on gene expression of bone morphogenic markers in rat., *Bull. Tokyo Dent. Coll.* 53 (2012) 45–50. doi:10.2209/tdcpublish.53.45.

- [498] S. Das, S. Gurav, V. Soni, A. Ingle, • Bhabani, S. Mohanty, P. Chaudhari, • Kiran Bendale, • Kanchan Dholam, • Jayesh, R. Bellare, Osteogenic Nanofibrous Coated Titanium Implant Results in Enhanced Osseointegration: In Vivo Preliminary Study in a Rabbit Model, *Tissue Eng. Regen. Med.* 15 (n.d.). doi:10.1007/s13770-017-0106-6.
- [499] A.B. Novaes, S.L.S. de Souza, R.R.M. de Barros, K.K.Y. Pereira, G. Iezzi, A. Piattelli, Influence of implant surfaces on osseointegration, *Braz. Dent. J.* 21 (2010) 471–481. doi:10.1590/s0103-64402010000600001.
- [500] G. Braun, D. Kohavi, D. Amir, M. Luna, R. Caloss, J. Sela, D.D. Dean, B.D. Boyan, Z. Schwartz, Markers of primary mineralization are correlated with bone-bonding ability of titanium or stainless steel in vivo, *Clin. Oral Implants Res.* 6 (1995) 1–13. doi:10.1034/j.1600-0501.1995.060101.x.
- [501] Z. Schwartz, D. Amir, B.D. Boyan, D. Cochavy, C.M. Mai, L.D. Swain, U. Gross, J. Sela, Effect of glass ceramic and titanium implants on primary calcification during rat tibial bone healing., *Calcif. Tissue Int.* 49 (1991) 359–64. doi:10.1007/bf02556260.
- [502] X. Zhang, Y. Wu, Y. Lv, Y. Yu, Z. Dong, Formation mechanism, corrosion behaviour and biological property of hydroxyapatite/TiO₂ coatings fabricated by plasma electrolytic oxidation, *Surf. Coatings Technol.* 386 (2020) 125483. doi:10.1016/j.surfcoat.2020.125483.
- [503] G. Wang, J. Li, K. Lv, W. Zhang, X. Ding, G. Yang, X. Liu, X. Jiang, Surface thermal oxidation on titanium implants to enhance osteogenic activity and in vivo osseointegration, *Sci. Rep.* 6 (2016) 1–13. doi:10.1038/srep31769.
- [504] ISO - ISO 10993-5:2009 - Biological evaluation of medical devices — Part 5: Tests for in vitro cytotoxicity, (n.d.). <https://www.iso.org/standard/36406.html> (accessed December 17, 2019).
- [505] M. Vaidulych, J. Hanuš, T. Steinhartová, O. Kylián, A. Choukourov, J. Beranová, I. Khalakhan, H. Biederman, Deposition of Ag/a-C:H nanocomposite films with Ag surface

- enrichment, *Plasma Process. Polym.* 14 (2017). doi:10.1002/ppap.201600256.
- [506] J. Hanuš, T. Steinhartová, O. Kylián, J. Kousal, P. Malinský, A. Choukourov, A. Macková, H. Biederman, Deposition of Cu/a-C:H Nanocomposite Films, *Plasma Process. Polym.* 13 (2016) 879–887. doi:10.1002/ppap.201500208.
- [507] A. Shelemin, D. Nikitin, P. Pleskunov, M. Vaidulych, R. Tafiichuk, A. Choukourov, P. Kúš, P. Solař, A. Kuzminova, O. Kylián, H. Biederman, Wetting on a-C:H coatings decorated with sub-micron structures, *Surf. Coatings Technol.* 367 (2019) 165–172. doi:10.1016/j.surfcoat.2019.03.060.
- [508] G.A. Sotiriou, S.E. Pratsinis, Antibacterial Activity of Nanosilver Ions and Particles, *Environ. Sci. Technol.* 44 (2010) 5649–5654. doi:10.1021/es101072s.
- [509] E. Körner, M.H. Aguirre, G. Fortunato, A. Ritter, J. Rühle, D. Hegemann, Formation and distribution of silver nanoparticles in a functional plasma polymer matrix and related Ag⁺ release properties, *Plasma Process. Polym.* 7 (2010) 619–625. doi:10.1002/ppap.200900163.
- [510] S. Lischer, E. Körner, D.J. Balazs, D. Shen, P. Wick, K. Grieder, D. Haas, M. Heuberger, D. Hegemann, Antibacterial burst-release from minimal Ag-containing plasma polymer coatings, *J. R. Soc. Interface.* 8 (2011) 1019–1030. doi:10.1098/rsif.2010.0596.
- [511] M. Ribeiro, F.J. Monteiro, M.P. Ferraz, Infection of orthopedic implants with emphasis on bacterial adhesion process and techniques used in studying bacterial-material interactions., *Biomater.* 2 (2012) 176–194.
- [512] L. Yang, B.W. Sheldon, T.J. Webster, Orthopedic nano diamond coatings: Control of surface properties and their impact on osteoblast adhesion and proliferation, *J. Biomed. Mater. Res. - Part A.* 91 (2009) 548–556. doi:10.1002/jbm.a.32227.
- [513] S.D. Kuhn, K. Sridharan, Z. Hao, P. Muir, M. Suresh, A. Singh, S. V. Raj, Biocompatibility of uncoated and diamond-like carbon coated Ti–20%Hf alloy, *Mater. Sci. Technol.* 24 (2008) 575–578. doi:10.1179/174328408x281903.
- [514] ISO 10993-5:2009 - Biological evaluation of medical devices -- Part 5: Tests for in vitro cytotoxicity, (n.d.). <https://www.iso.org/standard/36406.html> (accessed July 19,

- 2019).
- [515] C.N. Almeida, B.C. Ramos, N.S. Da-Silva, C. Pacheco-Soares, V.J. Trava-Airoldi, A.O. Lobo, F.R. Marciano, Morphological analysis and cell viability on diamond-like carbon films containing nanocrystalline diamond particles, *Appl. Surf. Sci.* 275 (2013) 258–263. doi:10.1016/j.apsusc.2012.12.122.
- [516] R. Hayashi, T. Ueno, S. Migita, Y. Tsutsumi, H. Doi, T. Ogawa, T. Hanawa, N. Wakabayashi, Hydrocarbon deposition attenuates osteoblast activity on titanium, *J. Dent. Res.* 93 (2014) 698–703. doi:10.1177/0022034514536578.
- [517] S. Nißen, J. Heeg, M. Wienecke, D. Behrend, M. Warkentin, K. Rokosz, S. Gaiaschi, P. Chapon, Surface Characterization and Copper Release of a-C:H:Cu Coatings for Medical Applications, *Coatings*. 9 (2019) 119. doi:10.3390/coatings9020119.
- [518] P. Guo, L. Sun, X. Li, S. Xu, P. Ke, A. Wang, Structural properties and surface wettability of Cu-containing diamond-like carbon films prepared by a hybrid linear ion beam deposition technique, (2015). doi:10.1016/j.tsf.2015.01.018.
- [519] A.Kuzminova, J. Beranová, O. Polonskyi, A. Shelemin, O. Kylián, A. Choukourov, D. Slavínská, H. Biederman, Antibacterial nanocomposite coatings produced by means of gas aggregation source of silver nanoparticles, *Surf. Coatings Technol.* 294 (2016) 225–230. doi:10.1016/J.SURFCOAT.2016.03.097.
- [520] Y.H. Kim, D.K. Lee, H.G. Cha, C.W. Kim, Y.C. Kang, Y.S. Kang, Preparation and Characterization of the Antibacterial Cu Nanoparticle Formed on the Surface of SiO₂ Nanoparticles, *J. Phys. Chem. B.* 110 (2006) 24923–24928. doi:10.1021/jp0656779.
- [521] J. Kratochvíl, J. Štěřba, J. Lieskovská, H. Langhansová, A. Kuzminova, I. Khalakhan, O. Kylián, V. Straňák, Antibacterial effect of Cu/C:F nanocomposites deposited on PEEK substrates, *Mater. Lett.* 230 (2018) 96–99. doi:10.1016/j.matlet.2018.07.082.
- [522] A. Ewald, C. Käppel, E. Vorndran, C. Moseke, M. Gelinsky, U. Gbureck, The effect of Cu(II)-loaded brushite scaffolds on growth and activity of osteoblastic cells, *J. Biomed. Mater. Res. Part A.* 100 (2012) n/a-n/a. doi:10.1002/jbm.a.34184.
- [523] C. Wu, Y. Zhou, M. Xu, P. Han, L. Chen, J. Chang, Y.X.-Biomaterials, undefined 2013, Copper-containing mesoporous

- bioactive glass scaffolds with multifunctional properties of angiogenesis capacity, osteostimulation and antibacterial activity, Elsevier. (n.d). <https://www.sciencedirect.com/science/article/pii/S0142961212010897> (accessed May 22, 2019).
- [524] O. Kylián, J. Kratochvíl, M. Petr, A. Kuzminova, D. Slavínská, H. Biederman, J. Beranová, Ag/C:F Antibacterial and hydrophobic nanocomposite coatings, *Funct. Mater. Lett.* 10 (2017) 1750029. doi:10.1142/s1793604717500291.
- [525] A. Kuzminova, J. Beranová, O. Polonskyi, A. Shelemin, O. Kylián, A. Choukourov, D. Slavínská, H. Biederman, Antibacterial nanocomposite coatings produced by means of gas aggregation source of silver nanoparticles, *Surf. Coatings Technol.* 294 (2016) 225–230. doi:10.1016/j.surfcoat.2016.03.097.
- [526] N. Alissawi, T. Peter, T. Strunskus, C. Ebbert, G. Grundmeier, F. Faupel, Plasma-polymerized HMDSO coatings to adjust the silver ion release properties of Ag/polymer nanocomposites, *J. Nanoparticle Res.* 15 (2013). doi:10.1007/s11051-013-2080-9.
- [527] L. Ploux, M. Mateescu, K. Anselme, K. Vasilev, Antibacterial Properties of Silver-Loaded Plasma Polymer Coatings, *J. Nanomater.* 2012 (2012) 1–9. doi:10.1155/2012/674145.
- [528] L. Song, M. Connolly, M.L. Fernández-Cruz, M.G. Vijver, M. Fernández, E. Conde, G.R. De Snoo, W.J.G.M. Peijnenburg, J.M. Navas, Species-specific toxicity of copper nanoparticles among mammalian and piscine cell lines, *Nanotoxicology.* 8 (2014) 383–393. doi:10.3109/17435390.2013.790997.
- [529] A.P. Ingle, N. Duran, M. Rai, Bioactivity, mechanism of action, and cytotoxicity of copper-based nanoparticles: A review, *Appl. Microbiol. Biotechnol.* 98 (2014) 1001–1009. doi:10.1007/s00253-013-5422-8.
- [530] Y. Zhuang, S. Zhang, K. Yang, L. Ren, K. Dai, Antibacterial activity of copper-bearing 316L stainless steel for the prevention of implant-related infection, *J. Biomed. Mater. Res. Part B Appl. Biomater.* (2019) jbm.b.34405. doi:10.1002/jbm.b.34405.
- [531] B. Cao, Y. Zheng, T. Xi, C. Zhang, W. Song, K. Burugapalli, H. Yang, Y. Ma, B. Cao, Y. Zheng, T. Xi, H. Yang, Y. Ma, C. Zhang, W. Song, K. Burugapalli, Concentration-dependent cytotoxicity of copper ions on mouse fibroblasts in vitro: effects of copper ion

- release from TCu380A vs TCu220C intra-uterine devices, *Biomed Microdevices*. 14 (2012) 709–720. doi:10.1007/s10544-012-9651-x.
- [532] M. Kalbacova, B. Rezek, V. Baresova, C. Wolf-Brandstetter, A. Kromka, Nanoscale topography of nanocrystalline diamonds promotes differentiation of osteoblasts, *Acta Biomater*. 5 (2009) 3076–3085. doi:10.1016/j.actbio.2009.04.020.
- [533] W. de M. Silva, C.A. Ribeiro, C.S. Marques, A.S. Tabata, M.J. Saeki, L.I. Medeiros, D.E. de Oliveira, Fibroblast and pre-osteoblast cell adhesive behavior on titanium alloy coated with diamond film, *Mater. Res.* 20 (2017) 284–290. doi:10.1590/1980-5373-mr-2016-0971.
- [534] R. Paul, Diamond-Like-Carbon Coatings for Advanced Biomedical Applications, *Glob. J. Nanomedicine*. 2 (2017).
- [535] E. O'Neill, G. Awale, L. Daneshmandi, O. Umerah, K.W.H. Lo, The roles of ions on bone regeneration, *Drug Discov. Today*. 23 (2018) 879–890. doi:10.1016/j.drudis.2018.01.049.
- [536] E. Filova, M. Vandrovcova, M. Jelinek, J. Zemek, J. Houdkova, Jan Remsa, T. Kocourek, L. Stankova, L. Bacakova, Adhesion and differentiation of Saos-2 osteoblast-like cells on chromium-doped diamond-like carbon coatings, *J. Mater. Sci. Mater. Med.* 28 (2017). doi:10.1007/s10856-016-5830-2.
- [537] R. Hang, A. Gao, X. Huang, X. Wang, X. Zhang, L. Qin, B. Tang, Antibacterial activity and cytocompatibility of Cu-Ti-O nanotubes, *J. Biomed. Mater. Res. - Part A*. 102 (2014) 1850–1858. doi:10.1002/jbm.a.34847.



Colorful abstract Plasma lightning background.